Synthesis and molecular properties of zwitterionic adducts of TCNQ and other related compounds

CROUCH, David James

Available from the Sheffield Hallam University Research Archive (SHURA) at:

http://shura.shu.ac.uk/3134/

A Sheffield Hallam University thesis

This thesis is protected by copyright which belongs to the author.

The content must not be changed in any way or sold commercially in any format or medium without the formal permission of the author.

When referring to this work, full bibliographic details including the author, title, awarding institution and date of the thesis must be given.

Please visit http://shura.shu.ac.uk/3134/ and http://shura.shu.ac.uk/information.html for further details about copyright and re-use permissions.

CITY CAMPUS, HOWARD STREET,
SHEFFIELD, S1 1WB.

101 610 865 6

REFERENCE

ProQuest Number: 10694400

All rights reserved

INFORMATION TO ALL USERS
The quality of this reproduction is dependent upon the quality of the copy submitted.

In the unlikely event that the author did not send a complete manuscript
and there are missing pages, these will be noted. Also, if material had to be removed,
a note will indicate the deletion.

ProQuest 10694400

Published by ProQuest LLC (2017). Copyright of the Dissertation is held by the Author.

All rights reserved.
This work is protected against unauthorized copying under Title 17, United States Code
Microform Edition © ProQuest LLC.

ProQuest LLC.
789 East Eisenhower Parkway
P.O. Box 1346
Ann Arbor, MI 48106 – 1346

SYNTHESIS AND MOLECULAR PROPERTIES OF ZWITTERIONIC ADDUCTS OF TCNQ AND OTHER RELATED COMPOUNDS

DAVID JAMES CROUCH B.Sc.(Hons)

A thesis submitted in partial fulfilment of the requirements of
Sheffield Hallam University
for the degree of Doctor of Philosophy

September 1999

Collaborating Organisation: The Health and Safety Executive

SHEFFIELD HALLAM UNIVERSITY
STACK NO
18173
ADSETTS CENTRE
STACK 1

Abstract

This thesis is concerned with the synthesis and characterisation of novel TCNQ (7,7,8,8-tetracyanoquinodimethane), TMTCNQ (2,3,5,6-tetramethyl-7,7,8,8-tetracyanoquinodimethane) and TCNQF$_4$ (2,3,5,6-tetrafluoro-7,7,8,8-tetracyanoquinodimethane) based zwitterionic D-π-A materials (where D and A are electron donors and acceptors respectively) of which the methylated Z-β-(N-methyl-4-quinolinium)-α-cyano-4-(2,3,5,6-tetrafluoro)styryldicyanomethanide [CH$_3$(4)Q3CNQF$_4$] is a typical example.

Synthetic modification of the donor moiety was also undertaken, resulting in a diverse range of pyridinium, quinolinium and benzothiazolium-based materials, which may have use in nonlinear optical research. For the quinolinium system an extensive range of both 2- and 4-substituted analogues have been prepared and their properties compared and contrasted.

The solvatochromic behaviour of these zwitterions was investigated in detail by dissolution in a range of organic solvents and measurement of their longest wavelength charge-transfer absorption bands using UV/Visible spectroscopy, which revealed that the substituents have a marked effect upon their solvatochromic properties. Most of the adducts studied display highly negative solvatochromism as the solvent polarity increases, in which their absorption maxima are linearly related with the normalised E^N_T values for the Reichardt dye. However the fluorinated quinolinium and pyridinium derivatives exhibit an unusual aggregation-induced reverse solvatochromism effect. The negative halochromic behaviour of selected zwitterions has also been investigated, with a hypsochromic shift of the longest wavelength CT absorption band being observed upon addition of electrolytes.

Increased polarisation within the fluorinated R(4)Q3CNQF$_4$ and R(2)Q3CNQF$_4$ adducts has been indicated by solution state dipole moment measurements indicating greater nonlinear optical potential. However this increased polarisation has also been shown to be a major cause of the limited stability of these materials to photo-oxidation. The behaviour of the R(4)Q3CNQF$_4$ and R(2)Q3CNQF$_4$ zwitterions on the subphase and their resultant Langmuir-Blodgett film forming ability was also studied. However unlike the TCNQ-based materials the fluorinated adducts have been shown to be poor LB film forming materials.

CONTENTS.

Abstract.
Dedication.
Contents. i
Acknowledgements. v

CHAPTER 1: Electroactive Organic Materials.

1.1. Historical Introduction. 1
1.2. Organic Charge-Transfer Complexes. 6
1.3. Organic Electron Donor Systems. 10
    1.3.1.Organic Superconductors. 13
1.4. Organic Electron Acceptor Systems. 15
    1.4.1.TCNQ Synthesis. 18
1.5. Conducting Polymers. 24
1.6. Structures and Nomenclature for the Donor-π-Acceptor Adducts Reported. 25
1.7. Zwitterionic Donor-π-Acceptor TCNQ Systems. 27
1.8. References. 35

CHAPTER 2: Synthesis.

2.1 Synthetic and Instrumental Techniques. 44
2.2 Synthesis of Electron Donors. 46
    2.2.1 N-Alkyl-4-methylquinolinium Bromides. 46
    2.2.2 N-Alkyl-2-methylquinolinium Bromides. 47
    2.2.3 N,N′-(*m* or *p*-Xylenyl)diquinolinium (or pyridinium) Dibromides. 49
    2.2.4 N-Methyl-2-methylpyridinium Iodide. 51
2.3 Synthesis of Electron Acceptors. 52
    2.3.1 11,11,12,12-Tetracyano-9,10-anthraquinodimethane. 52
    2.3.2 2,3,5,6-Tetramethyl-7,7,8,8-tetracyanoquinodimethane. 53
    2.3.3 2,3,5,6-Tetrafluoro-7,7,8,8-tetracyanoquinodimethane. 54
    2.3.4 N,N′-Dicyano-2,3,5,6-tetrafluorobenzoquinodiimine. 58

2.4 Synthesis of Zwitterionic D-π-A Adducts. 60
2.4.1 Synthesis of R(4)Q3CNQF$_4$ Adducts. 60
2.4.2 Synthesis of R(2)Q3CNQF$_4$ Adducts. 63
2.4.3 Synthesis of R(4)Q3CNTMQ Adducts. 66
2.4.4 Synthesis of R(4)Q3CNAQ Adducts. 68
2.4.5 Synthesis of *m*-C$_8$H$_8$(4)DQ6CNQ and Derivatives. 69
2.4.6 Synthesis of CH$_3$(2)P3CNQF$_4$. 71
2.4.7 Synthesis of C$_3$H$_7$(2)BT3CNQ. 73
2.4.8 Synthesis of C$_3$H$_7$(2)BT3CNQF$_4$. 74
2.4.9 Synthesis of C$_3$H$_7$(2)BT3CNTMQ. 76
2.5 Discussion of Synthetic Methods and Results. 79
2.5.1 N-Alkylation of Nitrogen Heterocycles. 79
2.5.2 Quinodimethanes/Quinodiimines by Knoevenagel Condensation. 81
2.5.3 Synthesis of 2,3,5,6-Tetrafluoro-7,7,8,8-tetracyanoquinodimethane. 83
2.5.4 Synthesis of Zwitterionic D-π-A Adducts of TCNQ. 85
2.6 Spectroscopic Studies of Zwitterionic D-π-A Adducts. 104
2.6.1 Ultra Violet/Visible Spectroscopy. 104
2.6.2 Infrared Spectroscopic Studies. 111
2.6.3 Mass Spectrometry Studies. 115
2.6.4 Nuclear Magnetic Resonance (NMR) Spectroscopy. 124
2.7 References. 128

Chapter 3: Solvatochromism and Halochromism Studies.

3.1 Solvent Polarity. 132
3.2 Solvatochromism and Solvatochromic Compounds. 133
3.3 Halochromism. 141
3.4 Solvatochromic Behaviour of Adducts. 143
3.4.1 Experimental. 144
3.4.2 Solvatochromic Characteristics of R(4)Q3CNQ and R(2)Q3CNQ Adducts. 145
3.4.3 Solvatochromic Characteristics of R(4)Q3CNQF$_4$ and R(2)Q3CNQF$_4$ Adducts. 151
3.4.4 Solvatochromic Characteristics of C$_3$H$_7$(2)BT3CNQ and C$_3$H$_7$(2)BT3CNQF$_4$ Adducts. 163

3.4.5 Solvatochromic Characteristics of $CH_3(2)P3CNQF_4$. 169
3.5 Halochromic Properties of Quinolinium and Benzothiazolium Betaines. 171
3.6 References. 176

Chapter Four: Studies on Selected Physical Properties.

4.1 Introduction. 182
4.2 Fundamental Principles of Nonlinear Optics. 183
4.3 Second Order Nonlinear Optical Materials and their Design. 185
4.4 TCNQ-based Nonlinear Optical Materials. 193
4.5 Dipole Moments of Highly Dipolar Nonlinear Optical Materials. 196
4.5.1 Experimental Apparatus and Procedure. 196
4.5.2 Solution State Dipole Moment Measurements. 199
4.6 ^{19}F NMR Dipole Moment Evolution Studies. 207
4.7 X-Ray Structural Studies. 210
4.7.1 Crystal Packing Effects. 219
4.8 Chemical Stability of Adducts. 223
4.8.1 Photo-Oxidation Experimental. 225
4.8.2 Experimental Results. 225
4.9 References. 230

Chapter Five: Langmuir-Blodgett Films, Experimental, Results and Discussion.

5.1 Historical Introduction. 237
5.2 Isotherm Measurement. 239
5.3 Deposition Principles and Mono/Multilayer Fabrication. 243
5.4 Langmuir-Blodgett Film Forming Materials and their Applications. 246
5.5 Langmuir-Blodgett Films - Experimental. 253
5.5.1 The Joyce-Loebl Mini Trough Monolayer Coating Unit. 253
5.5.2 The Compression System. 254
5.5.3 Surface Pressure Measurement. 255
5.6 Trough Operation. 257
5.6.1 Cleanliness. 257
5.6.2 Trough Calibration. 258
5.6.3 Calibration of Surface Area. 258

5.6.4 Calibration of Surface Pressure. 258
5.6.5 The Subphase. 259
5.6.6 Surface Cleaning. 259
5.6.7 Monolayer Material Preparation and Spreading. 260
5.6.8 Temperature of the Subphase. 261
5.6.9 Compression of the Monolayer. 262
5.6.10 Control of Surface Pressure. 262
5.6.11 Transfer of Monolayer. 262
5.7 Langmuir-Blodgett Films- Results and Discussion. 263
5.7.1 Langmuir Film Studies on R(4)Q3CNQF_4 and R(2)Q3CNQF_4 Adducts. 263
5.8 References. 285

Chapter 6: Conclusions.

6.1 Summary. 290
6.2 Future Work. 293
6.3 References. 294

Appendix I: 296
Appendix II: 298

Acknowledgments.

There are many people who I would like to acknowledge for their support and encouragement during this work. First and foremost I would like to thank all of the technical staff at Sheffield Hallam University especially Kevin, Lee, Ken and Lynn for providing assistance often at very short notice, for which I thank them. I would also like to thank Drs Peter Skabara and Alan Hewson for their helpful discussions on synthetic problems that were encountered and, for help in interpretation of mass spectra, Dr. John Little, all of Sheffield Hallam University. In addition I would also like to thank all my other friends and postgraduate colleagues at Sheffield Hallam for contributing to a most enjoyable atmosphere both in and out of the laboratory, in particular Jo, Steve, Scott, Rory, and Donna.

Apart from colleagues at Sheffield Hallam University I would also like to thank members of other academic institutions, in particular Dr. Marek Szablewski of the Department of Physics at Durham University, for his valued discussions on both chemistry and football and for the loan of materials. A special thanks also goes to Dr. Graham H. Cross, also of the Department of Physics for allowing me to conduct dipole moment measurements, as well as to Professor Mike C. Petty and Dr. Chris Pearson, of the Faculty of Engineering at Durham, for advice on Langmuir-Blodgett films and for allowing me to spend time in their laboratories. Many thanks are also due to Mr. Terry Finn for providing accommodation and sanity during my time in Durham.

I would also like to express my thanks to Mr. Derek White and his staff at Sheffield University for providing, not only accurate mass spectra and combustion analysis, but for excellent quality ^{1}H and ^{19}F NMR spectra as well.

In addition I would also like to thank all of the staff in the crystallographic departments of both Cardiff and Durham Universities, for providing the excellent crystal structures displayed in this text, in particular Dr. Simon Coles (Cardiff) and Professor Judith A. K. Howard (Durham).

I would also like to thank all the staff in the Personal Protective Equipment (PPE) Section of the Health and Safety Laboratory in Sheffield - in particular Dr. Steve Thorpe and Mr. Paul Lemon, without whose support much of this work would have been impossible. Additionally, I would like to thank my family for putting up with someone who refused to foresake the life of a student until the age of twenty-six, and to Sid for his support in providing many stress relieving nights out on the town, as well as to Rosie for the personal support that she has provided throughout the production of this thesis.

I would also like to express my warmest thanks to my supervisory team, Dr. Richard A. Broughton, of the Health and Safety Executive, and Dr. Derek J. Simmonds, of Sheffield Hallam University, who have both given great support and encouragement through some difficult times as well as for their many helpful discussions. A special thanks also goes to Dr. Chris Bradley for his kindness shown during my first few months at Sheffield Hallam, as well as for supplying me with quantities of the R(2)Q3CNQ type compounds. However above all I would most like to thank my Director of Studies, Dr. Norman A. Bell, without whom I would not have been able to complete this work. I wish to thank him for allowing me to undertake studies for a Ph.D and for his patience and kindness, which has been of the highest order, as has his unerring support through some often frustrating times. Working for Norman has been an honour and pleasure for which I again profoundly thank him.

Chapter 1: Electroactive Organic Materials.

1.1 Historical Introduction.

The fact that the electrical conductivity of most organic materials, when purified, is extremely low at room temperature ($\sigma_{rt}<10^{-10}Scm^{-1}$) has been known for many years. Nevertheless, it was suggested at the turn of the century by *McCoy*[1] that some organic solids may exhibit conductivities comparable with that of metals. This attracted little attention as organic materials were considered to form ordered assemblies of discrete, individual and separate molecules. However, in 1954 an unstable perylene bromide salt[2] (Figure 1.1) was found to exhibit "*metallic-like*" conductive properties.

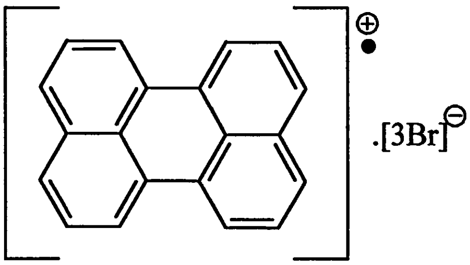

Figure 1.1 Akamatsu's Conducting Perylene Bromide Salt.

As a result of this discovery the area of organic-based electroactive materials has grown to become a major field of investigation. Over the last forty years a range of solid organic conductors has been developed which has led to two classes of organic materials now being recognized: -

1) Charge-transfer (CT) complexes

2) Conducting polymeric compounds

Of these, certain members exhibit conductivities similar to those of metals.

The study[3] of organic charge-transfer complexes goes back to around the time *McCoy*[1] predicted the existence of organic conductors. Such compounds are formed when strong π-molecular donor (D) and acceptor (A) molecules combine to produce either ion-radical salts (X.$^+$A.$^-$ or D.$^+$X.$^-$), where X is an appropriate cation or anion, or charge-transfer compounds in the form of a pseudo-ionic lattice (DA and D.$^+$A.$^-$). Conducting charge-transfer salts fall into two categories - either single chain conductors where the anion is a closed species, or a two-chain conductor, where both the donor and acceptor are open shell species that are able to form stable radical ions.

A stable charge-transfer (CT) complex is formed, as the name implies, by the transfer of an electron from a donor to an acceptor molecule. The more frequently encountered donors are amines, electron rich alkenes, heterocycles and simple alkali metals, whereas the more common acceptors include quinones, electron deficient alkenes, heterocycles and the halogen atoms. On examination, the crystal structures of such charge-transfer complexes were found to be of a mixed stacking type, in which the donor and acceptor molecules stack face-to-face alternately (Figure 1.2).

D A D A D
A D A D A
D A D A D
A D A D A

Figure 1.2 Mixed Donor-Acceptor Stacking.

In 1962 Acker and his co-workers[4] at Du Pont reported the synthesis of 7,7,8,8-tetracyano-p-quinodimethane (TCNQ), a powerful new organic electron acceptor (Figure 1.3).

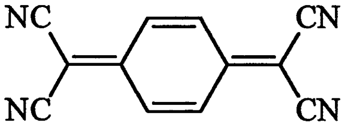

Figure 1.3 7,7,8,8-Tetracyano-p-quinodimethane (TCNQ).

Soon it was realised that TCNQ undergoes single electron reduction relatively easily to yield a number of stable anion-radical derivatives, many of which were found to be semiconductors[4-10] ($\sigma_{rt} \approx 10^{-5} Scm^{-1}$).

TCNQ is a strong π-acid and as such forms two types of salt-like charge-transfer complexes, each of which involve either partial or complete transfer of an electron to the TCNQ molecule, resulting in the formation of the TCNQ radical anion (Figure 1.4).

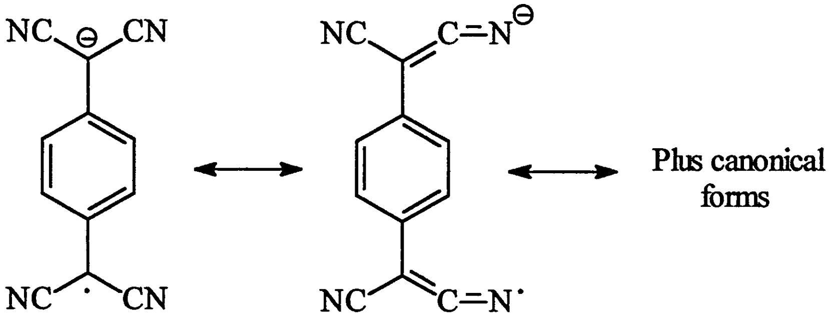

Figure 1.4 TCNQ Radical Anion.

The first type – simple TCNQ salts - have the general formula $M^{n+}(TCNQ^{-})_n$, e.g. LiTCNQ. In general, such complexes involve 100% charge transfer from the donor to the acceptor molecule accounting for the relatively low conductivities seen in such complexes (σ_{rt} = 10^{-3} to 10^{-12} Ω^{-1} cm^{-1}).[6] Some simple complexes such as $LiTCNQF_4$ (Figure 1.5) have shown current-controlled memory switching behaviour[11] and ferromagnetism.[12]

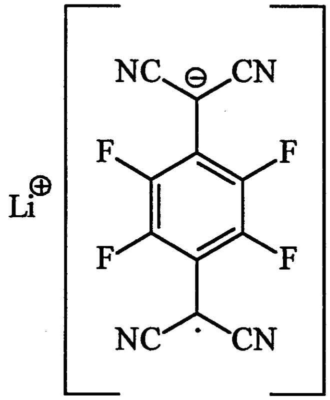

Figure 1.5 Simple TCNQ Salts that Exhibit Ferromagnetic Behaviour.

The second type of TCNQ complexes - complex radical-ion salts - generally have the formulae $M^+(TCNQ^{\cdot -}).(TCNQ^0)$, or $M^{2+}(TCNQ^{\cdot -})_2.(TCNQ^0)$. In the solid state, the donated electron is delocalised over both acceptor molecules, which results in a radical anion $(TCNQ)_2^{\cdot -}$. Quinolinium (Figure 1.6), morpholinium and pyridinium type electron donors[6] have given complex radical-ion salts that have remarkably high conductivities in the range 10^{-3} to $10^2\ \Omega^{-1}\ cm^{-1}$. The initial interest in nitrile-based electron acceptors, such as TCNQ, was itself sparked off by the discovery of tetracyanoethylene (TCNE),[13] which had already shown versatile chemistry and unique electrical properties when complexed with suitable electron donors.[14]

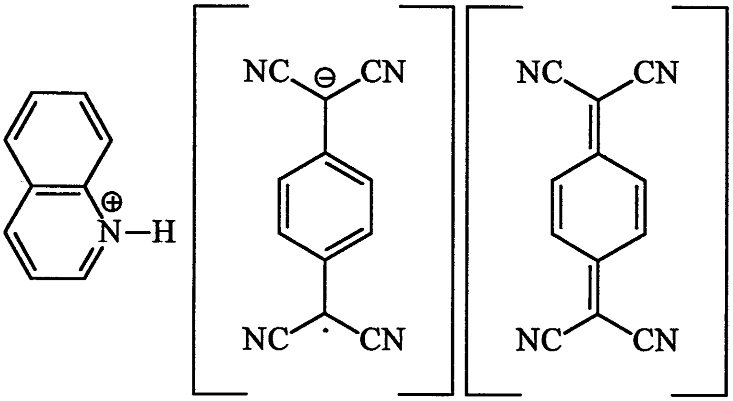

Figure 1.6 The Highly Conductive Quinolinium-TCNQ Charge Transfer Salt.

These large improvements in conductivity prompted renewed interest throughout the 1960's. The vast majority of this research focused upon TCNQ salts[15] and it was soon realised that the high conductivity observed in such complexes was associated with segregated stacks of donor and acceptor molecules. Again, these stack face-to-face (Figure 1.7) and result in the charge-transfer and π-overlap between molecules being very strong, with unpaired electrons partially delocalised along the one-dimensional stacks. The resultant conduction is highly anisotopic.

D A D A D
D A D A D
D A D A D
D A D A D

Figure 1.7 Segregated Donor and Acceptor Stacks.

During this period a powerful new donor, tetrathiafulvalene (TTF)[16] (Figure 1.8) was synthesised. However it required a further three years work before its TCNQ salt was prepared[17] which was found to be highly conducting at room temperature ($\sigma_{rt} \approx 500$ Scm^{-1}).

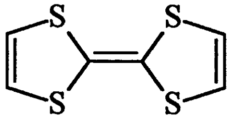

Figure 1.8 Tetrathiafulvalene (TTF).

The conductivity of the TTF-TCNQ salt dramatically increases below room temperature, rising to 10^4 Scm^{-1} at 60 K, and was the first organic solid to be classed as an organic metal. Below this temperature a transition (the Peierls distortion) to a metal-insulating state occurs which has been documented in other one-dimensional conducting organic lattices.[18,19]

1.2 Organic Charge-Transfer Complexes.

The complex formed between iodine and benzene[20] is an early example of a charge-transfer complex. Although not a conductor, it embodied many of the typical features found in subsequent charge-transfer complexes. Its ultraviolet/visible (UV/Vis) spectrum showed features that were characteristic of neither the solute or solvent, rather the features were associated with a separate complex formed between the two. Explanation of this observation led to an extension of Lewis acid-base theory and some other phenomena associated with molecular complexes were forthcoming, for instance the very intense UV/Vis absorption bands observed.

The molecular orbital bonding interactions that occur in such complexes was studied in the early 1950's by *Mulliken.*[21,22] In his series of papers he defined that the donor (D) possessing a HOMO (**H**ighest **O**ccupied **M**olecular **O**rbital) and the acceptor (A) possessing a LUMO (**L**owest **U**noccupied **M**olecular **O**rbital). The resultant charge-transfer, occurs between the HOMO of the donor and the LUMO of the acceptor, as the HOMO is of higher energy than the LUMO. The bonding between the donor (D) and acceptor (A) was described[23] by the following wave function:-

$$\boldsymbol{\Psi_N (A.D) = a\,\Psi_0 (A.D) + b\,\Psi_1 (A^-{-}D^+)} \qquad \text{Equation 1.1}$$

Where ‘**a**’ and ‘**b**’ are smaller integers, with $\mathbf{a>b}$; $\boldsymbol{\Psi_0}$ is the ‘no-bond’ contribution and $\boldsymbol{\Psi_1}$ is a dative bonding contribution. Thus $\boldsymbol{\Psi_N}$ **(A.D)** corresponds to the wave function which describes the combination of two extreme resonance forms. Equation 1.1 also shows that, while the degree to which charge transfer occurs may influence the nature of the complex, it does not dictate the bonding within that complex.

If charge transfer is to take place within such materials, then the energy levels of the donor and acceptor needed to be matched. In solution, this can be accomplished by reorientation of the solvent molecules around both donor and acceptor, whereas in the solid state it is achieved by reorientation and rotation of bonds. Thus, the energy barrier to electron transfer is the summation of these effects. The energy of this electronic transition is dependent on not only the ionization potential of the donor but also the electron affinity of the acceptor. If a strong donor is placed in close proximity to a strong acceptor, then the energy of the charge-transfer transition will be small and the ground state is essentially ionic as 100% charge-transfer occurs.

For weak donor and acceptors the converse is true, as the energy of charge-transfer is greater, which results in the ground state being neutral and the degree of charge-transfer being essentially zero. However, it has been shown that if partial charge-transfer takes place, where the energy of charge transfer is small and positive, then the resultant conductivity will be high as is seen in the TTF-TCNQ complex.[17]

The TTF-TCNQ complex was the prototype system for 'two-chain' organic conductors. The mixed valency and crystal packing of the complex results in a material that can maintain metallic-like conductivity. The partial charge transfer that occurs in this complex results in 59% of the TTF molecules being in the radical cation form and 59% of the TCNQ molecules being in the radical anion form, whilst the remaining TTF and TCNQ molecules are present as neutral species. Effectively the complex is self doped as both the donor and acceptor stacks are partially filled and both contribute towards the conductivity.

The crystal structure of the complex is of extreme importance to the conductivity. As the TTF-TCNQ complex consists of segregated stacks of donor and acceptor molecules, in which the distance between each TTF and TCNQ molecules is very small (3.47Å for TTF and 3.17Å for TCNQ),[24] formation of supra-molecular orbitals occurs due to combination of the π-orbitals of the donor and acceptor.

Nevertheless, despite this segregation, there is some interaction between the adjacent stacks, though electrical conductivity is about 1000× as great in the direction of the columns.[25-27]

The crystal structure also showed that molecules within the stacks do not lie directly on top of one another. Rather there is a sideways displacement in which the exocyclic C=C bond lies above the ring system of the adjacent molecule - in effect a 'ring-double bond overlap' (Figure 1.9). This sideways displacement of the molecules also gives rise to greater π-interactions along the stack. This further enhances the supra-molecular orbitals, creating a mass delocalisation of the electrons within each segregated column and thus giving rise to a highly conductive material.

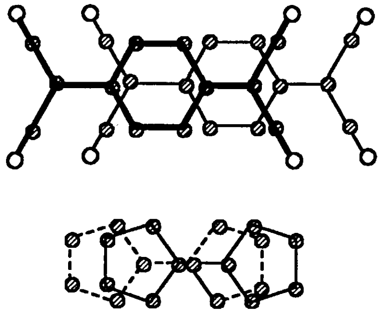

Figure 1.9 Ring-over Bond Overlapping.

As a result of the substantial research into the TTF-TCNQ complex it soon became clear that TTF and TCNQ had properties that made them unique amongst the other donor and acceptor molecules that were available at the time. They are both of similar size, both are planar with a high degree of symmetry, and the π-delocalisation is extensive. The ionization and electron affinities are very similar which tends to favour partial charge transfer and, thereby, high electrical conductivity.

Using this information researchers began to synthesise new electron donors and acceptors, to utilise and test the factors controlling these systems.[28,29] *Cowan et al*[30] published a set of design constraints for the formulation of good organic conductors. For good electrical conduction the components of such complexes should have the following properties:-

1. Stable open-shell (free-radical) species.
2. Planar molecules with delocalised π-molecular orbitals.
3. Inhomogeneous charge and spin distribution.
4. Segregated stacks of radical species.
5. No periodic distortion which opens a gap at the Fermi level (uniform stacks).
6. Little or no disorder (symmetrical radicals and/or radical anions and cations).
7. Molecular components of a similar size.
8. Fractional charge (mixed valence).
9. Relatively strong interchain coupling to suppress phase transitions such as Peierls distortions.
10. Cation and/or anion normally divalent.
11. Polarisable species.

So the last three decades have seen much effort associated with the synthesis of not only charge-transfer complexes, which exhibit the more glamorous phenomena of metallic conductivity and super-conductivity, but also with polymeric and dipolar D-π-A materials. These latter materials have recently attracted attention due to their novel magnetic and optical properties. As the work reported in this text is primarily concerned with the synthesis and characterisation of novel electroactive materials, further background on the chemistry and development of typical systems is discussed.

1.3 Organic Electron Donor Systems.

Since the discovery of the TTF-TCNQ charge-transfer complex the search for other conducting organic species has resulted in the synthesis of a multitude of other organic systems, some of the which show metallic conductivity, some superconductivity. In terms of new electron donor systems, most effort has been devoted to the synthesis of molecules derived from the tetrathiafulvalene (TTF) structure.[31-35] Initially the new donors were just simple derivatives with an extended σ-bond framework[36,37] e.g. tetramethyltetrathiafulvalene [TMTTF (1)]. However the subsequently prepared charge-transfer complexes are, like TTF-TCNQ, quasi one-dimensional materials and show a Peierls transition.

One can vary the heteroatom within the TTF skeleton, e.g. replacement of sulphur with selenium[38] [e.g. tetramethyltetraselenafulvalene-TMTSF (2)] or tellurium [e.g. hexamethylenetetratellurafulvalene-HMTTeF (3)].[38,39] The presence of selenium (or tellurium) atoms, which have a larger van der Waals radius, increased polarisability, band width and interchain interactions compared to the sulphur system. This enables the donor stacks to dominate the transport properties and in general complexes incorporating such derivatives with TCNQ result in increased metallic behaviour when compared to their

TTF counterparts. For example the HMTTeF-TCNQF$_4$ complex,[40,41] like its TTF analogue HMTTF-TCNQF$_4$ ($\sigma_{rt} \approx 10^{-4}$ Scm^{-1}),[42] was expected to be an insulator, as a result of the high electron affinity of TCNQF$_4$ causing complete charge-transfer. But as a result of the strong nonbonded tellurium-tellurium interactions, the complex was found to be highly conducting (1×10^{-1} Scm^{-1}), as a result of partial charge transfer ($\rho \approx 0.75$). This suppressed the Peierls distortion which is observed in the corresponding sulphur and selenium analogues.[41] Increases in dimensionality, which are essential in suppressing Peierls transitions, can also be achieved via the incorporation of group 16 elements, such as sulphur or oxygen etc., at the periphery of TTF type molecules. For instance the increased non-bonded S····S network in compounds such as BEDT-TTF (4) results in inter- as well as intra-stack interactions, which enable such multi-sulphur compounds to not only exhibit metallic conductivity but superconductivity as well. This is discussed further in Section 1.3.1.

In more recent times the emphasis has shifted towards π-extended donors, in which the conjugation between the two dithiolium rings is increased to allow better stabilisation of the dicationic state and thus conduction within such charge-transfer salts.[43] For example "stretched" TTF derivatives such as compounds (5)[44] and (6),[45] as well as the vinylogous derivative (7)[46] have all been shown to be very efficient π-donors. The introduction of group 16 elements into the periphery of polyaromatic systems has also been shown to lower the oxidation potential, one example being naphtho[1,8-*bc*;4,5-*b'c'*]dithiophene (8).[47]

The range is vast - from the simple functionalised derivatives,[48] such as tetrabromo-TTF,[49] to the more elaborate hybrid tetrachalcogeno- fulvalene derivatives,[50] such as DMDSTeF (9).[51]

For a more comprehensive overview of electron donors and conducting organic charge-transfer salts in general, the reader is referred to several excellent reviews by *Grossel* and *Weston*,[31] *Bryce*[32] and *Torrance*.[33]

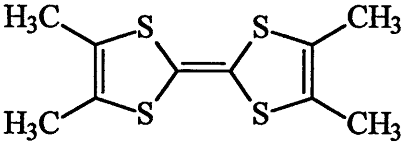
H3C
S
S
CH3
H3C
S
S
CH3

TMTTF(1)

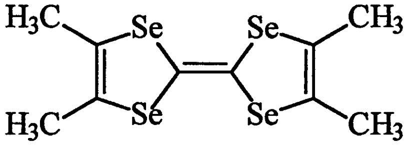
H3C
Se
Se
CH3
H3C
Se
Se
CH3

TMTSF(2)

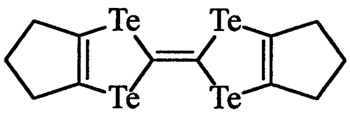

HMTTeF(3)

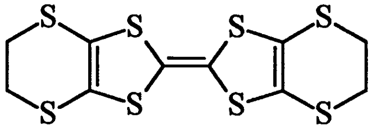

BEDT-TTF(4)

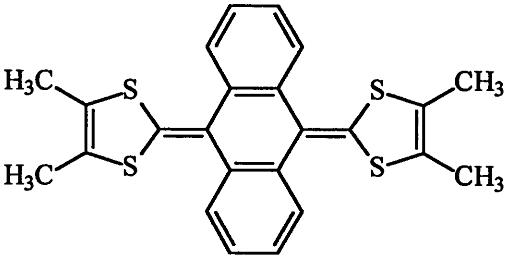
H3C
S
S
CH3
H3C
S
S
CH3

(5)

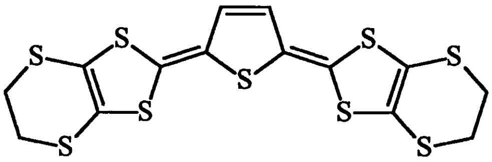

(6)

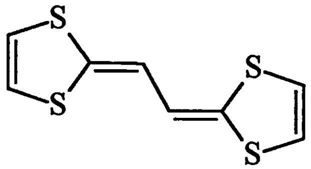

(7)

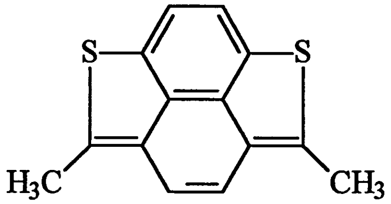

(8)

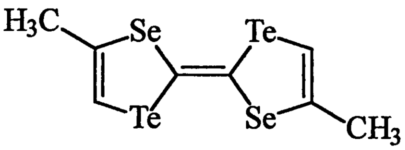
H3C
Se
Te
Te
Se
CH3

DMDSTeF(9)

1.3.1 Organic Superconductors.

The concept of superconductivity in metals and alloys was first introduced by Kamerlingh-Onnes in 1911.[52] Some years later, *Jacobsen et al*[53] showed that the charge-transfer compound TMTSF-2,5-DMTCNQ, which exhibits a truly conductive state when stabilised at liquid helium temperatures, was found to conduct electrically under pressure down to 1K and had an extremely high conductivity above 10 kbar ($\sigma_{\parallel}$ exceeds 10^5 Ωcm^{-1})[54]- a value which had not been observed in other organic conductors. It was proposed that this conductive state may be stabilised due to the super conducting pairing of electron states.[55,56]

Two years later, *Bechgaard* and his coworkers[57] showed that superconductivity could be achieved in organic based materials. The hexafluorophosphate salt of TMTSF, $(TMTSF)_2PF_6$ was found to exhibit superconductivity at 0.9K under a pressure of 12 kbar[57] and indeed many members of the $(TMTSF)_2X$ family, where X is an inorganic monovalent anion (ClO_4^-, ReO_4^-, FSO_3^-, etc.), were subsequently found to exhibit superconductivity. It was subsequently shown that with the proper choice, of the anion, superconductivity could be stabilised at ambient pressure below 1.2 K, as is the case with the $(TMTSF)_2ClO_4$ radical salt.

The theory of metallic superconductivity was first formulated by *Bardeen*, *Cooper* and *Schrieffer* in 1957[58] and is based upon the ordered motion of electron pairs. These electron pairs, termed Cooper pairs, interact with the lattice vibrations (phonons) such that the electrons are not scattered, rather they flow freely in a highly coordinated manner and carry super currents. Evidence appears to show that Cooper pairing does indeed occur in the *Bechgaard salts*.[59]

This pairing of electrons is localised along the donor chains, which are stacked in a zigzag arrangement between the monovalent anions, often at temperatures as high as 30 K which is well above the onset of bulk superconductivity (T_C).

In 1983 the sulphur-based $(BEDT\text{-}TTF)_2^+ ReO_4^-$ salt (Figure 1.10), showed the onset of superconductivity (T_C) at 1.5 K under a pressure of 7 kbar.[60]

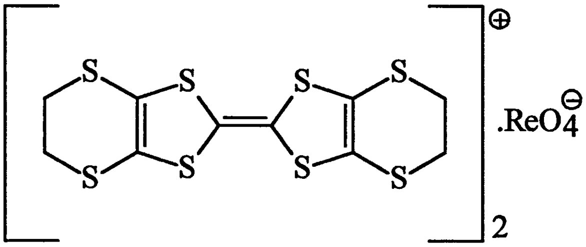

Figure 1.10 First Sulphur-Based Organic Superconductor.

Several other super conducting salts of BEDT-TTF have been found, such as the β-$(BEDT\text{-}TTF)_2^+I_3^-$ salt[61] which superconducts at ambient pressure and the κ-$(BEDT\text{-}TTF)_2Cu[N(CN)_2]Br$ salt[62] which currently has the highest onset temperature (T_C) among the TTF family of organic-based superconductors.[63] The BEDT-TTF series of compounds are all characterised by short sulphur-sulphur interactions which form two-dimensional sheets, rather than the one dimensional stacks of the $(TMTSF)_2X$ family of superconductors. Other families of salts also exhibit superconductivity e.g. hybrid compounds (10)[64]and (11)[65] illustrated in Figure 1.11. These are essentially produced by combining half of the TMTSF molecule with half of the BEDT-TTF molecule.

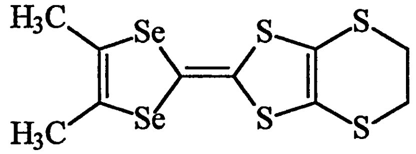

DMET(10)

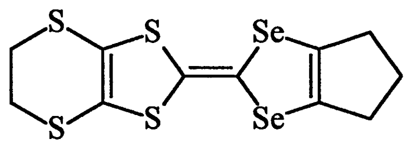

TMET-STF(11)

Figure 1.11 Hybrid Organic Superconductor Components.

Additionally alkali metal salts incorporating Fullerene donors have shown super conducting transitions at temperatures rivaling those observed in ceramic superconductors. For example the $Cs_2Rb[C_{60}]$ salt acts as a metal that becomes superconducting at 33 K (Figure 1.12).[66] More information on this topic can be found in several excellent papers by *Mori et al*[67] and *Jérome et al.*[68]

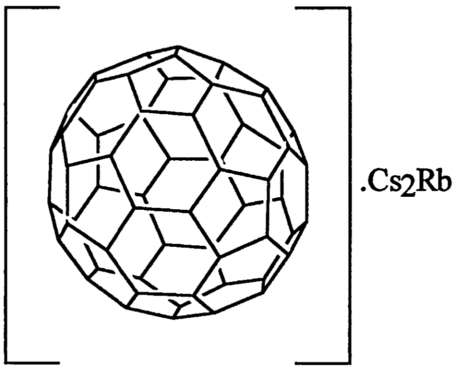

Figure 1.12 Highest T_C Organic-Based Superconductor.

1.4 Organic Electron Acceptor Systems.

The discovery of the TTF-TCNQ system, has resulted in much research in this area. Not only has this produced new electron donors, but also novel acceptors.

As a result of the high thermal stability of the intermediate radical anion of TCNQ, the vast majority of new electron acceptors that have been prepared have been TCNQ-based. These have ranged from simple ring substituted acceptors such as 2,3,5,6-tetrafluoro-

7,7,8,8-tetracyanoquinodimethane [$TCNQF_4$ (12)],[69] whose electronegative fluorine atoms make it a very strong electron acceptor, to the more complicated π-extended and heteroatom-containing acceptors such as 11,11,12,12-tetracyano-2,7-pyrenoquinodimethane [TCNPQ (13)][70] and bis[1,2,5]thiadiazolo-7,7,8,8-tetracyanoquinodimethane [BDTA-TCNQ (14)],[71] which reduce the intramolecular coulombic repulsion in the dianion and increase dimensionality as a result of greater intra- and inter-stack interactions. The strongest uncharged electron acceptor based upon the TCNQ system remains 2,5,7,7,8,8-hexacyano-p-quinodimethane [$TCNQ(CN)_2$, E_1 = 0.67 V versus Ag/AgCl in MeCN][72] as, although $TCNQ(CN)_4$ has a first reduction potential of 1.31 V, this latter compound is not stable in its oxidized form.[73]

The strongest uncharged electron acceptor is the 1,4-benzoquinone based compound, tetracyano-1,4-benzoquinone [cyanil –(15)][74] which shows a reduction potential of 0.90 V (versus Ag/AgCl in MeCN). Cyanil[74] is one of a number of strong acceptors based upon the 1,4-benzoquinone system (16) which includes 2,3-dichloro-5,6-dicyano-1,4-benzoquinone (DDQ),[75] as well as the halogenated derivatives, i.e. *p*-fluoranil, *p*-chloranil etc.

However, 1,4-benzoquinones are generally weaker electron acceptors when compared to their TCNQ counterparts[76] and so most research has been concentrated on TCNQ-based systems. The N,N′-dicyano-p-quinonediimine [DCNQI (17)] system, which was developed from TCNQ, is also of considerable interest as, unlike TCNQ, this forms highly conducting charge-transfer complexes and ion-radical salts that do not undergo a Peierls distortion even at low temperatures.[77] More recently researchers[78] have brought the TCNQ and DCNQI systems together by forming a hybrid type of electron acceptor.

These compounds which are termed N,7,7-tricyanoquinomethaneimines[TCNQI (18)] are like their TCNQ and DCNQI relatives in that they undergo one- and two-electron reductions.

Apart from the quinoidal TCNQ/DCNQI type electron acceptors mentioned, several other types of electron acceptors have been proposed. For example, cyanocarbons such as octacyanotetramethylenecyclobutadiendiide (19)[79] and hexacyanotriphenylene (20)[80] have been proposed as suitable organic ferromagnets, owing to their ability to stabilise anions and radical anions more effectively, due to their multiple cyano groups.[9] Fullerene electron acceptors based on C_{60} have also been examined.[81] However the electron acceptor ability of the C_{60} molecule was found to be weak - comparable with that of benzoquinone.-[82]

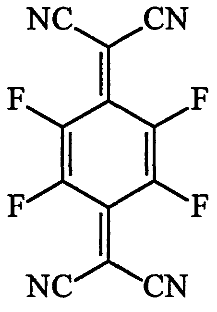

TCNQF4(12)

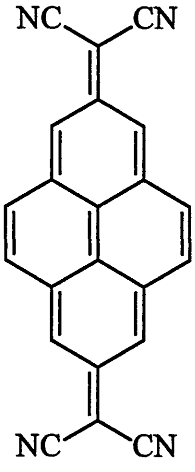

TCNPQ(13)

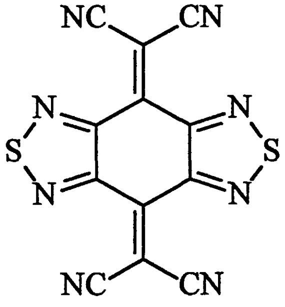

BTDA-TCNQ(14)

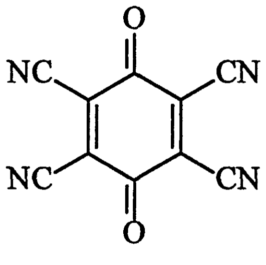

(15) Cyanil

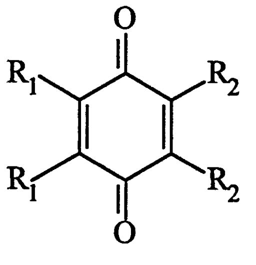

(16) R_1=Cl, R_2=CN, DDQ
R_1=R_2= Cl, *p*-Chloranil

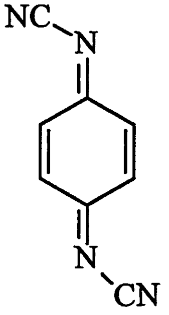

(17) DCNQI

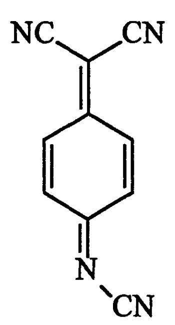

(18) TCNQI

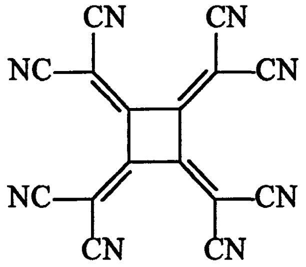

(19) $C_4[C(CN)_2]_4$

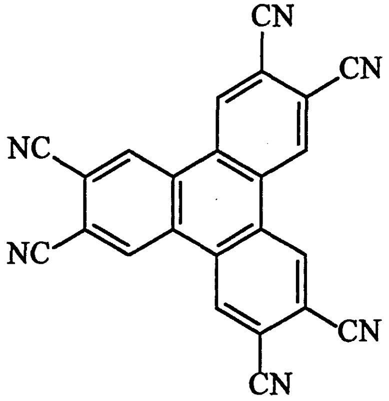

(20) Hexacyanotriphenylene

1.4.1 TCNQ Synthesis.

A major hurdle in the development of new organic materials is the difficulty in synthesising TCNQ derivatives, unlike the TTF skeleton, which has proved a particularly versatile building block for synthetic derivatives. The major problem confronting the synthetic chemist is that, in general TCNQ only undergoes reactions at the dicyanomethanide parts of the molecule - mainly 1,6-addition reactions-[83] and, substitution reactions involving the replacement of cyano groups with, for example primary and secondary amines.[7] Much effort has explored the displacement of hydrogen atoms on the quinoidal ring system. However, to date only one reaction of this type has been documented - the interaction of TCNQ with diphenyldiazomethane which results in the formation of 2-diphenylmethyl-TCNQ,[84] as illustrated in Figure 1.13.

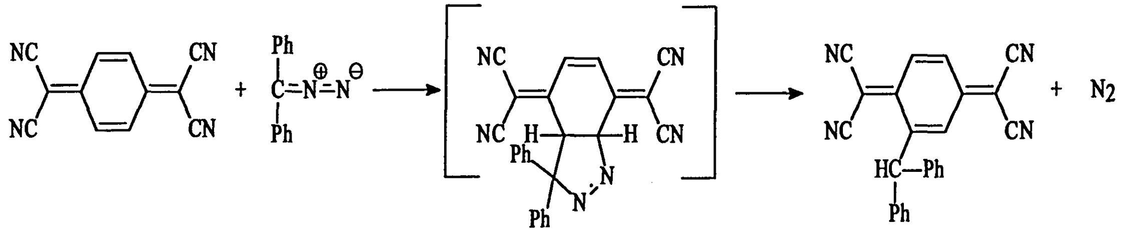

Figure 1.13 Ring Substitution of TCNQ.

The use of diazo-compounds to prepare substituted derivatives was never fully exploited despite the advantages of simplicity and effectiveness, and the use of TCNQ as starting material for the preparation of substituted derivatives was abandoned in favour of their synthesis by other means.

TCNQ itself was originally obtained[4] via a two step synthetic strategy, shown in Figure 1.14. In the first stage, malononitrile is condensed with 1,4-cyclohexanedione in benzene leading to a mixture of isomers (21) and (22). In aqueous media, a high yield of (21) is obtained directly from the reaction mixture.[83] The final stage involves the dehydrogenation of compound (21) - or a mixture of (21) and (22) - with reagents such as N-bromosuccinimide (NBS), bromine, selenium dioxide, or N-chlorosuccinimide (NCS). Best yields were obtained using bromine.

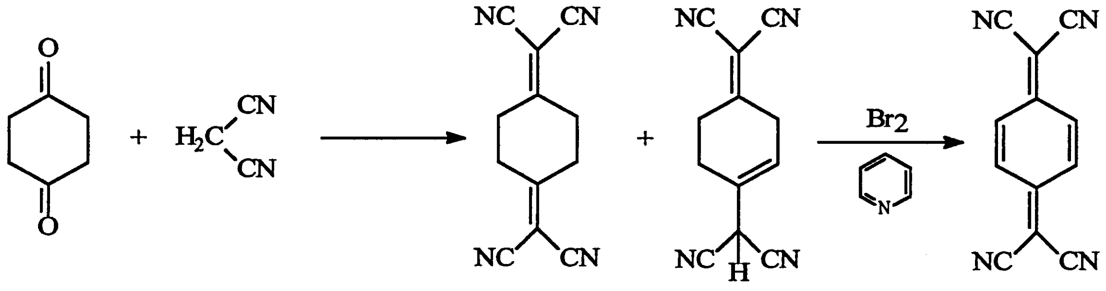

(21) (22) (23)

Figure 1.14 Original TCNQ Preparation.

The majority of the early substituted derivatives were obtained using similar procedures to that used for TCNQ (23) - for example, alkyl derivatives of TCNQ, i.e. 2-methyl-, 2-propyl-, and 2,5-dimethyl-TCNQ.[85] *Yamaguchi et al*[86] have extended the series to incorporate cyclobutane-fused derivatives of the type illustrated in Figure 1.15 which, like other alkyl derivatives, are generally weaker electron acceptors than TCNQ itself.[85]

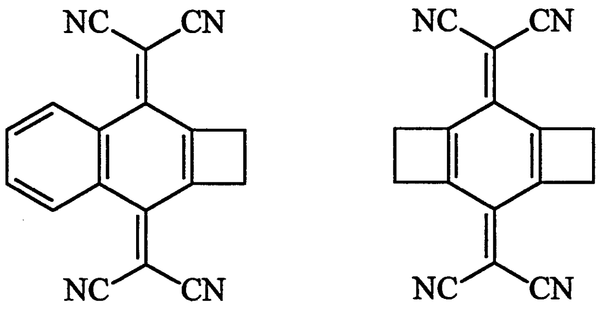
NC
CN
NC
CN
NC
CN
NC
CN

Figure 1.15 Yamaguchi's Tetra-substituted π-Acceptors.

The next significant development in the synthesis of TCNQ-derivatives came as a result of some excellent work by two researchers, *Robert C. Wheland* and *Elmore L. Martin*, at the du Pont Laboratories in Wilmington, U.S.A. This work published in 1975, showed that TCNQ-derivatives, which embodied both electron-withdrawing or -donating substituents, could be synthesised from simple substituted benzene compounds.[69] The synthetic strategy, which is illustrated in Figure 1.16, was very successful and could be applied to benzene derivatives embodying various functional groups ranging from halogens to ethers. This novel route resulted in twenty new TCNQ-based acceptors being demonstrated in the *Wheland* paper alone.[69] The method has been used by various other researchers to synthesise other TCNQ-derivatives - the powerful difluoro derivative ($TCNQF_2$)[87] and the relatively weak electron acceptor tetracyanodiphenoquinodimethane (TCNDQ),[88] for example.

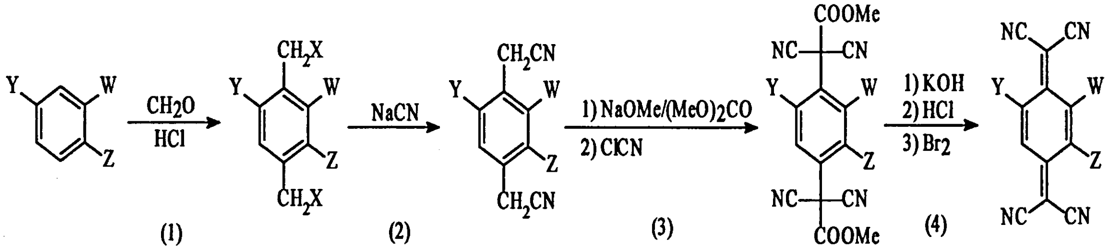
Y
W
Z
CH2O
HCl
(1)
CH2X
CH2X
NaCN
(2)
CH2CN
CH2CN
1) NaOMe/(MeO)2CO
2) ClCN
(3)
COOMe
NC
CN
COOMe
1) KOH
2) HCl
3) Br2
(4)
NC
CN

Figure 1.16 Wheland's Method of TCNQ preparation.

The Wheland and Martin method is not without its drawbacks and does suffer from some serious problems. The major problem is the hazardous nature of the reagents involved. Step 1 (Figure 1.16) involves the bischloromethylation of the appropriately substituted benzene compound with hydrogen chloride and formaldehyde which, when mixed at room temperature, may generate the potent carcinogens, chloromethyl methyl ether and bis (chloromethyl) ether.[88] The second and third steps also involve the use of highly toxic cyanide compounds. As a result an alternative methodology has been sought. The problematic third step, involving the use of cyanogen chloride has been addressed by introducing the second cyano group indirectly via conversion of the dicyano-p-xylene (24) into a bis-α-cyanoester (using base and dimethyl carbonate) followed by bis-demethoxylamination and dehydration of the resulting bisamide using either phosphorus pentachloride[89] or phosphorus oxychloride[85] (Figure 1.17)

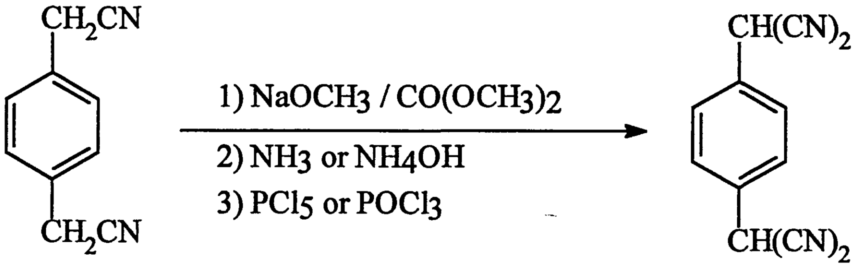

(24) (25)

Figure 1.17 Alternative to the Cyanogen Chloride Methodology for the Preparation of TCNQ Derivatives.

More recently, researchers at the Universities of Durham and Cranfield have shown that compounds such as 2-chlorobenzyl thiocyanate or arylselenocyanates are vastly superior to cyanogen chloride as a source of electrophilic cyanide for substituted-TCNQ synthesis.[89,90] 2-Chlorobenzyl thiocyanate is a non-toxic, shelf-stable liquid (Bpt 140^{0}C at 5 mm Hg) which can be prepared on a large scale with relative ease.[91]

Furthermore, unlike cyanogen chloride, 2-chlorobenzyl thiocyanate does not react with the phenylmalononitrile anion, so tricyanomethane products are not formed and hence there is no need to insert the ester groups and proceed via the scheme illustrated in Figure 1.16. Instead the phenylenedimalononitrile derivatives (25) are prepared in a one-pot procedure in 35-45% yields from di(cyanomethyl)benzenes (24) which can embody various electron-withdrawing or electron-donating substituents (Figure 1.18). These can then be oxidized to the TCNQ system as described previously.

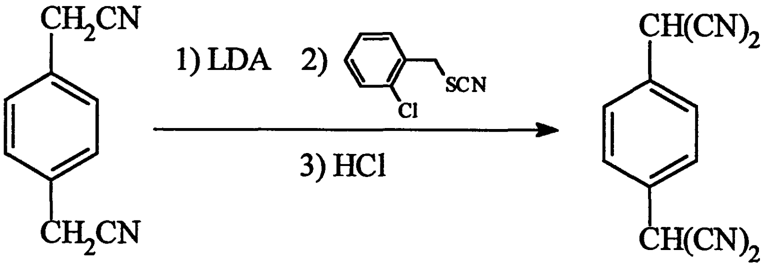

(24) (25)

Figure 1.18 Phenylenedimalononitrile Derivatives (25) via 2-Chlorobenzyl Thiocyanate.

Further simplification involved looking at key intermediates in the literature methods. It was clear that the major intermediate in substituted-TCNQ synthesis was phenylenedimalononitrile (25). If derivatives of compound (25) could be prepared in a single step from simple benzene derivatives, then the synthesis of substituted TCNQ derivatives could be limited to just two steps. Research groups in Japan[92] and Germany[93] have shown that substituted phenylenedimalononitrile derivatives can be obtained by copper (I)[92,93] or palladium (0 or II)[92] catalysed nucleophilic substitution reactions of diiodoarenes with malononitrile anions (Figure 1.19).

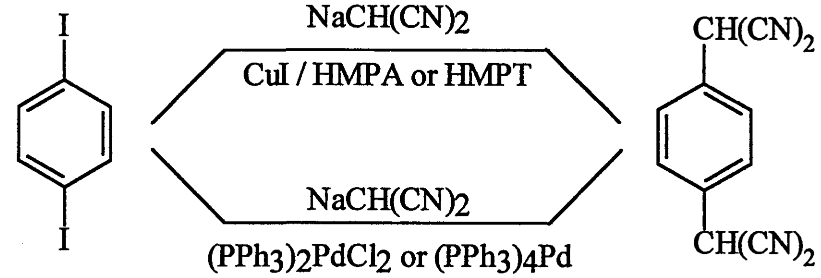

Figure 1.19 Metal-Catalysed Phenylenedimalononitrile Synthesis.

In the mid 1980's *Aumüller* and *Hünig*[94] showed that quinones could be directly bis(dicyanomethylated) in a single step using *Lehnert's* conditions (malononitrile, titanium (IV) chloride, pyridine),[95] as illustrated in Figure 1.20.

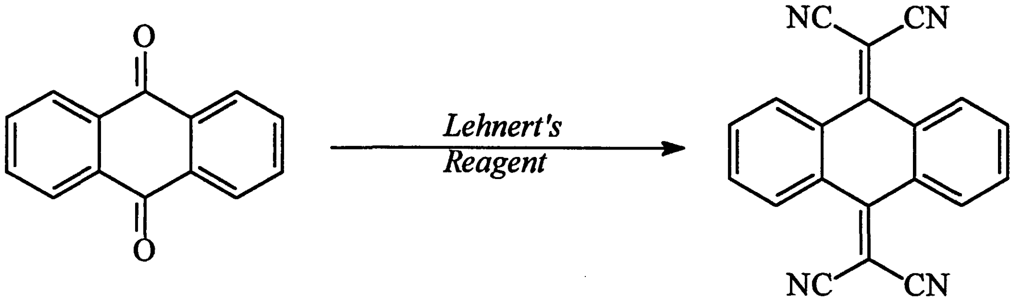

Figure 1.20 *Aumüller* and *Hünig*'s Modified *Lehnert* Procedure for Preparing TCNQ's.

However, the reaction can be capricious[96] and does not work with all quinones[97] (see Chapter 2). In general the reaction only seems applicable to tetra-substituted TCNQ derivatives,[98] though it has been successful in preparing a range of mono-, di-, tri- and tetra-substituted derivatives of the related DCNQI acceptor[99] Here, the reaction differs slightly from that used to prepare TCNQ derivatives, in that malononitrile is substituted for bis(trimethylsilyl)carbodiimide (BTC)[100] to enable the cyanoimine group to be introduced. Again as with the TCNQ reaction, preparation of the corresponding DCNQI compound requires the presence of titanium (IV) chloride since quinones do not yield quinodimethane or quinodiimines in the absence of this Lewis acid.[101]

Other methods have included that utilised by *Furuyama et al*[102] in which TCNQ is prepared in 80% yield by the single stage condensation of 1,4-cyclohexadiene with $(CN)_2CO$ or with phosgene in the presence of hydrogen cyanide or sodium cyanide. The methods described, are generally considered the more useful, and have been utilised to prepare a range of derivatives and not just individual examples. For a more comprehensive overview of TCNQ derivatives and their preparations the reader is referred to reviews by *Bespalov* and *Titov*,[83] *Grossel* and *Weston*,[31] *Kobayashi* and *Mazaki*[103] and the text by *Mártin et al*.[81]

1.5 Conducting Polymers.

Polymers have attracted extensive interest because of their perceived advantages such as processability, mechanical flexibility etc.

The first polymeric material to show conduction was the inorganic polymer poly(sulphur nitride) (26) which, in its polycrystalline form,[104] was found to be a semi-conductor. Subsequent research by *Walatka*[105] showed that single crystals of the polymer exhibited metal like conductivity ($\sigma_{rt} \approx 1730$ Scm^{-1}), and *Greene et al*[106] demonstrated that, when cooled to liquid helium temperatures, the polymer shows the onset of superconductivity. A wealth of new electrically conducting polymers is now documented in the literature - ranging from the simple hydrocarbon polymers polyacetylene (27) and poly (paraphenylene) (28) to the more elaborate polypyrrole (29) and polythiophene (30).

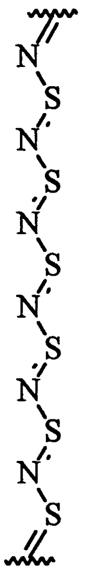

(26)

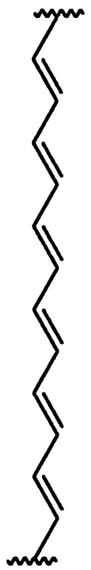

(27)

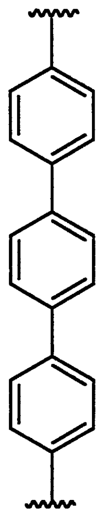

(28)

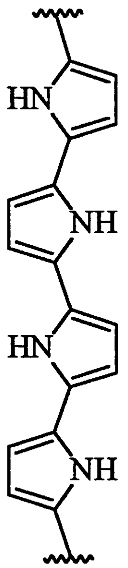

(29)

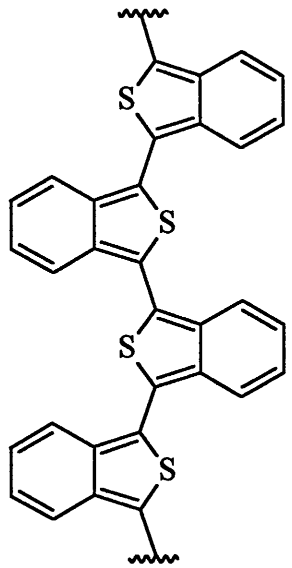

(30)

1.6 Structures and Nomenclature for the Donor-π-Acceptor Adducts Reported.

This report discusses the preparation and evaluation of a range of zwitterionic adducts prepared from quaternised N-heterocyclic donors and π-acceptors such as TCNQ. Adduct formation involves the creation of a new carbon to carbon double bond between the methyl carbon substituted on the donor N-heterocyclic ring and the dicyanomethanide carbon atom on the acceptor moiety. Formal loss of H^+ and HCN occurs during the preparation. A cipher nomenclature has been adopted to identify the various adducts. The ciphers are in two parts, first identifying the donor, then second the acceptor. So, the following:

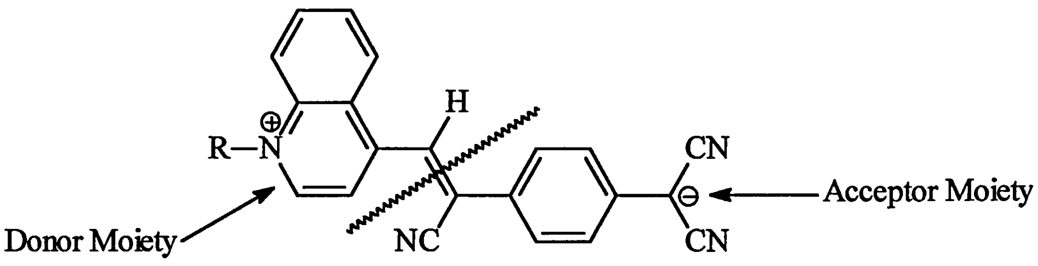

would have the cipher **R(4)Q3CNQ** where R(4)Q refers to the donor part ["R" identifies the quaternising alkyl group and "(4)Q" tells us that the heterocycle was 4-

methylquinolinium]. 3CNQ refers to the acceptor["3CN" tells us that 3 cyano groups remain, while "Q" at the end identifies TCNQ as the acceptor]. The donors used, with their letter ciphers, were

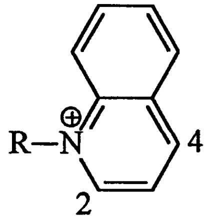

Quinolinium(Q)

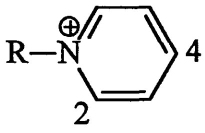

Picolinium(P)

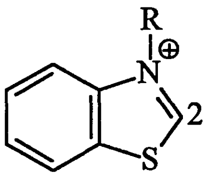

Benzothiazolium(BT)

The ciphers used for the symmetrical diquinolinium adducts were slightly different in that the m-C_8H_8 and p-C_8H_8 ciphers indicate the position of substitution on the bridging benzene ring between the two quaternised N-heterocyclic ring systems, i.e.

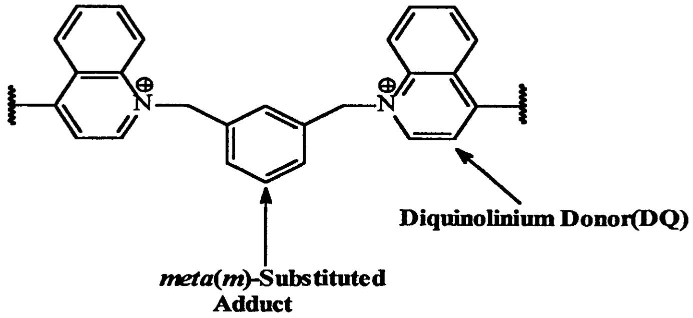
⊕
N
⊕
N
Diquinolinium Donor(DQ)
meta(m)-Substituted
Adduct

The acceptors used, with their ciphers, were

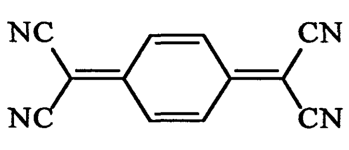

TCNQ(Q)

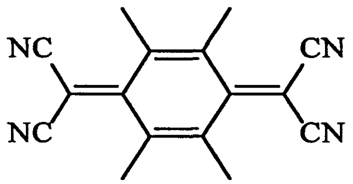

Tetramethyl-TCNQ(TMQ)

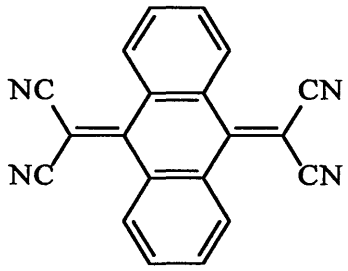

Tetracyano-Anthraquinodimethane(AQ)

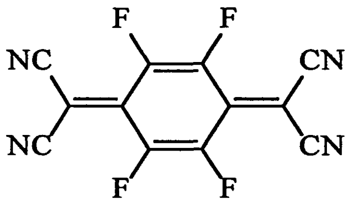
F
F
NC
NC
CN
CN
F
F

Tetrafluoro-TCNQ(QF 4)

1.7 Zwitterionic Donor-π-Acceptor TCNQ Systems.

Materials which consist of a donor part linked via an extended π-electron bridge to an acceptor part are not new to organic chemistry. Traditionally, such systems were used, due to their intense colours, as dyestuffs for colouring fabrics.[107] In more recent times D-π-A materials have found numerous other roles, ranging from the use of cyanines (31) and hemicyanines dyes (32) as spectral sensitisers in photography[108] to merocyanines (33) in the treatment of leukemic cancers.[109]

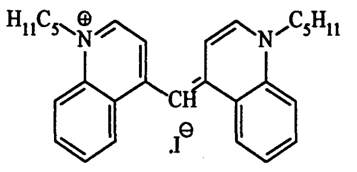

(31)

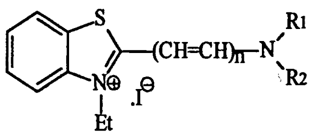

(32)

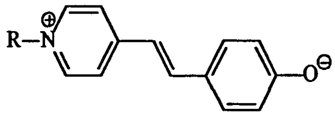

(33)

In the last few decades "push-pull" molecules have been the subject of renewed interest as candidate components of nonlinear optical (NLO) materials.[110] This area, traditionally dominated by inorganic materials, is discussed in more detail in Chapter 4.

In 1984[111] a new type of zwitterionic donor-π-acceptor material was found, when researchers at Sheffield Hallam University (formerly Sheffield City Polytechnic) synthesised: Z-β-(N-methyl-2-pyridinium)-α-cyano-styryldicyanomethanide (Figure 1.21) - trivial name picolyltricyanomethanide. Significantly the formation of the π-bridge C=C bond constituted a new type of reaction undertaken by TCNQ.

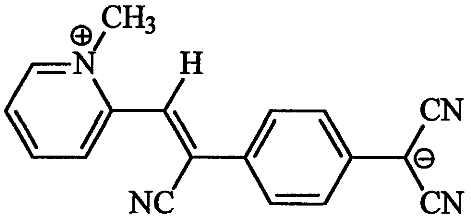

Figure 1.21 Picolyltricyanomethanide.

X-ray crystallographic characterisation of the adduct by *Metzger et al*[111] (Figure 1.22), demonstrated that C12 to C15 corresponded to a carbon-carbon double bond whilst the benzenoid nature of the two rings is also confirmed by bond length assessment.[111] The molecule was found to be non-planar with the pyridinium ring being twisted from the benzeniod TCNQ ring by 30.13^0. The UV/Vis spectrum of this material in acetonitrile, does not show the typical TCNQ band characteristic of the radical anion, rather a broad band centred on 592nm which is suggested to be due to an intramolecular charge-transfer transition.

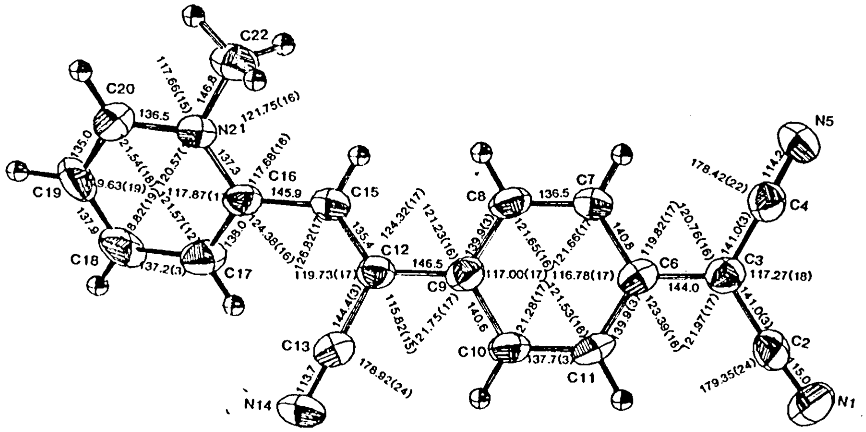
C22
C20
N21
136.5
146.8
121.75(16)
C16
145.9
C15
C19
135.0
137.9
C18
137.2(3)
C17
C12
146.5
119.73(17)
C9
117.00(17)
116.78(17)
C8
136.5
C7
C6
144.0
C3
117.27(18)
C4
N5
178.42(22)
C2
N1
179.35(24)
C13
N14
178.92(24)
C10
137.7(3)
C11

Figure 1.22 Crystal Structure of Picolyltricyanomethanide.[111]

Further evidence for its zwitterionic nature has been shown in subsequent atom-in-molecule calculations, which show the charge distribution of the molecule to be typical of a charge-separated species. The very large computed dipole moment of 26.16 D[111] also supports a zwitterionic structure, as does the observation of two distinct nitrile-stretching frequencies in the infrared spectrum, characteristic of a monosubstituted malononitrile anion. The adduct has also been studied in its solid state by polarised reflection spectroscopy,[112] in which an intermolecular charge-transfer transition was observed at 537nm. This results from head-to-tail stacking of the molecules (Figure 1.23) in the solid state.

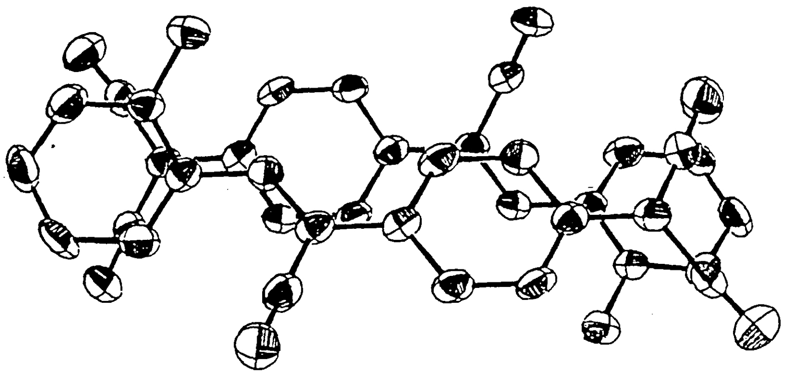

Figure 1.23 Overlap of Two Picolyltricyanomethanide Molecules Stacking along the b-axis.

Such a head-to-tail arrangement has been observed in other zwitterionic adducts, such as the D-σ-A compound formed between $TCNQF_4$ and N,N,N′,N′-tetramethyl-*p*-phenylenediamine (TMPD)[113](34). Another related example is the pyridyl substituted pyrazino-TCNQ derivative[114](35) in which the donor moiety is attached to the pyrazino ring in order to reduce the steric hindrance and degree of non-planarity.

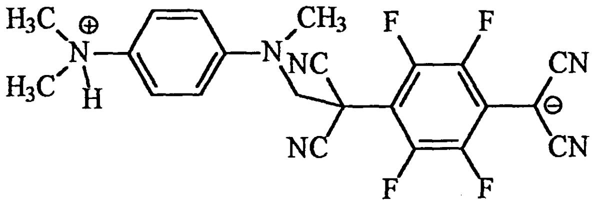

(34)

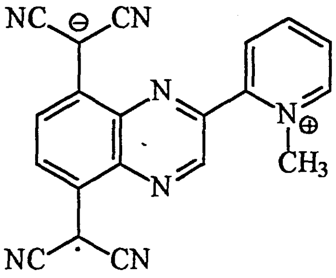

(35)

However, like the simple pyridinium-TCNQ complexes made by *Hertler et al*,[7] picolyltricyanomethanide is a very low conducting material and hence has relatively little appeal for incorporating into electronic devices.

The conduction mechanism in picolyltricyanomethanide is dependent upon the excitation of an electron from one ionic state to another. In this mechanism two conduction electrons are placed on the same TCNQ site:

$$\mathrm{TCNQ}^{\ominus}\,\mathrm{TCNQ}^{\ominus} \longrightarrow \mathrm{TCNQ}^{0}\,\mathrm{TCNQ}^{2\ominus}$$

Therefore, if the coulombic repulsion energy (U) between electrons on adjacent sites is considered the width of the band gap can be determined:

$$\mathbf{U = e^2 / 4\pi\varepsilon_o d} \qquad \text{Equation 1.2}$$

Where e = the unit of electronic charge

ε_o = the permittivity of free space

d = the charge separation measured in angstroms (Å)

Thus for two electrons:-

$$\mathbf{U = 14.4eV / d} \qquad \text{Equation 1.3}$$

The conduction pathway itself can be represented schematically (Figure 1.24) by considering the dicyanomethanide end of the charge-transfer compound.

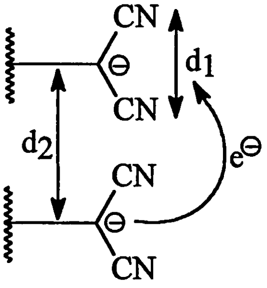

Figure 1.24 Proposed Intermolecular Conduction Pathway.

If such conduction is to occur as shown, then an electron would move from one acceptor unit to the next adjacent acceptor, resulting in two conduction electrons located on the same TCNQ site creating a vacant hole below for further conduction to occur. It has been shown from X-ray crystallography that the distance **d_1** (5.5Å) is smaller than the distance **d_2** (9.0Å).[115] Thus two electrons occupying the same site will have a greater repulsion energy **Ed_1** (2.6 eV) than if the electrons were on adjacent sites (**Ed_2** = 1.6 eV).[115] So the electrical conductivity of such a simple complex is low (pyridinium-TCNQ salts $\sigma_{rt} = 10^{-6}$ to 10^{-8} Scm^{-1}),[6] as placing two electrons on the same TCNQ site is energetically unfavourable.

Nevertheless, despite the low conductivity exhibited by picolyltricyanomethanide, the characterisation by *Metzger et al*[111,112] clearly showed that the structure displayed scope for synthetic manipulation of the core framework and, to that end, various analogues have been synthesised. Initial work concentrated upon long chain γ-(36) and α-(37) substituted pyridinium adducts such as those illustrated in Figure 1.25.

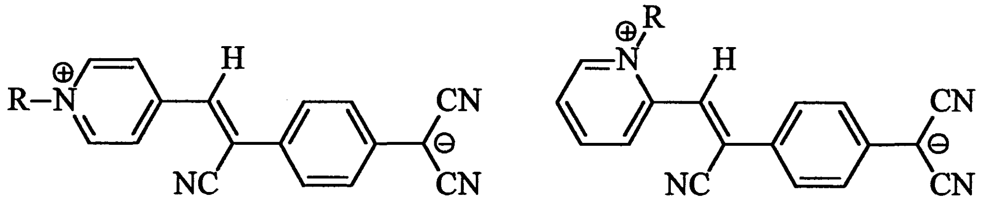

(36) (37)

Figure 1.25 Initially Studied R(4)P3CNQ (36) and R(2)P3CNQ (37) Type Adducts.

Like picolyltricyanomethanide, these materials formed a centrosymmetric head-to-tail arrangement in the solid state. Further work has synthesised and characterised quinolinium derivatives of the type shown in Figure 1.26.

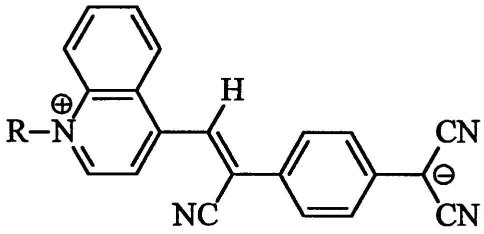

Figure 1.26 R(4)Q3CNQ Type Adducts.

As a result of extensive research into these quinolinium-based compounds, several interesting features were noted. For instance the Langmuir-Blodgett (LB) film properties shown by the R(4)Q3CNQ compounds are dependent upon the hydrophobic chain length, for n ≥16 the films are purple (λ_{max} = 563±5 nm) and the second harmonic generation (SHG) is similar to that obtained from corresponding films of hemicyanine halides.[115-118] For n ≤15 the films are turquoise (λ_{max} = 614±5 nm) and the SHG is very weak. The reason for this shift is attributed to a change in molecular tilt within the films which causes the charge-transfer transition, observed in such materials, to alter from an intermolecular to an intramolecular process, a phenomenon that is discussed in greater detail in Chapter 5.

Other properties were noted. For instance, the adducts also show unimolecular electrical rectification,[117,119,120] when sandwiched between metal electrodes, as well and photo-[121] and solvatochromism.[115,116,118] These observations prompted the synthesis of other zwitterionic TCNQ-based D-π-A systems. These ranged from the fairly simple α-substituted quinolinium adducts (38)[122,123] to the more elaborate benzothiazolium (39)[124] and pyridazine (40) based systems,[125] which, like the R(4)Q3CNQ compounds all, show significant nonlinear optical behaviour.

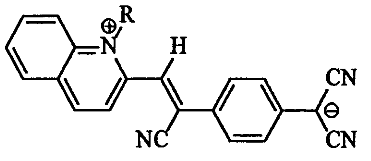

(38)

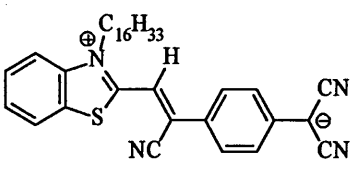

(39)

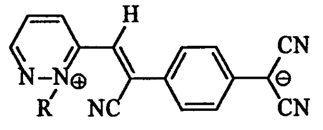

(40)

More recently another type of TCNQ-based zwitterion was synthesised by *Szablewski*:[126] the Z-β-[(N,N-diethylmethylimmonium)-α-cyano-4-styryldicyano-methanide] DEMI compound (41) via the reaction of triethylamine (TEA) with TCNQ (Figure 1.27). The reaction is unusual as tertiary amines in general are not expected to react with TCNQ because they do not possess an amino hydrogen which could be abstracted to produce the 1,6-addition intermediate. It is thought however that in the above reaction TCNQ abstracts hydrogen (H_2) from the tertiary amine to yield an enamine and dihydro-TCNQ. The enamine then attacks the TCNQ in a Stork-enamine manner, with subsequent elimination of HCN yielding the DEMI zwitterion (41).

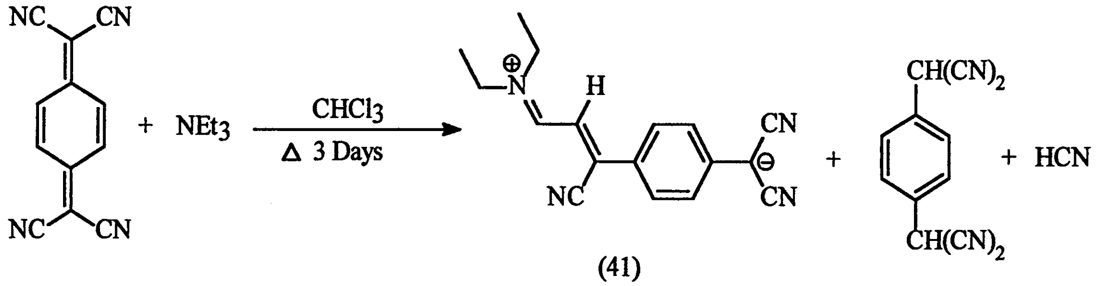

(41)

Figure 1.27 Novel TCNQ-based Zwitterions via Stork-enamine Reactions.

This novel Stork-enamine reaction has been used with various tertiary ethyl amines, to afford a range of DEMI-type zwitterions (42-44).[127] The spectral properties of these are very similar, consisting of a broad charge-transfer band in the middle of the visible region. The low optical absorption between 450 and 470nm has earned them the title of "blue-window" materials and makes them excellent candidates for frequency doubling applications.

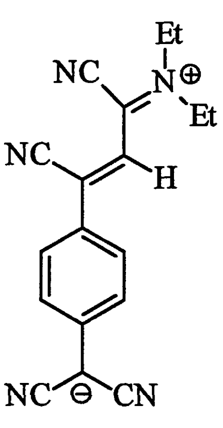
(42)

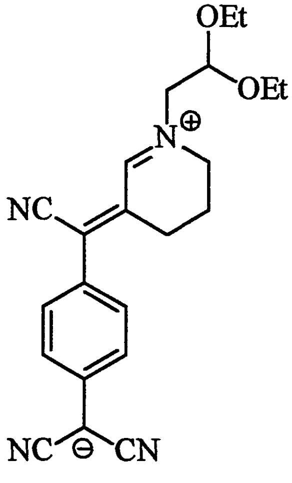
(43)

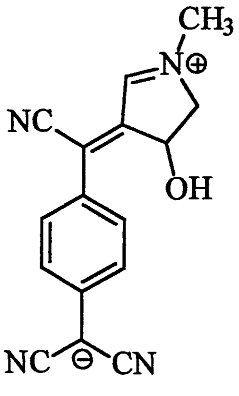
(44)

The majority of structural alterations investigated have been associated with the donor part of the molecule. Despite the numerous TCNQ derivatives that are currently available, very few have been incorporated into zwitterionic type structures.[116,118,127] If different electron acceptors were to be incorporated into the structures, then the properties observed in such compounds could, perhaps, be further tuned through careful choice of substituents.

Of the zwitterionic TCNQ-based compounds that have appeared in the literature,[116,118,127] all incorporate electronegative substituents in the TCNQ ring system e.g. fluorine ($TCNQF_4$),[116,118] or bromine ($TCNQBr_2$).[116] Research into the properties exhibited by such derivatives is limited. For example, unlike the unsubstituted R(4)Q3CNQ[115,116,118] and R(2)Q3CNQ[122,123] compounds, no chain length dependency or geometric studies have been attempted. The aim of this work was to look at these properties.

The main emphasis was strongly towards the use of substituted TCNQ acceptors, ranging from the fluorinated derivative $TCNQF_4$, to the relatively weak electron acceptor 2,3,5,6-tetramethyl-7,7,8,8-tetracyano-p-quinodimethane (TMTCNQ). The LB film-forming properties of such adducts would be studied to see if there was a similar chain length dependency to that found for the R(4)Q3CNQ compounds. Additionally the effect of the electropositive and electronegative substituents upon the linear and nonlinear optical properties could also be studied. The synthesis of various adducts, along with the subsequent characterisation by techniques such as UV/Vis spectroscopy and Langmuir-Blodgett film studies etc, are repeated in the forthcoming chapters.

1.8 References.

1. H. N. McCoy and W. C. Moore, *J. Am. Chem. Soc.*, 1911, **33**, 273.
2. H. Akamatsu, H. Inokuchi and Y. Matsunaga, *Nature*, 1954, **173**, 168.
3. H. Kraus, *J. Am. Chem. Soc.*, 1913, **34**, 1732.
4. (a) D. S. Acker and D. C. Blomstrom, *U.S.Patent No 3,115,506* (1963). (b) D .S. Acker and W. R. Hertler, *J. Am. Chem. Soc.*, 1962, **84**, 3370.
5. D. S. Acker, R. J. Harder, W. R. Hertler, W. Mahler, L. R. Melby, R. E. Benson and W. E. Mochel, *J. Am. Chem. Soc.*, 1960, **82**, 6403.
6. L. R. Melby, R. J. Harder, W. R. Hertler, W. Mahler, R. E. Benson and W. E. Mochel, *J. Am. Chem. Soc.*, 1962, **84**, 3374.
7. W. R. Hertler, H. D. Hartzler, D. S. Acker and R. E. Benson, *J. Am. Chem. Soc.*, 1962, **84**, 3387.
8. W. R. Hertler and R. E. Benson, *J. Am. Chem. Soc.*, 1962, **84**, 3474.
9. J. K. Williams, *J. Am. Chem. Soc.*, 1962, **84**, 3478.
10. W. R. Hertler, W. Mahler, L. R. Melby, J. S. Miller, R. E. Putscher and O. W. Webster, *Mol. Cryst. Liq. Cryst.*, 1989, **171**, 205.
11. R. S. Potember, T. O. Poehler, A. Rappa, D. O. Cowan and A. N. Bloch, *Synth. Met.*, 1982, **4**, 371.

12. T. Sugimoto, K. Ueda, N. Kanehisa, Y. Kai, M. Shiro, N. Hosoito, N. Takeda and M. Ishikawa, *ACS Aymposium Series*, 1996, **644**, 276.
13. (a) T. L. Cairns, R. A. Carboni, D. D. Coffmann, V. A. Englehardt, R. E. Herkert, E. L. Little, E. G. McGeer, B. C. McKusick and W. J. Middleton, *J. Am. Chem. Soc.*, 1957, **79**, 2340. (b) R. E. Heckert and E. L. Little, *U.S.Patent No. 2,794,824* (1957). (c) R. E. Heckert, *U.S.Patent No. 2,794,823* (1957).
14. T. L. Cairns, R. A. Carboni, D. D. Coffmann, V. A. Englehardt, R. E. Herkert, E. L. Little, E. G. McGeer, B. C. McKusick, R. E. Merrifield, W. J. Middleton, H. F. Mower, W. D. Philips, G. N. Sausen, R. M. Scribner, C. M. Theobald and H. E. Winberg, *J. Am. Chem. Soc.*, 1958, **80**, 2775, plus ten other publications-Cyanocarbon Chemistry II - XI, *J. Am. Chem. Soc.*, 1958, **80**, 2778-2846.
15. I. F. Shegolev, *Phys. Stat. Sol.*, (A), 1972, **12**, 9.
16. F. Wudl, G. M. Smith and E. J. Hufnagel, *J. Chem. Soc., Chem. Commun.*, 1970, 1453.
17. J. Ferraris, D. O. Cowan, V. V. Walatka and J. M. Perlstein, *J. Am. Chem. Soc.*, 1973, **95**, 948.
18. (a) H. Fröhlich, *Proc. Roy. Soc. Ser. A*, 1954, **223**, 296. (b) J-Q. Liang, F. Peng and X. X. Ding, *Phys. Lett. A*, 1995, **201**, 369.
19. R. E. Peierls, *Quantum Theory of Solids*, Oxford University Press, 1955.
20. H. A. Benisi and J. H. Hildenbrand, *J. Am. Chem. Soc.*, 1949, **71**, 2703.
21. R. S. Mulliken, *J. Am. Chem. Soc.*, 1950, **72**, 600.
22. R. S. Mulliken, *J. Am. Chem. Soc.*, 1950, **74**, 811.
23. R. S. Mulliken and W. B. Person, *Molecular Complexes*- A lecture and reprint volume, J. Wiley and Sons Inc., London, 1969.
24. T. E. Phillips, T. J. Kistenmacher, J. P. Ferraris and D. O. Cowan, *J. Am. Chem. Soc.*, 1973, **95**, 471.

25. M. J. Cohen, L. B. Coleman, A. F. Garito and A. J. Heeger, *Phys. Rev. B*, 1974, **10**, 1298.
26. S. K. Khanna, A. F. Garito, A. J. Heeger and R. C. Taklevic, *Solid State Commun.*, 1975, **16**, 667.
27. R. P. Groff, A. Suna and R. E. Merrifield, *Phys. Rev. Lett.*, 1974, **33**, 418.
28. R. C. Wheland, *J. Am. Chem. Soc.*, 1976, **98**, 3926.
29. D. O. Cowan, A. Kini, L-Y. Chiang, K. Lerstrup, D. R. Talham, T. O. Poehler and A. N. Bloch, *Mol. Cryst. Liq. Cryst.*, 1982, **86**, 1.
30. D. Cowan, P. Shu, C. Hu, W. Krug, T. Carruthers, T. Poehler and A. Bloch, *Chemistry and Physics of One-Dimensional Metals*, Plenum Press, New York, 1977.
31. M. C. Grossel and S. C. Weston, *Contemporary Organic Synthesis*, 1994, **1**, 367.
32. M. R. Bryce, *J. Mater. Chem.*, 1995, **5**, 1481.
33. J. B. Torrance, *Acc. Chem. Res.*, 1979, **12**, 79.
34. M. R. Bryce and A. J. Moore, *Tetrahedron Lett.*, 1988, **29**, 1075.
35. Proceedings of the International Conference on Science and Technology of Synthetic Metals, Santa Fe 1988 (ICSM 88), published in *Synth. Met.*, 1988, 27-29.
36. R. L. Greene, J. J. Mayerle, R. Schumaker, G. Castro, P. M. Chaikin, E. Etemad and S. J. Laplaca, *Solid State Commun.*, 1976, **20**, 943.
37. Y. Ueno, A. Nakayama and M. Okawara, *J. Chem. Soc., Chem. Commun.*, 1978, 74.
38. F. Wudl and E. Aharon-Shalom, *J. Am. Chem. Soc.*, 1982, **104**, 1154.
39. J. B. Torrance, J. J. Mayerle, K. Bechgaard, B. D. Silverman and Y. Tomkiewicz, *Phys. Rev. B*, 1980, **22**, 4960.
40. Z. S. Li, S. Matsuzaki, M. Onomichi and M. Sano, *Synth. Met.*, 1986, **16**, 71.
41. J. Pouget, M. D. Mays and D. O. Cowan, *J. Mater. Chem.*, 1995, **5**, 1629.

42. J. B. Torrance, J. J. Mayerle, K. Bechgaard, B. D. Silverman and Y. Tomkiewicz, *Phys. Rev. B*, 1980, **22**, 4960.

43. T. Jorgsensen, T. K. Hansen and J. Becker, *Chem. Soc. Rev.*, 1994, **23**, 41.

44. M. R. Bryce, A. J. Moore, D. Lorcy, A. S. Dhindsa and A. Robert, *J. Chem. Soc., Chem. Commun.*, 1990, 471.

45. K. Takahashi, T. Shirahata and K. Tomitani, *J. Mater. Chem.*, 1997, **8**, 2375.

46. M. R. Bryce, M. A. Coffin and W. Clegg, *J. Org. Chem.*, 1992, **57**, 1696.

47. A. Moradpour, *J. Chem. Soc., Perkin. Trans. I*, 1993, 7.

48. P. J. Alonso, J. Garin, J. Orduna, S. Uriel and J. M. Fabre, *Synth. Met.*, 1993, 55-57, 2169.

49. C. Weng, J. Y. Becker, J. Bernstein, A. Ellern and V. Khodorkovsky, *J. Mater. Chem.*, 1995, **5**, 1559.

50. Y. Yamashita and M. Tomura, *J. Mater. Chem.*, 1998, **8**, 1933.

51. K. Takimiya, A. Morikami, Y. Aso and T. Otsubo, *J. Chem. Soc., Chem. Commun.*, 1997, 1925.

52. H. K. Onnes, *Comm. Phys. Lab. Leiden.*, 1911, Nos. 119, 120, 122.

53. C. S. Jacobsen, K. Mortensen, J. R. Anderson and K. Bechgaard, *Phys. Rev. B*, **18**, 1978, 905.

54. D. Jérome, *Phys. Bull.*, 1986, 37.

55. A. Andrieux, C. Dorouré, D. Jérome and K. Bechgaard, *J. Phys. Paris. Lett.*, 1979, **40**, L381.

56. D. Jérome, *Phil. Trans. Roy. Soc.*, A, 1985, **314**, 69.

57. K. Bechgaard, C. S. Jacobsen, K. Mortensen, H. J. Pedersen, N. Thorup, *Solid State Commun.*, 1980, **38**, 1119.

58. J. Bardeen, L. N. Cooper and J. R. Schieffer, *Phys. Rev.*, 1957, **108**, 1175.

59. K. Bechgaard and D. Jérome, *Sci. Am.*, 1982, **247**, 50.

60. S. S. P. Parkin,, E. M. Engler, R. R. Schumaker, R. Lagier, V. Y. Lee, J. C. Scott and R. L. Greene, *Phys. Rev. Lett.*, 1983, **50**, 270.

61. G. W. Crabtree, K. D. Carlson, L. N. Hall, P. T. Copps, H. H. Wang, T. J. Emge, M. A. Beno and J. M. Williams, *Phys. Rev. B*, 1984, **30**, 2958.

62. J. M. Williams, A. M. Kini, H. H. Wang, K. D. Carlson, U. Geiser, L. K. Montgomery, G. J. Pyrka, D. M. Watkins, J. M. Kommers, S. J. Boryschuk, A. V. Strieby-Crouch, W. K. Kwok, J. E. Schirber, D. L. Overmyer, D. Jung and M-H. Whangbo, *Inorg. Chem.*, 1990, **29**, 3262.

63. J. M. Williams, J. R. Ferraro, R. J. Thorn, K. D. Carlson, U. Geiser, H. H. Wang, A. M. Kini and M-H. Whangbo, *Organic Superconductors*, Prentice Hall, Englewood Cliffs, 1992, 400.

64. E. Demiralp and W.A. Goddard III, *Synth. Met.*, 1995, **72**, 297.

65. R. Kato, K. Yamamoto, Y. Okano, H. Tajima and H. Sawa, *J. Chem. Soc., Chem. Commun.*, 1997, 947.

66. K. Tanigaki, T. W. Ebbessen, S. Saito, J. Mizuli, J. S. Tsai, Y. Kubo and S. Kuroshima, *Nature*, 1991, **352**, 222.

67. H. Mori, *Int. J. Mod. Phys.*, B, 1994, **1-2**, 1.

68. D. Jérome, *Solid State Commun.*, 1994, **92**, 89.

69. R. C. Wheland and E. L. Martin, *J. Org. Chem.*, 1975, **40**, 3101.

70. N. Acton, D. Huo, J. Schwarz and T. J. Katz, *J. Org. Chem.*, 1982, **47**, 1011.

71. Y. Yamashita, T. Suzuki, T. Mukai and G. Saito, *J. Chem. Soc., Chem. Commun.*, 1985, 1044.

72. S. Iwatsuki, M. Kubo and H. Iwase, *Chem. Lett.*, 1993, 517.

73. L. Bucsis and K. Friedrich, *Chem. Ber.*, 1976, **109**, 2469.

74. C. Vazquez, J. C. Calabrese, D. A. Dixon and J. S. Miller, *J. Org. Chem.*, 1993, **58**, 65.

75. J. Thiele and F. Gunther, *Justus. Liebigs. Ann. Chem.*, 1906, **349**, 45.

76. (a) W. P. Roberts and C. L. Ebner, *J. Org. Chem.*, 1987, **52**, 2297. (b) R. C. Wheland and J. L. Gillson, *J. Am. Chem. Soc.*, 1976, **98**, 3916.

77. (a) S. Hünig and P. Erk, *Adv. Mater.*, 1991, 225. (b) S. Hünig, *J. Mater. Chem.*, 1995, **5**, 1469.

78. (a) M. R. Bryce and S. R. Davies, *J. Chem. Soc., Chem. Commun.*, 1989, 329. (b) S. Iwatsuli, T. Itoh and H. Itoh, *Chem. Lett.*, 1988, 1187.

79. G. Seitz, R. Sutrisno, B. Geracht, G. Offermann, R. Schmidt and W. Massa, *Angew. Chem.*, 1982, **21**, 285.

80. J. S. Miller, D. A. Dixon, J. C. Calabrese, C. Vazquez, P. J. Krusic, M. D. Ward, E. Wasserman and R. L. Harlow, *J. Am. Chem. Soc.*, 1990, **112**, 381.

81. N. Martin, J. L. Segura and C. Seoane, *J. Mater. Chem.*, 1997, **7**, 1661.

82. G. Saito, T. Teramoto, A. Otsuka, Y. Sugita, T. Ban, M. Kusunoki and K. Sakaguchi, *Synth. Met.*, 1994, **64**, 359.

83. B. P. Bespalov and V. V. Titov, *Russ. Chem. Rev.*, 1975, **44**, 1091.

84. H. D. Hartzler, *J. Org. Chem.*, 1965, **30**, 2456.

85. J. Diekmann, W. R. Hertler and R. E. Benson, *J. Org. Chem.*, 1963, **28**, 2719.

86. S. Yamaguchi, H. Tatemitsu, Y. Sakata, T. Enoki and S. Misumi, *J. Chem. Soc., Chem. Commun.*, 1982, 1065.

87. A. W. Addison, N. S. Dalal, Y. Hoyano, S. Huizinga and L. Weiler, *Can. J. Chem.*, 1977, **55**, 4191.

88. Fed. Regist., 1974, 39, Part III, Department of Labour, Occupational Safety and Health Administration, Carcinogens, Occupational Health and Safety Standards.

89. (a) J. C. Hessler, *J. Am. Chem. Soc.*, 1904, **32**, 119. (b) W. A. Davis and M. P.Cava, *J. Org. Chem.*, 1983, **48**, 2774.

90. (a) M. R. Bryce, M. Hasan and G. J. Ashwell, *J. Chem. Soc., Chem. Commun.*, 1989, 529. (b) M. R. Bryce, A. M. Grainger, M. Hasan, G. J. Ashwell, M. A. Bates and M. Hursthouse, *J. Chem. Soc., Perkin Trans. I*, 1992, 611.

91. A. H. Schlesinger and D. T. Mowry, *J. Am. Chem. Soc.*, 1954, **76**, 585.

92. (a) M. Uno, K. Seto, M. Masuda, W. Ueda and S. Takahashi, *Tetrahedron Lett.*, 1985, **26**, 1553. (b) H. Suzuki, T. Kobayashi and A. Osuka, *Chem. Lett.*, 1983, 589.

93. B. Rosenau, C. Krieger and H. A. Staab, *Tetrahedron Lett.*, 1985, **26**, 2081.

94. A. Aumüller and S. Hünig, *Liebigs. Ann. Chem.*, 1984, 618.

95. (a) W. Lehnert, *Tetrahedron Lett.*, 1970, **54**, 4723. (b) W. Lehnert, *Synthesis*, 1974, 667 and references within.

96. M. R. Bryce, S. R. Davies, A. M. Grainger, J. Hellburg, M. B. Hursthouse, M. Mazid, R. Bachmann and F. Gerson, *J. Org. Chem.*, 1992, **57**, 1690.

97. (a) J. Y. Becker, J. Bernstein, S. Bittner, E. Harlev, and J. A. R. P. Sarma, *J. Chem. Soc., Perkin. Trans. II*, 1989, 1157. (b) T. Czekanski, M. Hanack, J. Y. Becker, J. Bernstein, S. Bittner, L. Kaufman-Orenstein and D. Peleg, *J. Org. Chem.*, 1991, **56**, 1569.

98. (a) K. Kobayashi and C.L Gajurel, *J. Chem. Soc., Chem. Commun.*, 1986, 1779. (b) Y. Yamashita, T.Suzuki, T. Mukai and G. Saito, *J. Chem. Soc., Chem. Commun.*, 1985, 1044. (c) P. Bando, K. Davidkov, N. Martín, J. L. Segura, C. Seoane, A. González and J. M. Pingarrón, *Synth. Met.*, 1993, **55-57**, 1726.

99. A. Aumüller and S. Hünig, *Liebigs. Ann. Chem.*, 1986, 165.

100. L. Birkofer, *Tetrahedron Lett.*, 1962, 195.

101. A. Fatiadi, *Synthesis*, 1978, 165.

102. T. Furuyama, *Japanese Patent. P.7410 666*, 1974; Chem Abs., 1974, **73**, 25200a.

103. K. Kobayashi and Y. Mazaki, *J. Synth. Org. Chem. (Jpn).*, 1988, **46**, 638.

104. D. Chapman, R. J. Wam, A. G. Fitzgerald and A. D. Yoffe, *Trans. Faraday Soc.*, 1964, **60**, 294.

105. V. V. Walakta, *Phys. Rev. Lett.*, 1973, **31**, 1139.

106. R. L. Greene, G. B. Street and L. J. Suter, *Phys. Rev. Lett.*, 1975, **34**, 577.

107. C. H. G. Williams, *Trans. R. Soc. Edinburgh.*, 1856, **21**, 377.

108. T. H. James, *The Theory of Photographic Processes*, 4th edn, MacMillan Publishing, New York, 1977.

109. F. Sieber, L. O. Spivak and A. Sutcliffe, *Proc. Natl. Acad. Sci. USA.*, 1984, **81**, 7584.

110. D. S. Chemla and J. Zyss, *Nonlinear Optical Properties of Organic Molecules and Crystals*, Volume 1, Academic Press Inc., London, 1987.

111. R. M. Metzger, N. E. Heimer and G. J. Ashwell, *Mol. Cryst. Liq. Cryst.*, 1984, **107**, 133.

112. S. Akhtar, J. Tanaka, R. M. Metzger and G. J .Ashwell., *Mol. Cryst. Liq. Cryst.*, 1986, **139**, 353.

113. J. S. Miller and J. C. Calabrese, *J. Chem. Soc., Chem. Commun.*, 1988, 63.

114. Y. Tsubata, T. Suzuki, T. Miyashi and Y. Yamashita, *J. Org. Chem.*, 1992, **57**, 6749.

115. R. A. Broughton, PhD Thesis, *Sheffield Hallam University*, 1993.

116. (a) G. J. Ashwell, E. J. C. Dawnay, A. P. Kuczyñski, M. Szablewski, I. M. Sandy, M. R. Bryce, A. M. Grainger and M. Hasan, *J. Chem. Soc., Faraday Trans.*, 1990, **86**, 1117. (b) G. J. Ashwell, G. Jefferies, E. J. C. Dawnay, A. P. Kuczyñski, D. E. Lynch, Y. Gongda and D. G. Bucknall, *J. Mater. Chem.*, 1995, **5**, 975. (c) N. A. Bell, R. A. Broughton, J. S. Brooks, T. A. Jones and S. C. Thorpe, *Int. J. Electronics*, 1994, **76**, 751.

117. R. M. Metzger, B. Chen, U. Höpfner, M. V. Lakshmikantham, D. Vuillaume, T.

Kawai, X. Wu, H. Tachibana, T. V. Hughes, H. Sakurai, J. W. Baldwin, C. Hosch, M. P. Cava, L. Brehmer and G. J. Ashwell, *J. Am. Chem. Soc.*, 1997, **119**, 10455.

118. M. Szablewski, PhD Thesis, *Cranfield Institute of Technology*, 1991.

119. (a) A. Aviram and M. A. Ratner, *Bull. Am. Phys. Soc.*, 1974, **19**, 341. (b) A. Aviram and M. A. Ratner, *Chem. Phys. Lett.*, 1974, **29**, 277.

120. G. J. Ashwell, J. R. Sambles, A. S. Martin, W. G. Parker and M. Szablewski, *J. Chem. Soc., Chem. Commun.*, 1990, 1374.

121. H. Heller, *IIE. Proc.*, 1983, **130**, 209.

122. C. S. Bradley, PhD Thesis, *Sheffield Hallam University*, 1999.

123. G. J. Ashwell, *Thin Solid Films*, 1990, **186**, 155.

124. G. J. Ashwell, M. Malhotra, M. R. Bryce and A. M. Grainger, *Synth. Met.*, 1991, **41-43**, 3173.

125. C. S. Bradley, *Personal Communication.*

126. M. Szablewski, *J. Org. Chem.*, 1994, 59, 954.

127. M. Szablewski, P. R. Thomas, A. Thornton, D. Bloor, G. H. Cross, J. M. Cole, J. A. K.Howard, M. Malagoli, F. Meyers, J-L. Brédas, W. Wenseleers and E. Goovaerts, *J. Am. Chem. Soc.*, 1997, **119**, 3144.

Chapter 2: Synthesis.

2.1 Synthetic and Instrumental Techniques.

Experimental.

Reagents.

All reagents were purchased from Aldrich-Sigma Chemical Company Limited and were not further purified prior to use.

Solvents.

All solvents used were purchased from Aldrich-Sigma Chemical Company Limited and dried using standard literature methods.[1]

Synthetic Procedures.

All synthetic procedures were carried out in a fume cupboard due to the extremely hazardous nature of some of the compounds involved.

Microanalysis.

Microanalytical data were obtained from the Micro-Analytical Service of the Centre for Chemical Instrumental Analysis Services, University of Sheffield and from Medac Limited at Brunel University.

Instrumentation.

Infrared Spectroscopy.

Infrared spectra were recorded from 4000 cm^{-1} to 500 cm^{-1}, using both Nujol and KBr sample preparation techniques, using an ATI Mattson Genesis series FTIR instrument.

Ultraviolet/Visible (UV/Vis) Spectroscopy.

UV/Vis spectra were recorded using a Hitachi U-2000 Spectrophotometer in the range 210-1100 nm, using a 1 cm path length quartz cell.

Mass Spectrometry.

Mass spectra were recorded using a VG Micromass 7070F mass spectrometer using EI/FAB modes of ionisation. A direct insertion probe was used. Accurate FAB and electrospray mass spectra were obtained courtesy of the analytical services of the University of Sheffield.

^{1}H, ^{13}C and ^{19}F NMR Spectroscopy.

^{1}H and ^{13}C NMR spectra were recorded using a Bruker AC250 NMR spectrometer. Samples were dissolved in various deuterated solvents depending on their relative solubilities. ^{19}F NMR spectra were obtained courtesy of the University of Sheffield. Coupling constant (J) values where illustrated are given in Hertz (Hz)

Differential Scanning Calorimetry (DSC).

DSC measurements were carried out on a Mettler Toledo TA8000 Thermal Analysis System (DSC30S/Ceramic sensor method) in a dynamic nitrogen atmosphere using an aluminium 40 μl crucible. Scans were made over the range 30^{0}C to 500^{0}C at a rate of 5-10^{0}C min^{-1}.

Thermogravimetric Analysis (TGA).

TGA measurements were carried out on a Mettler Toledo TA8000 Thermal Analysis System (TG50/M3 method) in a dynamic nitrogen atmosphere using an aluminium 70 μl crucible. Scans were made over the range 30^{0}C to 500^{0}C at a rate of 5-10^{0}C min^{-1}.

2.2 Synthesis of Electron Donors.

2.2.1 N-Alkyl-4-methylquinolinium Bromides.[2-4]

Equation:

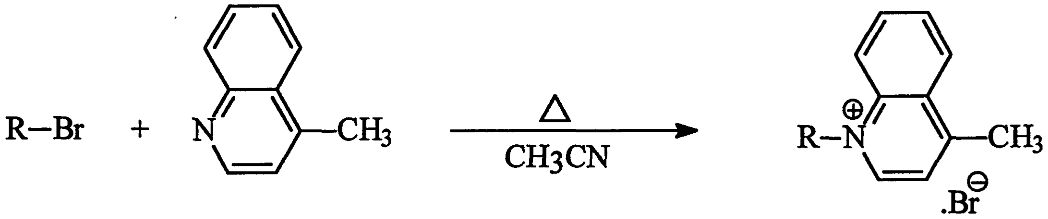

A range of derivatives from R= CH_3 to $C_{18}H_{37}$ and $PhCH_2$ have been synthesised. The method used was the same in all cases and the preparation of N-decyl-4-methyl-quinolinium bromide is described below as an illustrative example.

1-Bromodecane (7.72g, 0.035mol) was added to a solution of lepidine (5.00g, 0.035mol) in dry acetonitrile (5cm^3) and gently refluxed for 8 hours. The initial pale brown colour of the reaction became darker as the reaction proceeded. The reaction mixture was cooled in ice, before excess diethyl ether was added to precipitate out the salt as pink crystals. The recovered product was recrystallised from methanol/diethyl ether to yield 12.47g (98%) of fine pink crystals (Mpt 73-76^{0}C).

Analytical Data:

IR (KBr): 2954, 2942 (C-H str), 1602, 1529 (Ar C=C str) cm^{-1}.

^{1}H NMR ($CDCl_3$): δ= 0.9 (t, 3H, CH_3-R, J=12.5), 1.2 [s, 14H, $(CH_2)_6$], 1.4 (m, 2H, CH_3CH_2), 2.0 (m, 2H, $CH_2CH_2N^+$), 3.0 (s, 3H, Ar-CH_3), 5.3 (t, 2H, CH_2N^+, J=12.5), 8.0 (m, 2H, Ar-**H**), 8.2 (t, 2H, Ar-**H**, J=10), 8.4 (d, 1H, Ar-**H**, J=7.5) and 10.2 (d, 1H, Ar-**H**, J=7.5).

MS (70eV): *m/z* =283 (28%, M^+-HBr), 170 (52%, M^+-HBr-C_8H_{17}), 156 (69%, M^+-HBr-C_9H_{19}), 142 (100%, M^+-HBr-$C_{10}H_{21}$).

UV/Vis (CH_3OH): λ_{max}= 236, 316nm.

Reaction data for the series is shown in Table 2.1.

R Group$^{2-4}$	R-Br* (g)	Lepidine (g)	Reaction Time (hrs)	Yield (%)	Mpt (^{0}C)	λ_{max} (nm) (CH_3OH)
CH_3	3.96	4.00	1.00	7.6 (95)	164-166	234, 316
C_2H_5	4.18	5.00	2.00	7.1 (81)	58-60	234, 316
C_8H_{17}	6.74	5.00	7.00	5.1 (43)	84-87	236, 316
C_9H_{19}	7.30	5.00	7.00	10.2 (83)	86-89	238, 316
$C_{10}H_{21}$	7.72	5.00	8.00	12.4 (98)	73-76	236, 316
$C_{11}H_{13}$	8.30	5.00	7.00	11.0 (83)	74-77	236, 316
$C_{12}H_{13}$	8.80	5.00	7.00	11.5 (84)	62-65	236, 316
$C_{13}H_{13}$	8.2	5.00	7.00	12.0 (84)	67-71	236, 316
$C_{14}H_{13}$	9.70	5.00	7.00	11.8 (80)	82-86	236, 316
$C_{15}H_{13}$	9.20	4.50	12.00	12.5 (91)	84-87	236, 316
$C_{16}H_{33}$	10.68	5.00	17.00	12.5 (80)	81-85	236, 316
$C_{18}H_{37}$	11.64	5.00	17.00	12.7 (76)	88-91	236, 316
$PhCH_2$	5.96	5.01	9.00	8.6 (78)	210-212	240, 316

* Methyl iodide was used instead of bromomethane for the N-methyl derivative.

Table 2.1 Reaction Data For the γ-Substituted Quinolinium Salts.

2.2.2 N-Alkyl-2-methylquinolinium Bromides.[4]

Equation:

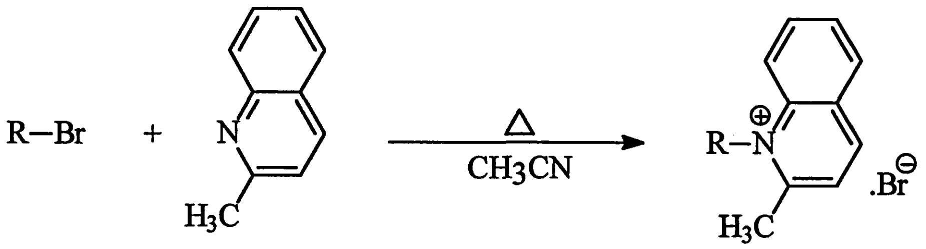

Where R= CH_3 and $C_{10}H_{21}$ to $C_{18}H_{37}$

The procedure for the preparation of the above mentioned α-substituted cations was similar to that for the γ-substituted cations (Section 2.2.1). For example the addition of 1-bromodecane (7.72g, 0.035mol) to a solution of quinaldine (5.00g, 0.035mol) in dry acetonitrile (5cm^3) yielded 4.86g (38%) of fine purple crystals after reflux, isolation and recrystallisation from methanol/diethyl ether (Mpt 138-141^{0}C).

Analytical Data:

IR (KBr): 2954, 2942 (C-H str), 1602, 1529 (Ar C=C str) cm^{-1}.

^{1}H NMR ($CDCl_3$): δ= 0.9 (t, 3H, $\mathbf{CH_3}$-R, J=12.5), 1.3 [s, 14H, $(\mathbf{CH_2})_6$], 1.6 (m, 2H, $CH_3\mathbf{CH_2}$), 2.0 (m, 2H, $\mathbf{CH_2}CH_2N^+$), 3.4 (s, 3H, Ar-$\mathbf{CH_3}$), 5.15 (t, 2H, $\mathbf{CH_2}N^+$, J=12.5), 7.9 (m, 2H, Ar-**H**), 8.15 (t, 2H, Ar-**H**, J=10), 8.3(d, 1H, Ar-**H**, J=7.5) and 9.0 (d, 1H, Ar-**H**, J=7.5).

MS (70eV): *m/z* =283 (29%, M^+-HBr), 268 (64%, M^+-HBr-CH_3), 170 (65%, M^+-HBr-C_8H_{17}), 156, (69%, M^+-HBr-C_9H_{19}), 142 (100%, M^+-HBr-$C_{10}H_{21}$).

UV/Vis (CH_3OH): λ_{max}= 238, 318nm.

Reaction data for the series is shown in Table 2.2

R Group[4]	R-Br* (g)	Quinaldine (g)	Reaction time (days)	Yield (%)	Mpt (^{0}C)	λ_{max} (nm) (CH_3OH)
CH_3	3.96	4.00	0.16	7.2 (90)	177-179	233, 320
$C_{10}H_{21}$	7.72	5.00	4.00	4.8 (38)	138-141	238, 316
$C_{11}H_{23}$	8.21	5.00	4.00	4.2 (32)	136-140	238, 318
$C_{12}H_{25}$	8.69	5.00	4.00	4.7 (34)	137-140	238, 320
$C_{13}H_{27}$	9.19	5.00	4.00	2.6 (18)	136-139	238-320
$C_{14}H_{29}$	9.70	5.00	4.00	5.4 (37)	116-119	238, 318
$C_{15}H_{31}$	10.17	5.00	5.00	5.7 (38)	132-135	238, 320
$C_{16}H_{33}$	10.68	5.00	6.00	4.4 (28)	122-125	238, 320
$C_{18}H_{37}$	11.64	5.00	6.00	4.80 (29)	139-142	236, 320

* Methyl iodide was used instead of bromomethane for the N-methyl derivative.

Table 2.2 Reaction Data For the α-Substituted Quinolinium Salts.

2.2.3 N,N′-(*m* or *p*-xylenyl)bisquinolinium (or pyridinium) Dibromides.

Equation:

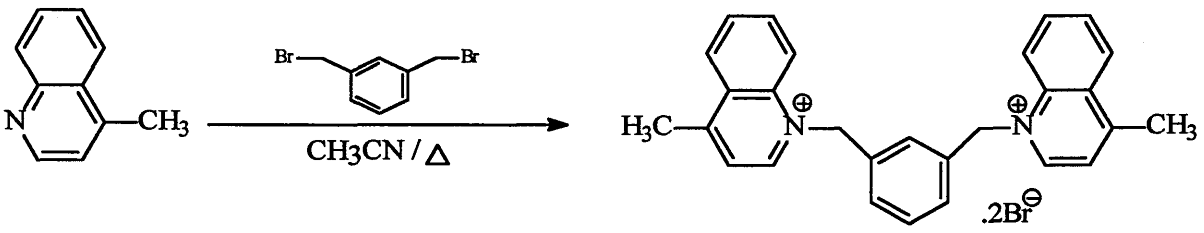

A range of derivatives has been synthesised, utilising the isomeric *m*- and *p*-xylene dibromide compounds in reactions with both lepidine and 4-picoline. The methods used were the same in all cases and the preparation of N,N′-(*m*-xylenyl)-bis(4-methylquinolinium) dibromide is described below as an illustrative example of the series. α,α′-Dibromo-*m*-xylene (2.00g, 0.0076mol) was refluxed with lepidine (2.17g, 0.015mol) in dry acetonitrile (50cm^3) for twenty-four hours during which time the initial colourless solution gave way to a lilac colour as the reaction proceeded. A yellow solid began to precipitate out of solution after about three hours and deposition appeared complete after about twenty-four hours. The reaction was monitored by tlc (dichloromethane/methanol 90:10) for the disappearance of lepidine and the appearance of the dibromide salt. The reaction mixture was cooled in ice and ice-cold diethyl ether was added to precipitate out more of the product as yellow crystals. Recrystallisation from methanol/diethyl ether afforded 2.44g (58%) of fine yellow crystals (Mpt 188-190°C).

Analytical Data:

IR (KBr): 3019 (Ar-H str), 2924 (C-H str), 1601, 1530 (Ar C=C str) cm^{-1}.

^{1}H NMR (CD_3OD): δ= 3.1 (s, 6H, 2CH_3), 6.35 (s, 4H, 2CH_2N^+), 7.4 (m, 4H, *m*-C_6H_4), 8.1 (m, 6H, Ar-**H**), 8.3 (d, 2H, Ar-**H**, J=7.5), 8.6 (d, 2H, Ar-**H**, J=7.5) and 9.45 (d, 2H, Ar-**H**, J=7.5).

MS (FAB): m/z =389 (8%, M^+-H-2Br), 247 (62%, M^+-2Br-lepidine), 231 (10%, 247 peak-CH_3), 156, (12%, 247 peak-benzyl), 104 (100%, C_8H_8).

UV/Vis (CH_3OH): λ_{max} = 236, 316nm.

$C_{28}H_{26}N_2Br_2$ (550.34)   Calc: C 61.11 H 4.76 N 5.09 Br 29.04 %

Found: C 58.95 H 5.09 N 4.85 Br 26.10 %

$C_{28}H_{26}N_2Br_2.2CH_3OH$ (614.42)   C 58.64 H 5.57 N 4.55 Br 26.01 %

TGA/DSC: Sample showed weight loss equivalent to 10.28 % of the sample mass (calculated weight loss for two CH_3OH molecules = 10.41 %)

Analytical data for the series is shown in Table 2.3.

Compound	Yield (%)	Mpt (^{0}C)	λ_{max} (CH_3OH) (nm)	Micro analysis
p-Diquinolinium Salt	6.83 (82)	268-270	236, 316	$C_{28}H_{26}N_2Br_2$ (550.34) Calc: C 61.11 H 4.76 N 5.09 % Found: C 59.21 H 5.30 N 4.91 % $C_{28}H_{26}N_2Br_2.2CH_3OH$ (614.42) Calc: C 58.64 H 5.57 N 4.55 % 10.375 % weight loss (TGA)
p-Dipyridinium Salt	7.80 (70)	322-324 (D)†	222, 256	$C_{20}H_{22}N_2Br_2$ (450.19) Calc: C 53.36 H 4.93 N 6.22 % Found: C 53.29 H 4.79 N 5.99 %
m-Dipyridinium Salt	3.50 (51)	138-142	222, 256	$C_{20}H_{22}N_2Br_2$ (450.19) Calc: C 53.36 H 4.93 N 6.22 % Found: C 53.69 H 4.96 N 6.53 %

† decomposition (D).

Table 2.3 Analytical Data for Symmetrical Dibromide Salts.

2.2.4 N-Methyl-2-methylpyridinium Iodide.[5]

Equation:

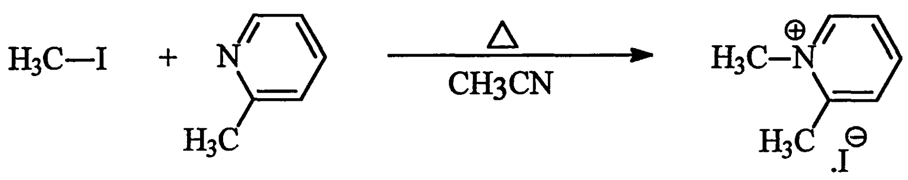

Methyl iodide (6.1g, 0.043mol) was **carefully** added dropwise, over a period of twenty minutes, with stirring to a warm solution of 2-picoline (4.00g, 0.043mol) in dry acetonitrile (5cm^3). This addition resulted in the immediate formation of a fine gelatinous yellow precipitate, which was soluble in water. The suspension was allowed to stir for one hour under a condenser, after which the reaction mixture was diluted with diethyl ether and collected. The crude product was washed with further portions of diethyl ether until the washings were colourless and then recrystallised from methanol/diethyl ether to yield 9.26g (92%) of a fine white solid (Mpt 225-228^{0}C).

Analytical Data:

IR (KBr): 3021 (C-H str), 1637, 1515 (Ar C=C str) cm^{-1}.

^{1}H NMR (D_2O): δ= 2.8 (s, 3H, Ar-**CH_3**), 4.2 (s, 3H, **CH_3**N^+), 7.85 (t, 1H, Ar-**H**, J=5), 7.9 (d, 1H, Ar-**H**, J=5), 8.35 (t, 1H, Ar-**H**, J=5) and 8.75 (d, 1H, Ar-**H**, J=5).

MS (70eV): *m/z* =142 (91%, CH_3I decomposition product), 127 (85%, I^+), 107 (58%, M^+-HI), 93, (100%, M^+-CH_3I), 78 (44%, M^+-CH_3I-CH_3), 66 (80%, 78 peak-HCN).

UV/Vis (CH_3OH): λ_{max} = 266nm.

2.3 Synthesis of Electron Acceptors.

2.3.1 11,11,12,12-Tetracyano-9,10-anthraquinodimethane (TCAQ).[6]

Equation:

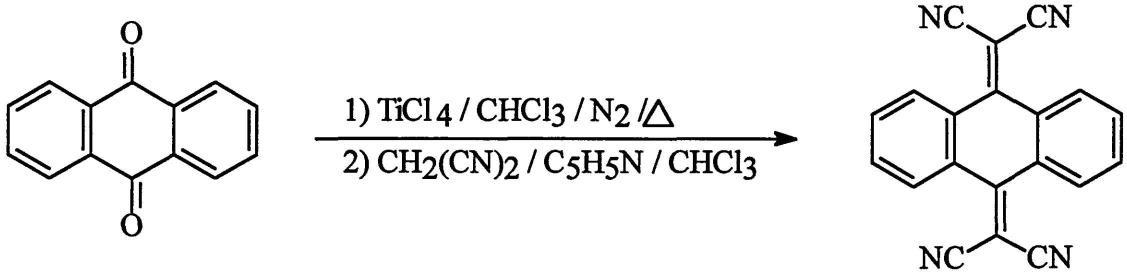

Titanium (IV) chloride (9.5g, 0.05mol) was added to a solution of 9,10-anthraquinone (5.2g, 0.025mol) in dry chloroform (250cm^3). The resultant yellow suspension was refluxed under a dry nitrogen atmosphere for half an hour. After cooling, the suspension was poured into a solution of malononitrile (33.0g, 0.5mol) and pyridine (79.5g, 1.0mol) in dry chloroform (300cm^3). The black solution was refluxed for a further thirteen hours under nitrogen. After cooling in ice, the reaction mixture was poured into water (100cm^3) and shaken vigorously. The resulting layers were separated and the aqueous layer was extracted with chloroform (3×100cm^3). The combined extracts were washed with 10% aqueous sodium hydroxide (2×50cm^3) and water (1×200cm^3), then dried over magnesium sulphate. The yellow extract was reduced in volume to ca 50cm^3 (rotary evaporator) and 40/60 petroleum ether was added to precipitate out the product as yellow crystals. The recovered solid was recrystallised from acetonitrile to yield 2.75g (36%) of yellow crystals (Mpt >360^{0}C).

Analytical Data:

IR (KBr): 2229 (C≡N str), 1581, 1556, 1546 (Ar C=C str) cm^{-1}.

^{1}H NMR (D$_6$-DMSO): δ= 7.91-8.36 (m, 8H, Ar-**H**)

MS (70eV): *m/z* =304 (100%, M$^+$), 277 (21%, M$^+$-HCN), 250 (11%, M$^+$-2HCN).

UV/Vis (CH$_3$CN): λ_{max}= 280, 304, 344nm.

$C_{20}H_8N_4$ (304.2) Calc: C 78.94 H 2.65 N 18.40 %

Found: C 78.69 H 2.60 N 18.31 %

2.3.2 2,3,5,6-Tetramethyl-7,7,8,8-tetracyano-p-quinodimethane (TMTCNQ).[7]

Equation:

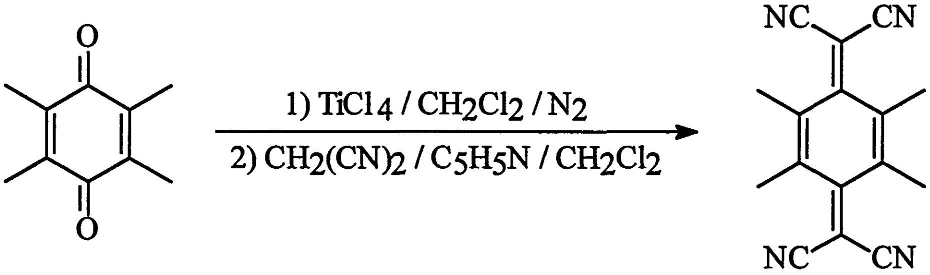

Titanium (IV) chloride (14.44g, 0.076mol) was added to a solution of duroquinone (5.03g, 0.03mol) in dry dichloromethane (150cm^3). The resultant yellow/orange suspension was stirred under a dry nitrogen atmosphere for thirty minutes. Then a solution of malononitrile (5.02g, 0.076mol) and pyridine (12.04g, 0.152mol) in dry dichloromethane (100cm^3) was added dropwise to yield a black solution which was stirred under nitrogen at room temperature for twenty-four hours. The reaction mixture was poured into water (100cm^3) and shaken vigorously. The resultant layers were separated and the aqueous layer was extracted with dichloromethane (3×100cm^3). The combined organic extracts were washed with 10% aqueous sodium hydroxide (2×50cm^3) and water (1×200cm^3), then dried over magnesium sulphate. The yellow extract was reduced in volume to ca 50cm^3 (rotary evaporator) and 40/60 petroleum ether was added to precipitate out the product as a fine yellow solid. The recovered solid was recrystallised from acetonitrile to yield 1.97g (25%) of fine yellow crystals (Mpt 242-244^{0}C decomp).

Analytical Data:

IR (KBr): 2964, 2926, 2858 (C-H str), 2220 (C≡N str), 1671 (C=C str) cm^{-1}.

^{1}H NMR ($CDCl_3$): δ= 2.38 (s, 4CH_3).

^{13}C NMR ($CDCl_3$): δ=18.43 (s, $4CH_3$), 83.83 (s, C_7, C_8), 112.40 (s, C≡N), 137.51 (s, $C_{2,3,5,6}$) and 163.80 (s, $C_{1,4}$).

MS (70eV): *m/z* =260 (100%, M^+), 233 (72%, M^+-HCN), 205 (20%, M^+-2HCN).

UV/Vis (CH_3CN): λ_{max} = 260, 368, 386nm.

$C_{16}H_{12}N_4$ (260.3)	Calc:	C 73.83	H 4.65	N 21.52 %
	Found:	C 73.77	H 4.58	N 21.44 %

2.3.3 2,3,5,6-Tetrafluoro-7,7,8,8-tetracyano-p-quinodimethane ($TCNQF_4$).[8]

$TCNQF_4$ was prepared, starting from acetone, using a five step synthetic strategy.[8] Experimental details are given below for the various steps:

Isopropylidenemalononitrile.[9]

Equation:

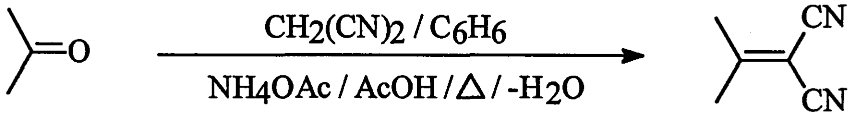

Acetone (118.0g, 2.03mol) was added to a solution of malononitrile (132.28g, 2.0mol), ammonium acetate (30.03g, 0.39mol) and acetic acid (96.04g, 1.59mol) in benzene (400cm^3). The resultant liquor was refluxed under a Dean-Stark trap until the water ceased to separate (≈7 hours). The mixture was washed with water (3×250cm^3) and saturated sodium chloride (1×250cm^3) before being dried over magnesium sulphate. The benzene was removed under reduced pressure and the resultant crude brown liquor was distilled under reduced pressure to yield 126.4g (60%) of a colourless oil (Bpt 112-114^{0}C / 9.5mm Hg).

Analytical Data:

IR (KBr): 3000 (C-H str), 2232 (C≡N str), 1607 (C=C str) cm^{-1}.

^1H NMR ($CDCl_3$): δ= 2.21 (s, $2CH_3$).

^{13}C NMR ($CDCl_3$): δ=23.79 (q, 2CH_3), 6.04 (s, R_2-C=), 112.31 (s, C≡N), 180.02 [s, =$C(CN)_2$].

MS (70eV): *m/z* =106 (88%, M^+), 79 (92%, M^+-HCN), 66 (72%, M^+-CH_2CN), 52 (75%, M^+-2HCN).

tert-Butylmalononitrile.[8]

Equation:

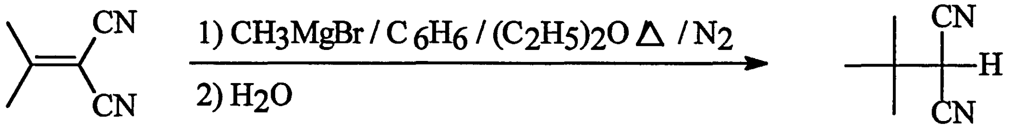

A solution of isopropylidenemalononitrile (51.2g, 0.483mol) in anhydrous benzene (200cm^3) was added dropwise to a solution of 3M methylmagnesium bromide (178cm^3, 0.531mol) in anhydrous diethyl ether (150cm^3) under an atmosphere of dry nitrogen at a temperature of 30-35^{0}C. The resultant mixture was stirred at 45-48^{0}C for one hour then poured onto excess ice. The mixture was made faintly acidic with 20% sulphuric acid and the layers were separated. The resultant aqueous layer was extracted once with 1:1 ether-benzene mixture (200cm^3). The combined organic layers were washed twice with water (2×200cm^3) then made faintly acidic with dilute hydrochloric acid before being washed twice with saturated sodium chloride solution (2×200cm^3). After drying with magnesium sulphate and concentration under reduced pressure, the pale brown liquor was distilled under reduced pressure yielding 30.2g (51%) of *tert*-butylmalononitrile (Bpt 112-116^{0}C / 11mm Hg) as a white waxy solid that melted at 80^{0}C.

Analytical Data:

IR (KBr): 2973, 2942, 2877 (C-H str), 2254 (C≡N str) cm^{-1}.

^1H NMR ($CDCl_3$): δ= 1.25 (s, 9H, 3CH_3), 3.5 (s, C-**H**).

^{13}C NMR ($CDCl_3$): δ=25.08 [s, R_2-CCH$(CN)_2$], 27.09 (s, 3CH_3), 36.03 [s, CH$(CN)_2$], 112.57 (s, C≡N).

MS (70eV): *m/z* =107 (28%, M^+-CH_3) 57 (100%,^{t}butyl), 41 (72%, M^+-CH_3CCCN).

2,3,5,6-Tetrafluoro-1,4-bis(*tert*-butyldicyanomethyl)benzene.[8]

Equation:

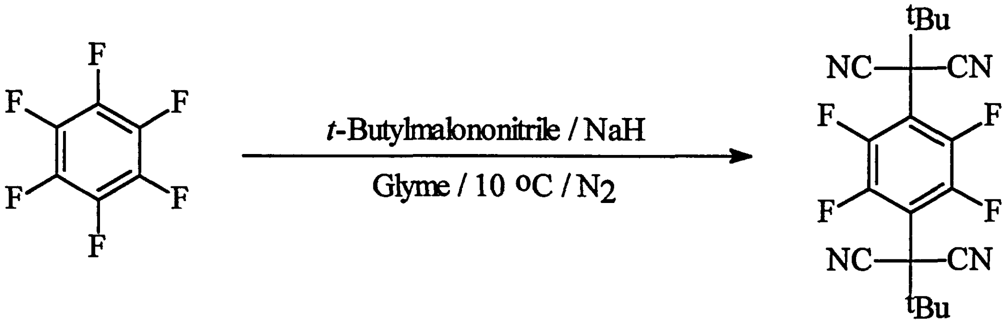

A solution of *tert*-butylmalononitrile (15.0g, 0.12mol) in anhydrous ethyleneglycol dimethylether (20cm^3) was **carefully** added dropwise to a stirred suspension of sodium hydride (2.88g, 0.12mol) in the same solvent (40cm^3) at 10-15^{0}C under an atmosphere of dry nitrogen. The resulting golden brown homogeneous solution was stirred for a few minutes before hexafluorobenzene (9.3g, 0.05mol) in anhydrous ethyleneglycol dimethylether (10cm^3) was added rapidly in one portion and the mixture heated to reflux. After about two hours a white solid appeared and precipitation seemed complete after about 16 hours. Most of the solvent was then removed by distillation under reduced pressure and the reaction mixture was diluted with water. The recovered solid was washed until neutral with water, then with methanol until the washings were colourless, and finally with diethyl ether. The resultant pale yellow solid was recrystallised from a very large volume of acetone to yield 13.73g (70%) of colourless crystals of 2,3,5,6-tetrafluoro-1,4-bis(*tert*-butyldicyanomethyl)benzene (Mpt 296-300^{0}C).

Analytical Data:

IR (KBr): 2983, 2943, 2894 (C-H str), 2255 (C≡N str), 1470 (Ar C=C str) cm^{-1}.

^1H NMR [$(CD)_2CO$]: δ= 1.35 (s, 6H, $2CH_3$), 2.9 (s, 12H, $4CH_3$).

^{13}C NMR [$(CD)_2CO$]: Signal too weak.

^{19}F NMR [$(CD)_2CO$]: Signal too weak.

MS (70eV): *m/z* =391 (6%, M^+), 375 (12%, M^+-CH_3), 362 (24%, M^+-CN), 355 (26%, M^+-^{t}butyl), 226 (28%, M^+-$4CH_3CN$), 57 (100%, ^{t}butyl), 41 (74%, CH_3CN).

$C_{20}H_{18}N_4F_4$ (391.4)	Calc:	C 61.53	H 4.65	N 14.34	F 19.41 %
	Found:	C 61.24	H 4.48	N 14.31	F 19.38 %

2,3,5,6-Tetrafluoro-7,7,8,8-tetracyano-p-quinodimethane ($TCNQF_4$).[8]

Equation:

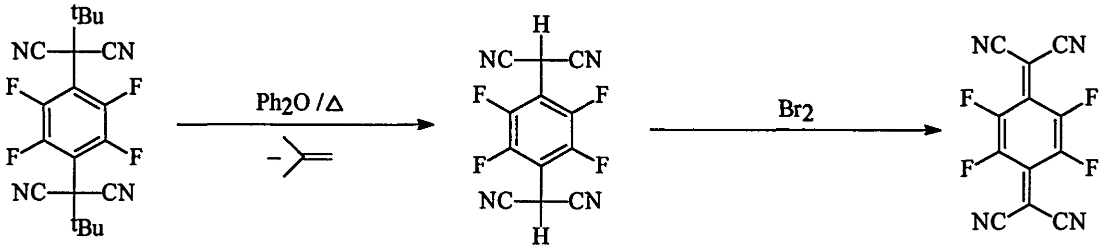

Diphenylether ($350cm^3$) was heated to reflux under an atmosphere of nitrogen and 2,3,5,6-tetrafluoro-1,4-bis(*tert*-butyldicyanomethyl)benzene (7.8g, 0.02mol) was added rapidly in one portion. The resulting solution was heated to reflux for four minutes (**Caution** reaction liberates highly flammable iso-butene gas), before being allowed to cool in air to 195^0C and then in an ice bath to 40^0C. An equal volume of diethyl ether was then added followed by 4% aqueous sodium bicarbonate ($100cm^3$). The mixture was shaken vigorously, and the organic layer extracted with three further portions of 1% aqueous sodium bicarbonate ($3\times30cm^3$). The combined aqueous layers were filtered and extracted once with diethyl ether ($50cm^3$).

The aqueous solution was then treated with potassium acetate (7.5g) and acetic acid (5cm^3) before bromine water was added, until a positive test for free bromine was obtained, to precipitate out the TCNQF$_4$. The yellow precipitate was filtered, washed with water and the moist filter cake was then dissolved in about two and a half litres of dichloromethane. The aqueous layer was separated and the remaining organic layer was treated with magnesium sulphate and decolourising charcoal. The resulting clear bright yellow filtrate was concentrated until a thick paste of TCNQF$_4$ was obtained to which excess 40/60 petroleum ether was added to maximise the product recovery. The recovered solid was repeatedly recrystallised (~ 4 times) from acetonitrile to yield 2.39g (43%) of rusty yellow crystals (Mpt 297-300^{0}C decomp).

Analytical Data:

IR (KBr): 2225 (C≡N str), 1594 (C=C str), 1337 (C-F str) cm^{-1}.

^{1}H NMR (CDCl$_3$): No peaks found except those associated with the deuterated solvent.

^{13}C NMR (CDCl$_3$): signal too weak

^{19}F NMR (CDCl$_3$): δ= -130.67 (broad s, 4F, C-**F**)

MS (70eV): *m/z* =276 (100%, M$^+$), 250 (4%, M$^+$-CN), 224 (24%, M$^+$-2CN),

UV/Vis (CH$_3$OH): λ_{max} = 348, 366, 390nm

$C_{20}N_4F_4$ (276.1)	Calc:	C 52.19	H 0.00	N 20.28	F 27.52 %
	Found:	C 52.08	H 0.00	N 20.30	F 27.32 %

2.3.4 N,N'-Dicyano-2,3,5,6-tetrafluoro-1,4-benzoquinodiimine (DCNQIF$_4$).[10]

Equation:

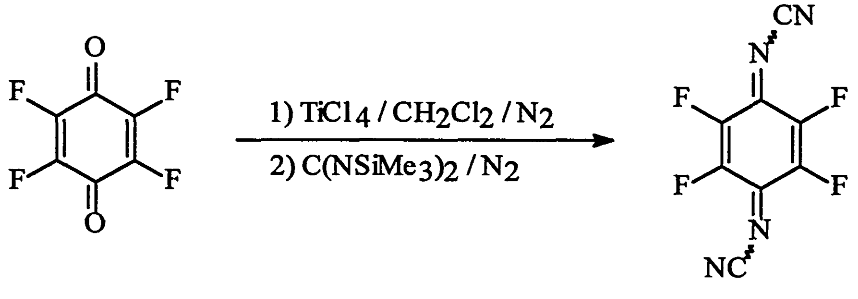

Titanium (IV) chloride (15.272g, 0.0805mol) was added to a stirred solution of *p*-fluoranil (2.89g, 0.0161mol) in dry dichloromethane (200cm^3). The pale brown solution was stirred under an atmosphere of dry nitrogen for twenty minutes. Bis(trimethylsilyl)carbodiimide (15.00g, 0.0805mol) was added rapidly to yield a fine brick red precipitate which was allowed to stir under nitrogen for a further three hours. The reaction mixture was poured into ice cold water (500cm^3) and shaken. The organic phase was diluted with dichloromethane until a clear solution was obtained. The layers were separated and the organic extract was dried over magnesium sulphate. The solvent was reduced in volume to about 20cm^3 (rotary evaporator) and excess 40/60 petroleum ether was added to precipitate out the product as dark crystals. The recovered solid was recystallised from toluene/methyl-cyclohexane to yield 1.7g (46%) of fine brown solid (Mpt 202-205^{0}C decomp).

Analytical Data:

IR (KBr): 2183 (C≡N str), 1643 (C=C str), 1596 (C=N str), 1337 (C-F str) cm^{-1}.

^{13}C NMR: product too insoluble

^{19}F NMR: product too insoluble

MS (70eV): *m/z* =228 (100%, M$^+$), 176 (69%, M$^+$-2CN).

UV/Vis (CH_3CN): λ_{max} = 330, 346nm

$C_8N_4F_4$ (228.11)	Calc:	C 42.10	H 0.00	N 24.57	F 33.33 %
	Found:	C 41.88	H 0.00	N 24.38	F 32.91 %

2.4 Synthesis of Zwitterionic D-π-A Adducts.

2.4.1 Synthesis of R(4)Q3CNQF$_4$ Adducts.

Equation:

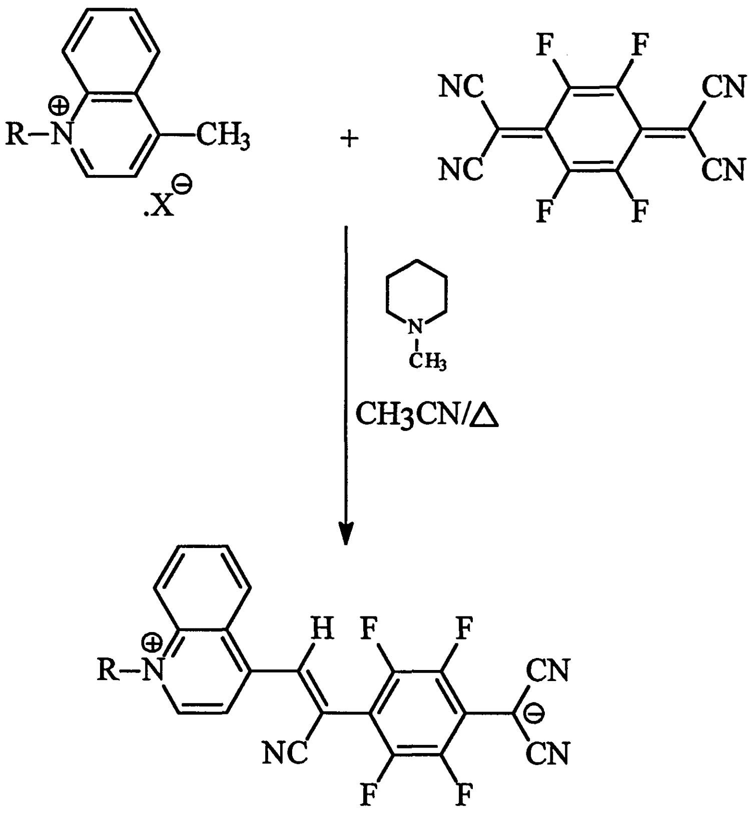

A range of derivatives, from N-methyl to long chain compounds, where R= C_{10} to C_{18}, and N-benzyl has been synthesised. The general method used was the same in each case and the preparation of (Z)-β-(N-decyl-4-quinolinium)-α-cyano-4-(2,3,5,6-tetrafluoro) styryldicyanomethanide [$C_{10}H_{21}$(4)Q3CNQF$_4$] is described below as a representative example:

N-Decyl-4-methylquinolinium bromide (0.4g, 0.0011mol) was refluxed with N-methyl piperidine (0.1g, 0.0011mol) in dry acetonitrile (20cm^3) for twenty minutes, during which time the initial dark brown colour gave way to a deep blue colour. After cooling slightly, 2,3,5,6-tetrafluoro-7,7,8,8-tetracyano-p-quinodimethane (TCNQF$_4$) (0.3g, 0.0011mol) was added and the solution was refluxed for a further hour, during which time the colour changed from the original deep blue colour to an emerald green shade. After a further twenty-four hours reflux the solution which had turned a deep brown colour was cooled producing a fine black powder. The product was isolated by vacuum filtration and washed with diethyl ether (3×25cm^3) to remove any unreacted TCNQF$_4$. The crude product was recrystallised several times from large volumes of methanol to yield 0.1897g, (33%) of deep purple solid (Mpt 252-255^{0}C).

Analytical Data:

IR (KBr): 2922, 2854 (C-H str), 2182, 2152 (C≡N str), 1625 (C=C str), 1496 (Ar C=C str), 1226 (C-F str) cm^{-1}.

^{1}H NMR (d$_6$-DMSO): δ= 0.9 (t, 3H, **CH$_3$**-R, J=12.5), 1.3 [s, 14H, (**CH$_2$**)$_7$], 2.0 (m, 2H, **CH$_2$**CH$_2$N$^+$), 5.1 (t, 2H, **CH$_2$**N$^+$, J=12.5), 8.0 (d, 1H, Ar-**H**, J=5), 8.2 (t, 1H, Ar-**H**, J=5), 8.4 (t, 1H, Ar-**H**, J=5), 8.65 (s, 1H, π-bridge-**H**), 8.7 (d, 1H, Ar-**H**, J=5), 9.3 (d, 1H, Ar-**H**, J=5), 9.7 (d, 1H, Ar-**H**, J=5).

^{13}C NMR (d$_6$-DMSO): Signal too weak.

^{19}F NMR (d$_6$-DMSO): δ= -143.9, 144.0 (d, 2F, C-**F**, $J_{F,F}$=24), -147.53, 147.59 (d, 2F, C-**F**, $J_{F,F}$=24).

MS (70eV): *m/z* =532 (5%, M$^+$), 392 (86%, M$^+$-R), 373 (50%, M$^+$-R-F), 327 [48%, M$^+$-R-C(CN)$_2$].

UV/Vis (CH$_3$CN): λ_{max} = 242, 342, 566(CT)nm

$C_{31}H_{28}N_4F_4$ (532.55)	Calc:	C 69.91	H 5.29	N 10.52	F 14.27 %
	Found:	C 69.63	H 5.38	N 10.29	F 14.22 %

A collection of analytical data for the series is shown in Tables 2.4 and 2.5.

Zwitterion	Yield (%) / g	Mpt (^{0}C)	R*f**	λ_{max} (CH_3CN) (nm)
CH_3(4)Q3CNQF_4	0.180 (63)	>300	0.52	572
$C_{11}H_{23}$(4)Q3CNQF_4	0.181 (31)	252-254	0.40	566
$C_{12}H_{25}$(4)Q3CNQF_4	0.152 (25)	259-262	0.46	566
$C_{13}H_{27}$(4)Q3CNQF_4	0.220 (35)	268-271	0.51	566
$C_{14}H_{29}$(4)Q3CNQF_4	0.141 (22)	248-251	0.40	566
$C_{15}H_{31}$(4)Q3CNQF_4	0.187 (28)	262-265	0.47	564
$C_{16}H_{33}$(4)Q3CNQF_4	0.151 (23)	260-263	0.51	564
$C_{18}H_{37}$(4)Q3CNQF_4	0.200 (29)	266-269	0.53	566
PhCH_2(4)Q3CNQF_4	0.188 (36)	225-229	0.42	580

* 90:10 DCM/CH_3OH eluent.

Table 2.4 Analytical Data for the R(4)Q3CNQF_4 Adducts.

Zwitterion	C(%) Found (Calc)	H(%) Found (Calc)	N(%) Found (Calc)	F(%) Found (Calc)
CH_3(4)Q3CNQF_4	65.08 (65.03)	2.66 (2.48)	13.61 (13.78)	18.62 (18.71)
$C_{11}H_{23}$(4)Q3CNQF_4	69.94 (70.31)	5.53 (5.53)	10.21 (10.25)	13.76 (13.90)
$C_{12}H_{25}$(4)Q3CNQF_4	70.21 (70.69)	5.83 (5.75)	10.04 (9.99)	13.46 (13.55)
$C_{13}H_{27}$(4)Q3CNQF_4	70.77 (71.06)	5.96 (5.96)	9.78 (9.75)	13.18 (13.22)
$C_{14}H_{29}$(4)Q3CNQF_4	71.48 (71.40)	6.35 (6.16)	9.48 (9.51)	12.72 (12.91)
$C_{15}H_{31}$(4)Q3CNQF_4	70.84 (71.74)	6.39 (6.35)	9.22 (9.29)	12.58 (12.61)
$C_{16}H_{33}$(4)Q3CNQF_4	71.52 (72.06)	6.60 (6.54)	8.69 (9.08)	12.18 (12.32)
$C_{18}H_{37}$(4)Q3CNQF_4	72.65 (72.65)	6.98 (6.88)	8.50 (8.68)	11.65 (11.79)
PhCH_2(4)Q3CNQF_4	68.89 (69.71)	3.04 (2.92)	11.54 (11.61)	15.46 (15.75)

Table 2.5 Micro-analytical Data for the R(4)Q3CNQF_4 Adducts.

2.4.2 Synthesis of R(2)Q3CNQF$_4$ Adducts.

Equation:

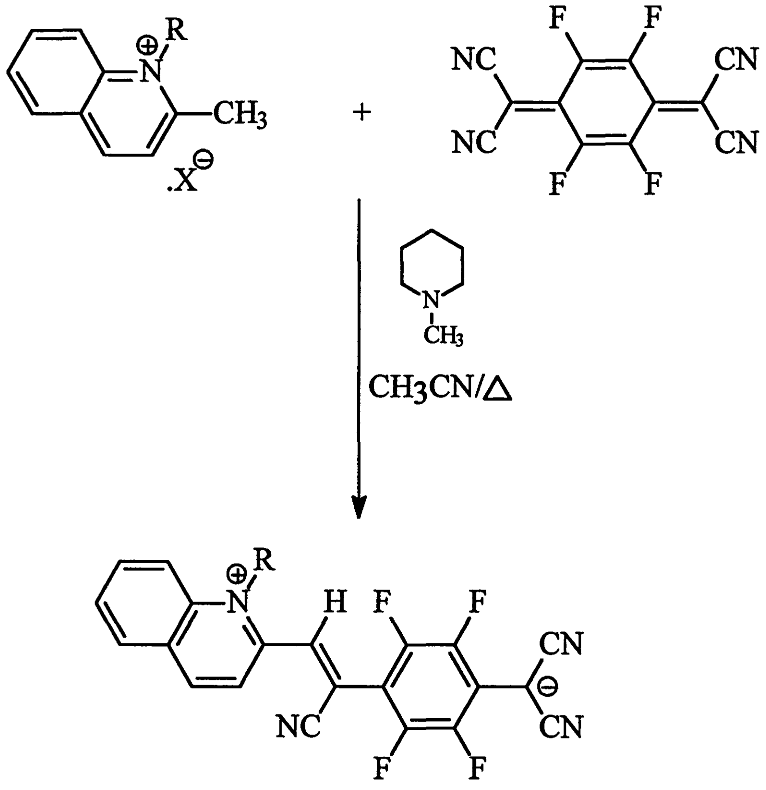

A range of derivatives, from N-methyl to long chain compounds (where R=C_{10} to C_{16}), has been synthesised. Again the general method used was the same in each case and the preparation of (Z)-β-(N-decyl-2-quinolinium)-α-cyano-4-(2,3,5,6-tetrafluoro)styryl-dicyanomethanide [$C_{10}H_{21}$(2)Q3CNQF$_4$] is described below as a representative example.

N-Decyl-2-methylquinolinium bromide (0.4g, 0.0011mol) was refluxed with N-methyl piperidine (0.1g, 0.0011mol) in dry acetonitrile (20cm^3) for twenty minutes, during which time the initial dark brown colour gave way to a deep purple colour. After cooling slightly 2,3,5,6-tetrafluoro-7,7,8,8-tetracyano-p-quinodimethane (0.3g, 0.0011mol) was added and the solution was refluxed for a further hour, during which time the colour changed from the original deep purple to an emerald green shade.

After a further forty-nine hours reflux the solution, which had turned a deep blue colour, was cooled producing a fine black powder. The product was isolated by vacuum filtration and washed with diethyl ether (3×25cm^3) to remove any unreacted TCNQF$_4$. The crude product was recrystallised several times from acetonitrile to yield 0.1841g (32%) of deep purple solid (Mpt 160-164^{0}C).

Analytical Data:

IR (KBr): 2925, 2853 (C-H str), 2184, 2152 (C≡N str), 1635 (C=C str), 1496 (Ar C=C str), 1227 (C-F str) cm^{-1}.

^{1}H NMR (d$_6$-DMSO): δ= 0.85 (t, 3H, **CH$_3$**-R, J=12.5), 1.25 [s, 12H, (**CH$_2$**)$_6$], 1.5 (m, 2H, CH$_3$**CH$_2$**-R) 1.95 (m, 2H, **CH$_2$**CH$_2$N$^+$), 5.05 (t, 2H, **CH$_2$**N$^+$, J=12.5), 8.05 (d, 1H, Ar-**H**, J=5), 8.3 (s, 1H, π-bridge-**H**), 8.35 (t, 1H, Ar-**H**, J=5), 8.55 (d, 1H, Ar-**H**, J=5), 8.65 (d, 1H, Ar-**H** J=5), 8.7 (d, 1H, Ar-**H**, J=5), 9.45 (d, 1H, Ar-**H**, J=5).

^{13}C NMR (d$_6$-DMSO): Signal too weak.

^{19}F NMR (d$_6$-DMSO): δ= -142.56, 142.62 (d, 2F, C-**F**, $J_{F,F}$=24), -146.88, 146.94 (d, 2F, C-**F**, $J_{F,F}$=24).

MS (70eV): *m/z* =532 (5%, M$^+$), 392 (28%, M$^+$-R), 373 (15%, M$^+$-R-F), 327 [12%, M$^+$-R-C(CN)$_2$].

UV/Vis (CH$_3$CN): λ_{max} = 246, 338, 568(CT)nm

$C_{31}H_{28}N_4F_4$ (532.55) Calc: C 69.91 H 5.29 N 10.52 F 14.27 %

Found: C 69.97 H 5.27 N 10.26 F 14.28 %

A collection of analytical data for the series is shown in Tables 2.6 and 2.7.

Zwitterion	Yield (%) / g	Mpt (^{0}C)	Rf^*	λ_{max} (CH_3CN) (nm)
$CH_3(2)Q3CNQF_4$	0.140 (48)	>300	0.41	570
$C_{12}H_{25}(2)Q3CNQF_4$	0.170 (28)	162-165	0.49	570
$C_{13}H_{27}(2)Q3CNQF_4$	0.150 (24)	163-166	0.46	568
$C_{14}H_{29}(2)Q3CNQF_4$	0.073 (11)	167-170	0.47	568
$C_{16}H_{33}(2)Q3CNQF_4$	0.088 (13)	168-171	0.48	570

* 90:10 DCM/CH_3OH eluent.

Table 2.6 Analytical Data for the $R(2)Q3CNQF_4$ Adducts.

Zwitterion	C(%) Found (Calc)	H(%) Found (Calc)	N(%) Found (Calc)	F(%) Found (Calc)
$CH_3(2)Q3CNQF_4$	64.93 (65.03)	2.45 (2.48)	13.78 (13.78)	18.51 (18.71)
$C_{12}H_{25}(2)Q3CNQF_4$	70.41 (70.69)	5.93 (5.75)	9.75 (9.99)	-
$C_{13}H_{27}(2)Q3CNQF_4$	70.77 (71.06)	5.96 (5.96)	9.78 (9.75)	13.10 (13.22)
$C_{14}H_{29}(2)Q3CNQF_4$	71.26 (71.40)	6.31 (6.16)	9.39 (9.51)	-
$C_{16}H_{33}(2)Q3CNQF_4$	72.55 (72.06)	6.72 (6.54)	8.98 (9.08)	12.44 (12.32)

Table 2.7 Micro-analytical Data for the $R(2)Q3CNQF_4$ Adducts.

2.4.3 Synthesis of R(4)Q3CNTMQ Adducts.

Equation:

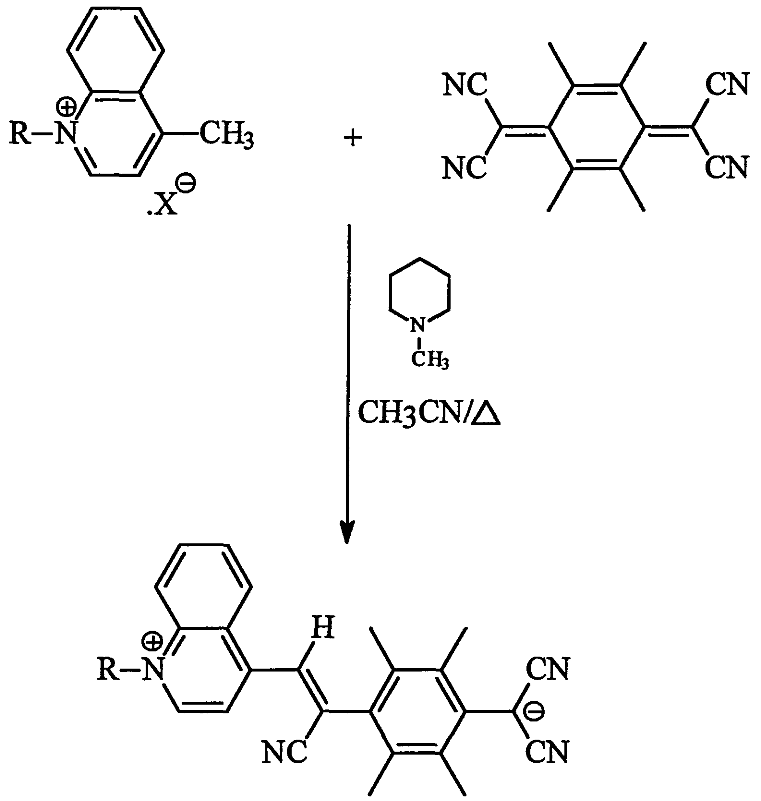

A range of derivatives, having R from CH$_3$ to C$_{16}$H$_{33}$, has been synthesised. The general method employed was the same in each case and the preparation of (Z)-β-(N-methyl-4-quinolinium)-α-cyano-4-(2,3,5,6-tetramethyl)styryldicyanomethanide [CH$_3$(4)Q3CNTMQ] is described below as an illustrative example.

N-Methyl-4-methylquinolinium iodide (0.4g, 0.0014mol) was refluxed with N-methyl piperidine (0.12g, 0.0014mol) in dry acetonitrile (20cm^3) for twenty minutes, during which time the initial dark brown colour gave way to a deep blue colour. After cooling slightly, 2,3,5,6-tetramethyl-7,7,8,8-tetracyano-p-quinodimethane (0.36g, 0.0014mol) was added and the solution was refluxed for a further hour, during which time the colour changed from the original deep blue colour to an emerald green shade. After a further seventy two hours reflux the solution, which had turned an intense royal blue colour, was cooled producing a fine purple/black powder.

The product was recovered by vacuum filtration and washed with diethyl ether ($3\times25cm^3$) to remove any unreacted TMTCNQ. The crude solid was recrystallised several times from methanol to yield 0.045g (8%) of deep purple solid (Mpt 241-245^{0}C decomp).

Analytical Data:

IR (KBr): 3425 (O-H str), 2928, 2855 (C-H str), 2153, 2090 (C≡N str), 1612 (C=C str), 1497 (Ar C=C str)cm^{-1}.

^{1}H NMR: Insufficient sample available

^{13}C NMR: Insufficient sample available

MS (70eV): *m/z* =390 (8%, M$^+$), 375 (5%, M$^+$-CH_3), 284 [27%, M$^+$-$C(CN)_2$-CH_3CN], 270 [45%, M$^+$-$C(CN)_2$-CH_3CN-CH_3].

UV/Vis (CH_3CN): λ_{max} = 582(CT)nm

$C_{26}H_{22}N_4$ (390.4)	Calc: C 79.97	H 5.68	N 14.34 %
	Found: C 77.75	H 5.40	N 13.45 %
$C_{26}H_{22}N_4.CH_3OH$ (422.4)	C 76.75	H 6.20	N 13.25 %

A collection of analytical data for the series of R(4)Q3CNTMQ adducts is shown in Tables 2.8 and 2.9.

Zwitterion	Yield (%) / g	Mpt (^{0}C)	R*f**	λ_{max} (CH_3CN) (nm)
C_2H_5(4)Q3CNTMQ	0.030 (9)	247-251 (D)†	0.43	583
$C_{10}H_{21}$(4)Q3CNTMQ	0.103 (17)	244-249 (D)†	0.47	580
$C_{14}H_{29}$(4)Q3CNTMQ	0.078 (12)	248-253 (D)†	0.40	581
$C_{16}H_{33}$(4)Q3CNTMQ	0.040 (6)	256-261 (D)†	0.42	582

* 90:10 DCM/CH_3OH eluent, † decomposition (D).

Table 2.8 Analytical Data for the R(4)Q3CNTMQ Adducts.

Zwitterion	C (%) Found (Calc)	H (%) Found (Calc)	N (%) Found (Calc)
C_2H_5(4)Q3CNTMQ	71.82 (80.17)	6.79 (5.98)	13.53 (13.84)
$C_{10}H_{21}$(4)Q3CNTMQ	75.78 (81.35)	8.15 (7.80)	9.27 (10.84)
$C_{14}H_{29}$(4)Q3CNTMQ	70.10 (81.77)	7.75 (8.45)	7.56 (9.78)
$C_{16}H_{33}$(4)Q3CNTMQ	70.33 (81.95)	9.16 (8.72)	6.76 (9.32)

Table 2.9 Micro-analytical Data for the R(4)Q3CNTMQ Adducts.

2.4.4 Synthesis of R(4)Q3CNAQ Adducts (cf p.90).

Equation:

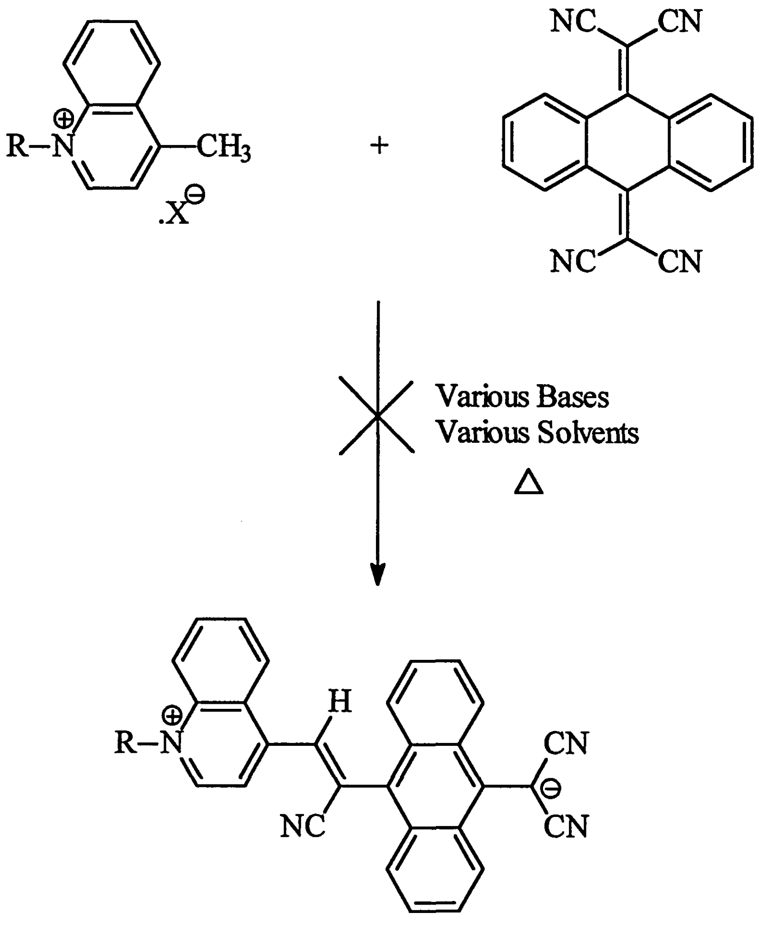
R–N
CH3
.X
+
NC
CN
NC
CN
Various Bases
Various Solvents
Δ
R–N
H
NC
CN
CN

2.4.5 Synthesis of *m*-C_8H_8(4)DQ6CNQ and Derivatives.

Equation:

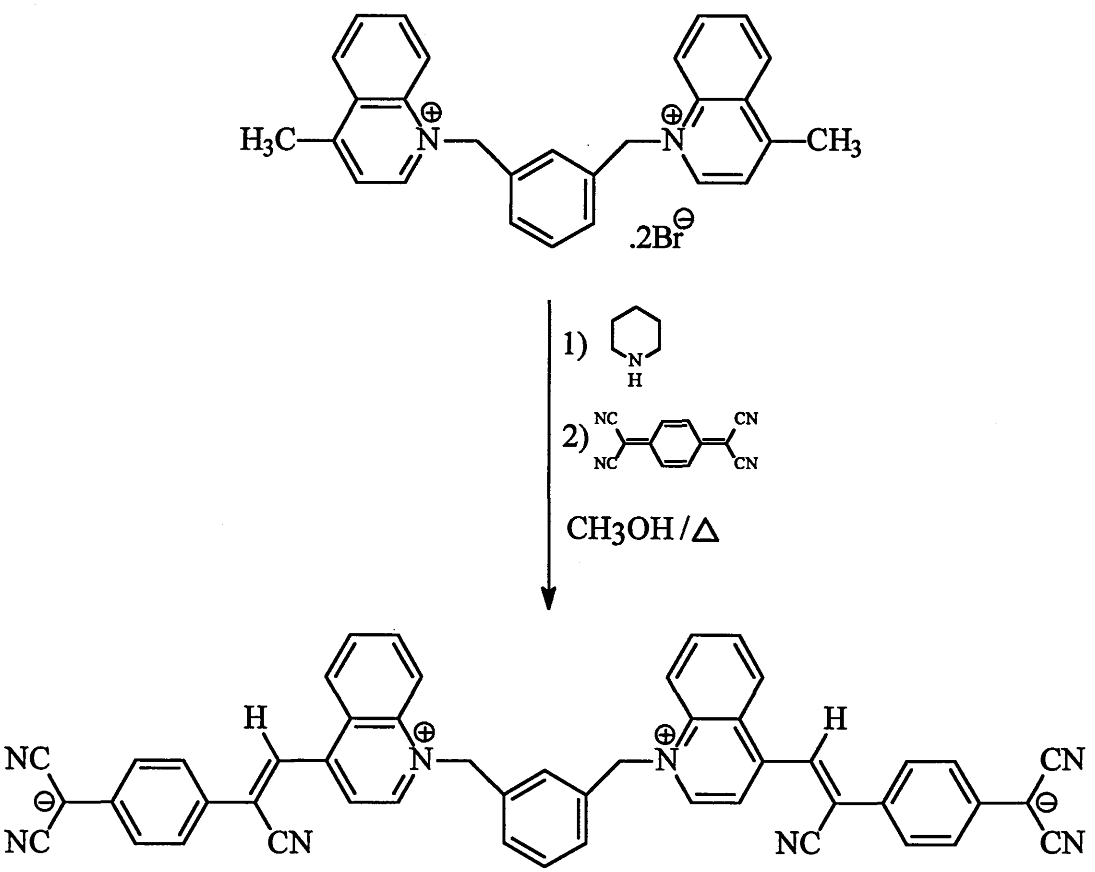

A range of derivatives, involving the dipyridinium and diquinolinium salts with various electron acceptors such as TCNQ, TMTCNQ etc, have been synthesised. The general method used was the same in each case and the preparation of *m*-C_8H_8(4)DQ6CNQ is described below as a representative example:

N,N'-(*m*-Xylenyl)-bis(4-methylquinolinium bromide) (0.67g, 0.0012mol) was refluxed with piperidine (0.2g, 0.0024mol) in dry methanol (40cm^3) for twenty minutes, during which time the initial pale pink colour gave way to a deep purple colour. After cooling slightly, 7,7,8,8-tetracyano-p-quinodimethane (0.5g, 0.0024mol) was added and the solution changed colour from the original deep purple to black. After about half an hour of gentle reflux a black solid began to deposit on the sides of the flask, precipitation appearing complete after about twenty-nine hours. The reaction mixture was cooled resulting in further precipitation of the black solid. The product was isolated by vacuum filtration and washed with diethyl ether (3×25cm^3) to remove any unreacted TCNQ. The crude product was recrystallised from methanol/N-methylformamide (NMF) to yield 0.473g (52%) of a fine black solid (Mpt 210-213^{0}C decomp).

Analytical Data:

IR (KBr): 3429 (O-H str), 2171, 2122 (C≡N str), 1535 (C=C str) cm^{-1}.

^{1}H NMR (d$_1$-TFA): See section 2.6.4

^{13}C NMR (d$_1$-TFA): signal too weak

MS (FAB): *m/z* =743 (7%, M$^+$), 566 (5%, M$^+$-TCQ), 423 (8%, M$^+$-QTCQ)

UV/Vis (NMF): λ_{max} = 728(CT)nm

$C_{50}H_{30}N_8$ (742.9)	Calc:	C 80.85	H 4.07	N 15.08 %
	Found:	C 77.00	H 4.22	N 13.74 %
$C_{50}H_{30}N_8.2CH_3OH$ (806.52)		C 77.39	H 4.75	N 13.88 %

TGA/DSC: Sample showed weight loss equivalent to 7.71 % of the sample mass (calculated weight loss for two CH_3OH molecules = 7.94 %)

A collection of analytical data for the series is shown in Tables 2.10 and 2.11 and 2.12.

Zwitterion	Yield (%) / g	Mpt (^{0}C)	λ_{max} (NMF) (nm)
m-C_8H_8(4)DQ6CNQ	0.473 (52)	210-213 (D)†	728
p-C_8H_8(4)DQ6CNQ	0.298 (33)	226-229 (D)†	720
m-C_8H_8(4)DQ6CNTMQ	0.0781 (16)	>300	568
p-C_8H_8(4)DQ6CNTMQ	0.0704 (14)	>300	578

† decomposition (D).

Table 2.10 Analytical Data for the Diquinolinium Adducts.

Zwitterion	C (%) Found (Calc)	H (%) Found (Calc)	N (%) Found (Calc)
p-C_8H_8(4)DQ6CNQ	77.22 (80.85)	4.35 (4.07)	13.95 (15.08)
+ 2 CH_3OH	77.22 (77.39)	4.35 (4.75)	13.95 (13.88)
m-C_8H_8(4)DQ6CNTMQ	77.97 (81.47)	5.65 (5.42)	12.75 (13.10)
+ 2 CH_3OH	77.97 (78.41)	5.65 (5.92)	12.75 (12.19)
p-C_8H_8(4)DQ6CNTMQ	78.68 (81.47)	5.45 (5.42)	12.14 (13.10)
+ 2 CH_3OH	78.68 (78.41)	5.45 (5.92)	12.14 (12.19)

Table 2.11 Micro-analytical Data for the Diquinolinium Adducts.

Zwitterion	Calc (%) loss of 2 CH_3OH	Found (%) loss of 2 CH_3OH
p-C_8H_8(4)DQ6CNQ	7.942	7.963
m-C_8H_8(4)DQ6CNTMQ	6.972	6.426
p-C_8H_8(4)DQ6CNTMQ	6.972	6.152

Table 2.12 TGA Data for the Diquinolinium Adducts.

2.4.6 Synthesis of CH_3(2)P3CNQF_4.

Equation:

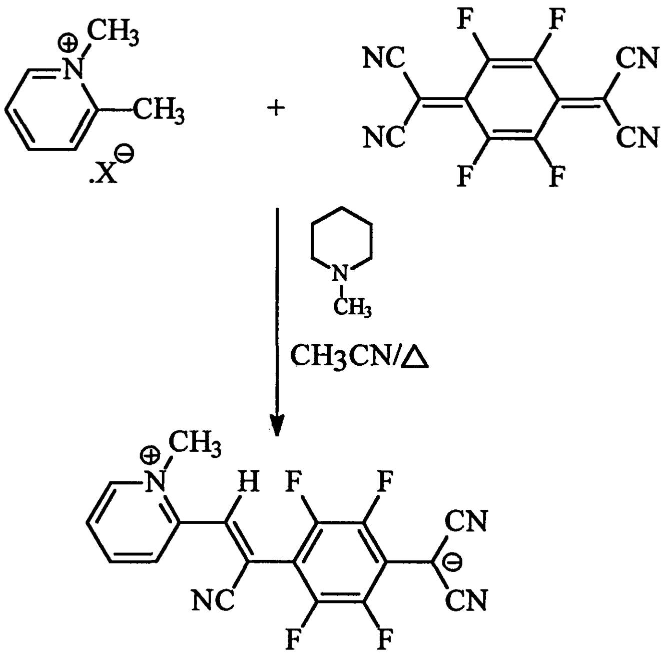

N-Methyl-2-methylpyridinium iodide (0.34g, 0.0014mol) was refluxed with N-methyl piperidine (0.14g, 0.0014mol) in dry acetonitrile (15cm^3) for twenty minutes, during which time the initial pale yellow colour gave way to a deep canary yellow. After cooling slightly, 2,3,5,6-tetrafluoro-7,7,8,8-tetracyano-p-quinodimethane (0.4g, 0.0014 mol) was added and the solution was refluxed for a further hour, during which time the colour changed from the original canary yellow colour to emerald green. After a further four hours reflux the solution, which had turned a deep red/brown colour, was cooled producing a fibrous brick red solid. The product was isolated by vacuum filtration and washed with diethyl ether (3×25cm^3) to remove any unreacted $TCNQF_4$. The crude product was recrystallised from acetonitrile to yield 0.20g (39%) of a brick red solid (Mpt >296^{0}C decomp).

Analytical Data:

IR (KBr): 2995 (C-H str), 2183, 2149 (C≡N str), 1625 (C=C str), 1586, 1491 (Ar C=C str), 1222 (C-F str) cm^{-1}.

^{1}H NMR (d_6-DMSO): δ= 4.35 (s, 3H, $\mathbf{CH_3}N^+$), 7.95 (s, 1H, π-bridge-**H**), 8.2 (t, 1H, Ar-**H**, J=5), 8.65 (d, 1H, Ar-**H**, J=5), 8.75 (t, 1H, Ar-**H**, J=5), 9.2 (d, 1H, Ar-**H**, J=5).

^{13}C NMR (d_6-DMSO): Signal too weak.

^{19}F NMR (d_6-DMSO): δ= -148.42, 148.30 (d, 2F, C-**F**, $J_{F,F}$=48), -144.47, 144.35 (d, 2F, C-**F**, $J_{F,F}$=48).

MS (70eV): *m/z* =356 (14%, M^+), 342 (46%, M^+-CH_2), 329 (50%, M^+-HCN), 323 (100%, M^+-CH_3F).

UV/Vis (CH_3CN): λ_{max} = 310, 510(CT)nm

$C_{18}H_8N_4F_4$ (356.26) Calc: C 60.68 H 2.26 N 15.72 F 21.33 %

Found: C 60.51 H 2.40 N 15.45 F 21.26 %

2.4.7 Synthesis of $C_3H_7(2)BT3CNQ$.[4]

Equation:

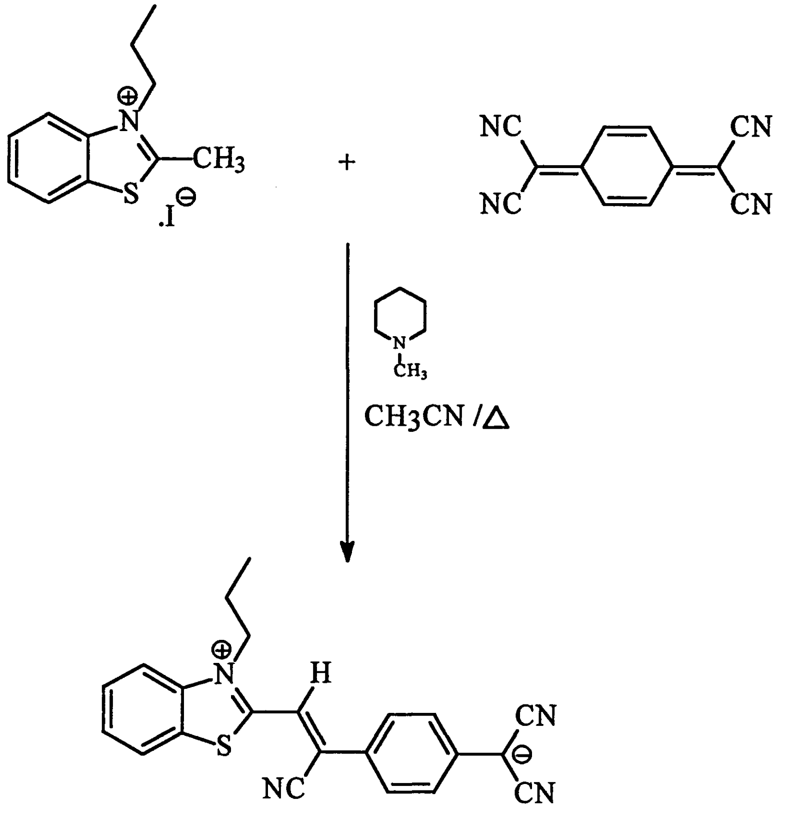

2-Methyl-3-propylbenzothiazolium iodide (0.78g, 0.0024mol) was refluxed with N-methylpiperidine (0.05g, 0.0005mol) in acetonitrile (30cm^3) for twenty minutes, resulting in a colour change from pale yellow to pink. After cooling, 7,7,8,8-tetracyano-p-quinodimethane (0.5g, 0.0024mol) was added and the solution changed again from pink to emerald green. After about half an hour of gentle reflux a green solid began to precipitate out of the solution and deposition appeared complete after about three hours. After this period the solution, which had turned a deep emerald green colour, was cooled producing more of the emerald green solid. The product was isolated by vacuum filtration, washed with diethyl ether (3×25cm^3) to remove any unreacted TCNQ, and methanol (3×25cm^3) to remove any unreacted iodide, yielding 0.52g (57%) of an emerald green solid (Mpt >300^{0}C) that required no further purification to provide an analytically pure sample.

Analytical Data:

IR (KBr): 2930 (C-H str), 2175 (C≡N str), 1601 (C=C str), 1496 (Ar C=C str) cm^{-1}.

^{1}H NMR: Product too insoluble

^{13}C NMR: Product too insoluble

MS (70eV): *m/z* =368 (100%, M$^+$), 326 (96%, M$^+$-C_3H_6), 299 (12%, M$^+$-R-HCN), 289 [8%, M$^+$-R-C(CN)$_2$].

UV/Vis (CH_3CN): λ_{max} = 738(CT)nm

$C_{22}H_{16}N_4S$ (368.4)	Calc:	C 71.72	H 4.38	N 15.21	S 8.70 %
	Found:	C 71.56	H 4.32	N 15.14	S 8.92 %

2.4.8 Synthesis of C_3H_7(2)BT3CNQF$_4$.

Equation:

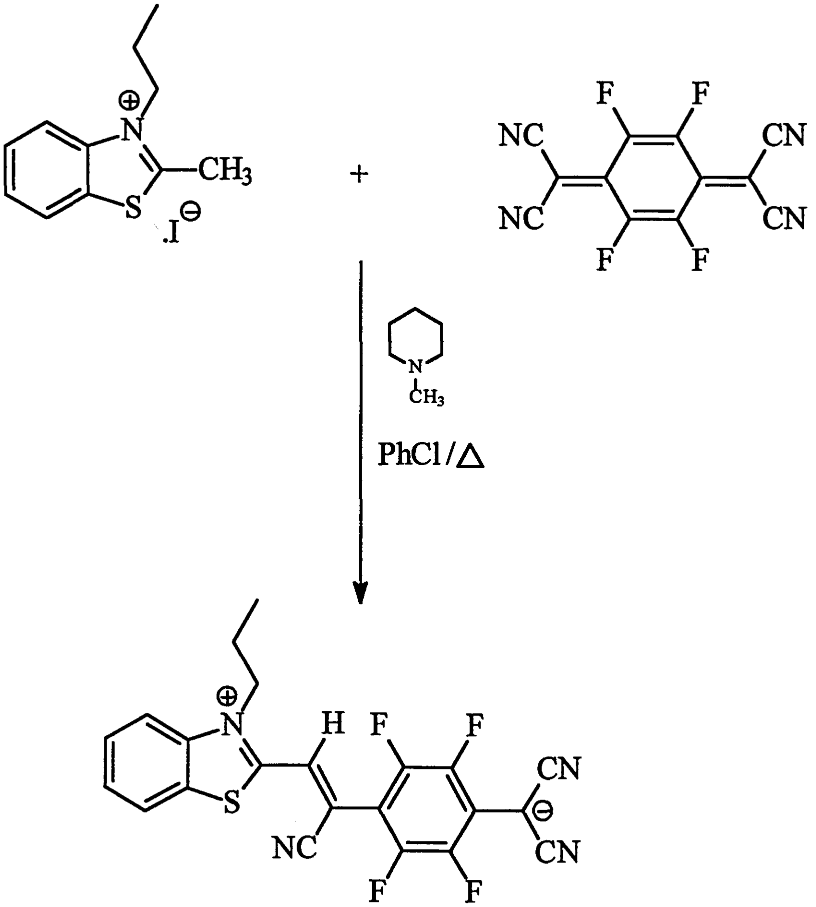

2-Methyl-3-propylbenzothiazolium iodide (0.23g, 0.00072mol) was refluxed with N-methylpiperidine (0.07g, 0.00072mol) in chlorobenzene (30cm^3) for twenty minutes, resulting in a colour change from pale yellow to poppy red. After cooling 2,3,5,6-tetrafluoro-7,7,8,8-tetracyano-p-quinodimethane (0.2g, 0.00072mol) was added and the solution changed from poppy red colour to emerald green. After about half an hour of gentle reflux a gold/green solid began to precipitate out of solution and precipitation appeared complete after about six hours. After this period the solution, which had turned a deep blue colour, was cooled producing more of the gold/green solid. The product was isolated by vacuum filtration and washed with diethyl ether (3×25cm^3) to remove any unreacted TCNQF$_4$. The crude product was recrystallised from acetonitrile to yield 0.170g (54%) of golden green needles (Mpt >304^{0}C).

Analytical Data:

IR (KBr): 2971, 2918 (C-H str), 2192, 2166 (C≡N str), 1631 (C=C str), 1496 (Ar C=C str), 1227 (C-F str) cm^{-1}.

^{1}H NMR (d$_6$-DMSO): δ= 1.0 (t, 3H, **CH$_3$**-R, J=12.5), 1.9 (m, 2H,R-**CH$_2$**), 4.9 (t, 2H, **CH$_2$**N$^+$, J=12.5), 8.0 (m, 2H, Ar-**H**), 8.35 (s, 1H, π-bridge-**H**), 8.5 (d, 1H, Ar-**H**, J=5), 8.6 (d, 1H, Ar-**H**, J=5).

^{13}C NMR (d$_6$-DMSO): Signal too weak.

^{19}F NMR (d$_6$-DMSO): δ= -148.28, 148.31 (d, 2F, C-**F**, $J_{F,F}$=16), -143.09, 143.13 (d, 2F, C-**F**, $J_{F,F}$=16).

MS (70eV): *m/z* =441 (5%, M$^+$), 415 (15%, M$^+$-CN), 398 (16%, M$^+$-CH$_3$CN), 378 [34%, M$^+$-C(CN)$_2$], 333 [14%, M$^+$-R-C(CN)$_2$].

UV/Vis (CH$_3$CN): λ_{max} = 332, 664(CT)nm

$C_{22}H_{12}N_4F_4S$ (440.39) Calc:	C 60.00	H 2.75	N 12.72	F 17.25	S 7.28 %
Found:	C 59.95	H 2.77	N 12.59	F 17.21	S 7.19 %

2.4.9 Synthesis of C_3H_7(2)BT3CNTMQ.

Equation:

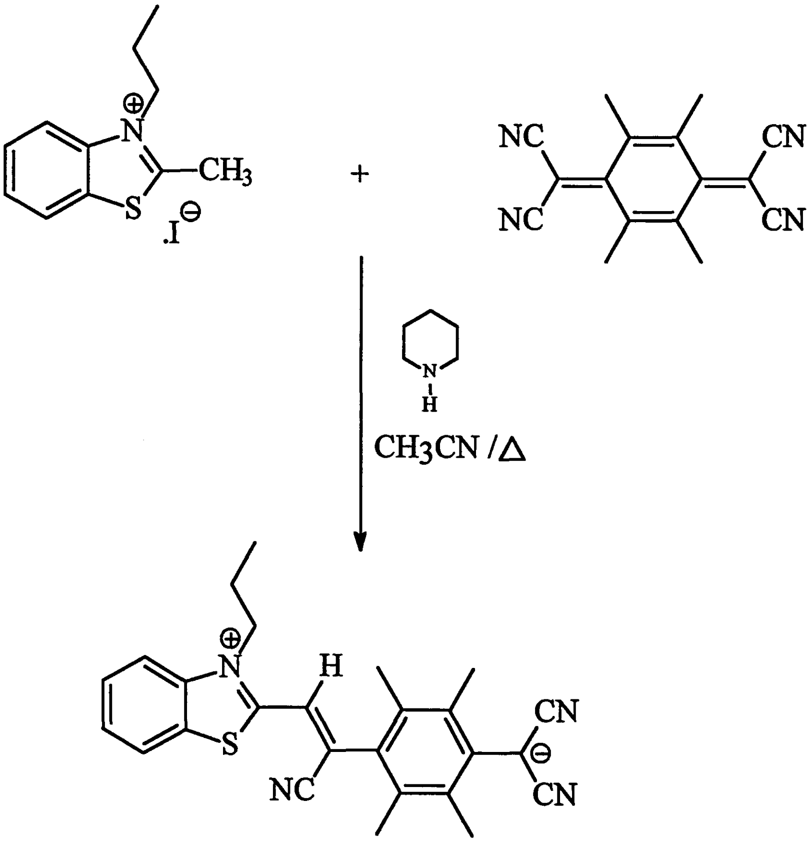

2-Methyl-3-propylbenzothiazolium iodide (0.29g, 0.00094mol) was refluxed with piperidine (0.08g, 0.00094mol) in dry acetonitrile ($30cm^3$) for twenty minutes, resulting in a colour change from pale yellow to poppy red. After cooling, 2,3,5,6-tetramethyl-7,7,8,8-tetracyano-p-quinodimethane (0.25g, 0.00094mol) was added and the solution deepened to a blood red colour. After about three hours reflux the blood red solution, which had become more intense in colour, was cooled producing a brown/yellow powder. The product was isolated by vacuum filtration and washed with diethyl ether ($3\times25cm^3$) to remove any unreacted TMTCNQ. The crude product was chromatographed on a silica gel column (90:10 dichloromethane-methanol) to yield 0.040g (10%) of a canary yellow powder (Mpt >300^0C).

Analytical Data:

IR (KBr): 3447 (O-H str), 2960, 2930, 2873 (C-H str), 2157, 2099 (C≡N str), 1564 (C=C str), 1508 (Ar C=C str) cm^{-1}.

^1H NMR (d_6-DMSO): δ= 1.1 (t, 3H, **CH_3**-R, J=12.5), 1.9 (m, 2H,R-**CH_2**), 2.3 (s, 12H, 4**CH_3**) 5.0 (t, 2H, **CH_2N^+**, J=12.5), 7.9 (t, 1H, Ar-**H**, J=5), 8.0 (t, 1H, Ar-**H**, J=5), 8.4 (d, 1H, Ar-**H**, J=5), 8.55 (d, 1H, Ar-**H**, J=5). 8.95 (s, 1H, π-bridge-**H**).

^{13}C NMR (d_6-DMSO): Signal too weak.

MS (70eV): *m/z* =424 (6%, M^+), 382 (84%, M^+-CH_2CN), 367 (22%, M^+-CH_3CN-CH_3), 318 [9%, M^+-R-C$(CN)_2$], 43 (100%, CH_3CN)

UV/Vis (CH_3CN): λ_{max} = 594(CT)nm

$C_{26}H_{24}N_4S$ (424.53) Calc: C 73.55 H 5.70 N 13.19 %

Found: C 70.31 H 5.62 N 11.61 %

$C_{26}H_{24}N_4S.CH_3OH$ (456.53) C 71.03 H 6.18 N 12.27 %

In an attempt at improving the yield of the above compound it was decided to increase the reflux time since significant amounts of TMTCNQ were being recovered. This met with startling consequences as the initial reaction mixture, which gave a peak at 344nm in the UV/Vis spectra and a yellow spot at R*f* = 0.44 (90:10 DCM/CH_3OH), began to change in appearance with time. The reaction, which had now become a darker red colour, began to show signs of a new red fraction at R*f* ~0.56 (90:10 DCM/CH_3OH) upon TLC analysis, and a new UV/Vis band at ~550nm. As the reaction progressed further, TLC analysis suggested an increase in the relative concentration of this red fraction coupled with consumption of the above adduct (adduct 1). The formation of this new product (adduct 2) appeared complete after about six hours (Figure 2.1), after which time the reaction was cooled, resulting in a brick red solid precipitate.

The recovered solid was washed with diethyl ether (3×25cm^3) to remove any unreacted TMTCNQ.

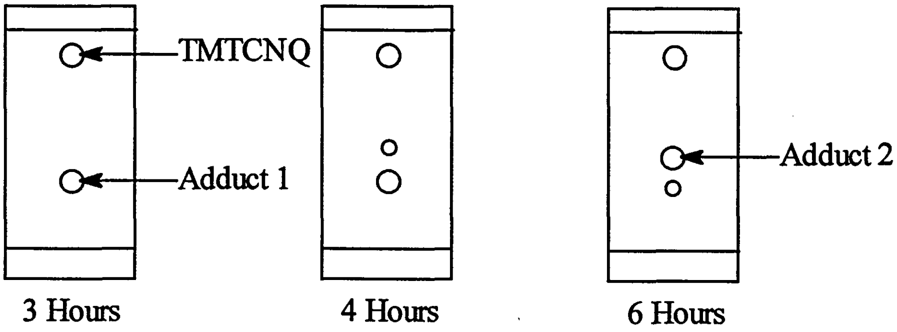

Figure 2.1 TLC Analysis of New Product Formation.

The crude product was chromatographed on a silica gel column (90:10 dichloromethane :methanol), then recrystallised from acetonitrile/diethylether to yield 0.050g (8.47%) of this unidentified brick red coloured powder (Mpt >300^{0}C). The compound was found to give the following analytical data:

IR (KBr): 2923, 2869 (C-H str), 2151, 2089 (C≡N str), 1671, 1563 (C=C str), 1506 (Ar C=C str) cm^{-1}.

^{1}H NMR (d$_6$-DMSO): See section 2.5.4

^{13}C NMR (d$_6$-DMSO): Signal too weak.

MS (FAB): *m/z* =614 (100%, M$^+$+H), 572 (6%, M$^+$-R), 507 [5%, M$^+$-R-C(CN)$_2$].

UV/Vis (CH$_3$CN): λ_{max} = 520, 544(CT)nm

Accurate Mass:	mDa	PPM	Calc.Mass	DBE	C	H	N	S
614.242632	-1.4	-2.3	614.241215	22.5	37	36	5	2

A proposed structure and other relevant details of this benzothiazolium derived adduct will be discussed in Section 2.5 and 2.6.

2.5 Discussion of Synthetic Methods and Results.

2.5.1 N-Alkylation of Nitrogen Heterocycles.

As with most quaternisation reactions,[11] the preparation of N-alkylated pyridinium/ quinolinium salts proceeds via S_N2 type substitution. Also known as the *Menshutkin* reaction,[12,13] this N-alkylation involves displacement of the halide from an alkyl halide by the heterocyclic nitrogen as illustrated (Figure 2.2) by the N-alkylation of lepidine to produce the corresponding γ-substituted quinolinium salt. Formation of the other quaternised salts used in this work follows a similar mechanistic pathway.

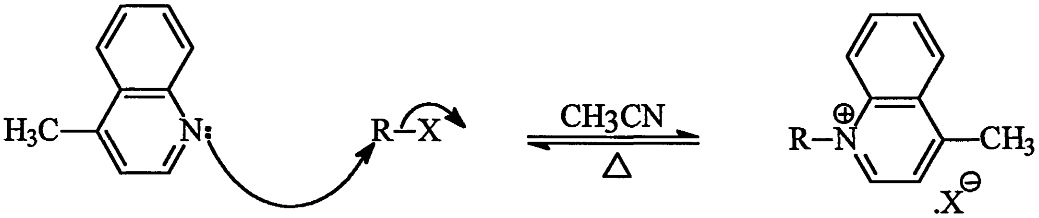

Figure 2.2 Preparation of Quaternised Nitrogen Heterocycles.

Of the various methods available[2,3,5,14] for the preparation of such quaternised salts, a modified version was used to that of *Broughton et al*,[2] who directly refluxed the alkyl halide and the nitrogen heterocycle, resulting in a slight decomposition of the salt. The modified version involves dilution of the reagents with a little acetonitrile solvent, which reduces the reaction temperature and limits the amount of decomposition giving better yields. However longer reaction times are necessary except for N-methylations for which reflux[5] was not required due to the high reactivity of methyl iodide (care was taken as the addition of MeI was potentially explosive).

The choice of alkyl halides was based upon the fact that LB films have been fabricated from other zwitterionic adducts having alkyl chain lengths varying from eight to twenty carbons.[2,15-17] Thus it was decided to try and cover as much of this previously tried and tested range as possible. The C_{16} homologues were especially desirable as studies of area per molecule and UV/Vis spectra of LB films of the unsubstituted R(4)Q3CNQ compounds[2,15-17] had shown an abrupt change in film behaviour occurring at chain lengths greater than or equal to fifteen carbons. It was hoped that this phenomenon would be repeated in the new adducts of substituted-TCNQ's and further investigated, leading to a possible explanation.

The yield of product in most cases was respectable, with the γ-substituted quinolinium salts typically giving yields of 80-90% comparable to, if not slightly larger than, the same compounds prepared by different methods.[2,3,5,14] As expected the α-substituted quinolinium salts, with ortho-methyl steric hindrance of the reaction site gave lower yields,[4] typically around 40%. This was significant even in the N-methylations as the α-substituted quinolinium salt gave a slightly smaller yield than that of the related γ-substituted compound, despite the relatively small incoming methyl group. Another common trend shown by the quinolinium salts (both α and γ) was a decrease in yield with increasing chain length probably attributable to the decreased reactivity and increased size of the larger alkyl halides.

The symmetrical dipyridinium/diquinolinium salts, despite their apparent bulk, gave similar yields to the mono-substituted benzylic quinolinium salt, although yields for the *para*-substituted compounds were somewhat larger than for the corresponding *meta*-compounds.

2.5.2 Quinodimethanes/Quinodiimines by Knoevenagel Condensation.

Synthesis of the electron acceptors, TMTCNQ,[7,18] and TCAQ[6,19,20] can be achieved by exploiting various documented methods. However, of all the possible synthetic routes, the simplest and most widely used is the modified Lehnert procedure,[21,22] first reported by *Hünig et al*,[6] involving direct condensation of the appropriate quinone (i.e. duroquinone in the case of TMTCNQ) with *Lehnert's* reagent[21,22] (malononitrile, pyridine and titanium (IV) chloride). Because other methods require multi-step procedures,[18,20] it was decided to utilise the modified Lehnert procedure to prepare TMTCNQ and TCAQ.

In this *Knoevenagel*[23,24] type reaction the titanium (IV) chloride acts as a Lewis acid, in the absence of which quinones in general do not yield quinodimethanes but undergo conjugate reactions to form phenolic/heterocyclic products.[7,23,25,26] The titanium (IV) chloride activates the quinone carbonyl group by forming a metal-oxygen bond, increasing the polarisation of the carbon-oxygen bond and thus promoting nucleophilic attack at the carbonyl carbon and inhibiting 1,4-addition.[27] (Figure 2.3)

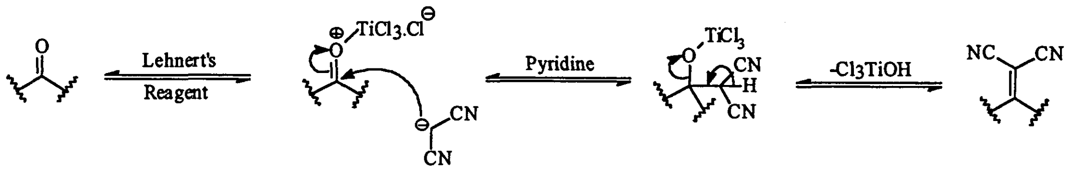

Figure 2.3 Titanium (IV) Chloride Mediated Condensation.

However in the preparation of tetramethyl-TCNQ the use of Lehnert's reagent, which normally results in quinodimethane formation (i.e. 1,2-addition) as the major or sole pathway,[7] leads to side reactions[23,28] resulting in relatively small yields. The unwelcome phenolic by-product (1), which presumably arises from 1,6-addition of malononitrile to the intermediate quinomethane system (2) followed by 1,2-elimination of hydrogen cyanide, is conveniently removed by a dilute alkali wash during workup.

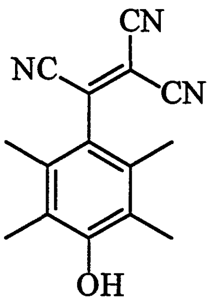

(1)

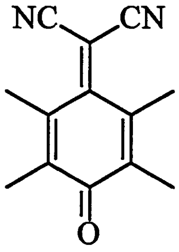

(2)

The overall yield of TMTCNQ, which has been shown to be dependent upon the scale of the reaction[25] (i.e. <6mmol of duroquinone results in no TMTCNQ being formed) was improved by minor modifications. The standard Lehnert method involves the addition of $TiCl_4$ to a solution of the quinone in malononitrile and pyridine. Subsequent work has shown that addition of $TiCl_4$ to a solution of the quinone, followed by dropwise addition of malononitrile and pyridine to the already formed metal-oxygen complex, resulted in larger overall yields (~25%).[25] However the improved yields still remain poor compared to the 55% yield quoted by *Cowan et al.*[7] The Hünig method[6] for preparing TCAQ also required slight modifications as attempts to repeat the literature method failed. Hence an approach similar to that for the tetramethyl acceptor was tried although it resulted in a poorer overall yield of TCAQ relative to the literature method (36% compared to 78%) of *Hünig et al.*[6]

Nevertheless the modified Lehnert procedure for TCNQ derivatives does have its limitations as the reaction can be capricious[25] and does not work for all quinones.[27,29] It seems really successful only for the preparation of tri- and tetra-substituted TCNQ derivatives.[6,7,30-32] This was borne in the attempted preparation of $TCNQF_4$ in a manner comparable to the related N,N'-dicyano-2,3,5,6-tetrafluoro-1,4-benzoquinodiimine[10] whose synthesis follows a very similar mechanistic pathway to the above (Figure 2.3). This was a relatively straightforward procedure requiring only a modified $TiCl_4$-mediated condensation of *p*-fluoranil with bis(trimethylsilyl)carbodiimide (BTC)[33] to afford the desired product. This preparation of the tetra-fluorinated diimine electron acceptor from the corresponding *p*-benzoquinone led to the false hope that the corresponding fluorinated-TCNQ derivative could also be prepared by a Knoevenagel reaction (Figure 2.4). However the attempted preparation of this powerful and extremely expensive electron acceptor (5mg = £18.50),[34] via a $TiCl_4$-mediated condensation reaction, resulted in failure.[35]

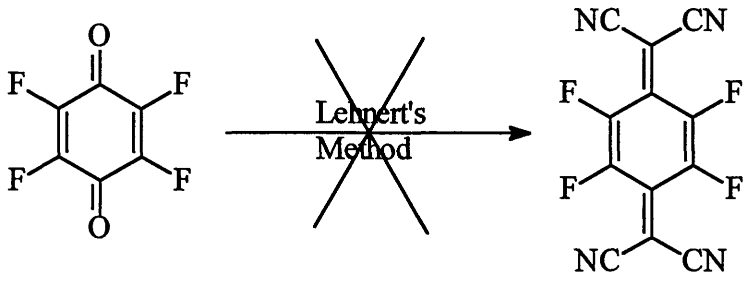

Figure 2.4 Synthesis of $TCNQF_4$ via Lehnert's Method.

This seems quite surprising in a nucleophilic process since the relatively unreactive duroquinone, with its electron donating methyl groups, does form a quinodimethane while the tetra-halogenated benzoquinone, with its electron withdrawing fluorine substituents, does not.

2.5.3 Synthesis of 2,3,5,6-Tetrafluoro-7,7,8,8-tetracyano-p-quinodimethane.

The preparation of this powerful electron acceptor was eventually achieved using a five step route via isopropylidenemalononitrile. The approach was essentially that of *Wheland* and *Martin* in their original synthesis of $TCNQF_4$,[8] although slight modifications were required.

The published preparation of isopropylidenemalononitrile,[36] using the supposedly superior β-alanine as a catalyst[23] was found to be capricious in large scale reactions and an alternative was sought. This type of Knoevenagel reaction[34] is usually catalysed by base, of which many have been tried and tested.[23,34,37-39] However superior results were reported, in terms of ease of preparation, when using an ammonium acetate/acetic acid catalyst.[9] Despite the relatively low yield of this reaction (~60%), it can easily be scaled up so that large quantities (>200g) of isopropylidenemalononitrile are available in less than a day.

The preparation of *t*-butylmalononitrile was achieved using the original *Wheland* method,[8] in which the aliphatic dicyano compound is prepared via a *Michael* reaction[40] using methylmagnesium bromide. Yields of the reaction, in which isopropylidenemalononitrile is the *Michael* acceptor, varied upon the rate of addition of the alkene which resulted in the formation of a yellow/orange suspension. If the addition was too fast then the viscosity of the suspension became so thick that the reaction could not be stirred leading to smaller yields. This problem was slightly alleviated by the addition of more diethyl ether (150cm^3) to the reaction mixture which, despite increasing the yield slightly (51%), still gave a smaller yield than that quoted (75%) in the original paper.[8]

Access to 2,3,5,6-tetrafluoro-1,4-bis(*tert*-butyldicyanomethyl)benzene involves a nucleophilic aromatic substitution reaction via a resonance stabilised hexadienyl anion intermediate[41,42] which is stabilised by the electron-attracting fluorine atoms. Subsequent ejection of two fluorine ions completes the addition-elimination mechanism (Figure 2.5), giving the 2,3,5,6-tetrafluoro-1,4-bis(*tert*-butyldicyanomethyl)benzene product in yields consistent with those reported by *Wheland et al.*[8]

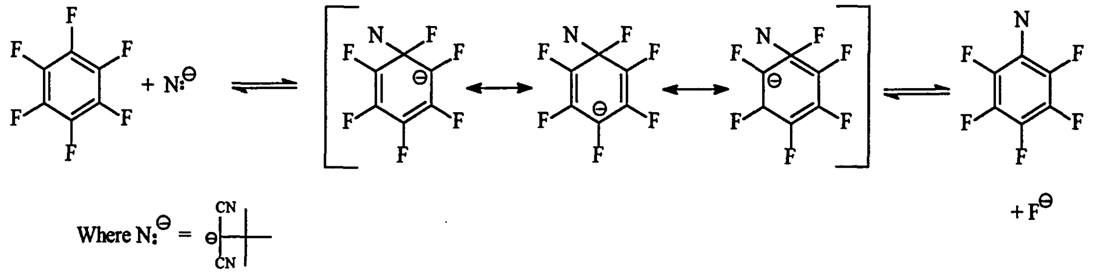

Figure 2.5 Nucleophilic Aromatic Substitution of Hexafluorobenzene.

The final two steps of the preparation were achieved in a one-pot procedure. The 2,3,5,6-tetrafluoro-1,4-bis(*tert*-butyldicyanomethyl)benzene product (from above) was pyrolysed resulting in the loss of 2 equivalents of isobutene and the formation of the intermediate 2,3,5,6-tetrafluoro-1,4-phenylenedimalononitrile. This, in turn was treated with excess bromine water to yield the powerful electron acceptor $TCNQF_4$. However this oxidation using excess bromine water was not so straightforward as claimed by *Wheland*[8] since it gave relatively large quantities of $TCNQF_4(H_2)$ as well as the desired $TCNQF_4$ which was only isolated by repeated recrystallisation from acetonitrile or by cold-finger sublimation leading to much smaller yields than those quoted in the original paper (72-85%).[8]

2.5.4 Synthesis of Zwitterionic D-π-A Adducts of TCNQ.

Synthesis of the zwitterionic D-π-A adducts of substituted electron acceptors such as $TCNQF_4$ involves substitution of a nitrile group in the relevant electron acceptor by the appropriate quinolinium/picolinium or benzothiazolium donor moiety. The preparation of such compounds has varied, with numerous methods being documented in the literature.[15,16,43-45] The zwitterions were originally obtained by prolonged reaction of the appropriate N-alkylated donor with the lithium salt of TCNQ (Li^+TCNQ^-) in hot acetonitrile[17,43] (diagrammatically illustrated in Figure 2.6).

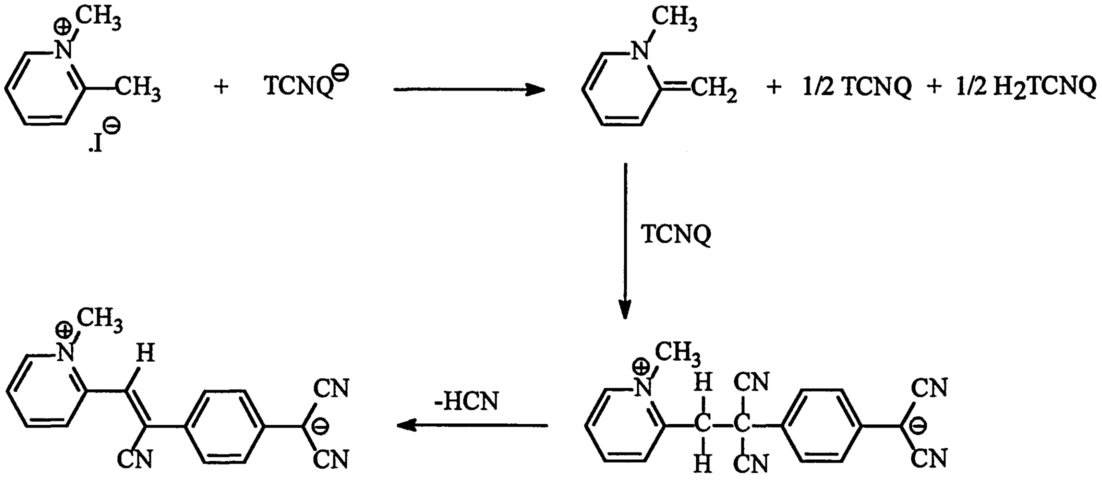

Figure 2.6 Proposed Mechanism for the Synthesis of $CH_3(2)P3CNQ$ using LiTCNQ

This method was refined by *Ashwell et al*[45] giving shorter reaction times and improved yields. However the modification involves the lithium salt of the corresponding TCNQ which has not been accessible in the case of TCAQ and TMTCNQ. The preparation of the only reported fluorinated zwitterion[3,46] [$C_{16}H_{33}(4)Q3CNQF_4$] used the lithium salt but gave a relatively poor yield.

Another approach, and that most widely used[15-17,44] for the preparation of adducts, involves the use of piperidine or N-methylpiperidine as a base to remove a proton from the ring methyl group of the N-alkylated donor. This is very similar to the method used for the preparation of merocyanine/hemicyanine dyes from N-alkyl benzo[c]quinolizinium/quinolinium salts in which piperidine is again used as base.[47,48]

The removal of the methyl proton produces a relatively stable species having a resonance form in which the lone pair of electrons is situated on the electron deficient nitrogen. The resulting, nucleophile active at the exocyclic methylene, reacts with

TCNQ, or one of its derivatives, forming a new carbon-carbon double bond between what started as a methyl carbon substituted on the donor N-heterocycle ring and a $\underline{C}(CN)_2$ carbon atom on the acceptor moiety. Because of the shortcomings of the LiTCNQ methods,[43,45] such as low yields and long reaction times, the alternative piperidine/N-methyl piperidine method was employed for the vast majority of the synthetic work undertaken. Despite the apparent structural differences in the various adducts, they were all approached using this same methodology. The same mechanistic pathway, illustrated in Figure 2.7 by the synthesis of an R(4)Q3CNQF$_4$ type adduct, is probable for all the preparations.

While neither approach gave huge yields our preparations using piperidine/N-methylpiperidine gave markedly better yields than those observed by other authors using the LiTCNQ method.[3] This was probably because piperidine/N-methylpiperidine are much stronger bases than LiTCNQ (cf. Figures 2.6 and 2.7).

The majority of synthetic work used N-methylpiperidine as base since piperidine, a secondary amine, may react with TCNQ[49] leading to side products causing the desired product to be somewhat impure,[2] a major limitation of the piperidine method. N-Methylpiperidine, being a tertiary amine (much less nucleophilic), will not react with TCNQ or its derivatives,[49] although the desired reaction is somewhat slower. Steric factors also affect the yield and rate of reaction, as shown by the reduced yields and increased reaction times of the more sterically crowded R(2)Q3CNQF$_4$ adducts relative to their R(4)Q3CNQF$_4$ counterparts. The length of the alkyl chain of the adducts also has a noticeable effect on yield and reaction time, as the yield diminishes with increasing chain length for both α- and γ-substituted fluorinated compounds.

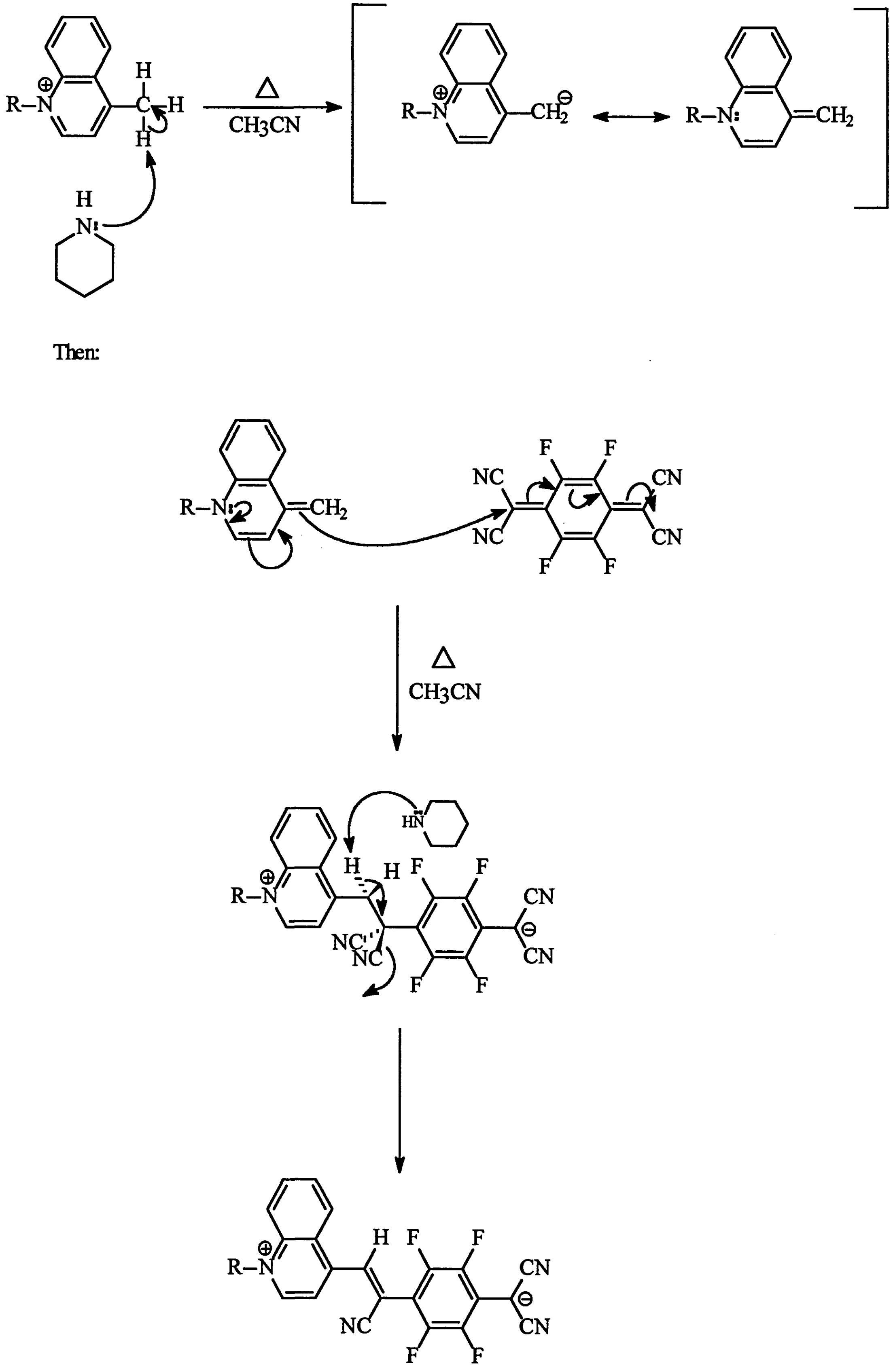
R–N
H
C
H
H
Δ
CH3CN
H
N:
R–N
CH2
R–N:
=CH2
Then:
R–N:
=CH2
NC
NC
F
F
F
F
CN
CN
Δ
CH3CN
HN
R–N
H
H
F
F
CN
CN
NC
NC
F
F
R–N
H
F
F
CN
CN
NC
F
F

Figure 2.7 Proposed Mechanism for the Synthesis of R(4)Q3CNQF$_4$ using Piperidine.

The use of acetonitrile as opposed to a polar protic solvent like methanol, which has been employed before,[15] is preferable since methanol would tend to solvate the carbanionic resonance structure of the nucleophile formed in the reaction, hence limiting its reactivity. The use of acetonitrile does, however, raise the possibility of photolytic side reactions occurring between the solvent and the TCNQ derivative,[50] resulting in potentially smaller and impure yields.

The use of chlorobenzene, shown by *Ashwell et al*[16] to improve the yield and ease of preparation in TCNQ-based adducts, had negligible effects upon the yields obtained for our substituted-TCNQ adducts, which were similar for both solvents. However the yield of C_3H_7(2)BT3CNQF_4 was increased by some twenty percent upon switching to chlorobenzene.

The yields obtained for the benzothiazolium-based adducts were about twenty percent higher than those observed for the fluorinated quinolinium-based adducts. Exceptions were the fluorinated N-methyl adducts which, in the case of the γ-substituted compound, gave the greatest yield of any of the adducts prepared. The increased yields of benzothiazolium compounds (the exception being the tetramethyl-adduct) is thought to be a consequence of the increased stabilisation of the exo-methylene nucleophile. The presence of a sulphur heteroatom, with its lone pair of electrons, in the electron donor moiety (Figure 2.8) can help accommodate the charge and thus provide another resonance canonical form.

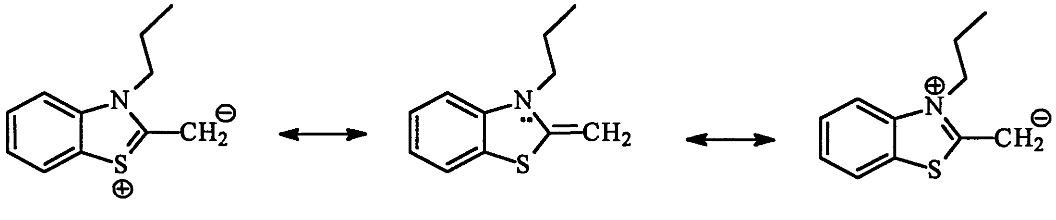

Figure 2.8 Resonance Forms of the Benzothiazolium Intermediate.

On the other hand the attempted synthesis of TCAQ-based adducts, using a similar approach to that used in the formation of the other quinolinium-based adducts, resulted in failure (See Section 2.4.4). Various experimental conditions, including standard literature methods,[15,16] were employed as well as the variation of solvent (i.e. $CHCl_3$, CH_3CN, C_2H_5CN and PhCl), base (i.e. piperidine, N-methylpiperidine, DBU, DBN, DABCO) and of the reaction time (i.e. from twenty-four hours to thirty-five days). The reactions were monitored by looking for the characteristic long-wavelength charge-transfer (CT) absorption band exhibited by such compounds. In some cases CT bands were observed to a small extent and in others not at all. In all cases a colour change was observed during the reaction (red to black) and black microcrystalline solids were isolated along with unreacted starting materials. However, the isolated solids did not give the correct analytical data for the required product.

The failure may be due to a number of reasons. The first is that 11,11,12,12-tetracyano-9,10-anthraquinodimethane (TCAQ) is not a planar molecule.[51] The non-planarity is due to strong non-bonding interactions between the cyano groups and the aromatic hydrogens in the peri positions on the anthracene ring (Figure 2.9).

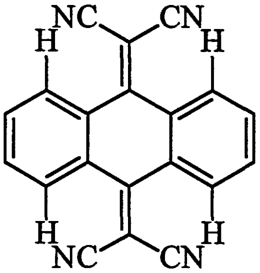

Figure 2.9 Distortion in TCAQ.

For a planar conformation the C-H and N$\cdots$H distances between the cyano groups and the peri hydrogen are calculated to be 1.898 Å and 2.256 Å[52] respectively. To avoid these interactions and thus alleviate the steric strain, the central TCNQ ring folds producing a butterfly structure in which the benzene rings (the "wings of the butterfly") point upwards and the dicyanomethanide units point downwards. Thus there is a loss of planarity as confirmed by an X-ray structure of TCAQ.[51] The distortion makes charge-transfer within the system difficult due to the poor overlap of the π-orbitals,[26,51] thus discouraging formation of the adduct.

Another possible reason behind the failure is the increased benzannelation in TCAQ which has the effect of reducing the overall electron accepting capability of the molecule.[6,20] This, together with its non-planar structure, makes TCAQ an unsatisfactory acceptor for the production of D-π-A adducts, as has been observed by other authors.[4,53] Furthermore the TCAQ system, which embodies two extra benzene rings, is very much larger than TCNQ creating steric hindrance to attack by the quinolinium nucleophile. This, aided by the poor electron-accepting capability of TCAQ,[6,20] further diminishes the chance of a successful reaction.

Despite the discouraging lack of success in preparing adducts from the non-planar TCAQ, subsequent work showed that the equally distorted tetramethyl-TCNQ derivative (TMTCNQ)[18] did, unexpectedly, form D-π-A adducts with quinolinium and benzothiazolium donors. In the case of the quinolinium-based adducts however, the analytical data seemed contradictory. On the one hand the appearance of a molecular ion and its identifiable mass spectral fragments (see Section 2.6.3), along with two nitrile stretching bands in the infrared spectrum (see Section 2.6.2), seemed to confirm successful coupling of the quinolinium heterocycle with the distorted electron acceptor. On the other hand, however, elemental analysis suggested that the adducts were far from pure whereas thin layer chromatography (TLC) using 90:10 dichloromethane:

methanol, implied purity by the observation of a single spot. This discrepancy could be attributed to the presence of methanol trapped in the crystal lattice[54] of the adduct. Evidence for this hypothesis is observed in infrared spectra, which all show a broad band at ≈3400 cm^{-1} consistent with an O-H stretching frequency.

The intense O-H stretching frequency is thought to arise from methanol molecules associated with the adducts, either by hydrogen bonding or by physical entrapment in the lattices, during recrystallisation. However this hypothesis must be treated with caution as the lack of physical evidence (i.e. no NMR or DSC/TGA data due to insufficient sample resulting from the very low yields obtained) means that any conclusions drawn may be open to other interpretations.

Bis-Adduct from TMTCNQ.

An unexpected and unique observation arose while preparing adducts of tetramethyl-TCNQ (TMTCNQ). Attempts to form a benzothiazolium adduct were thwarted by low yields and, as a result, we investigated strategies involving longer reaction times and varying quantities of reactants/reagents. Improved conditions were indeed found, involving a prolonged reaction time, whereby adequate conversion to a mono-adduct occurred. TLC monitoring, however, indicated that a second, dark red adduct began to form once some of the anticipated, yellow adduct was present. Further investigations led to the observation that the new product was actually formed using the mono-adduct as starting material. The new adduct (as well as the mono-adduct) was eventually isolated in sufficient quantities for structural analysis and was shown to be a 1:2 bis-adduct of TMTCNQ with the benzothiazolium system in a highly conjugated, delocalised structure of formula $C_{37}H_{35}N_5S_2$. A proposed structure is shown in Figure 2.10(a) and evidence for the structure is presented in the following pages.

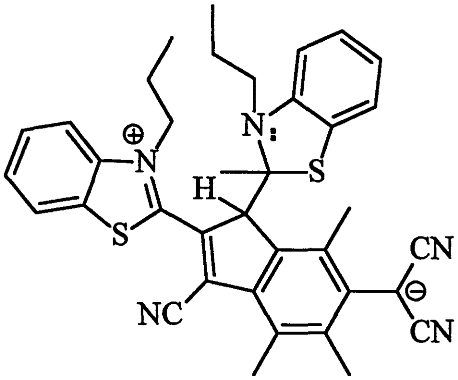

Figure 2.10(a) Proposed Structure for the New Bis-Adduct.

Elucidation of the Proposed Structure.

The formation of bis-adducts from TCNQ with nucleophiles is not new and literature precedent[49] suggests that both nucleophiles will attach, in sequence, at the same end of the TCNQ substrate. Such a reaction in this case would lead to the formation of the bis-adduct shown in Figure 2.10(b).

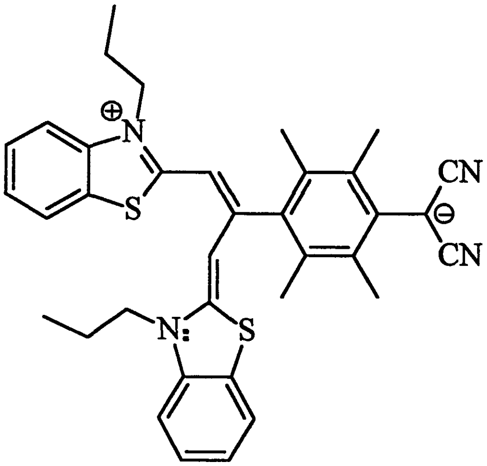

Figure 2.10(b) Possible Bis-Adduct from Literature Precedent.[49]

The structure in Figure 2.10(b) is, in fact, untenable for several reasons including its incompatibility with most of the analytical data obtained. It was not, in any case, given serious credence since comparable bis-adducts were not seen in any of the other preparations with other heterocyclic nucleophiles or, crucially, with any other TCNQ acceptors including both TCNQ itself and tetrafluoro-TCNQ both of which should give bis-adducts more easily than TMTCNQ (less hindered and more electrophilic).

After thorough purification spectroscopic data was obtained for the new adduct which, together with other observations, led us to the following stipulations for its structure and for the mechanism of its preparation.

1. It is formed from the mono-benzothiazolium TMTCNQ adduct and the TMTCNQ methyl groups are a key to its formation.

2. The IR Spectrum (Figure 2.11) suggests two types of environment for nitrile groups and, together with the molecular formula, supports the presence of three nitrile groups (with N_2S_2 arising from two benzothiazolium moieties).

3. It has RMM = 613/614 (FAB-MS with peak-match mass measurement- e.g. Figure 2.12) implying a molecular formula of $C_{37}H_{35}N_5S_2$ (= 613.8).

4. Electron impact MS generates small fragments of the molecule two of which (m/z = 227.9 and 184.9) suggest a benzothiazolylacrylonitrile feature in the adduct as found in mono-adducts also [Figure 2.10(c)].

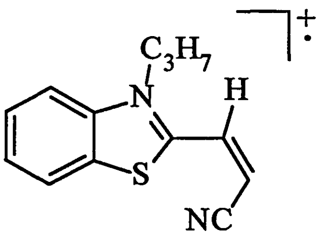

$m/z = 228$
(loss of C_3H_7 gives 185)

Figure 2.10(c) Benzothiazolylacrylonitrile Fragment.

However the vinyl H shown is probably not present in the intact molecule since such a proton occurs at ca. 9δ in the NMR of adducts containing the feature, whereas no such signal appears in the spectrum of the new adduct (Figure 2.13).

5. The ^{1}H NMR (Figure 2.13) implies that only three of the four TMTCNQ methyls have survived the reaction intact, with two appearing at 2δ and the third at 2.6δ.

6. NMR also confirms two benzothiazolium moieties in two different environments, as shown by the comparable $C\underline{H}_3CH_2C\underline{H}_2$-N signals at 0.8 and 1.2δ and 4.6 and 4.9δ (cf 1.7 and ca 2.05δ for the central CH_2) and also by the pairs of signals in the benzene ring part of the spectrum (7.2 - 8.5δ).

7. UV/Vis spectroscopy shows charge-transfer activity (Figure 2.14) suggesting that the structure should be capable of equilibrating between uncharged and zwitterionic forms.

The structure proposed in Figure 2.10(a) results from consideration of each of the foregoing points together with a careful analysis of the high resolution NMR spectrum and an attempt to plot a mechanistic pathway, from the mono-adduct as substrate, that makes chemical sense.

The NMR spectrum (Figure 2.13) is marred slightly by additional, non-integral signals. Low solubility led to the use of d_6-DMSO as NMR solvent. DMSO itself appears separate from significant signals at 2.5δ but the water peak (3.35δ) almost masks a sharp singlet which corresponds quite well with CH_3 attached to a benzothiazolium moiety. Other non-integral signals (from solvents?) appear at 1.5δ, 1.95δ, 2.25δ and

2.65δ (all sharp) and, probably under the CH_3 signal at 2.3δ. The only other signal is a sharp, one-proton singlet at 6.3δ while notably absent are any doublets/triplets etc in the vinyl part of the spectrum and certainly the grouping H-C=C-CN is absent since there is no signal at 9δ. The spectrum suggests that the mono-adduct substrate has reacted with a second molecule of N-propyl-2-methylbenzothiazolium iodide via one of the TMTCNQ methyl groups giving a product of low solubility that contains three TMTCNQ derived methyls, one methyl derived from the 2-methylbenzothiazolium group and just one other (uncoupled) proton, at 6.3δ, apart from benzene ring protons and N-propyl protons of the two benzothiazolium groups.

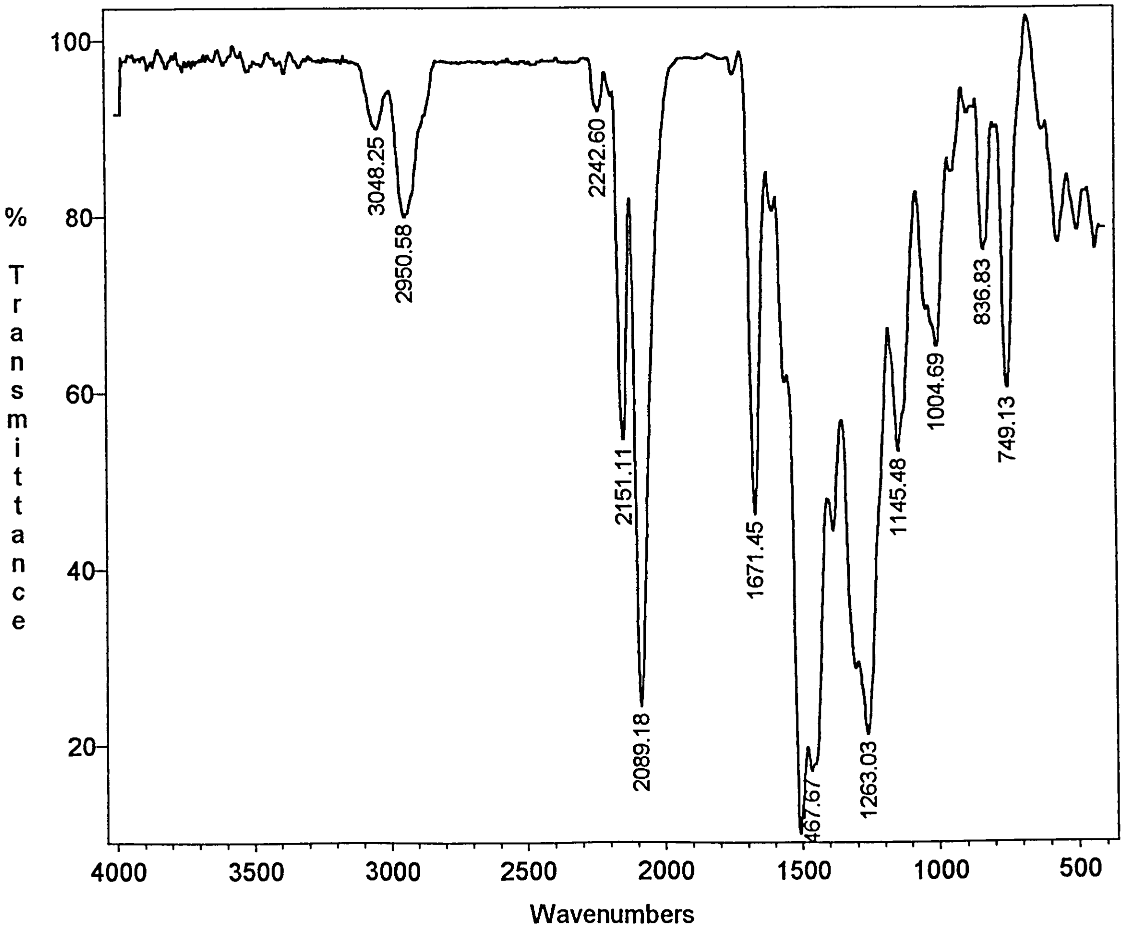

Figure 2.11 Infrared Spectrum Obtained for the C_3H_7(2)BT3CNTMQ Bis-adduct.

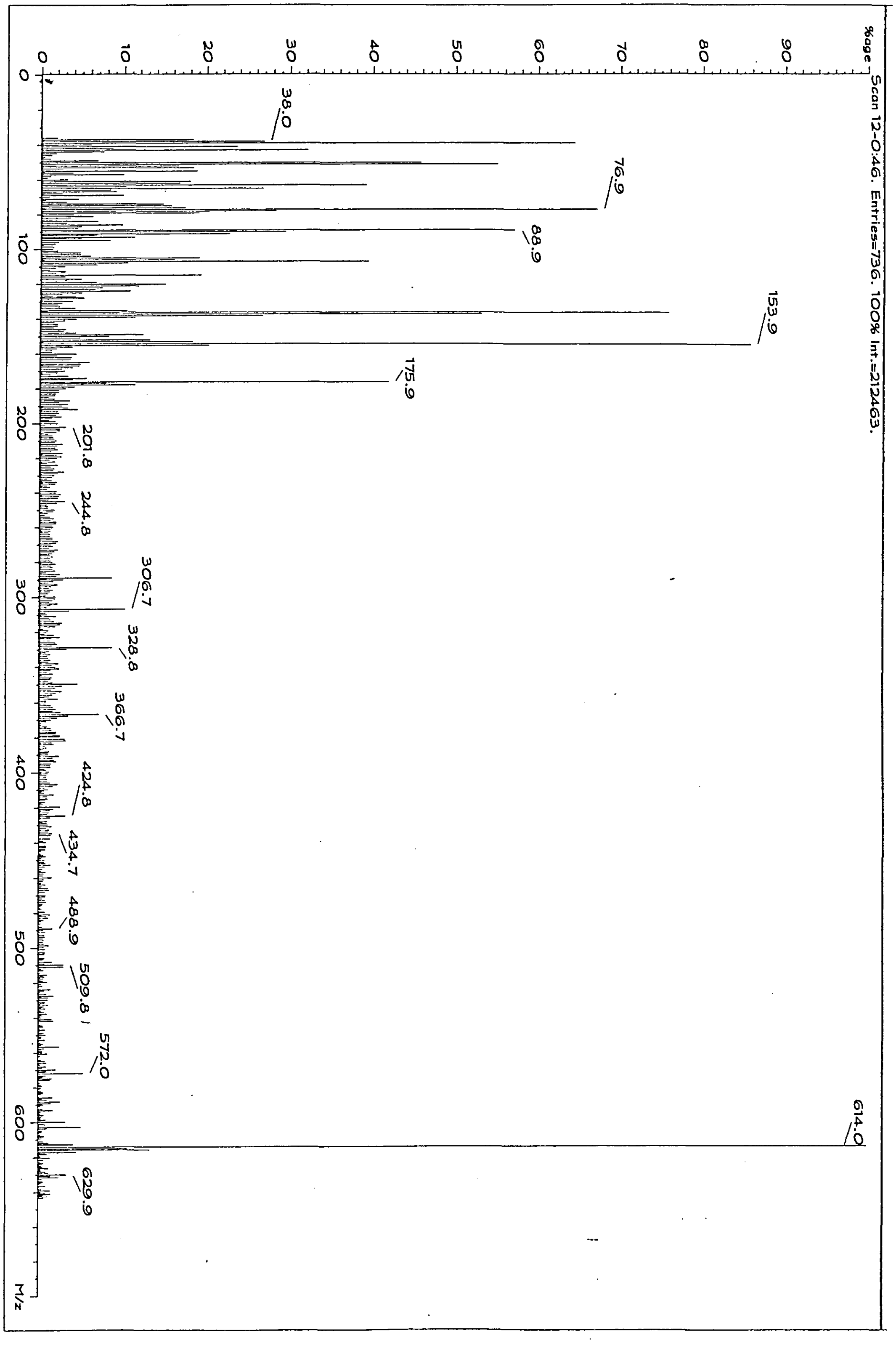

Figure 2.12 FAB-MS Spectrum Obtained for the C_3H_7(2)BT3CNTMQ Bis-Adduct.

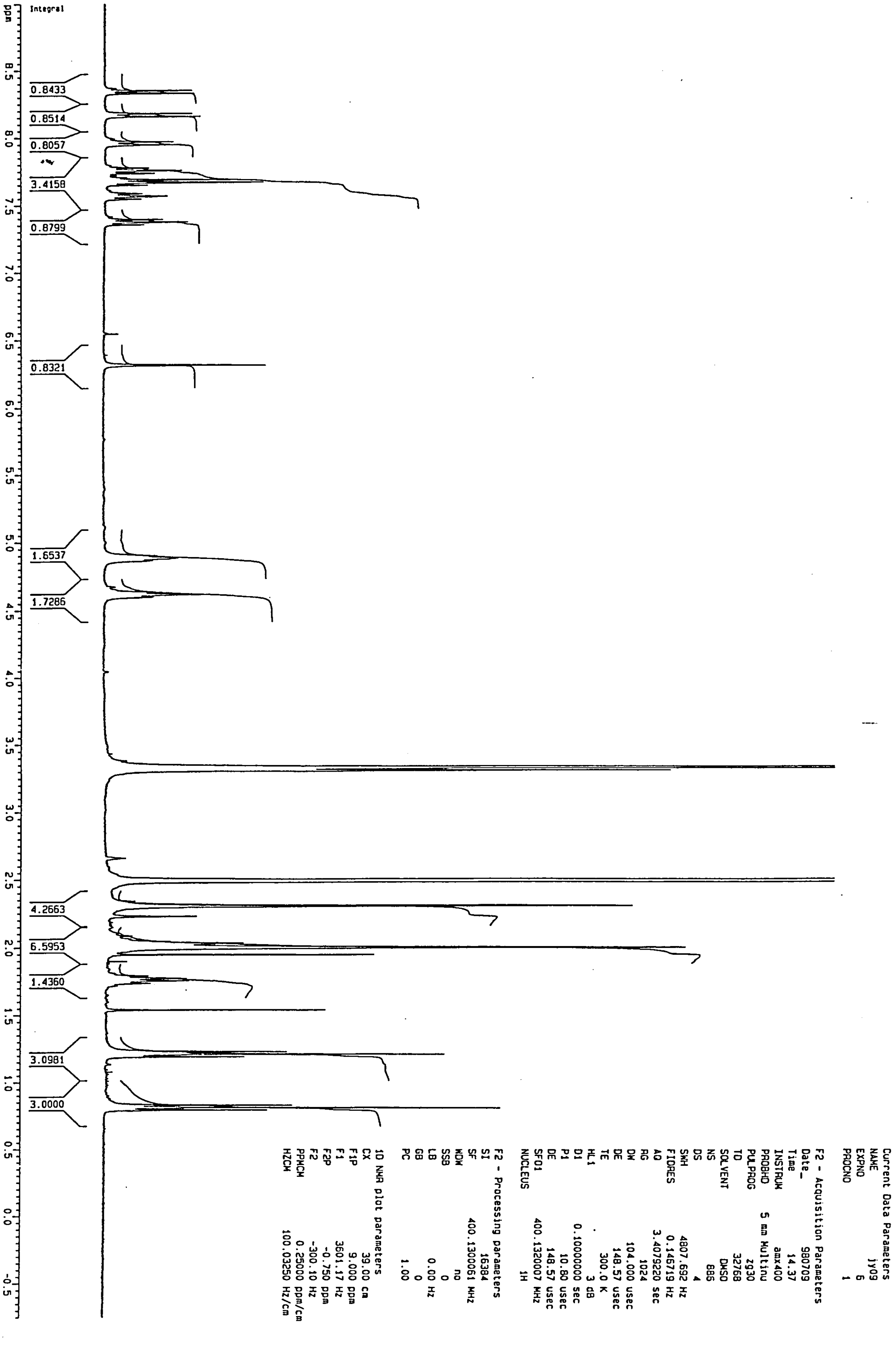

```
Current Data Parameters
NAME              jy09
EXPNO                6
PROCNO               1

F2 - Acquisition Parameters
Date_           980709
Time             14.37
INSTRUM         amx400
PROBHD    5 mm Multinu
PULPROG           zg30
TD               32768
SOLVENT           DMSO
NS                 886
DS                   4
SWH           4807.692 Hz
FIDRES        0.146719 Hz
AQ           3.4079220 sec
RG                1024
DW             104.000 usec
DE              148.57 usec
TE               300.0 K
HL1                  3 dB
D1          0.10000000 sec
P1               10.80 usec
DE              148.57 usec
SF01       400.1320007 MHz
NUCLEUS             1H

F2 - Processing parameters
SI               16384
SF         400.1300061 MHz
WDW                 no
SSB                  0
LB                0.00 Hz
GB                   0
PC                1.00

1D NMR plot parameters
CX               39.00 cm
F1P              9.000 ppm
F1             3601.17 Hz
F2P             -0.750 ppm
F2             -300.10 Hz
PPMCM          0.25000 ppm/cm
HZCM         100.03250 Hz/cm
```

Figure 2.13 ^{1}H NMR Spectrum Obtained for the C_3H_7(2)BT3CNTMQ Bis-Adduct.

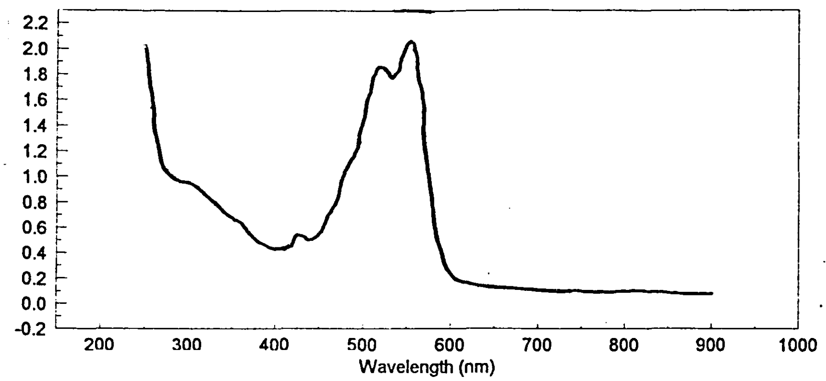

Figure 2.14 C_3H_7(2)BT3CNTMQ Bis-Adduct in Acetonitrile.

Possible Mechanism for the New Adduct.

The exclusive nature of bis-adduct formation, only from the TMTCNQ and 2-methylbenzothiazolium iodide, suggests that the mechanism begins via reactivity of the TMTCNQ methyl groups. It is proposed therefore that the base present abstracts a proton from one of the "acidic" methyl groups and that the resultant nucleophile attacks a benzothiazolium molecule that acts as electrophile (leading to retention of its 2-methyl group) as shown in Figure 2.15.

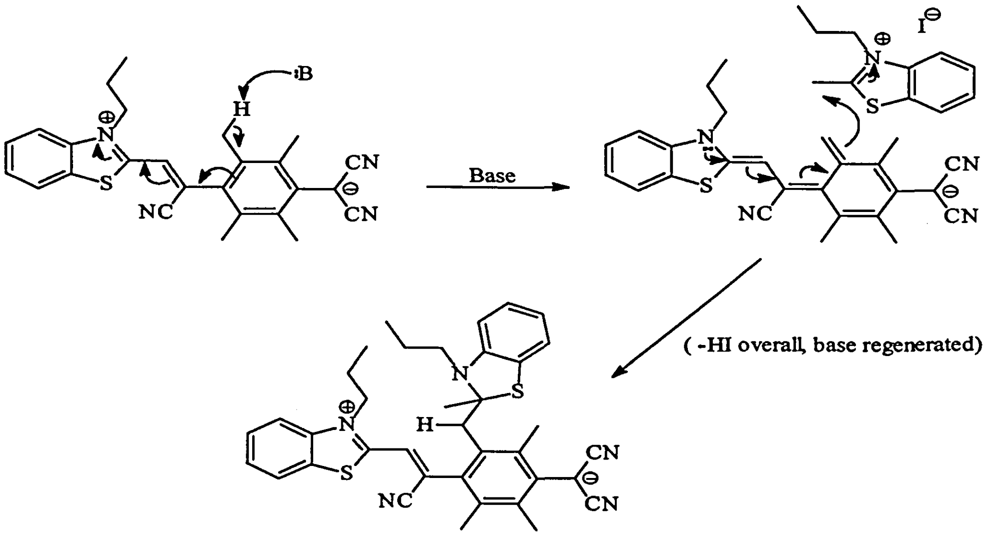
:B
H
N
S
NC
CN
CN
Base
I
N
S
NC
CN
CN
(-HI overall, base regenerated)
N
S
H
N
S
NC
CN
CN

Figure 2.15 Generation and Reaction of C_3H_7(2)BT3CNTMQ Nucleophile.

The initial product (above) still contains an acidic (benzylic) proton and the anion formed by its removal is ideally arranged to close a five membered ring via Michael attack at the acrylonitrile moiety (Figure 2.16).

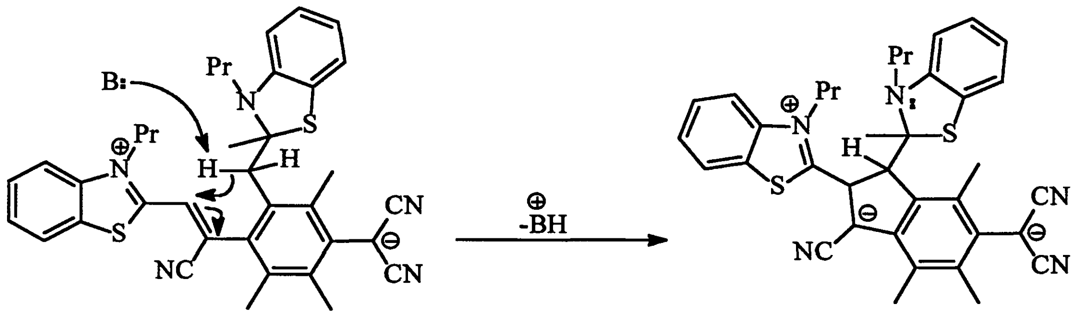

Figure 2.16 Five-Membered Ring Formation.

A formal Michael addition can be completed via protonation of the new carbanion but the anion itself suggests that a driving force for the novel reaction could be aromatisation. Dehydrogenation of the anion creates a 10π benzocyclopentadienyl anion rather like cyclohexa-1,3-diene leads to benzene [Figure 2.17(a)].

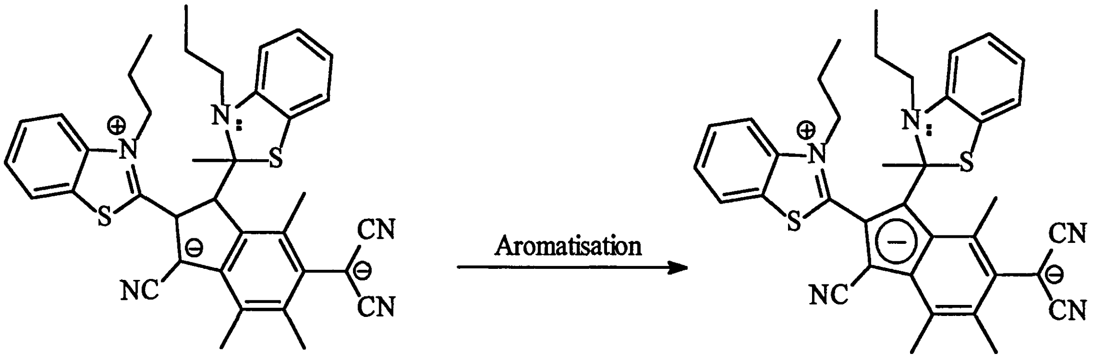

Figure 2.17(a) Formation of 10π Benzocyclopentadienyl Anion.

It is proposed that the aromatisation process could involve unreacted TMTCNQ as reagent and could proceed via hydride expulsion onto TMTCNQ followed by deprotonation (by either TMTCNQ^{-} or piperidine) to the aromatic anion as shown in the partial structures of Figure 2.17(b)

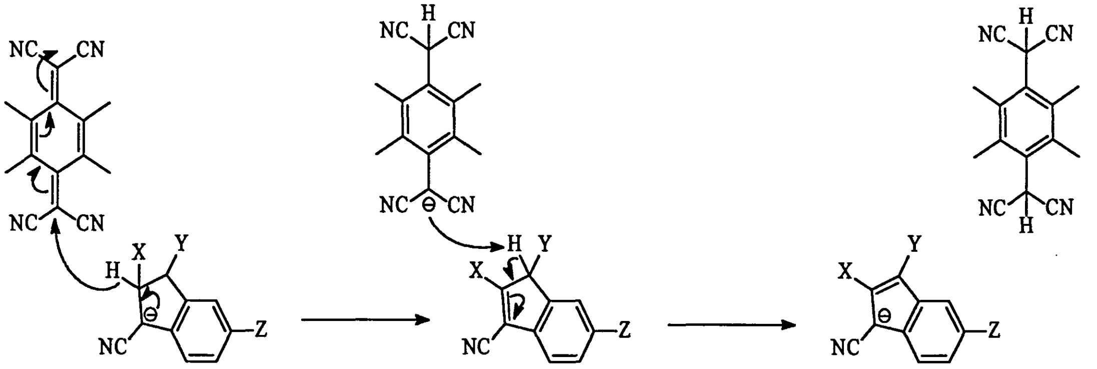

Figure 2.17(b) Possible Aromatisation Mechanism.

A neutral form of the bis-adduct product can then arise by protonation of the aromatic anion (e.g. by ^{+}BH from Figure 2.16) giving $C_{37}H_{35}N_5S_2$ but the resulting C-H bond would be highly acidic and the proton highly mobile through a range of isomeric structures. UV/Vis spectroscopy suggests that a favoured form would allow a simple equilibrium between uncharged and zwitterionic forms. That form, the proposed final structure, could arise via allylic rearrangement of the structure generated in Figure 2.17(a/b) after protonation, as shown in Figure 2.18.

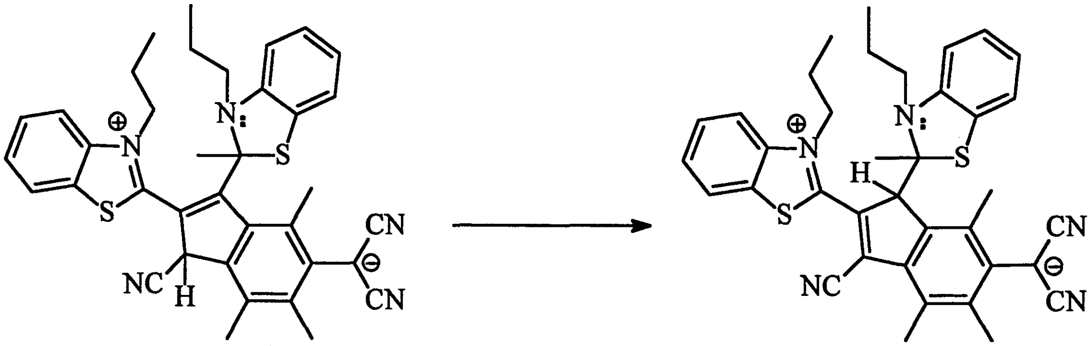

Figure 2.18 Allylic Rearrangement to the Proposed Structure.

The proposed structure seems consistent with MS and IR data, and seems to provide a reasonable fit with the NMR data if the signals at 3.3δ (shoulder to H_2O peak) and 6.3δ are assigned to the quaternary methyl on the upper heterocycle and to the allylic H respectively. The structure is also consistent with the UV/Vis observation (Figure 2.14) of a charge-transfer process which would be as shown in Figure 2.19.

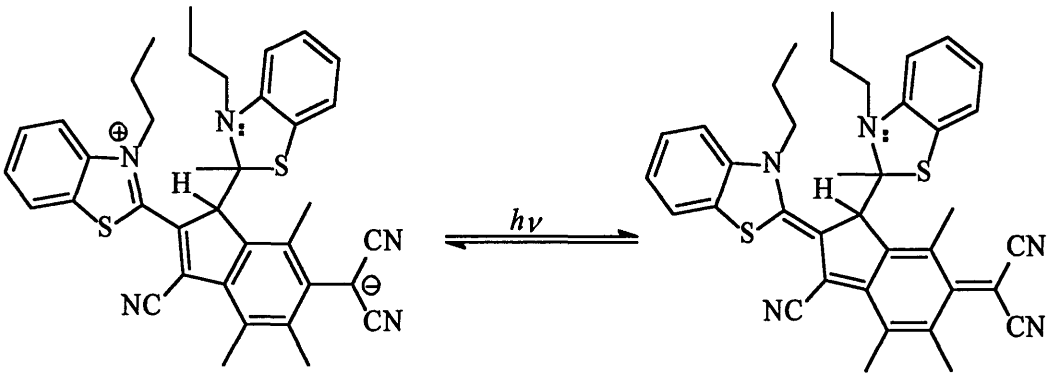

Figure 2.19 Charge-Transfer Process of the Proposed Structure.

If aromaticity is indeed a driving force of the reaction leading to the proposed structure then it seems that the new bis-adduct, like the conventional mono-adducts, may correspond to a benzothiazolium donor moiety separated from a dicyanomethanide acceptor moiety by a π-system with a substantially aromatic structure. An interesting alternative canonical form of the new bis-adduct, with an entirely aromatic intervening π-system is shown in Figure 2.20 and corresponds to a neutral molecule that is a bis-zwitterion. Clearly further work needs to be done to firmly establish (or disprove) the proposed structure, to further investigate the mechanism of its formation and to examine, in more detail, the behaviour of a rather novel system.

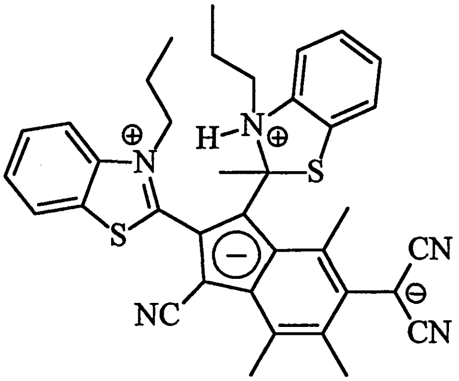

Figure 2.20 Bis-Zwitterion Form of the Proposed Structure.

Symmetrical Diquinolinium Adducts.

The synthesis of the structurally complicated TCNQ- and TMTCNQ-based diquinolinium adducts was in fact relatively straightforward and very similar to that of the related mono-quinolinium adducts (see Figure 2.7). Synthesis was aided by the fact that the products were insoluble in methanol and deposited out of solution making work-up straightforward. The yields, in the case of the TCNQ-based compounds, were quite surprising being comparable to those of the mono-quinolinium adducts despite their increased complexity. As expected the TMTCNQ-based adducts gave much smaller yields consistent with those observed in other TMTCNQ-based compounds.

A major problem with the diquinolinium adducts was their insolubility, making practical details such as TLC and recrystallisation very difficult. This had consequences in terms the range of derivatives prepared, which included examples of $TCNQF_4$- and dipyridinium-based adducts that could be purified sufficiently to afford analytically pure samples. A list of adducts that were prepared but not considered pure enough to include in this text despite having been characterised are listed in Appendix 1. The main analytical technique used with such adducts was UV/Vis spectroscopy which provided an adequate means of monitoring reaction progress despite the insolubility of the product.

Analytical data, in conjunction with the phase (DSC) and weight (TGA) changes (Table 2.12) (Appendix 2.), confirmed the inclusion of methanol in the crystal lattices of symmetrical diquinolinium salts and subsequently prepared adducts. Because of the limited solubility and subsequent observation of solvent inclusion in their lattices, the potential applications of these novel compounds is limited.

2.6 Spectroscopic Studies of Zwitterionic D-π-A Adducts.

2.6.1 Ultra Violet/Visible Spectroscopy.

Ultra violet/visible (UV/Vis) spectroscopy was engaged to monitor reaction mixtures for the various adducts to determine when a reaction had run its course. Small aliquots were monitored at intervals throughout the reaction's lifetime, with the UV/Vis spectra giving clear indication of the changes that occurred. Initially a spectrum shows λ_{max} bands characteristic of the added TCNQ derivative, i.e. 854nm ($TCNQF_4^-$) and 410nm ($TCNQF_4$) in the case of the fluorinated adducts though, as the reaction proceeds, these bands diminish as the TCNQ derivative is consumed. Correspondingly a broad band characteristic of the particular zwitterionic product begins to appear as the adduct is formed. This band grows in intensity as more product is formed, until a point is reached when all the TCNQ derivative has been spent, and the reaction is terminated. An illustrative example of the change in UV/Vis spectra during the course of the preparation for $C_{10}H_{21}(2)Q3CNQF_4$ is shown in Figure 2.21.

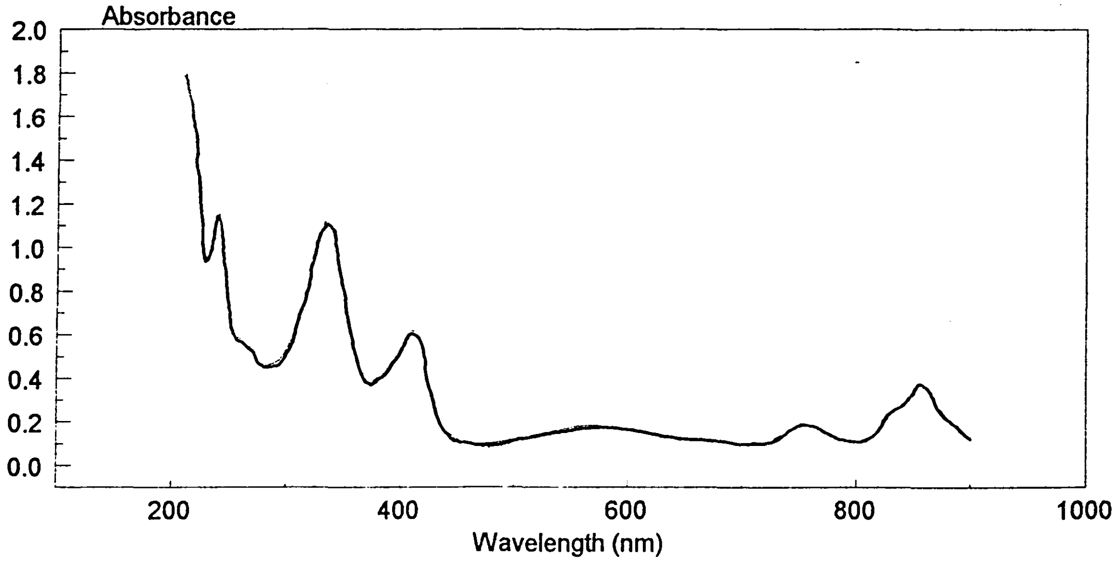

i) Starting Materials.

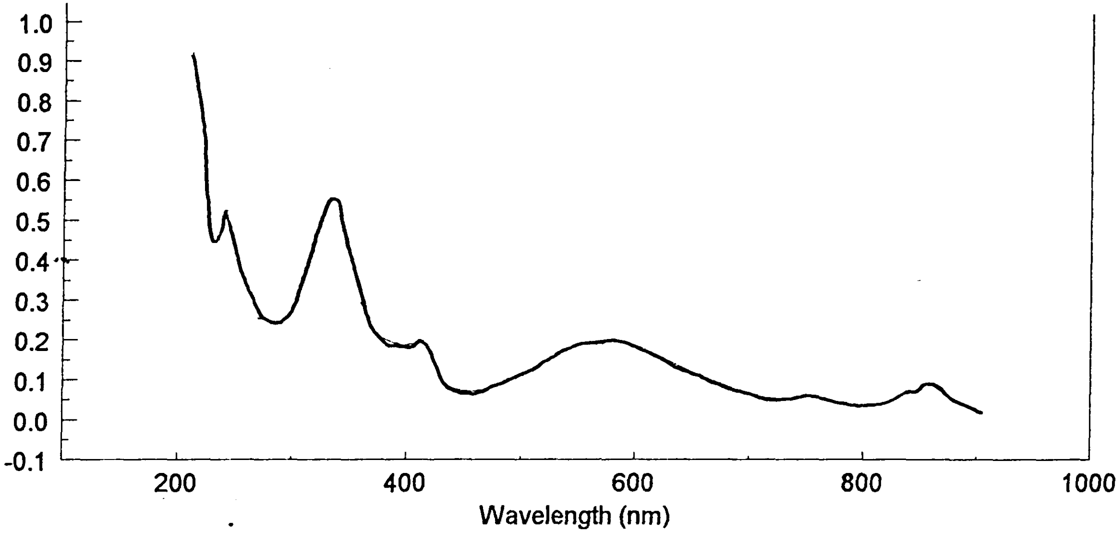

ii) **Reaction after 1 hour.**

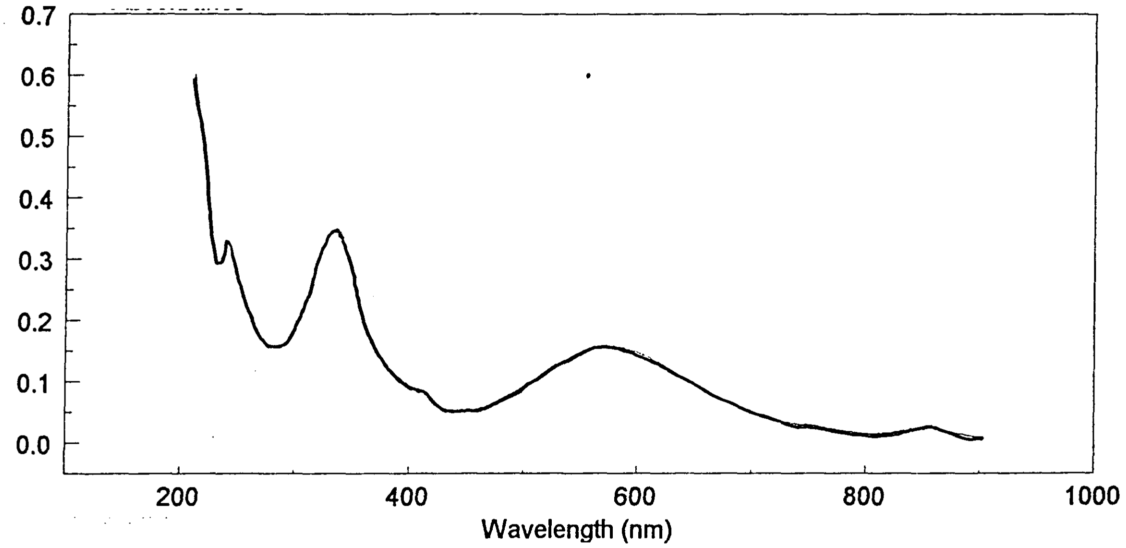

iii) **Reaction after 12 hours.**

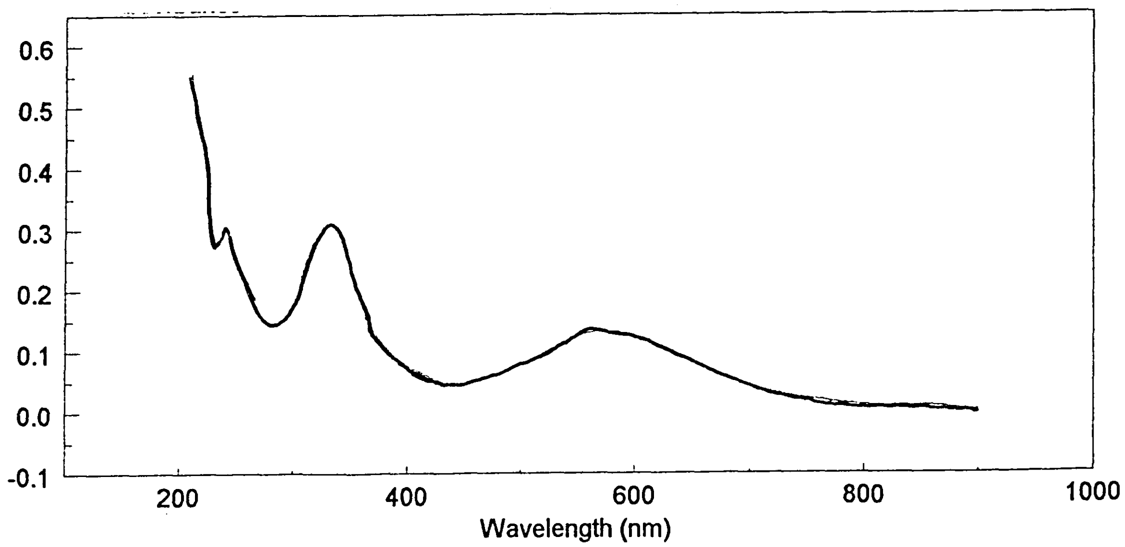

iv) **Reaction after 48 hours**

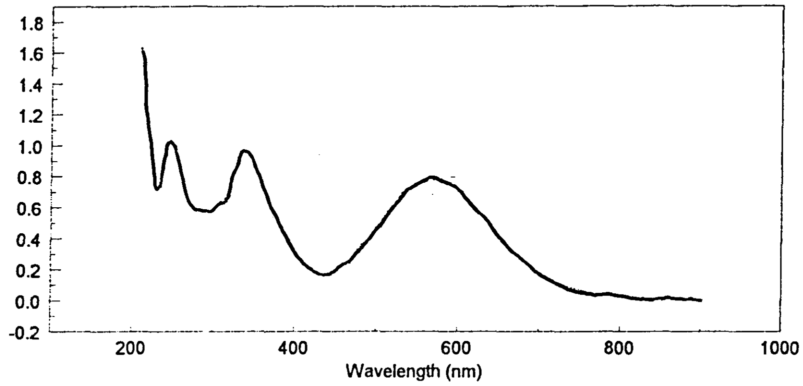

v) Pure $C_{10}H_{21}(2)Q3CNQF_4$.

Figure 2.21 UV/Vis Spectra Showing the Course of the Reaction Between $TCNQF_4$ and N-Decyl-2-methylquinolinium Bromide.

Almost all of the pure adducts show an intense, broad top transition centred around 500-750nm in acetonitrile solution. Characteristic spectra are illustrated in Figures 2.23 to 2.25. The position and intensity of this transition, which has been attributed to an intramolecular charge-transfer process from the negatively charged dicyanomethanide group to the positively charged nitrogen heterocycle[43] (Figure 2.22), is dependent upon the type of adduct and the electron-inductive effects of its substituents.

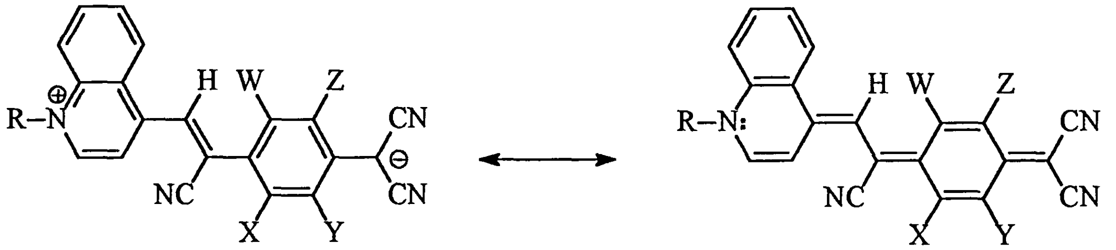

Figure 2.22 Light Induced Charge Transfer Process.

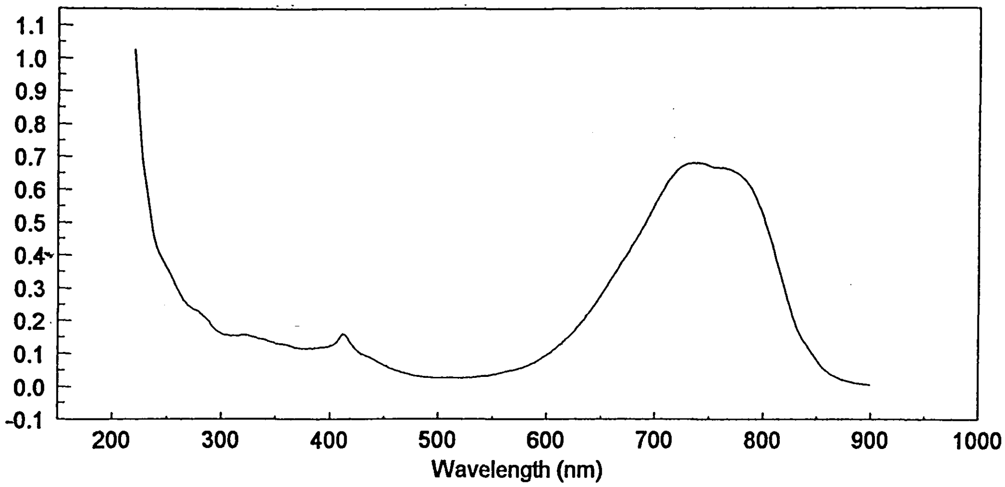

Figure 2.23 C_3H_7(2)BT3CNQ in Acetonitrile.

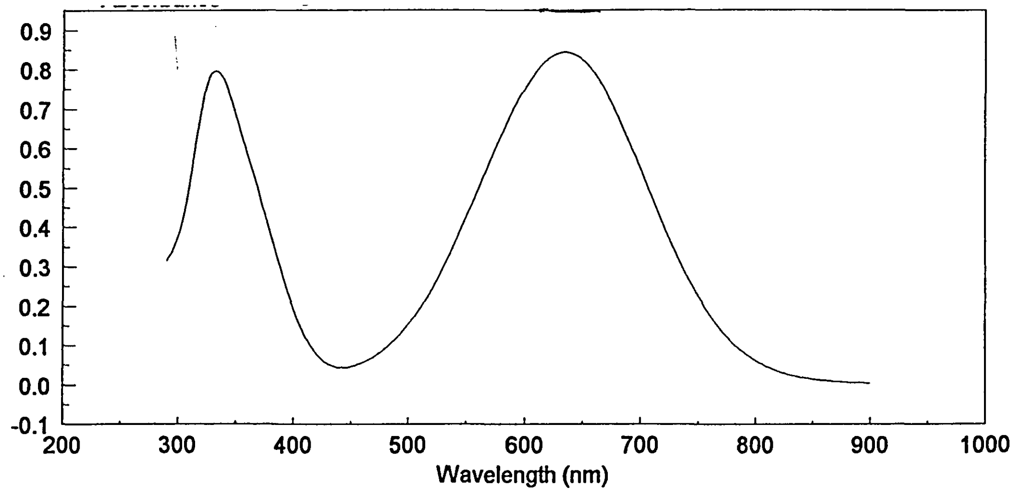

Figure 2.24 C_3H_7(2)BT3CNQF_4 in Acetonitrile.

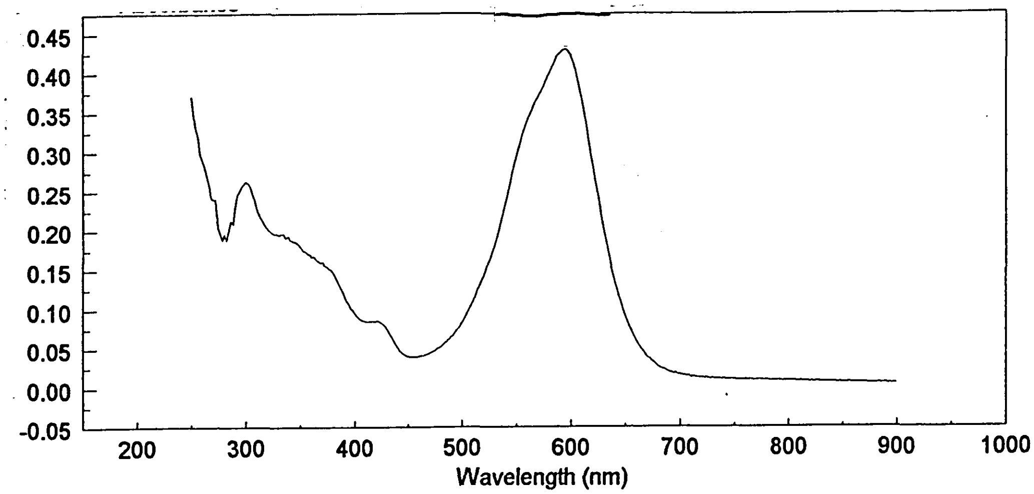

Figure 2.25 C_3H_7(2)BT3CNTMQ in Acetonitrile.

For example the fluorinated adducts such as $C_{10}H_{21}(2)Q3CNQF_4$ exhibit intramolecular transitions at shorter wavelengths (higher energy) relative to those seen in the corresponding unsubstituted adducts.[2,4] This is a direct consequence of the powerful electronegative fluorine atoms increasing the ionisation potential of the dicyanomethanide group, resulting in a higher energy charge-transfer process.

Surprisingly the tetra-methyl adducts show a similar trend in that their charge-transfer absorption band appears at higher energies relative to the unsubstituted compounds. This is attributed to the positive-inductive effect of the methyl groups on the acceptor ring which push electrons into the dicyanostyrylmethanide moiety, thus creating coulombic repulsion between these electrons and the electron which is trying to escape through the charge-transfer route. A higher energy system is created, resulting in a shift of the absorption band to shorter wavelengths, as shown in Table 2.13 by the differences in λ_{max} for the different adducts.

Zwitterion	CH_3CN λ_{max} (nm)
$C_{10}H_{21}(4)Q3CNQ$[4]	710
$C_{10}H_{21}(2)Q3CNQ$[11]	702
$C_{10}H_{21}(4)Q3CNQF_4$	566
$C_{10}H_{21}(2)Q3CNQF_4$	568
$C_{10}H_{21}(4)Q3CNTMQ^*$	582
$C_3H_7(2)BT3CNQ$	738
$C_3H_7(2)BT3CNQF_4$	664
$C_3H_7(2)BT3CNTMQ^*$	594
$C_3H_7(2)BT3CNTMQ$ (red spot)	520, 544

* Contain methanol of crystallisation

Table 2.13 λ_{max} of Selected Adducts in Acetonitrile.

Despite this shift in absorption band the fluorinated compounds were expected to show properties similar to those of their unsubstituted counterparts, in that the energy of the transition should be independent of chain length[2,3,15] since the active portion of the compound, the chromophore, is the same for each zwitterionic compound. However the fluorinated compounds did not follow this trend apart from the longer chain (n>6) derivatives. The N-methyl derivatives, of both the α- and γ-quinolinium based adducts, exhibited bands that were different from their longer chain homologues.

There were also differences observed in the solvatochromic behaviour of the adducts, which is discussed in Chapter 3. These observed differences could be attributed to the fact that at low concentrations the longer chain fluorinated derivatives deviate from the Beer-Lambert law, thus indicating non-intramolecular behaviour[2] of the transition as a result of the zwitterions forming aggregates. The relatively poorer solubility, in solvents of medium to low polarity, of the N-methylated derivatives compared to their longer chain counterparts presumably results in their forming aggregates more easily and giving transitions that are not of true intramolecular origin. The dimer pairs formed in such aggregation would interact with each other thus stabilising the electronic ground state of each chromophore and resulting in a shift to higher energy of the observed intramolecular transition. This hypothesis is also based on the fact that in higher polarity solvents such as DMSO, DMF etc, in which the shorter chain homologues are more soluble, the observed transitions are very similar to those observed for the long chain derivatives (Chapter 3) indicating that the transition arises solely from an intramolecular charge-transfer process.

The intramolecular charge-transfer transition of the much larger symmetrical diquinolinium adducts was only observed in N-methylformamide (NMF) as a consequence of the compound's insolubility in all other solvents (Figures 2.26 and 2.27). Hence the solvent dependent nature of the absorption band of these highly novel zwitterionic adducts could not be studied. The solvatochromic behaviour of the TMTCNQ-based quinolinium and benzothiazolium adducts was not studied either, as a result of their crystal lattices being adjudged to contain methanol which when dissolved in solution would produce an undetermined binary solvent mixture, thus rendering any observed transitions difficult to quantify.

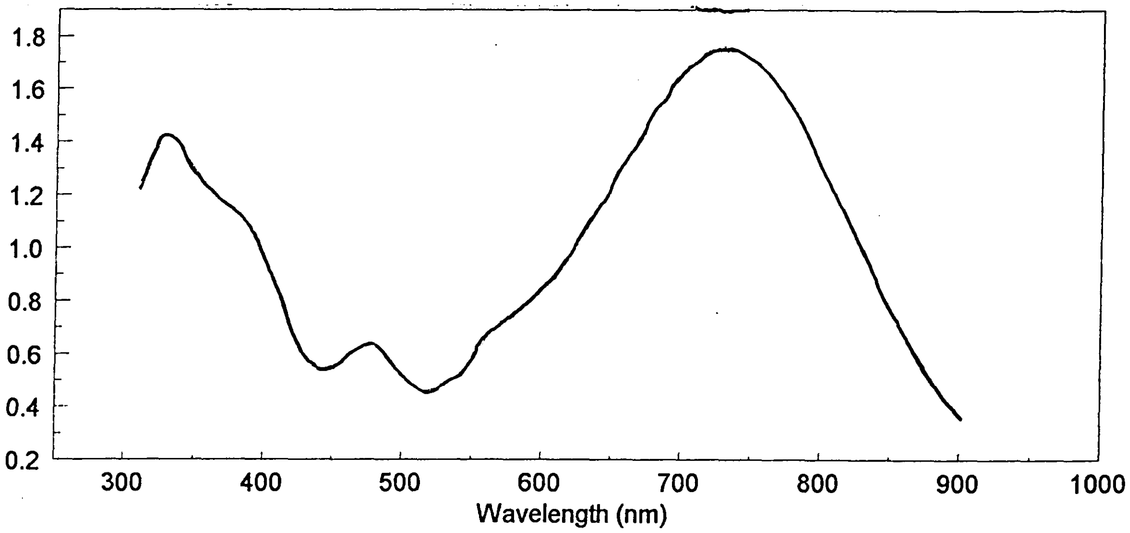

Figure 2.26 **m-C_8H_8(4)DQ6CNQ in N-methylformamide (NMF).**

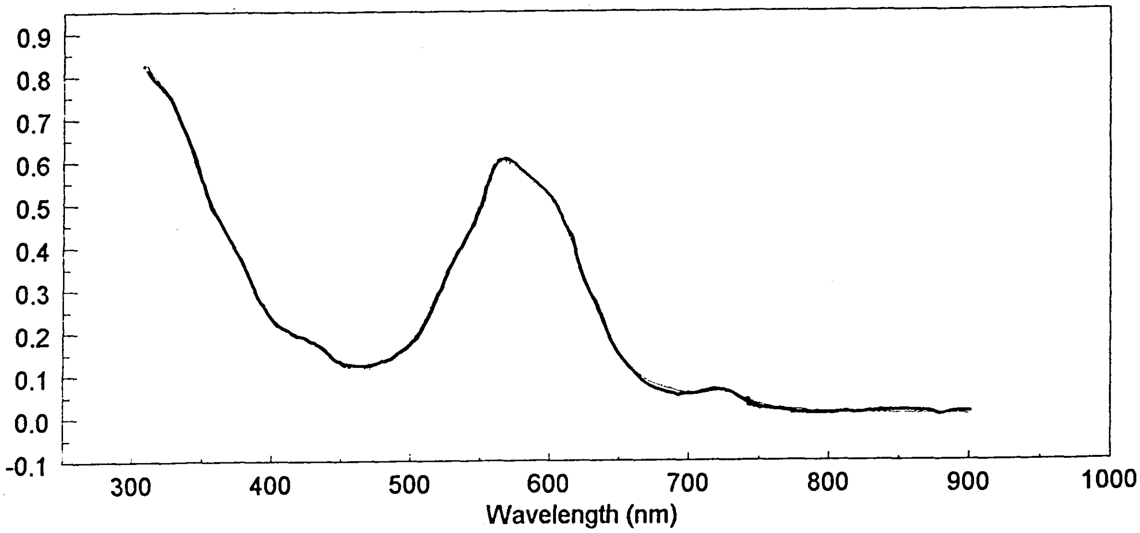

Figure 2.27 **m-C_8H_8(4)DQ6CNTMQ in N-methylformamide (NMF).**

2.6.2 Infrared Spectroscopic Studies.

As expected, all the adducts gave similar infrared spectra. Like other zwitterionic donor-π-acceptor adducts of TCNQ,[2,3,55] the infrared spectrum of each adduct studied showed a doublet at the C≡N stretching frequencies of ~2150-2180cm^{-1} and ~2080-2166cm^{-1}. Such a doublet is characteristic of zwitterionic materials containing the dicyanomethanide group,[2,3,55] as the cyano stretching frequencies compare well with those of TCNQ^0 and TCNQ$^-$.[56,57] Typically neutral nitriles normally cover the range 2260cm^{-1} to 2200cm^{-1}. However the presence of two cyano stretching frequencies is indicative of two distinct cyano environments.[58] The band at ~2180cm^{-1} represents the neutral environment of the nitrile substituent embodied into the π-bridge (Figure 2.28) whilst the band at ~2150cm^{-1} is characteristic of the 3-carbon dicyanomethanide unit over which the negative charge is delocalised.

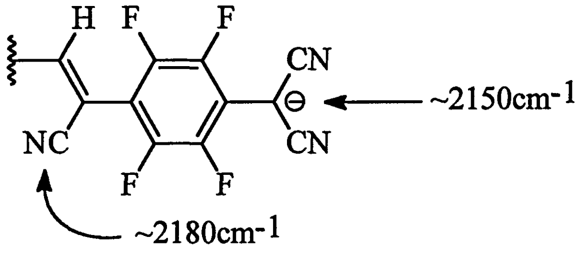

Figure 2.28 Infrared Cyano Environments of R(4)Q3CNQF$_4$ Adducts.

Delocalisation of the negative charge reduces the strength of the C-N bond and the stretching frequency is reduced accordingly. In the case of the C_3H_7(2)BT3CNQ adduct, which has been previously documented,[4] only a single nitrile band is observed. This anomaly is thought to occur as a result of the two cyano environments giving bands which are very close in terms of energy and hence only a broad single nitrile band is observed due to overlap of the two expected bands which are observed in the longer chain $C_{16}H_{33}$(2)BT3CNQ derivative prepared by *Ashwell et al.*[59]

This anomaly is diagrammatically illustrated in Figure 2.29 along with a selection of spectra (Figure 2.30 and 2.31) for the other adducts studied, and with the relevant cyano stretching and other frequency assignments in Tables 2.14 and 2.15.

Zwitterion	Nitrile Stretch (ionic)	Nitrile Stretch (neutral)
R(4)Q3CNQ[2,3]	2137 ± 3cm^{-1}	2137 ± 3cm^{-1}
R(2)Q3CNQ[4]	2132 ± 3cm^{-1}	2175 ± 0cm^{-1}
R(4)Q3CNQF$_4$	2152 ± 2cm^{-1}	2182 ± 1cm^{-1}
R(2)Q3CNQF$_4$	2155 ± 2cm^{-1}	2183 ± 2cm^{-1}
R(4)Q3CNTMQ	2092 ± 2cm^{-1}	2153 ± 2cm^{-1}
C_3H_7(2)BT3CNQ[4]	2175 cm^{-1}	2175 cm^{-1}
C_3H_7(2)BT3CNQF$_4$	2166 cm^{-1}	2192 cm^{-1}
C_3H_7(2)BT3CNTMQ (red spot)	2089 cm^{-1}	2151 cm^{-1}
(*m*- or *p*-)-C_8H_8(4)DQ6CNQ	2121 ± 1cm^{-1}	2170 ± 1cm^{-1}
(*m*- or *p*-)-C_8H_8(4)DQ6CNTMQ	2088 ± 1cm^{-1}	2157 ± 1cm^{-1}

Table 2.14 Nitrile Stretching Frequencies for Various Adducts.

Absorption Band	Assignment[60]
3600-3200 cm^{-1} (s)	- O-H stretch
2995-2850 cm^{-1} (s)	- C-H stretch (sp^3 centre)
2185-2150 cm^{-1} (vs)	- C≡N stretch (neutral sp centre)
2170-2085 cm^{-1} (vs)	- C≡N stretch (ionic sp centre)
~1650 cm^{-1} (s)	- C=C stretch (sp^2 centre)
~1600 cm^{-1} (s)	- C=C (aromatic sp^2 centre)
~1500 cm^{-1} (s)	- C=C (aromatic sp^2 centre)
1300-1200 cm^{-1} (s)	- C-F stretch (sp^3 centre)

Note: (s) strong, (vs) very strong.

Table 2.15 Infrared Spectral Bands Common to the Various Adducts.

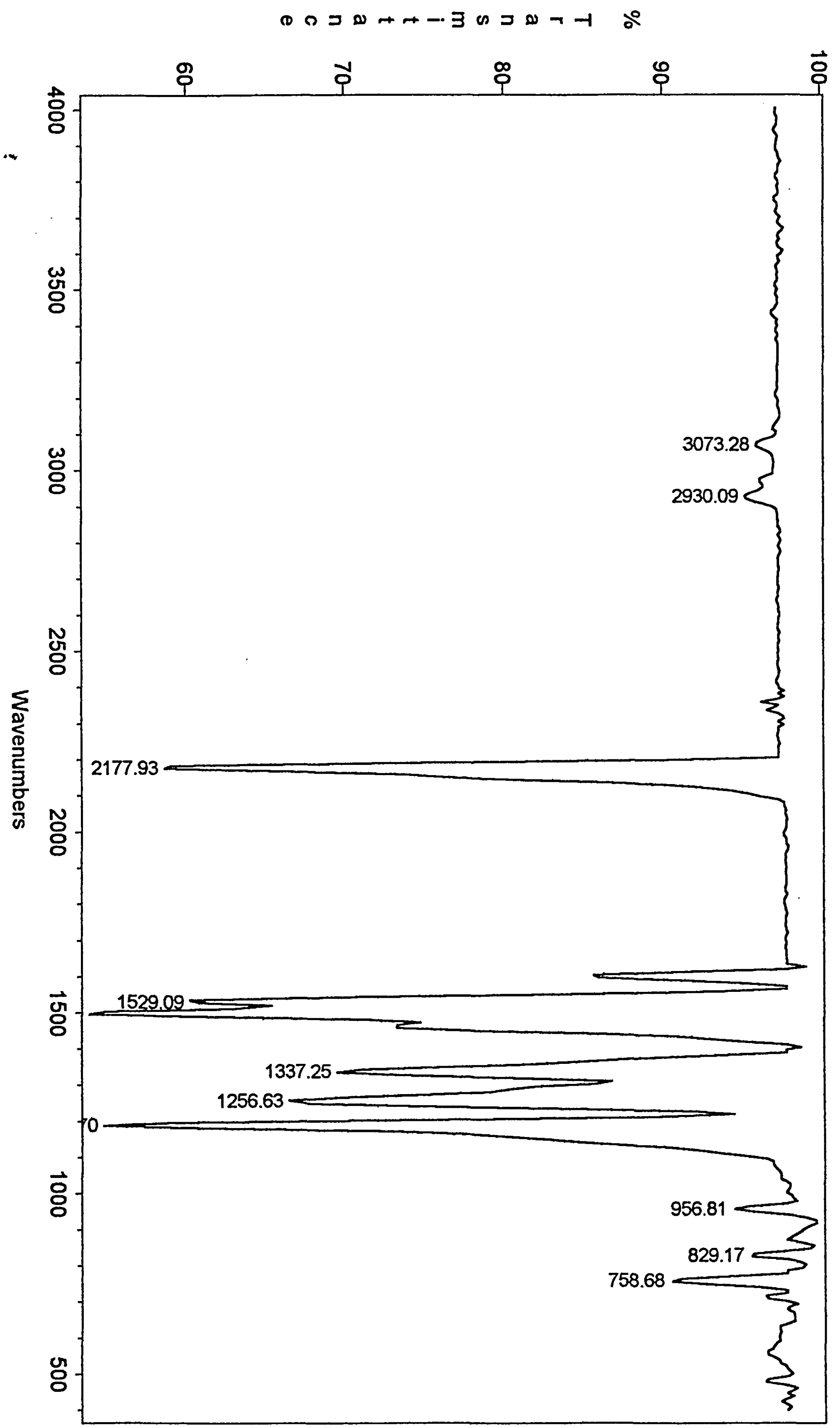

Figure 2.29 Infrared Spectrum of C_3H_7(2)BT3CNQ.

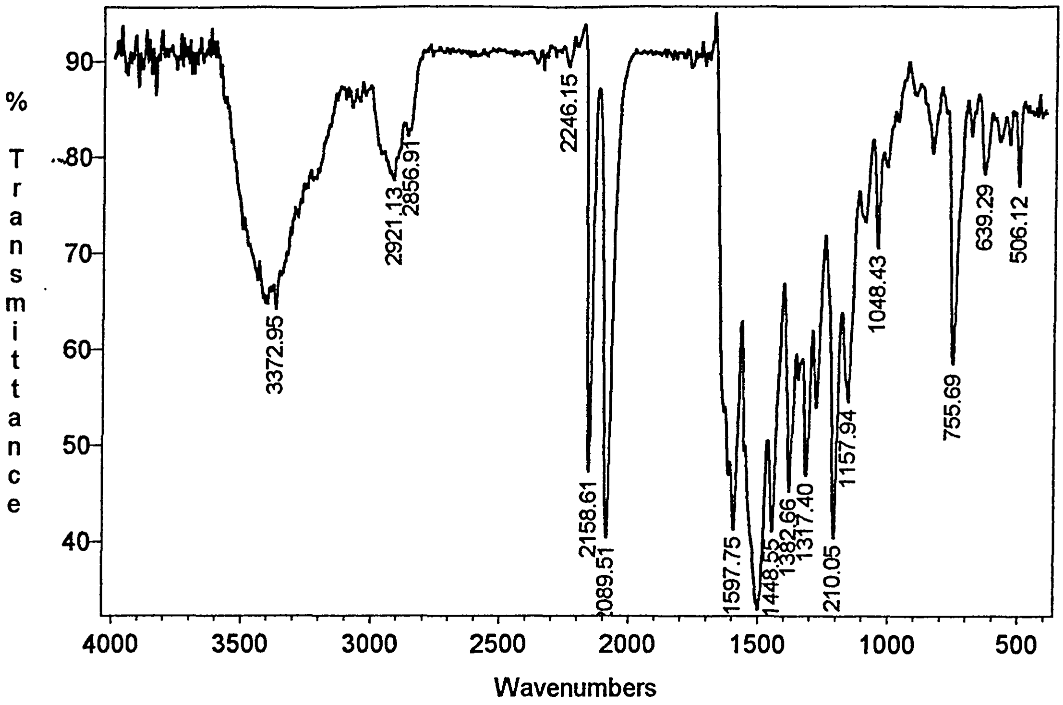

Figure 2.30 Infrared Spectrum of *m*-C_8H_8(4)DQ6CNTMQ.

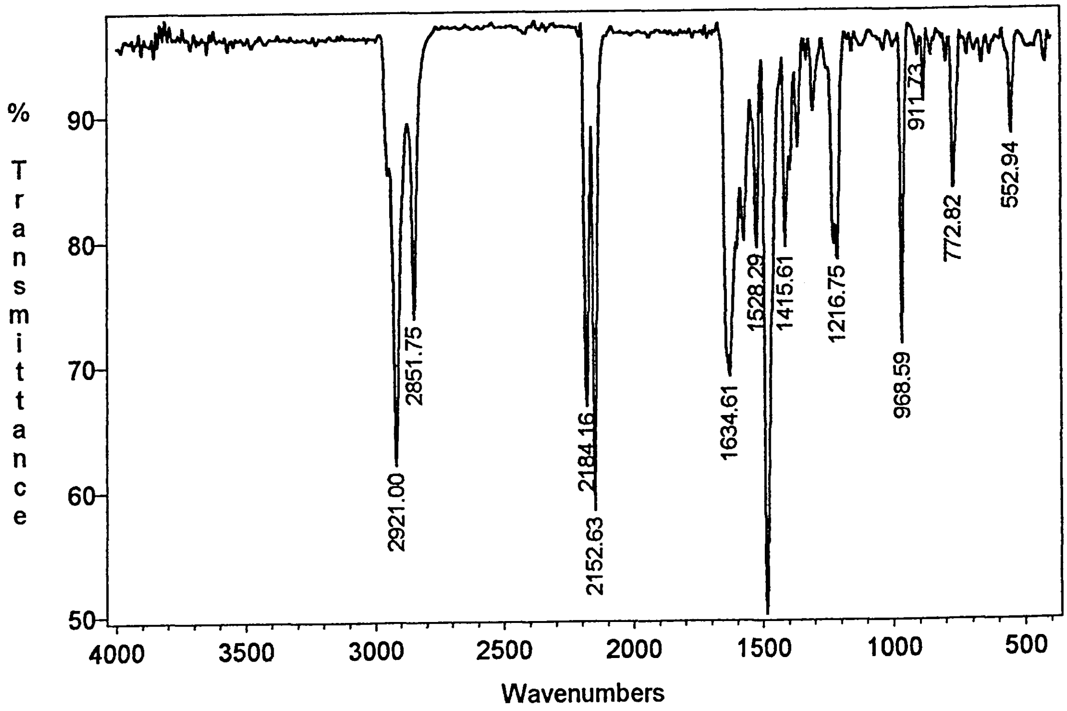

Figure 2.31 Infrared Spectrum of $C_{11}H_{23}$(4)Q3CNQF_4.

2.6.3 Mass Spectrometry Studies.

Mass spectrometry was a major tool in the characterisation of the prepared adducts. The basis of the mass spectrometry technique is the production of ions from neutral species on bombardment with high energy particles. In the case of electron impact (EI) ionisation mass spectrometry this leads to the formation of a positively charged molecular ion (M^{+}) which may then break into smaller fragment ions. The processes can be summarised as shown below:

$$1)\ M + e^{\ominus} \longrightarrow M^{\dot{+}} + 2e^{\ominus}$$

i.e. loss of an electron leads to a radical cation.

$$2)\ M^{\dot{+}} \begin{cases} \xrightarrow{A} M_1^{\dot{+}} + M_2 \\ \xrightarrow[B]{} M_1^{+} + \dot{M_2} \end{cases}$$

Pathway A leads to the formation of a new radical cation and a neutral molecule, and B to the formation of a cation and a radical. Mass spectrometric data for the range of quinolinium, benzothiazolium and picolinium based adducts prepared has been documented and interpreted; illustrative examples are given in Figures 2.32 to 2.37. The data obtained from the fluorinated quinolinium adducts shows very similar fragmentation to that observed in their unsubstituted counterparts,[2] as expected considering the structural similarities. However, the fluorinated adducts seem less stable than their unsubstituted counterparts displaying much smaller molecular ions and more substantive fragmentation in the electron impact spectra as illustrated for C_3H_7(2)BT3CNQF_4 (Figure 2.32) and C_3H_7(2)BT3CNQ (Figure 2.33). The benzothiazolium adducts are unique in that they show fragmentation corresponding to the loss of both hydrogen cyanide (-27 Da) and acetonitrile (-41 Da), something which is not observed in most of the quinolinium compounds apart from the TMTCNQ-based compounds.

The characterisation of the symmetrical diquinolinium adducts was achieved using the less energetic Fast Atom Bombardment (FAB) ionisation technique, since the increased fragmentation observed in the higher energy electron impact technique made conclusive characterisation difficult. FAB is a method which uses high energy particle collisions with a sample/viscous liquid matrix to afford ionisation of the sample,[61] a lower energy process that resulted in the observation of molecular ions (M+H ions) for the TCNQ-based diquinolinium adducts, with fragmentation limited to the loss of a tricyano-quinodimethane (TCQ) moiety (Figure 2.34).

The TMTCNQ-based compounds showed differing mass spectrometric stabilities. The quinolinium-based and C_3H_7(2)BT3CNTMQ adducts were differentiated and characterised using electron impact, with molecular ions observed in both spectra (see Figures 2.35 and 2.36). However the fragmentation observed in the electron impact spectrum of the bis-C_3H_7(2)BT3CNTMQ compound (incorporating the second benzothiazolium ring) was so similar to that observed in the mono C_3H_7(2)BT3CNTMQ compound that it made characterisation difficult. However this problem was overcome by using the FAB technique, whereby the spectrum (see Figure 2.12) obtained using this technique gave a molecular ion (M+H) of 614 Daltons which is consistent with the proposed structure [Figure 2.10(a)]. Subsequent fragmentation of the compound, i.e. loss of the dicyanomethanide swallow tail and two propyl groups, also support the proposed structure. Characterisation and differentiation of the TMTCNQ-based diquinolinium compounds was more difficult as neither FAB nor EI spectra showed adequate signs of structural differentiation. However this problem was resolved using electrospray mass spectrometry, a process which involves the dissolved sample being pumped through a stainless capillary held at ca. 5KV (Figure 2.38).

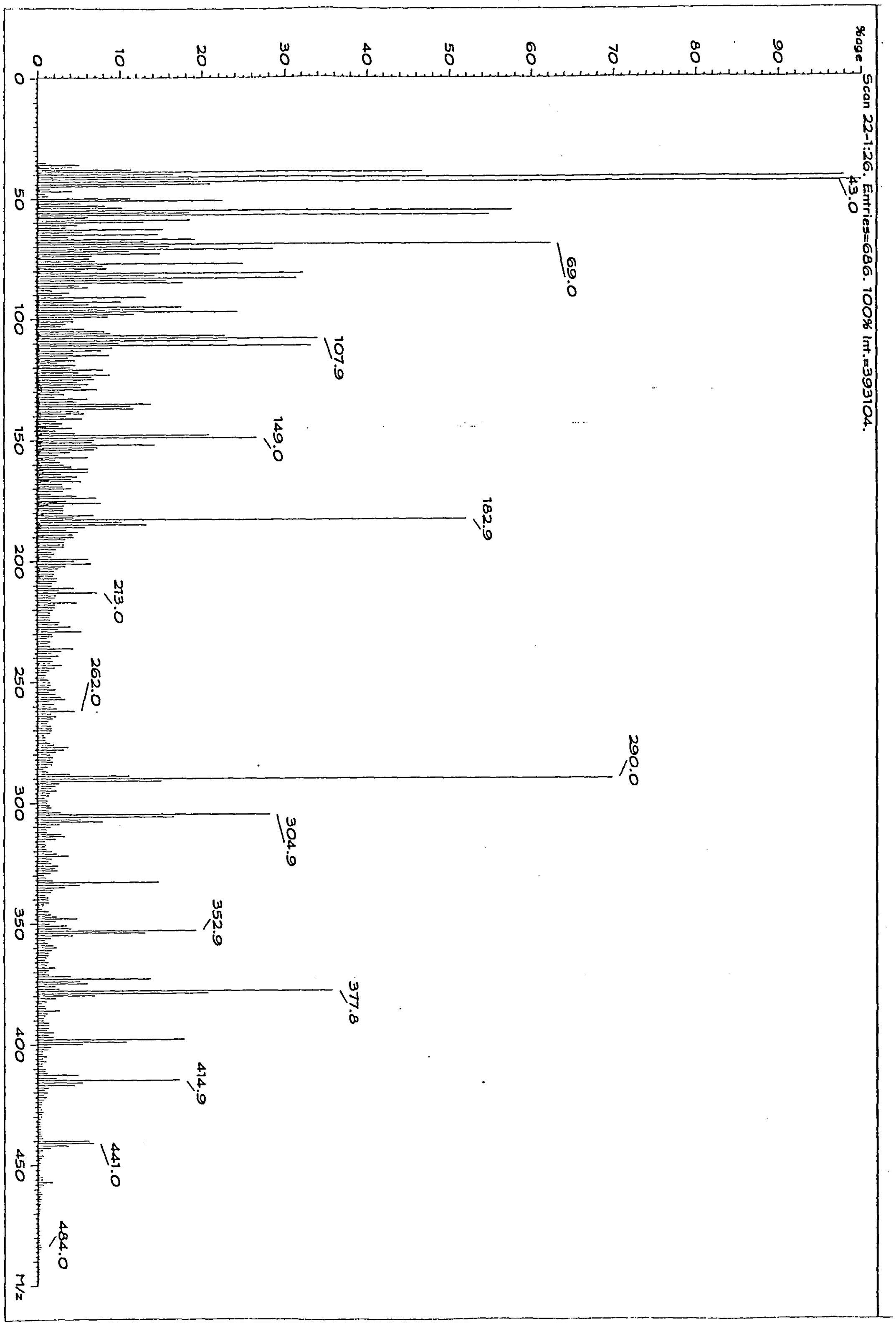

Figure 2.32 Electron Impact Mass Spectrum of $C_3H_7(2)BT3CNQF_4$.

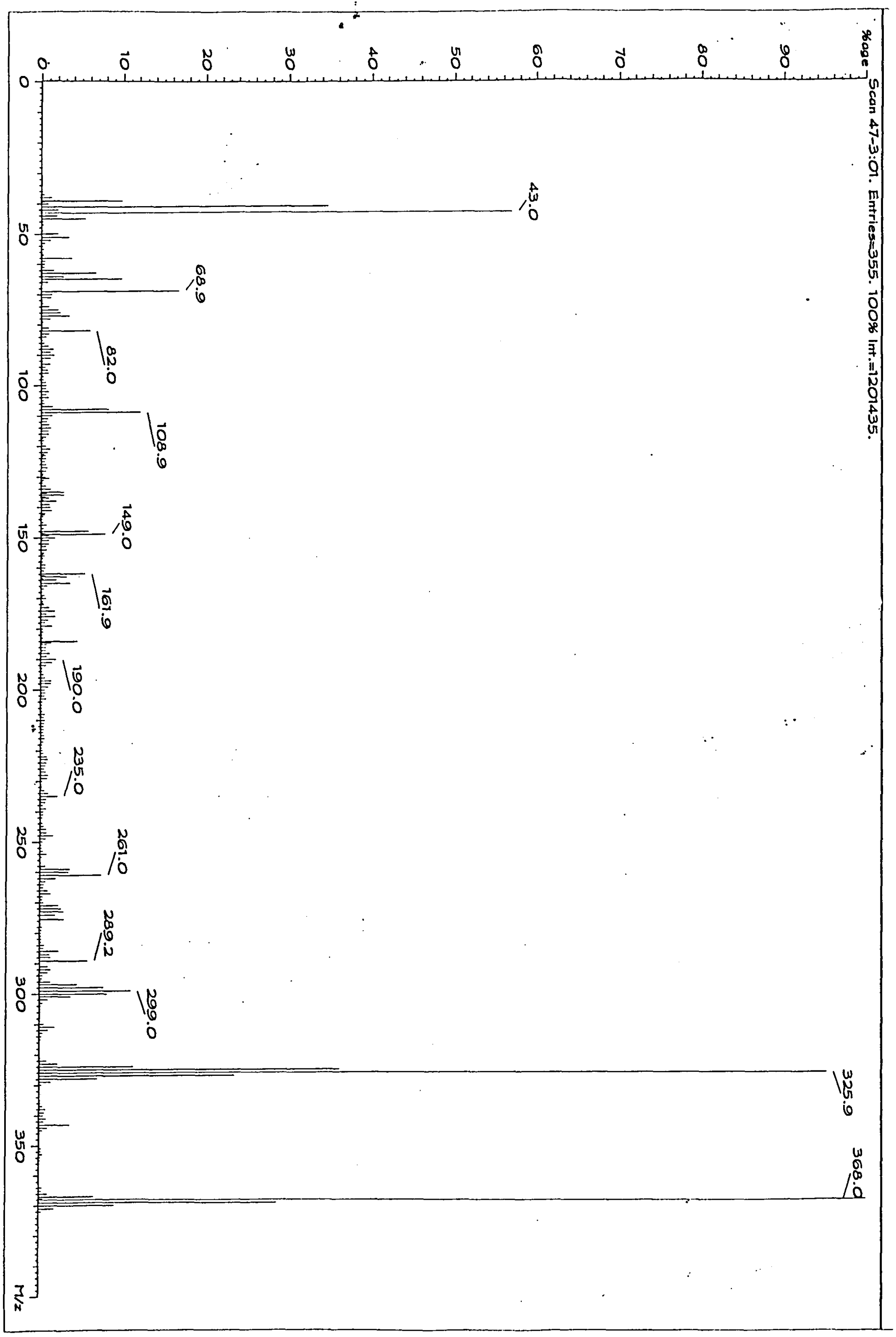

Figure 2.33 Electron Impact Mass Spectrum of C_3H_7(2)BT3CNQ.

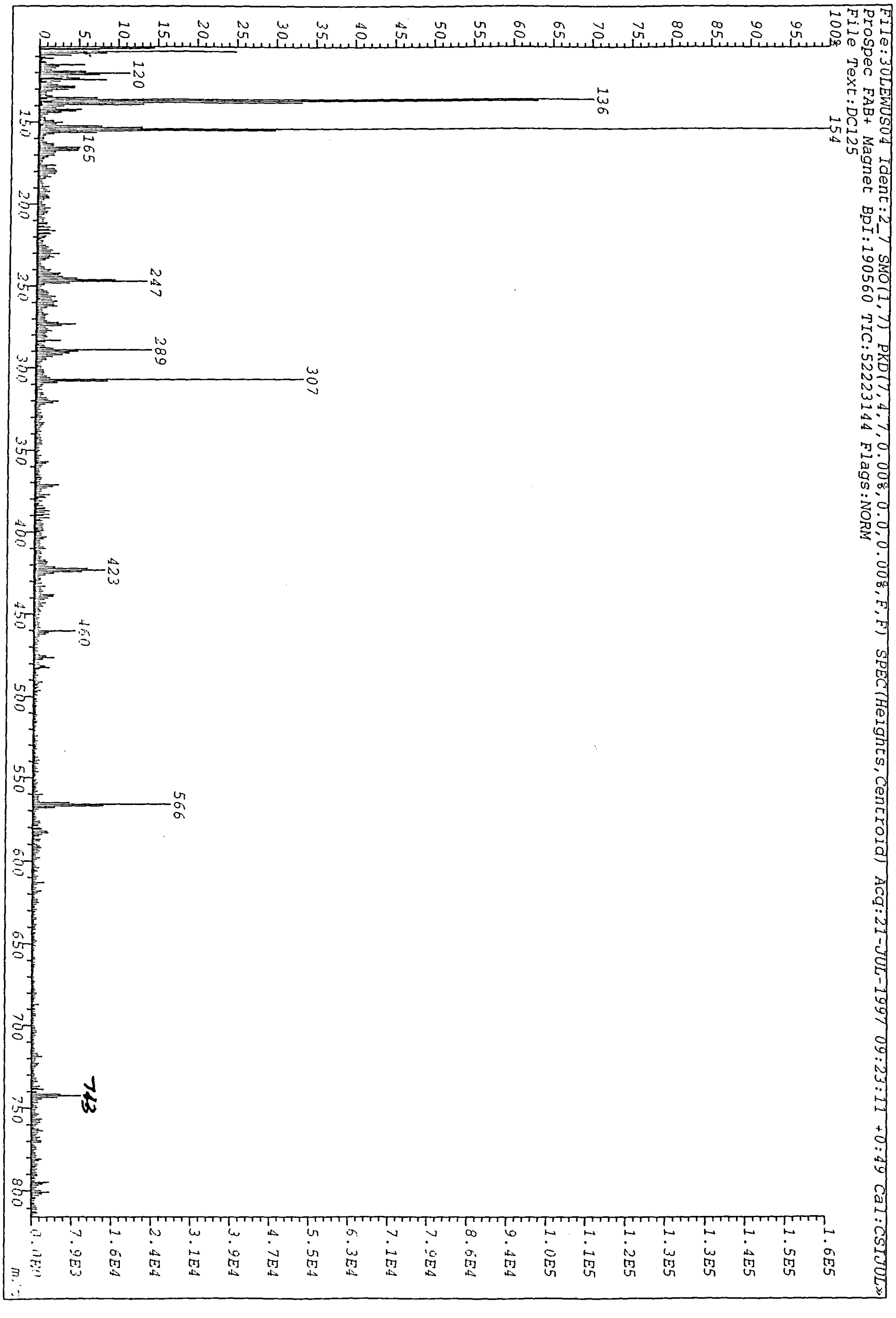

Figure 2.34 FAB Mass Spectrum of *p*-C_8H_8(4)DQ6CNQ.

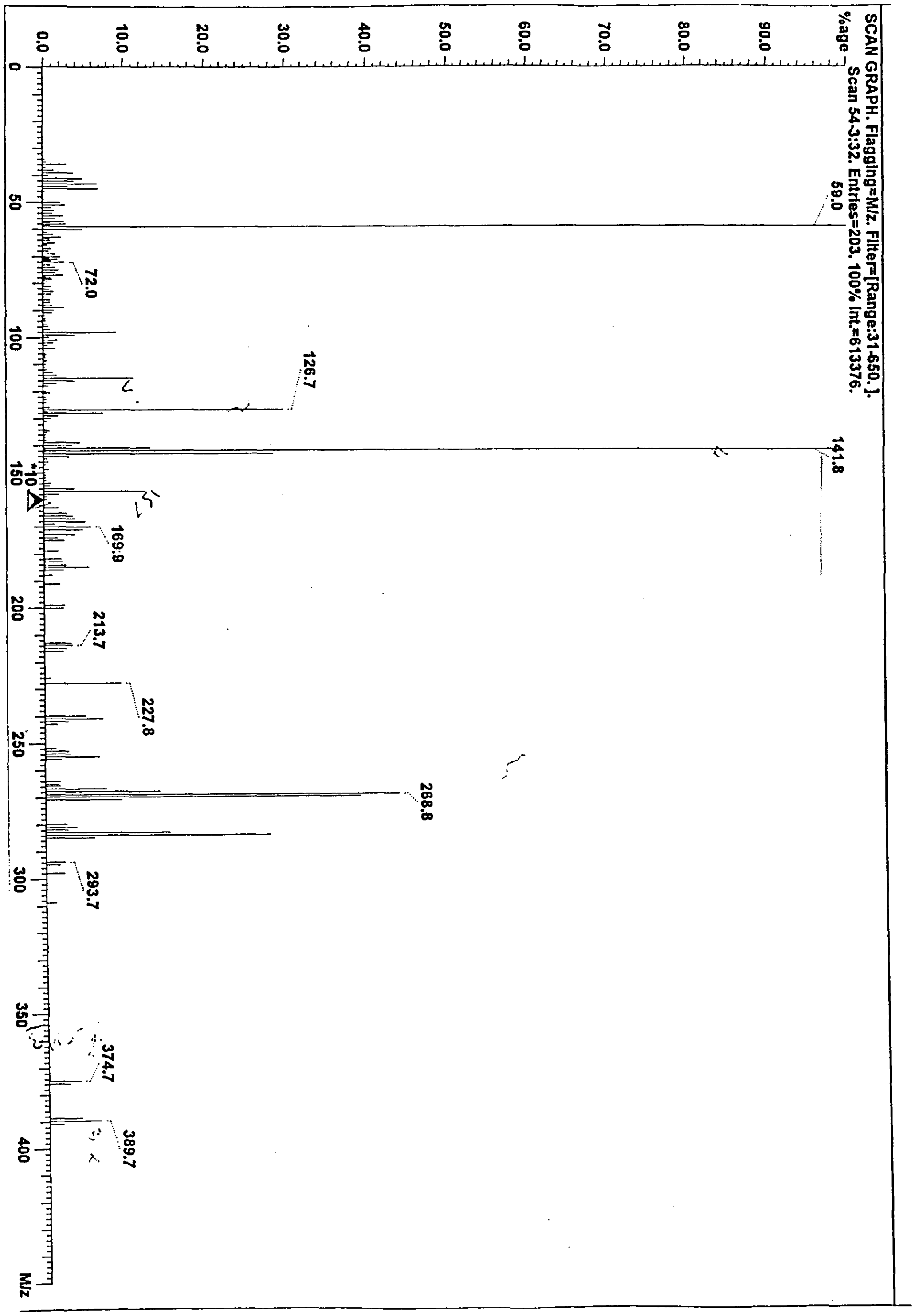

Figure 2.35 Electron Impact Mass Spectrum of CH_3(4)Q3CNTMQ.

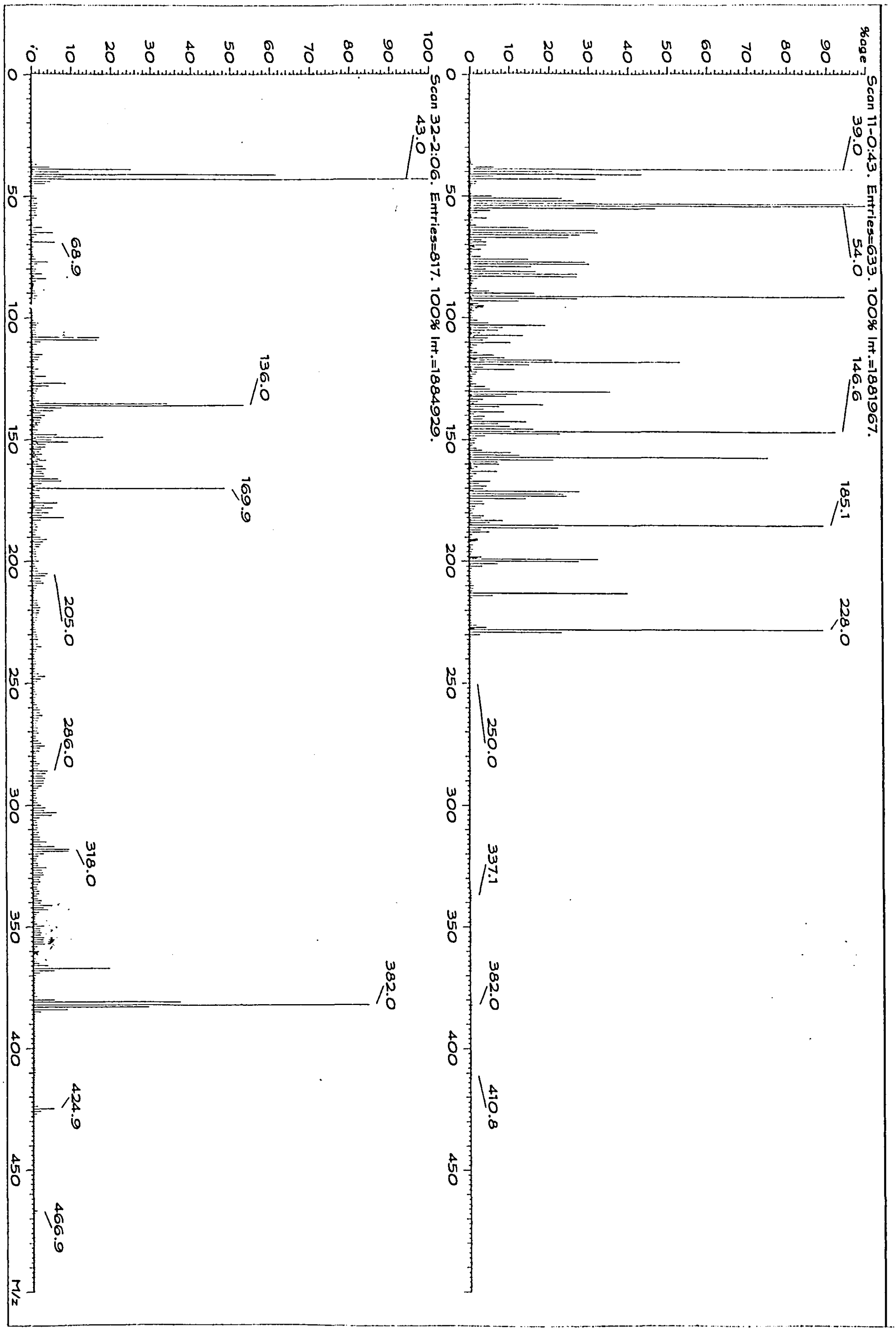

Figure 2.36 Electron Impact Mass Spectrum of C_3H_7(2)BT3CNTMQ.

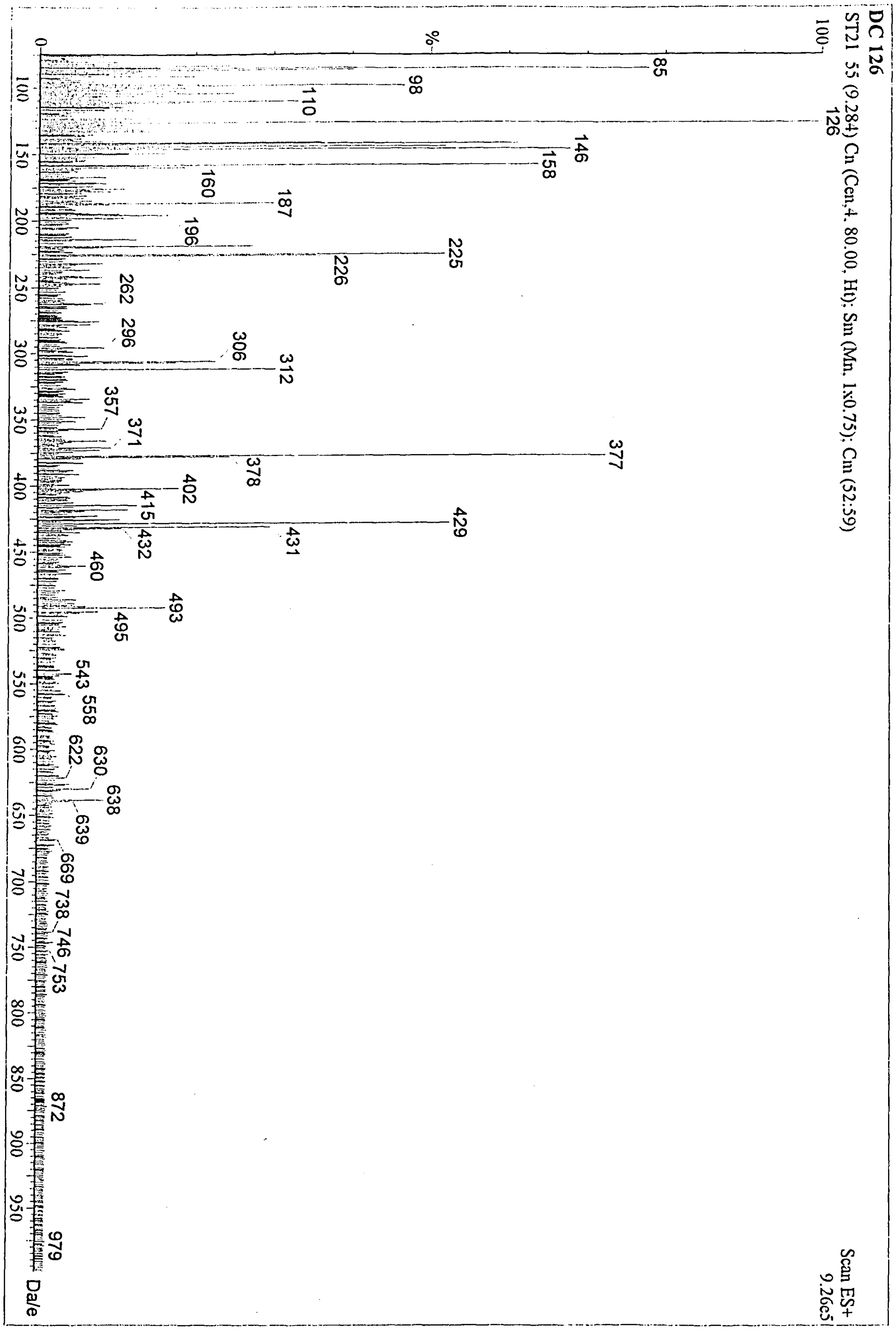

Figure 2.37 Electrospray Mass Spectrum of *p*-C_8H_8(4)DQ6CNTMQ.

The potential field held at the exit of the capillary creates a spray of highly charged droplets (hence the name "*electrospray*"), which results in ionisation by a purely ion evaporation process.

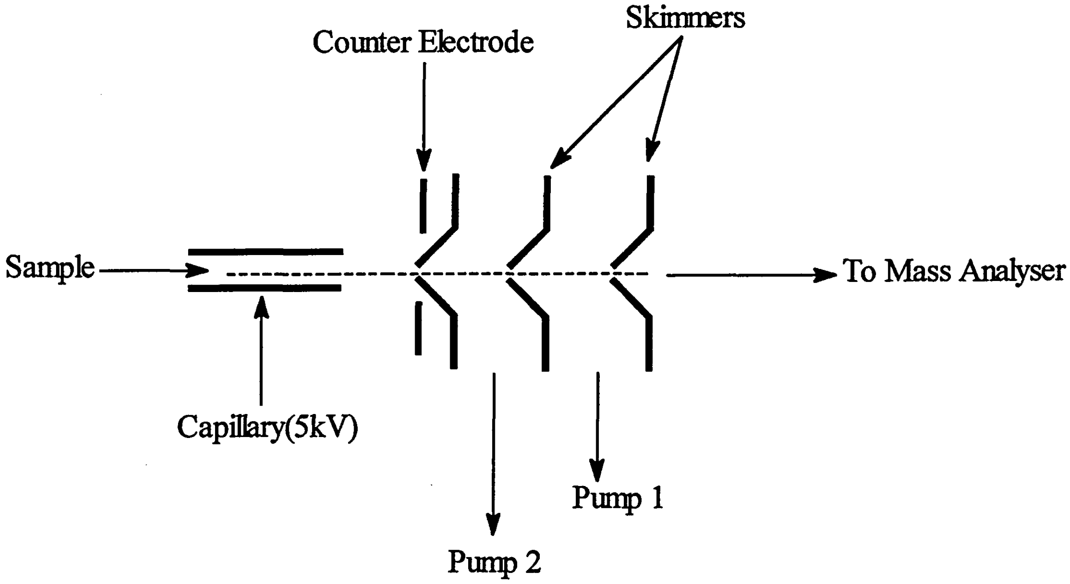

Figure 2.38 Electrospray Ionisation Source.

As a result of the high potential field employed, the spectra obtained usually show evidence of multiply charged ions e.g. $(M+2H)^{2+}$ which are on the m/z axis of the mass spectrum at values corresponding to:

$$= \frac{M + nH}{n}$$

Where M = the RMM of the molecule, H = the mass of 1 proton, and n = the number of charges on the ion. In the case of the spectra obtained for the TMTCNQ-based diquinolinium compounds peaks were observed at 429 and 312 Daltons, corresponding to $(M+2H)^{2+}$ and $(M+2H\text{-}TCQ)^{2+}$ ions respectively (Figure 2.37). Similar peaks were observed in the electrospray spectra obtained for the TCNQ-based diquinolinium compounds as well, thus confirming the structures of both types of compound.

2.6.4 Nuclear Magnetic Resonance (NMR) Spectroscopy.

Nuclear magnetic resonance spectroscopy was a major tool in the characterisation of the adducts as a result of its sensitivity towards different chemical environments. In general the compounds, which are all based upon the same π-bridge backbone, exhibited very similar proton NMR spectra. Typical spectra are illustrated in Figures 2.39 and 2.40. From the different spectra examined various trends were observed. The singlet observed for the alkene proton of the π-bridge, which was expected to appear at ~7.5ppm,[60] was generally found further down field in the range 7.95-8.95ppm, as a result of deshielding of the proton's electronic environment caused by the charge separation state of the zwitterions. The more polar fluorinated adducts surprisingly exhibited very similar shifts to those observed in the TCNQ-based adducts.

The ^{19}F NMR shifts observed in the fluorinated adducts appear at much higher field (i.e. –142 to –149ppm) as a result of the increased electronic environment in the charge separated compound, relative to that of neutral $TCNQF_4$ (-130ppm). The appearance of the peaks is also different, with the fluorinated adducts showing near perfect doublets arising from the two distinct fluorine environments (Figure 2.41). In contrast the ^{19}F NMR spectrum of $TCNQF_4$ shows a very broad singlet, as a result of the highly reactive $TCNQF_4$ molecule reacting with impurities in the deuterated solvent. This results in the formation of radicals, which affect the electronic environment of the fluorine atoms and the NMR peak accordingly.

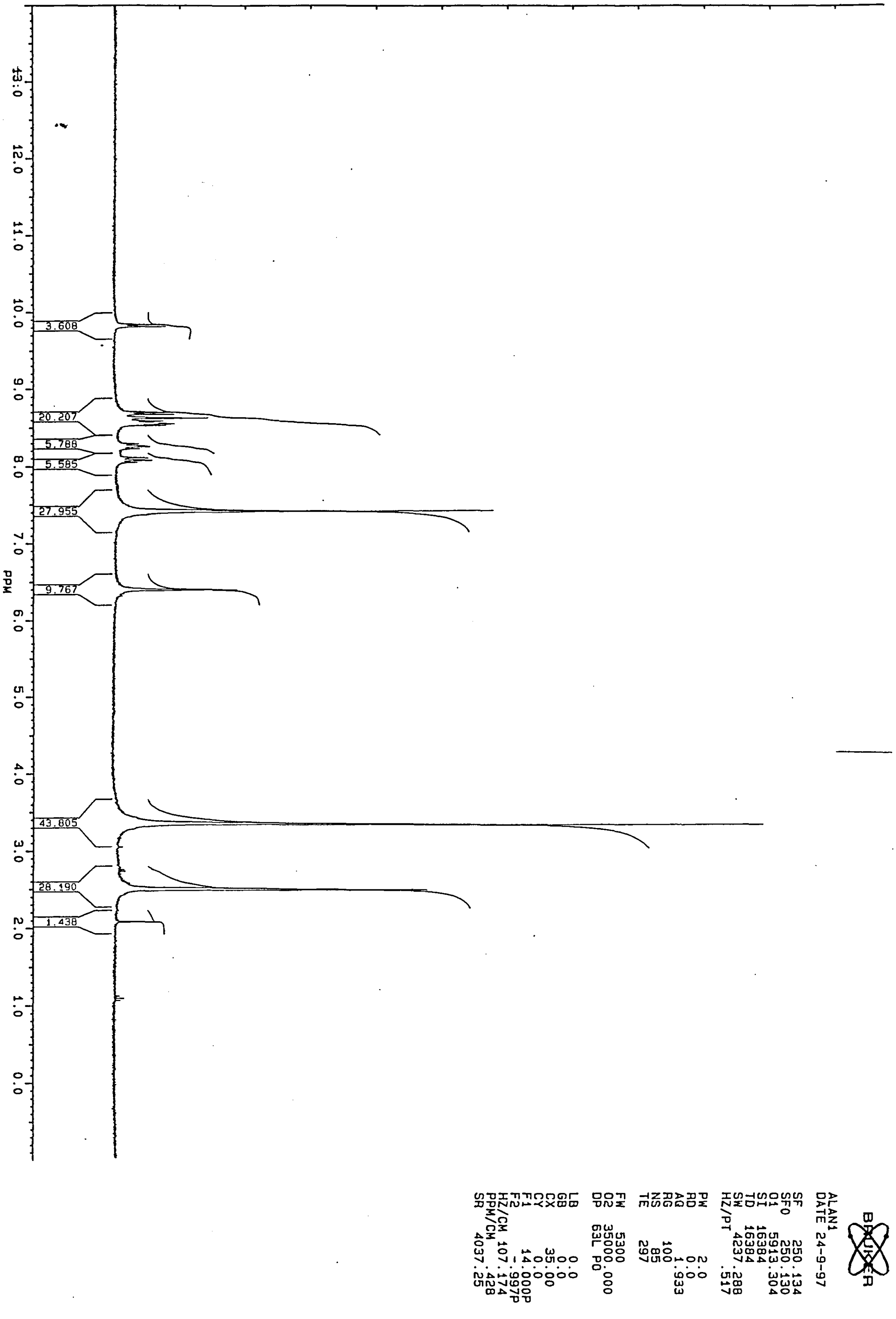

Figure 2.39 ^{1}H NMR Spectrum of PhCH$_2$(4)Q3CNQF$_4$ in d$_6$-DMSO.

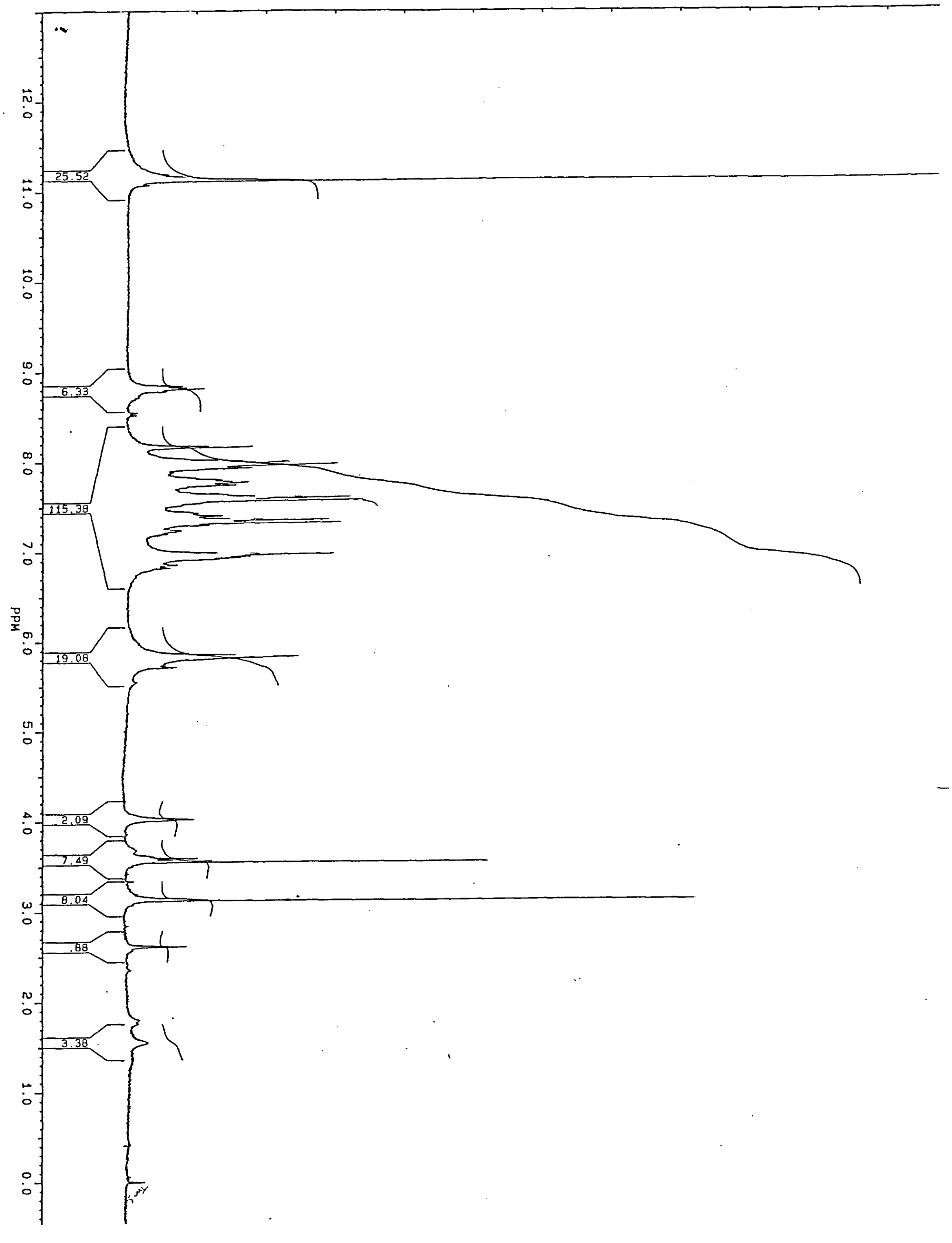

Figure 2.40 ^{1}H NMR Spectrum of p-C_8H_8(4)DQ6CNQ in d_1-TFA.

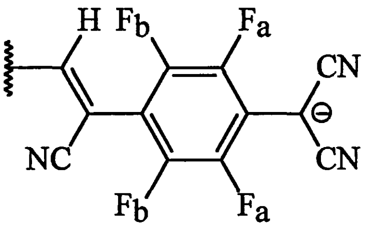

Figure 2.41 Two Distinct Fluorine Environments.

NMR characterisation of the diquinolinium adducts was hampered by their poor solubility in solvents used for the other compounds (e.g. d_6-DMSO, d_6-acetone etc). However this problem was resolved by the use of deuterated trifluoroacetic acid (d_1-TFA), although this did result in the protonation of the two dicyanomethanide swallowtails (Figure 2.42) which was observed at 3.6ppm as a singlet.

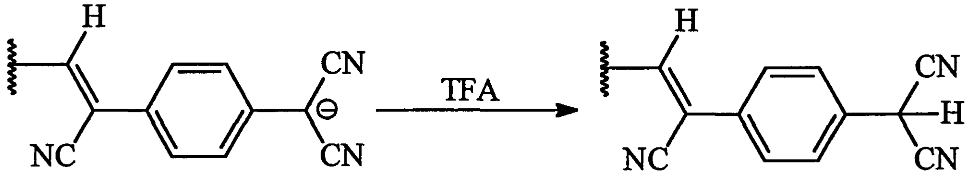

Figure 2.42 Protonation of Dicyanomethanide Swallowtail By TFA.

Spectra obtained for the TCNQ-based diadducts were quite similar in that complex aromatic regions were observed as expected. The most important feature in these spectra was the appearance of two singlet peaks at 3.2 and 4.1ppm (Figure 2.40) which corresponds to the NMR shifts of methanol[60] thus confirming the inclusion of solvent molecules in the crystal lattice.

On the other hand the spectra acquired for the TMTCNQ-based diadducts were quite different. The complicated array of peaks observed between 2.00 and 3.00ppm were thought to be characteristic of the four methyl groups of the TMTCNQ acceptor moiety in such compounds. However the poor quality of the aromatic region of the spectra obtained, together with the fact that subsequent TLC analysis (90:10 DCM/CH_3OH eluant) of the dissolved adducts has shown several spots, led to the conclusion that the trifluoroacetic acid had caused decomposition of the TMTCNQ-based diadducts. Hence characterisation of these diadducts was obtained via other techniques such as infrared spectroscopy, mass spectrometry etc.

2.7 References.

1. A. J. Riddick, W. B. Bunger and T. K. Sakano, *Organic Solvents., Physical Properties and Methods of Purification*, 4th ed., John Wiley and Son Inc., New York, 1986.
2. R. A. Broughton, PhD Thesis, *Sheffield Hallam University*, 1993.
3. M. Szablewski, PhD Thesis, *Cranfield Institute of Technology*, 1991.
4. C. S. Bradley, PhD Thesis, *Sheffield Hallam University*, 1999.
5. P. Murrill, *J. Am. Chem. Soc.*, 1899, **21**, 828.
6. A. Aumüller and S. Hünig, *Liebigs Ann. Chem.*, 1984, 618.
7. A. Kini, M. Mays and D. Cowan, *J. Chem. Soc., Chem. Commun.*, 1985, 286.
8. R. C. Wheland and E. L. Martin, *J. Org. Chem.*, 1975, **40**, 3101.
9. J. Mirck, M. Adamczyk and M. Mokrosz, *Synthesis*, 1980, 296.
10. A. Aumüller and S. Hünig, *Liebigs Ann. Chem.*, 1986, 142.
11. J. A. Zoltewicz and L. W. Deady, *Adv. Heterocycl. Chem.*, 1978, **22**, 71.
12. N. Menschutkin, *Z. Phys. Chem.*, 1890, **6**, 41.
13. A. T. Bottini, *Sel. Org. Transform.*, 1970, **1**, 89.

14. T. Watson, MSc Thesis, *Cranfield Institute of Technology*, 1986.

15. G. J. Ashwell, E. J. C. Dawnay, A. P. Kuczyñski, M. Szablewski, I. M. Sandy, M. R. Bryce, A. M. Grainger and M. Hasan, *J. Chem. Soc., Faraday Trans.*, 1990, 86, 1117.

16. G. J. Ashwell, G. Jefferies, E. J. C. Dawnay, A. P. Kuczyñski, D. E. Lynch, Y. Gongda and D.G. Bucknall, *J. Mater. Chem.*, 1995, **5**, 975.

17. N. A. Bell, R. A. Broughton, J. S. Brooks, T. A. Jones and S. C. Thorpe, *Int. J. Electronics*, 1994, **76**, 751.

18. B. Rosenau, C. Krieger and H. A. Staab, *Tetrahedron Lett.*, 1985, **26**, 2081.

19. S. Yamaguchi, H. Tatemitsu, Y. Sakata and S. Misumi, *Chem. Lett.*, 1983, 229.

20. A. M. Kini, D. O. Cowan, F. Gerson and R. Möckel, *J. Am. Chem. Soc.*, 1985, **107**, 556.

21. W. Lehnert, *Tetrahedron Lett.*, 1970, **54**, 4723.

22. W. Lehnert, *Synthesis*, 1974, 667.

23. A. J. Fatiadi, *Synthesis*, 1978, 165 and references cited therein.

24. E. Knoevenagel, *Ber. Dtsch. Chem. Ges.*, 1898, **31**, 2596.

25. M. R. Bryce, S. R. Davies, A. M. Grainger, J. Hellberg, M. B. Hursthouse, M. Mazid, R. Bachmann and F. Gerson, *J. Org. Chem.*, 1992, **57**, 1690.

26. B. S. Ong and B. Keoshkerian, *J. Org. Chem.*, 1984, **49**, 5002.

27. J. Y. Becker, J. Bernstein, S. Bittner, E. Harlev, and J. A. R. P. Sarma, *J. Chem. Soc., Perkin Trans. II.*, 1989, 1157.

28. P. Victory, J. I. Borrell, A. Vidal-Ferran, C. Seoane and J. L. Soto, *Tetrahedron Lett.*, 1991, **32**, 5375.

29. T. Czekanski, M. Hanack, J. Y. Becker, J. Bernstein, S. Bittner, L. Kaufman-Orenstein and D. Peleg, *J. Org. Chem.*, 1991, **56**, 1569.

30. K. Kobayashi and C. L. Gajurel, *J. Chem. Soc., Chem. Commun.*, 1986, 1779.

31. Y. Yamashita, T. Suzuki, T. Mukai and G. Saito, *J. Chem. Soc., Chem. Commun.*, 1985, 1044.

32. P. Bando, K. Davidkov, N. Martín, J. L. Segura, C. Seoane, A. González and J. M. Pingarrón, *Synth. Met.*, 1993, **55**, 1726.

33. L. Birkofer, A. Ritter and P. Richter, *Tetrahedron Lett.*, 1962, **5**, 195.

34. G. Jones, *Org. React.*, 1967, **15**, 204.

35. C. S. Bradley, Personal Communication.

36. F. S. Prout, *J. Org. Chem.*, 1953, **18**, 928.

37. F. Freemore, *Chem. Rev.*, 1969, **69**, 591.

38. F. Freemore, *Chem. Rev.*, 1980, **80**, 329.

39. F. Freemore, *Synthesis*, 1981, 925.

40. E. D. Bergmann, D. Ginsburg and R. Pappo, *Org. React.*, 1959, **10**, 182.

41. A. Streitwiesser, C. H. Heathcock and E. M. Kosower, *Introduction to Organic Chemistry*, 4th ed., MacMillan Publishers, 1992.

42. J. March, *Advanced Organic Chemistry*, 4th ed., Wiley Publishers, 1992, 641.

43. R. M. Metzger, N. E. Heimer and G. J. Ashwell, *Mol. Cryst. Liq. Cryst.*, 1984, **107**, 733.

44. N. A. Bell, R. A. Broughton, J. S. Brooks, T. A. Jones, S. C. Thorpe and G. J. Ashwell, *J. Chem. Soc., Chem. Commun.*, 1990, 325.

45. R. M. Metzger, B. Chen, U. Höpfner, M. V. Lakshmikantham, D. Vuillaume, T. Kawai, X. Wu, H. Tachibana, T. V. Hughes, H. Sakurai, J. W. Baldwin, C. Hosch, M. P. Cava, L. Brehmer and G. J. Ashwell, *J. Am. Chem. Soc.*, 1997, **119**, 10455.

46. G. J. Ashwell, *UK. Patent. Appl.*, No 9007230.7. (1990)

47. S. Arai, H. Arai, M. Hida and T. Yamagishi, *Heterocycles*, 1994, **38**, 2449.

48. G. J. Ashwell, T. W. Walker, I. R. Gentle, G. J. Foran, G. S. Bahra and C. R. Brown, *J. Mater. Chem.*, 1996, **6**, 969.

49. W. R. Hertler, H. D. Hartzler, D. S. Acker and R. E. Benson, *J. Am. Chem. Soc.*, 1962, **84**, 3387.
50. K. Tsujimoto, T. Fujimori and M. Ohashi, *J. Chem. Soc., Chem. Commun.*, 1986, 304.
51. U. Schubert, S. Hünig and A. Aumüller, *Liebigs Ann. Chem.*, 1985, 1216.
52. E. Ortí, R. Viruela and P. M. Viruela, *J. Mater. Chem.*, 1995, **5**, 1697.
53. M. Szablewski, Personal Communication.
54. G. J. Ashwell, I. M. Sandy, A. Chyla and G. H. Cross, *Synth. Met.*, 1987, **19**, 463.
55. M. Szablewski, P. R. Thomas, A. Thornton, D. Bloor, G. H. Cross, J. M. Cole, J. A. K. Howard, M. Malagoli, F. Meyers, J. L. Brédas, W. Wenseleers and E. Goovaerts, *J. Am. Chem. Soc.*, 1997, **119**, 3144.
56. J. S. Chappell, A. N. Bloch, W. A. Bryden, M. Maxfield, T. O. Poehler and D. O. Cowan, *J. Am. Chem. Soc.*, 1981, **103**, 2442.
57. A. Terzis, E. I. Kamitsos, V. Pscharis, J. S. Zambounis, J. Swiatek and J. Papavassilou, *Synth. Met.*, 1987, **19**, 481.
58. J. H. van der Maas, *Basic Infrared Spectroscopy*, 2nd ed.; Heyden & Sons Ltd; 1972
59. G. J. Ashwell, M. Malhotra, M. R. Bryce and A. M. Grainger, *Synth. Met.*, 1991, **41**, 3173.
60. D. H. Williams and I. Fleming, *Spectroscopic Methods in Organic Chemistry*, 3rd ed., McGraw-Hill Publishers, 1980.
61. (a) K. Biemann, *Anal. Chem.*, 1986, **58**, 1288A. (b) K. L. Rinehart Jr., *Science*, 1982, **218**, 254.

Chapter 3: Solvatochromism and Halochromism Studies.

3.1 Solvent Polarity.

It has long been known that choice of solvent can influence both the rate and equilibrium of chemical reactions,[1-3] as well as the position and intensity of spectral absorption bands.[4-6] Chemists have tried to understand the effect of different solvents in terms of "solvent polarity", which is not easy to define or express quantitatively. The simplistic idealised electrostatic models for describing the solvation of ions and molecules in solution has led to the use of specific solvent parameters such as the *dielectric constant* (ε_r), *permanent dipole moment* (μ), *refractive index* (n) or functions thereof. However, this approach is often inadequate as the intermolecular interactions between solute and solvent molecules are much more complicated than is often assumed. A fine example of this is shown by the solvatochromic shifts exhibited by Z-β-[(N,N-diethylmethylimmonium)-α-cyano-4-styryldicyanomethanide] DEMI (Figure 3.1)[7] for which the longest wavelength charge-transfer absorption band, measured in acetonitrile (λ_{max} = 698nm, ε_r = 35.94), appears at a longer wavelength than that measured in methanol (λ_{max} = 688nm, ε_r = 32.66). If the shift was proportional to solvent polarity in terms of dielectric constant, then the reverse would be expected.

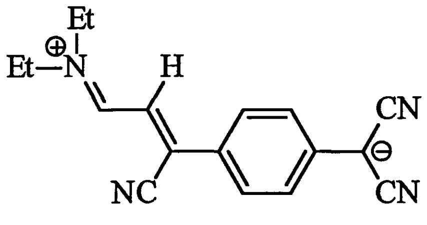

Figure 3.1 The Solvatochromic DEMI Compound.

The reason is the differential solvation of molecules in the corresponding ground and excited states. The extent to which this differential solvation occurs depends greatly upon the intermolecular forces between the solute and the surrounding solvent molecules. These intermolecular forces occur on a molecular microscopic level. They include: non-specific forces such as electrostatic forces arising from coulombic effects between charged ions and dipolar molecules (i.e. ion-ion, ion-dipole, dipole-dipole interactions); polarisation forces arising from dipole moments induced in molecules by nearby ions or dipolar molecules (i.e. ion-nonpolar molecule, dipolar-nonpolar molecule, two nonpolar molecules), and specific forces such as hydrogen bonding and electron pair donor (EPD) / electron pair acceptor (EPA) forces.[8] Single solvent parameters often fail due both to i) neglect of specific solute / solvent interactions, and ii) consideration of interactions only on a macroscopic level.[9]

Reichardt et al[4,10] defined solvent polarity as "the overall solvation capability (or solvent power) of a solvent" which in turn depends upon the action of every possible specific and non-specific intermolecular interaction between solute ions or molecules and solvent molecules, including solute-solute (at high solute concentrations) and solvent/solvent interactions. It excludes those interactions which lead to the definite chemical alteration of the solute (i.e. oxidation, reduction, protonation).

3.2 Solvatochromism and Solvatochromic Compounds.

Solvatochromism describes the change in λ_{max} (and sometimes intensity) of a UV/Vis absorption band of a chromophore accompanying a change in the polarity of the medium. This effect is caused by the differential solvation of the corresponding ground and first excited states of the light absorbing molecule.

If, with increasing medium polarity, the electronic ground state of the chromophore is more stabilised than that of the first excited state then a ***hypsochromic*** (blue) shift of the absorption band is observed (often termed ***negative*** solvatochromism). On the other hand, if greater stabilisation of the chromophore in its first excited state relative to the ground state occurs, then a ***bathochromic*** (red) shift will be observed (often termed ***positive*** solvatochromism).

The first excited state is the *Frank-Condon* state[4,11] which, in most cases, has the same solvation pattern as that of the corresponding ground state. The time required for the molecule to become electronically excited (about 10^{-15} s) is much shorter than that required for the nuclei of the absorbing entity to execute vibrations or rotations (about 10^{-12} to 10^{-10} s). So the nuclei of the absorbing entity do not appreciably alter their positions during the electronic transition.[11] Here, the solvatochromism observed depends upon the chemical structure and physical properties of the chromophore and the nature of the solvent. In general, dye molecules which show a large change in their permanent dipole moment upon excitation exhibit strong solvatochromism. If upon excitation the solute's dipole moment increases then a positive solvatochromism is normally observed.

This is the case for *p*-(N,N-dimethylamino)-*p*-nitro-transstilbene (NNS)[12] (Figure 3.2) which exhibits a maximum at 418 nm in heptane and 454 nm in dimethylsulphoxide - a bathochromic shift of +36 nm.

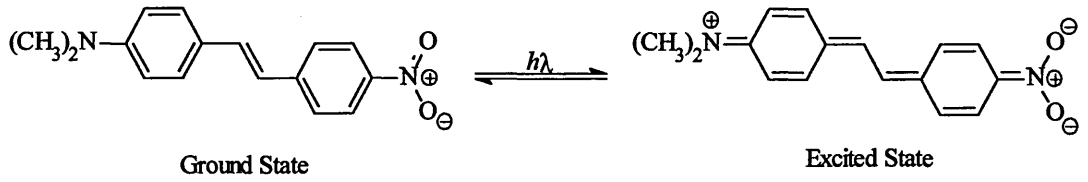

Figure 3.2 The Positively Solvatochromic NNS Chromophore.[12]

If, on the other hand, the dipole moment of the solute decreases upon excitation, then a negative solvatochromism is usually observed. For example the phosphonio-iminophenolate betaine dye prepared by *Allen et al*[13] (Figure 3.3) shows a distinct hypsochromic shift of −74 nm from tetrahydrofuran (578 nm) to acetonitrile (504 nm).

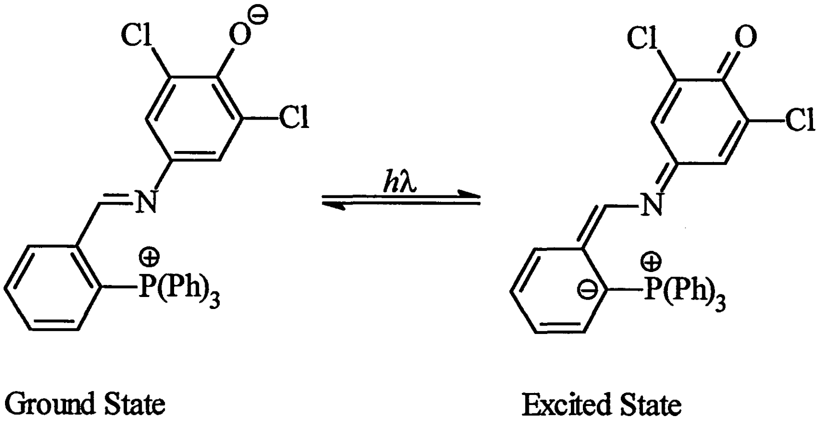
Cl
O⊖
Cl
N
⊕
P(Ph)3
hλ
Cl
O
Cl
N
⊖
⊕
P(Ph)3
Ground State
Excited State

Figure 3.3 Phosphonio-iminophenolate Betaine.

However, pronounced solvatochromic behaviour is not only limited to intramolecular processes. Large shifts are observed for compounds whose absorption bands arise from intermolecular charge-transfer. A striking example of this is the negative solvatochromic effect observed for the EPD/EPA complex of 1-ethyl-4-methoxycarbonylpyridinium iodide.[14] (Figure 3.4)

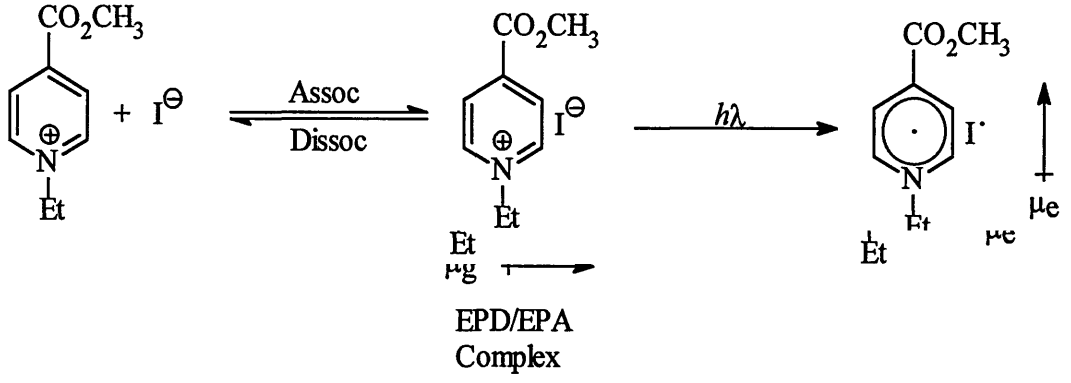
CO2CH3
⊕
N
Et
+ I⊖
Assoc
Dissoc
CO2CH3
⊕
N
Et
I⊖
Et
μg
EPD/EPA
Complex
hλ
CO2CH3
N
Et
I·
Et
μe
μe

Figure 3.4 Kosower's EPD/EPA Complex.[14]

The absorption band of this ground state ion-pair complex corresponds to an intermolecular transfer of an electron from the iodide to the pyridinium ion. This results in loss of charge and change in direction of the dipole moment of the complex during transition,[4,14] so that a hypsochromic shift of –88 nm occurs in the absorption band from pyridine (430 nm) to methanol (342 nm). This led Kosower[14] to use the compound for the development of the Z scale empirical parameter of solvent polarity.

In general, solvatochromic compounds either exhibit positive or negative solvatochromism. However, the existence of *reverse* (sometimes called "*inverse*") solvatochromism, in which a compound can show both positive and negative solvatochromism, has been observed in various compounds.[13,15,16] One of the more frequently quoted examples, is that of *Brooker's* merocyanine dye[17] 4-[(1-methyl-4(1H)-pyridinylidene)-ethylidene]-2,5-cyclohexadien-1-one (Figure 3.5), which shows a particularly interesting reverse solvatochromism. As the polarity of the medium is increased, it initially exhibits a bathochromic shift of +28 nm from cyclohexane (592 nm) to chloroform (620 nm) and then a hypsochromic shift of –178 nm on going from chloroform (620 nm) to water (442 nm).[18]

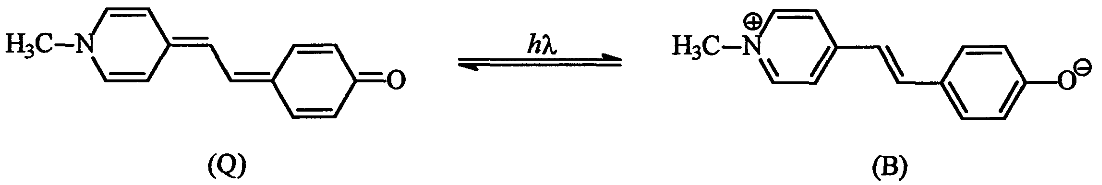

Figure 3.5 Brooker's Merocyanine Dye.[17]

The proposed reason for this reverse solvatochromism is the change from the neutral quinoidal structure (Q) to the charge-separated benzenoid structure (B) in the electronic ground state of the dye, with increasing solvent polarity.[19]

In solvents of low polarity such as cyclohexane, the uncharged quinoidal form (Q) is better stabilised via weak, non-polar solvent interactions, and therefore predominates. Thus a bathochromic shift is observed. As solvent polarity increases, the charge separated zwitterionic form (B) becomes dominant as the solvent, with its increased polarity, is better able to solvate the more polar, charge-separated state.[19] Hence observed solvatochromism switches from positive to negative due to the change in electronic ground state of the dye.

However, some authors[20] have suggested that inverse solvatochromism is attributed to an aggregation phenomenon, in which a head to tail arrangement of the dye units occurs, rather than a change in the structure. This stabilises the ground state molecules and so shifts of the spectral band to lower wavelengths with decreasing solvent polarity result, thereby producing a bathochromic shift of the absorption band.

Spectroscopic analysis (e.g. UV/Vis, near-IR) of known solvatochromics is then, a fairly simple empirical probe for solvent "polarity". Due to the inadequacy of idealised electrostatic models in discussing solvent polarity, solvatochromism provides a convenient means for its assessment. The common approach used in developing such empirical parameters is to assume that a particular spectral absorption band is a suitable and representative model for other solvent dependent processes.

The first real empirical parameter of solvent polarity was the Y scale introduced by *Winstein et al*[21], which uses the S_N1 heterolysis of *tert*-butylchloride as its model process. The first suggestion that solvatochromic dyes could be used as indicators of solvent polarity was made by *Brooker et al*[17,22] who defined the χ_R and χ_B scales.[22] *Kosower et al*[14] were the first to set up a real spectroscopic solvent scale, the Z scale[14] (see earlier).

Since then, various UV/Vis/near-IR based solvent polarity scales have been developed using compounds which exhibit positive and negative solvatochromism. Examples include: the PRM scale of *Dahne et al*,[23] the π^* scale of *Kamlet et al*,[24] the π^*_{azo} scale of *Buncel et al*,[25] the P_S scale of *Middleton et al*,[26] the $E_T(30)$ scale of *Dimroth* and *Reichardt*,[27] the E_K scale of *Walther et al*,[28] the ϕ scale of *Dubois et al*,[29] the S scale of *Zelinskii et al*[30] and the Py (or Pyrene) scale of *Dong* and *Winnik*.[31]

Because of the vast array of solvent polarity indicators, it is often difficult to know which one to use when correlating solvatochromic effects. However, four have been found to be particularly good models for the empirical determination of solvent parameters because of their pronounced solvatochromic properties:

1) The previously mentioned Z scale of *Kosower*;
2) The π^* scale developed by *Kamlet et al*[24];
3) The π^*_{azo} scale introduced by *Buncel et al*[25] (similar to the π^* scale), and
4) The $E_T(30)$ scale developed by *Dimroth* and *Reichardt*[27]

The $E_T(30)$ scale is probably the most widely used single parameter empirical scale to define solvent polarity. The scale is based upon the solvatochromic shift of the first absorption maximum of a pyridinium N-phenolate betaine dye (Figure 3.6). This negatively solvatochromic probe molecule exhibits one of the largest solvatochromic shifts observed. Its longest wavelength intramolecular absorption band is hypsochromically shifted by $-9730\ cm^{-1}$ (357 nm) on going from diphenyl ether (λ_{max} = 810 nm) to water (λ_{max} = 453 nm).

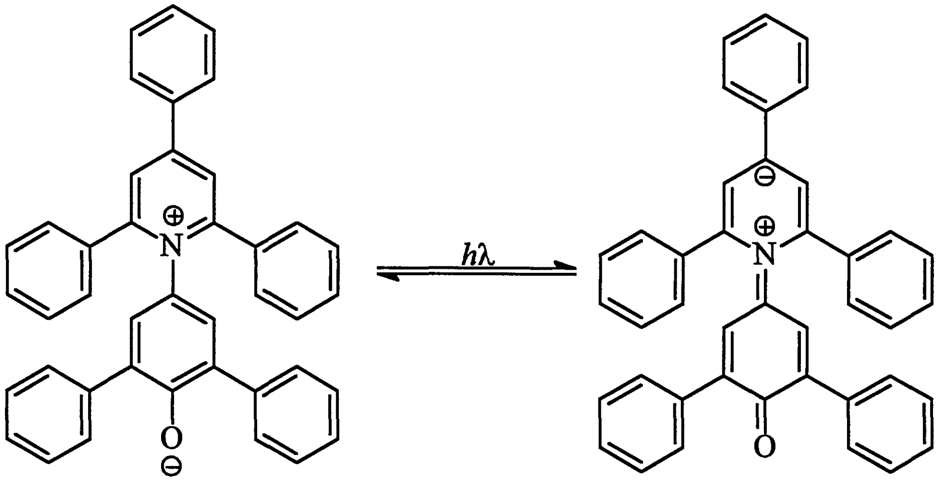

Figure 3.6 Reichardt's Dye.

Solutions of the probe are red in methanol, violet in ethanol, blue in isoamyl alcohol, green in acetone and yellow/green in ethyl acetate, thus covering the whole visible region and even allowing a visual estimate of the solvent polarity. This large solvatochromism stems from the unequal, differential solvation of its highly dipolar charge-separated ground state (μ_g =15D)[4,32] relative to its less dipolar excited state (μ_e = 6D).[4,32] $E_T(30)$ values are simply defined as the molar electronic transition energies (E_T), measured in kcal mol^{-1} at room temperature (25^{0}C) and normal pressure (1 bar), of the dye in a specific solvent (Figure 3.7) and according to Equation 3.1.

$$E_T(30)\,(\text{kcal mol}^{-1}) = hc.\nu.N_A = (2.8591\times10^{-3}).\nu = 28591 / \lambda_{\max}\,(\text{nm}) \qquad \text{Equation 3.1}$$

where h is Plancks constant, c is the speed of light in a vacuum, N_A is Avogadro's constant, and ν and λ_{max} are the respective frequency and wavelength of the π-π^* transition of Reichardt's dye.

$E_T(30)$ values range from an upper value of 63.1 kcal mol^{-1} for water to a lower limit of 30.7 kcal mol^{-1} for tetramethylsilane. Thus a high E_T (30) value corresponds to high solvent polarity and vice versa.

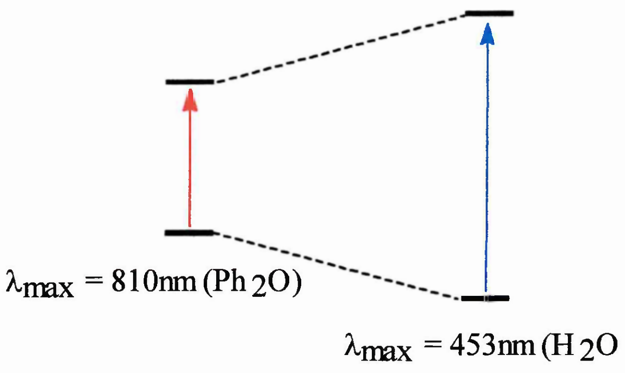
λ_{max} = 810nm (Ph 2O)
λ_{max} = 453nm (H 2O

Figure 3.7 Molar Transition Energy.

In order to avoid recalculation of $E_T(30)$ values from kcal mol^{-1} to KJ mol^{-1} a normalised and dimensionless E_T^N value was introduced. The new normalised values are defined by Equation 3.2[33] and use water and tetramethylsilane (TMS) as extreme polar and non-polar respectively.

$$\begin{aligned} E_T^N \text{ Value } &= [E_T(\text{solvent}) - E_T(\text{TMS})] \,/\, [E_T(\text{water}) - E_T(\text{TMS})] \qquad \text{Equation 3.2} \\ &= [E_T(\text{solvent}) - 30.7] / 32.4 \end{aligned}$$

So, normalised E_T^N scale values range from 0.00 (for TMS) to 1.00 (for water). Depending upon the conditions, the $E_T(30)$ values as well as the dimensionless E_T^N values can be used equally well. The $E_T(30)$ value has the advantage of giving an immediate insight into the magnitude of the solvent effects observed, whereas the E_T^N values are easier to handle particularly in multi-parameter correlation equations. The E_T^N and $E_T(30)$ scales roughly divide organic solvents into three groups:[4]

1) Apolar non-HBD (hydrogen bonding donor) solvents: $E_T(30)$: 30-40 kcal mol^{-1}; E_T^N: 0.0-0.3, e.g: cyclohexane, benzene.
2) Dipolar non-HBD (aprotic) solvents: $E_T(30)$: 40-47 kcal mol^{-1}; E_T^N: 0.3-0.5, e.g: acetone, N,N-dimethylformamide (DMF), dimethylsulphoxide (DMSO).
3) Dipolar HBD (protic) solvents: $E_T(30)$: 47-63 kcal mol^{-1}; E_T^N: 0.5-1.0, e.g: methanol, water.

As well as models for developing solvent polarity scales, compounds exhibiting solvatochromism are also of potential interest as systems which may exhibit nonlinear optical properties (Chapter 4), with many strongly solvatochromic compounds exhibiting second harmonic generation.[34]

3.3 Halochromism.

The addition of electrolytes, such as alkali metal salts to solutions of *Reichardt's* type dyes (Figure 3.6) often leads to a hypsochromic shift of the absorption band, depending upon the nature and concentration of the electrolyte added.[4,35] This phenomenon has been termed *halochromism.* An understanding of halochromism is made more difficult in comparison to solvatochromism due to the involvement of a three component system (solute, solvent and ionophore). Two distinct approaches have been put forward.

The first regards halochromic shifts as arising from alterations in the solvent structure, i.e. changes in the ionic strength of electric field[36] of the solvent, or it may be simply regarded as a structure making or structure breaking species which alters the bulk properties of the solvent.[37]

The second approach simply correlates the halochromic shifts with changes in the micro-environment of the dye (caused by the addition of the electrolyte) - the properties of which are not equivalent to those of the bulk medium. It is difficult to make an unambiguous choice between the two approaches,[38] because both specific and non-specific effects are likely to co-occur in such systems. However, it is generally accepted that halochromism results from changes in the micro-environment of the dye.[39] The halochromism exhibited by *Reichardt's* betaine dye is probably the best documented example. The shift of its longest wavelength charge-transfer (CT) absorption band depends upon the nature and concentration of the electrolyte added.[40] The shift increases with electrolyte order, that is with increasing effective cation charge. In contrast the anions seem to exert little or no influence on this type of halochromism. There exists an almost linear correlation between the salt-induced negative halochromic shift of the dye and the charge to size ratio of cations added.

The position of the CT absorption band depends on the ionisation energy of the electron donor and on the electron affinity of the electron acceptor. Hence, cations of the added electrolytes increase the ionisation energy of the phenoxide group by reducing the overall electron donating capability of the phenoxide moiety due to the electrostatic oxygen-metal interaction. This corresponds to an increase in the CT excitation energy and results in an electrolyte induced hypsochromic shift (termed as negative halochromism by Reichardt).

The search for compounds with ever larger halochromic shifts has led to many fascinating developments. One of the more important ones was made by Reichardt himself who found that introducing crown-ether linkages[41] into the framework of the dye resulted in a more cation-selective species (Figure 3.8) than the original dye itself.[42]

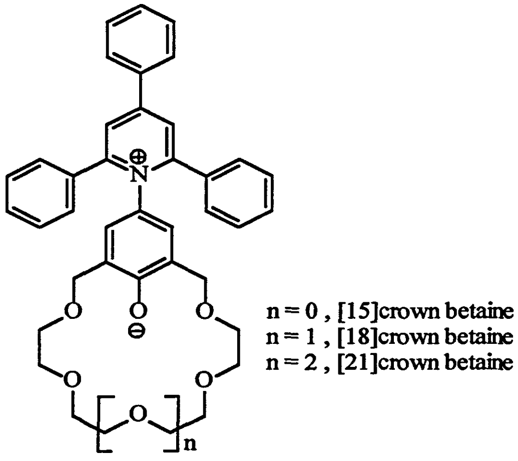
n = 0 , [15]crown betaine
n = 1 , [18]crown betaine
n = 2 , [21]crown betaine

Figure 3.8 Crown Ether Linked Betaines.

Hence, by altering the size of the cavity of the crown ether linkage, it was found that preferential complexation of a single type of cation could be achieved (e.g. [15]crown-4-betaine with Na^+). Because the absorption band of such systems lies within the visible region of the spectrum, the cation induced colour changes can be followed easily by the eye, thus enabling these chromoionophores to be used as cation indicators.

3.4 Solvatochromic Behaviour of Adducts.

As with other dipolar compounds[4,7,13] which exist in a charge-separated electronic ground state, almost all of the zwitterionic adducts synthesised in this work were found to exhibit pronounced negative solvatochromism. As an example, the fluorinated benzylic quinolinium betaine (Figure 3.9) gives a maximum frequency range of about –4813 cm^{-1} (198 nm) starting from an apple green colour in dichloromethane (λ_{max} =748 nm) through royal blue in acetone (λ_{max} =614 nm) to lilac in methanol (λ_{max} =550 nm).

This observation of negative solvatochromism is a reflection of the stabilisation of the dipolar betaine form (A) in increasingly more polar solvents relative to the less polar excited state (B). Further details follow.

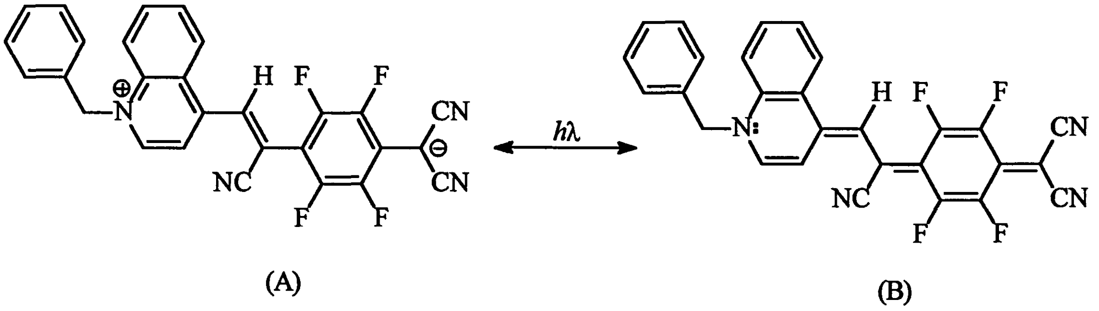

Figure 3.9 $PhCH_2(4)Q3CNQF_4$ Zwitterion.

3.4.1 Experimental.

The absorption spectra of twenty-three adducts have been measured in eighteen different solvents using a double beam ultra violet/visible (UV/Vis) ATI Unicam V2 spectrophotometer at 298K. Each spectrum was referenced to the solvent using two, 1cm path length quartz cuvettes, each filled with the solvent and inserted into the beam of the spectrophotometer. When this was complete, the sample cuvette was filled with a solution of chromophore of known concentration - typically 10^{-5}-10^{-6} mol dm^{-3}. Spectra were recorded in the range 210nm to 1100 nm - though of course dependent upon the UV cut off point of the solvent in question. All solvents used were HPLC grade (Aldrich-Sigma Co.) and dried to eliminate the effects of water using standard literature methods[43]. All measurements were carried out at room temperature.

The long-wavelength UV/Vis absorption charge-transfer absorption band of the adducts has also been measured in acetonitrile and methanol, with and without the addition of an excess of alkaline and alkaline earth salts (see Section 3.5). For the halochromic measurements, salt solutions of different concentrations [[salt]= 10^{-3}, 10^{-2} and 10^{-1} mol dm^{-3}] were prepared by dilutions of a stock solution [[salt]= 10^{-1} mol dm^{-3}].

The electrolyte was then thoroughly mixed with the appropriate amount of adduct solution (~10^{-4} mol dm^{-3} in acetonitrile or methanol) in the quartz cell to give the desired excess of electrolyte (i.e. tenfold, hundredfold, etc). Measurements were made against an electrolyte solution blank using matched 1cm quartz cells. The alkaline and alkaline earth salts were obtained form Aldrich-Sigma Co and were used without the further purification.

3.4.2 Solvatochromic Characteristics of R(4)Q3CNQ and R(2)Q3CNQ Adducts.

The solvatochromic behaviour of compounds of types (I) and (II) have been documented by others.[44-48]

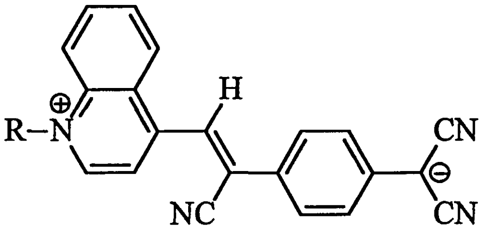

(I)

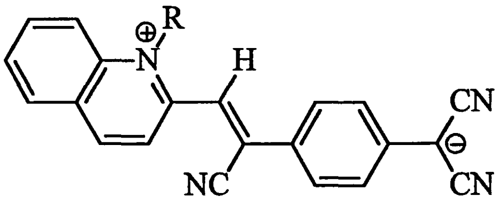

(II)

However, the range of solvents used in this previous work[44-48] was limited and insufficient to enable effective comparisons of the substituent effects on the solvatochromic behaviour to be drawn. Therefore the solvatochromic behaviour of these materials has been re-investigated using a more comprehensive range of solvents. The longest wavelength intramolecular CT absorption bands, λ_{max}, of representative examples of the isomeric compounds are listed below:

1) R(4)Q3CNQ Adducts (e.g. $C_{10}H_{21}(4)Q3CNQ$)[44,45]

Solvent	ε_r[49]	λ_{max} (nm)	Solvent	ε_r[49]	λ_{max} (nm)
NMF[a]	182.4	696	Acetone	20.56	760
DMSO[b]	46.45	692	2-Butanone	18.51	766
DMF[c]	36.71	722	4M2P[d]	13.11	826
Acetonitrile	35.94	708	Dichloromethane	8.93	890
Nitromethane	35.87	718	THF[e]	7.58	894
Methanol	32.66	674	Chlorobenzene	5.62	942
Benzonitrile	25.20	808	Chloroform	4.81	930

[a] N-methylformamide (NMF), [b] dimethylsulphoxide (DMSO), [c] N,N-dimethylformamide (DMF), [d] 4-methyl-2-pentanone (4M2P), [e] tetrahydrofuran (THF).

Table 3.4.1 Solvatochromic Shifts of the R(4)Q3CNQ Zwitterions.

The solvatochromism exhibited by the unsubstituted R(4)Q3CNQ homologues is independent of the alkyl chain length (R) and results in most long chain derivatives exhibiting very large negative solvatochromic shifts. For example the decyl derivative (Table 3.4.1) shows a hypsochromic shift of –4221 cm^{-1} (268 nm) on going from chlorobenzene (λ_{max} = 942 nm) to methanol (λ_{max} = 674 nm).

2) R(2)Q3CNQ Adducts (e.g. $C_{10}H_{21}(2)Q3CNQ$)[46]

Solvent	ε_r[49]	λ_{max} (nm)	Solvent	ε_r[49]	λ_{max} (nm)
NMF[a]	182.4	684	Acetone	20.56	754
DMSO[b]	46.45	680	2-Butanone	18.51	790
DMF[c]	36.71	704	4M2P[d]	13.11	798
Acetonitrile	35.94	702	Dichloromethane	8.93	848
Nitromethane	35.87	708	THF[e]	7.58	850
Methanol	32.66	664	Chlorobenzene	5.62	884
Benzonitrile	25.20	786	Chloroform	4.81	874

[a] N-methylformamide (NMF), [b] dimethylsulphoxide (DMSO), [c] N,N-dimethylformamide (DMF), [d] 4-methyl-2-pentanone (4M2P), [e] tetrahydrofuran (THF).

Table 3.4.2 Solvatochromic Shifts of the R(2)Q3CNQ Zwitterions.

In contrast the isomeric α-substituted derivatives show a distinctly smaller solvatochromic shift relative to their γ-substituted counterparts with the decyl analogue (Table 3.4.2) exhibiting a hypsochromic shift of –3748 cm^{-1} (220 nm) on going from chlorobenzene (λ_{max} = 884 nm) to methanol (λ_{max} = 664 nm).

The solvatochromic behaviour shown by the R(4)Q3CNQ and R(2)Q3CNQ type adducts is extremely large when compared to other TCNQ-based systems[7,50] and is consistent with a transition involving back charge-transfer from the negatively charged dicyanomethanide group to the positively charged nitrogen heterocycle resulting in a neutral excited state. The large negative solvatochromism exhibited by both isomers correlates well with various solvent polarity scales. Even the limited dielectric constant parameter gives a clear indication of the hypsochromic shifts observed in such compounds (Figure 3.10).

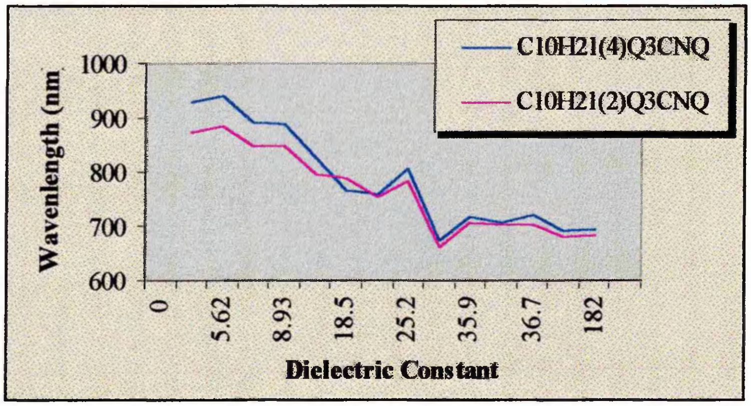

Figure 3.10 Negative Solvatochromism of the TCNQ-based Zwitterions.

However anomalies do occur with this scale, as protic solvents such as methanol tend to cause a much greater shift than expected. Because of this the $E_T(30)$ scale has been employed instead as a measure of the interaction of adduct molecules with the solvent systems.

The molar transition energy is used in the present discussion to compare various betaine-solvent media interactions. The normalised empirical solvent polarity parameters, E_T^N of Reichardt's dye, the longest wavelength intramolecular CT absorption band, ν_{max} ($=1/\lambda_{max}$), of the above zwitterions, and corresponding transition energies, E_T, are shown in Table 3.4.3.

Solvent	$E_T(30)$	$C_{10}H_{21}(4)Q3CNQ$		$C_{10}H_{21}(2)Q3CNQ$	
	E_T^N	ν_{max} $\times 10^3$ cm^{-1}	E_T kcal mol^{-1}	ν_{max} $\times 10^3$ cm^{-1}	E_T kcal mol^{-1}
Methanol	0.762	14.84	42.42	15.06	43.06
NMF[a]	0.722	14.37	41.08	14.62	41.80
Nitromethane	0.481	13.93	39.82	14.12	40.38
Acetonitrile	0.460	14.12	40.38	14.25	40.73
DMSO[b]	0.444	14.45	41.32	14.71	42.05
DMF[c]	0.386	13.85	39.56	14.20	40.61
Acetone	0.355	13.16	37.62	13.26	37.92
Benzonitrile	0.333	12.38	35.39	12.72	36.38
2-Butanone	0.327	13.06	37.33	12.63	36.19
Dichloromethane	0.309	11.24	32.12	11.79	33.72
4M2P[d]	0.269	12.11	34.61	12.53	35.83
Chloroform	0.259	10.75	30.70	11.44	32.71
THF[e]	0.207	11.19	31.98	11.76	33.64
Chlorobenzene	0.188	10.61	30.35	11.31	32.34

[a] N-methylformamide (NMF), [b] dimethylsulphoxide (DMSO), [c] N,N-dimethylformamide (DMF), [d] 4-methyl-2-pentanone (4M2P), [e] tetrahydrofuran (THF).

Table 3.4.3. Solvatochromic Shifts of the TCNQ-based Adducts.

For both of the above compounds, a plot of wavenumber, ν_{max}, for the longest wavelength visible absorption band of the unsubstituted quinolinium betaine against the normalised solvent polarity, E_T^N, for the Reichardt betaine is shown in Figure 3.11.

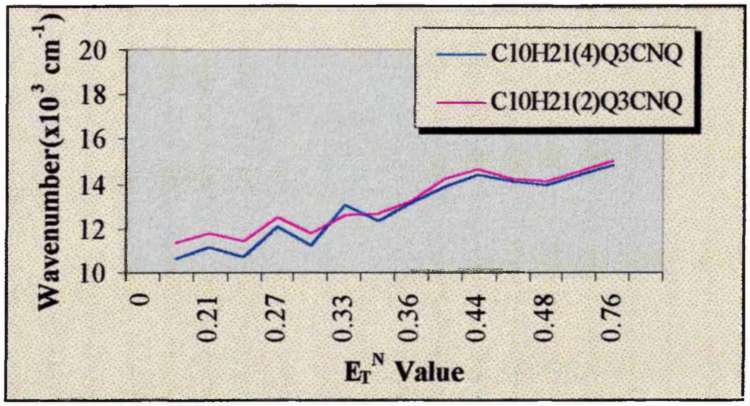

Figure 3.11 Solvatochromic Behaviour of the TCNQ-based Zwitterions.

The plot demonstrates solvent dependent behaviour of the unsubstituted quinolinium adducts revealing a negative solvatochromism. The plot is near linear, with positive slope. We can suggest that the hypsochromic shift observed in such compounds, which extends into the latter parts of the visible and fringes of the near-infrared regions of the spectrum makes them potential advanced optoelectronic materials, such as near infrared dyes.[51] Other push-pull chromophores such as *Otsubo's* diphenoquinoid compound (III),[52] have also been used in optoelectronic devices.

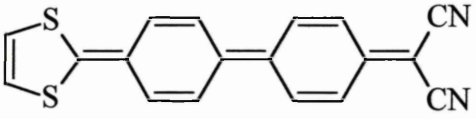

(III)

Although the solvatochromic behaviour of the above materials is less pronounced than that observed in compounds like Reichardt's dyes,[4] it does compare well with that observed in other D-π-A materials,[4] such as the long chain pyridinium iminophenolate betaine (IV) of *Li et al*[13,34] which exhibits a maximum shift of –3947 cm^{-1} (132 nm) on going from THF (λ_{max} = 648 nm) to methanol (λ_{max} = 516 nm).

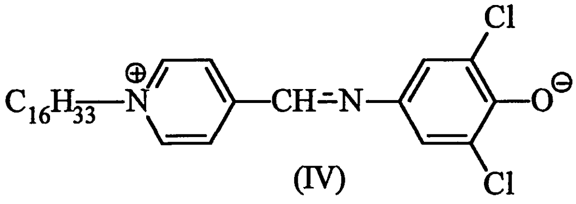
(IV)

The variation in solvatochromic behaviour exhibited by the two quinolinium isomers is attributed to the difference in ground state dipole moment (see Chapter 4) of the γ-derivative (31D in DCM), relative to that of its α-substituted counterpart (24D in DCM). The more polar γ-derivative is more polarisable and, as such, is likely to induce larger dipoles in the surrounding solvent cage, relative to that of the α-compound, resulting in a larger solvatochromic shift than the α-analogue. Despite this, the α-substituted compounds still exhibit a negative solvatochromism which is extremely large when compared to other TCNQ-based push-pull type systems.[7,53] For example, the series of TCNQ-based D-π-A materials developed at Durham University, of which DEMI (R^1=R^2=ethyl, Figure 3.12) was the first, exhibit only relatively small negative solvatochromic responses.[7,53] DEMI itself exhibits a shift of –684 cm^{-1} (34 nm) from chlorobenzene (λ_{max} = 722nm) to methanol (λ_{max} = 688 nm), despite its very large ground state dipole moment.[53]

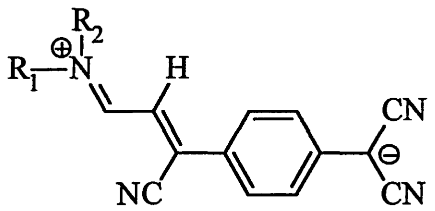

Figure 3.12 The Solvatochromic DEMI Chromophore.

3.4.3 Solvatochromic Characteristics of R(4)Q3CNQF$_4$ and R(2)Q3CNQF$_4$ Adducts.

The solvatochromic behaviour of a range of TCNQF$_4$-based adducts of the types R(4)Q3CNQF$_4$ and R(2)Q3CNQF$_4$ have also been studied. The longest wavelength intramolecular CT absorption bands, λ_{max}, are listed below.

1) C_nH_{2n+1}(4)Q3CNQF$_4$ (where n =10 to 18)

Solvent	ε_r^{49}	λ_{max} (nm)	Solvent	ε_r^{49}	λ_{max} (nm)
NMF[a]	182.4	554 ± 2	Acetone	20.56	596 ± 4
DMSO[b]	46.45	552 ± 2	2-Butanone	18.51	624 ± 2
DMF[c]	36.71	570 ± 2	4M2P[d]	13.11	660 ± 4
Acetonitrile	35.94	566 ± 1	Dichloromethane	8.93	720 ± 0
Nitromethane	35.87	570 ± 2	THF[e]	7.58	706 ± 4
Methanol	32.66	550 ± 3	Chlorobenzene	5.62	490 ± 8
Benzonitrile	25.20	650 ± 1	Chloroform	4.81	482 ± 6

[a] N-methylformamide (NMF), [b] dimethylsulphoxide (DMSO), [c] N,N-dimethylformamide (DMF), [d] 4-methyl-2-pentanone (4M2P), [e] tetrahydrofuran (THF).

Table 3.4.4 Solvatochromic Shifts of the Long Chain R(4)Q3CNQF$_4$ Zwitterions.

As with the unsubstituted compounds, the solvatochromism exhibited by the long chain fluorinated homologues (where R= C_{10} to C_{18}) is independent of chain length, with the shifts being the same in each solvent for all of the compounds examined. For example the decyl analogue (Table 3.4.4) exhibits a comprehensive hypsochromic shift of –4293 cm^{-1} (170 nm) on going from dichloromethane (λ_{max} = 720 nm) to methanol (λ_{max} = 550 nm). However in solvents of lower polarity than dichloromethane, the compounds then exhibit a significant bathochromic shift of +6857 cm^{-1} (238 nm), with an absorption maximum of 482 nm being observed in chloroform.

2) $CH_3(4)Q3CNQF_4$

Solvent	ε_r[49]	λ_{max} (nm)	Solvent	ε_r[49]	λ_{max} (nm)
NMF[a]	182.4	558	Acetone	20.56	588
DMSO[b]	46.45	558	2-Butanone	18.51	598
DMF[c]	36.71	574	4M2P[d]	13.11	588
Acetonitrile	35.94	572	Dichloromethane	8.93	590
Nitromethane	35.87	574	THF[e]	7.58	576
Methanol	32.66	574	Chlorobenzene	5.62	NS[†]
Benzonitrile	25.20	628	Chloroform	4.81	NS[†]

[a] N-methylformamide (NMF), [b] dimethylsulphoxide (DMSO), [c] N,N-dimethylformamide (DMF), [d] 4-methyl-2-pentanone (4M2P), [e] tetrahydrofuran (THF), [†] not soluble (NS).

Table 3.4.5 Solvatochromic Shifts of the $CH_3(4)Q3CNQF_4$ Zwitterion.

Only one short chain adduct ($CH_3(4)Q3CNQF_4$) was examined (Table 3.4.5) and in contrast to the series of longer chain homologues it exhibits only a relatively small negative solvatochromic response. Its intramolecular CT absorption band undergoes a hyposchromic shift of -1198 cm^{-1} (40 nm) on going from 2-butanone (λ_{max} = 598 nm) to DMSO (λ_{max} = 558 nm). Again, as with its longer chain homologues, the N-methyl adduct exhibits inverse solvatochromism although less pronounced than its longer chain derivatives due to insolubility in solvents less polar than 2-butanone.

3) $PhCH_2(4)Q3CNQF_4$

Solvent	ε_r[49]	λ_{max} (nm)	Solvent	ε_r[49]	λ_{max} (nm)
NMF[a]	182.4	566	Acetone	20.56	614
DMSO[b]	46.45	566	2-Butanone	18.51	638
DMF[c]	36.71	586	4M2P[d]	13.11	676
Acetonitrile	35.94	580	Dichloromethane	8.93	748
Nitromethane	35.87	586	THF[e]	7.58	734
Methanol	32.66	550	Chlorobenzene	5.62	530
Benzonitrile	25.20	668	Chloroform	4.81	524

[a] N-methylformamide (NMF), [b] dimethylsulphoxide (DMSO), [c] N,N-dimethylformamide (DMF), [d] 4-methyl-2-pentanone (4M2P), [e] tetrahydrofuran (THF).

Table 3.4.6 Solvatochromic Shifts of the $PhCH_2(4)Q3CNQF_4$ Zwitterion.

The benzylic betaine, $PhCH_2(4)Q3CNQF_4$, is readily soluble in all common organic solvents and displays the largest solvatochromic shift of all of the fluorinated γ-derivatives (Table 3.4.6). Its long wavelength absorption band extends over almost all of the visible region, from apple green in dichloromethane (λ_{max} = 748 nm) to lilac in methanol (λ_{max} = 550 nm), giving a maximum frequency range of –4813 cm^{-1} (198 nm). Again, as with other fluorinated γ-compounds, the benzylic homologue shows signs of inverse solvatochromism, with a bathochromic shift being observed in its absorption band in solvents of low polarity.

4) $C_nH_{2n+1}(2)Q3CNQF_4$ (where n =10 to 16)

Solvent	ε_r[49]	λ_{max} (nm)	Solvent	ε_r[49]	λ_{max} (nm)
NMF[a]	182.4	554 ± 2	Acetone	20.56	600 ± 1
DMSO[b]	46.45	552 ± 0	2-Butanone	18.51	622 ± 0
DMF[c]	36.71	570 ± 4	4M2P[d]	13.11	644 ± 1
Acetonitrile	35.94	568 ± 2	Dichloromethane	8.93	714 ± 1
Nitromethane	35.87	574 ± 2	THF[e]	7.58	698 ± 2
Methanol	32.66	550 ± 0	Chlorobenzene	5.62	798 ± 3
Benzonitrile	25.20	640 ± 2	Chloroform	4.81	482 ± 0

[a] N-methylformamide (NMF), [b] dimethylsulphoxide (DMSO), [c] N,N-dimethylformamide (DMF), [d] 4-methyl-2-pentanone (4M2P), [e] tetrahydrofuran (THF).

Table 3.4.7 Solvatochromic Shifts of the Long Chain $R(2)Q3CNQF_4$ Zwitterions.

α-substituted adducts also show extensive solvatochromic responses. The negative solvatochromism exhibited by these adducts, as with their γ-substituted analogues, is independent of chain length. For example, $C_{10}H_{21}(2)Q3CNQF_4$, (Table 3.4.7) shows a negative solvatochromic shift of –5650 cm^{-1} (248 nm) on going from chlorobenzene (λ_{max} = 798 nm) to methanol (λ_{max} = 550 nm). Although, as with their γ-substituted analogues, evidence of reverse solvatochromism is observed in solvents of low polarity.

5) $CH_3(2)Q3CNQF_4$

Solvent	ε_r[49]	λ_{max} (nm)	Solvent	ε_r[49]	λ_{max} (nm)
NMF[a]	182.4	550	Acetone	20.56	596
DMSO[b]	46.45	552	2-Butanone	18.51	612
DMF[c]	36.71	566	4M2P[d]	13.11	628
Acetonitrile	35.94	570	Dichloromethane	8.93	638
Nitromethane	35.87	570	THF[e]	7.58	618
Methanol	32.66	592	Chlorobenzene	5.62	NS[†]
Benzonitrile	25.20	636	Chloroform	4.81	NS[†]

[a] N-methylformamide (NMF), [b] dimethylsulphoxide (DMSO), [c] N,N-dimethylformamide (DMF), [d] 4-methyl-2-pentanone (4M2P), [e] tetrahydrofuran (THF),), [†] not soluble (NS).

Table 3.4.8 Solvatochromic Shifts of the $CH_3(2)Q3CNQF_4$ Zwitterion.

The short chain α-substituted betaine shows similar solvatochromic properties to that of its γ-substituted counterpart with the range of λ_{max} being much smaller than that exhibited by its longer chain analogues (c.f Table 3.4.7). Its absorption band undergoes a hypsochromic shift of -2507 cm^{-1} (88 nm) on going from dichloromethane ($\lambda_{max} = 638$ nm) to N-methylformamide ($\lambda_{max} = 550$ nm). Again, as with the other fluorinated adducts, evidence of reverse solvatochromism is observed in solvents of low polarity although, as with the short chain γ-homologue, this is limited due to insolubility in solvents such as chlorobenzene and chloroform.

The solvatochromic behaviour of the fluorinated quinolinium betaines is somewhat different compared to the related unsubstituted quinolinium betaines because the position of the absorption band is influenced by the nature of the betaine and its substituents.

The introduction of fluorine atoms into the acceptor ring system clearly shifts the CT absorption band to shorter wavelengths. The underlying reason for this is the electronegative effect of the fluorine atoms which reduce the overall efficiency of the charge-transfer process by increasing the ionisation potential of the TCNQ ring system, thus stabilising the charge-separated ground state (Figure 3.13) and shifting the absorption band hypsochromically to higher energies relative to that of the unsubstituted analogues.

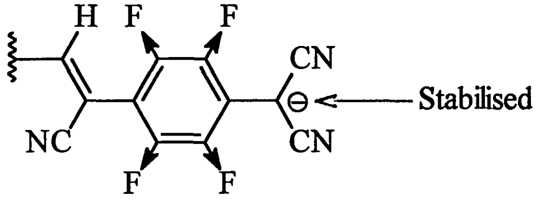

Figure 3.13 Fluorine Stabilisation of the Zwitterionic Ground State.

The normalised empirical solvent polarity parameter, E_T^N, of Reichardt's dye, the longest wavelength intramolecular CT absorption band, ν_{max} of the fluorinated γ-betaines, and the corresponding transition energies, E_T, are shown in Table 3.4.9.

Solvent		$CH_3(4)Q3CNQF_4$		$PhCH_2(4)Q3CNQF_4$		$C_{10}H_{21}(4)Q3CNQF_4$	
	E_T^N	$\nu_{max}^{\dagger}$	$E_T^{\ddagger}$	$\nu_{max}^{\dagger}$	$E_T^{\ddagger}$	$\nu_{max}^{\dagger}$	$E_T^{\ddagger}$
Methanol	0.762	17.42	49.81	18.18	51.98	18.18	51.98
NMF[a]	0.722	17.92	51.24	17.66	50.51	18.05	51.61
Nitromethane	0.481	17.42	49.81	17.06	48.79	17.54	50.16
Acetonitrile	0.460	17.48	49.98	17.24	49.29	17.66	50.51
DMSO[b]	0.444	17.92	51.24	17.66	50.51	18.12	51.79
DMF[c]	0.386	17.42	49.81	17.06	48.79	17.54	50.16
Acetone	0.355	17.00	48.62	16.28	46.45	16.78	47.97
Benzonitrile	0.333	15.92	45.53	14.97	42.80	15.38	43.98
2-Butanone	0.327	16.72	47.81	15.67	44.81	16.02	45.81
Dichloromethane	0.309	16.95	48.46	13.37	38.22	13.88	39.71

4M2P[d]	0.269	17.00	48.62	14.79	42.29	15.15	43.32
Chloroform	0.259	NS[*]	NS[*]	19.08	54.56	20.74	59.32
THF[e]	0.207	17.36	49.64	13.62	38.95	14.16	40.49
Chlorobenzene	0.188	NS[*]	NS[*]	18.87	53.94	20.41	58.35

[a] N-methylformamide (NMF), [b] dimethylsulphoxide (DMSO), [c] N,N-dimethylformamide (DMF), [d] 4-methyl-2-pentanone (4M2P), [e] tetrahydrofuran (THF),), [*] not soluble (NS), [†] units are $\times 10^3$ cm^{-1} , [‡] units are kcal mol^{-1}.

Table 3.4.9 Solvatochromic Shifts of the R(4)Q3CNQF$_4$ Adducts.

Figure 3.14 shows the plots of wavenumber, ν_{max}, for the CT absorption band of the above γ-fluoro-betaines against the normalised solvent polarity, E_T^N, parameter. For comparison the variation of ν_{max} with E_T^N for the unsubstituted decyl γ-betaine is also included.

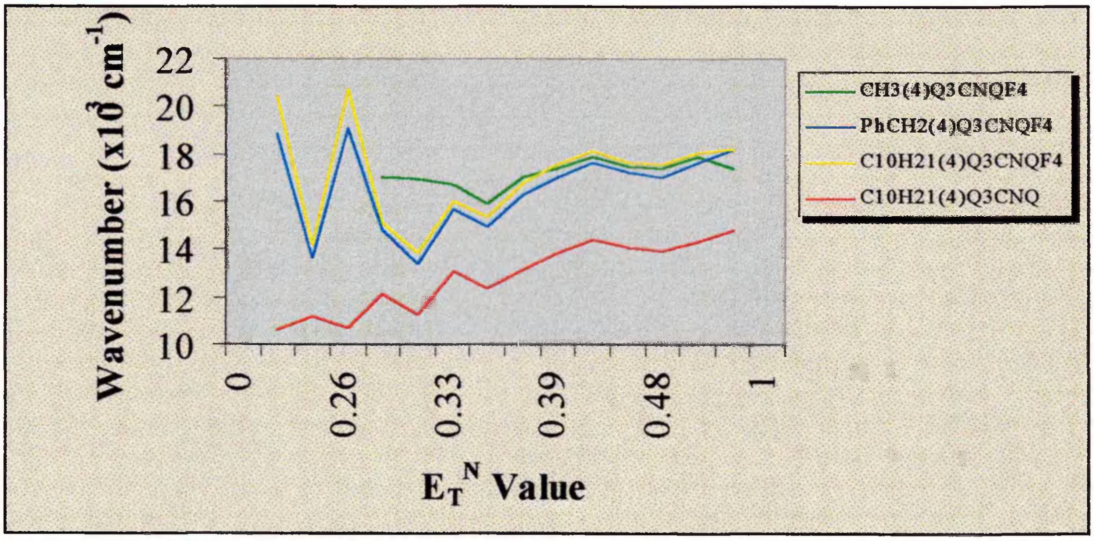

Figure 3.14 Solvatochromic Response of the Fluorinated γ-Betaines.

The negative solvatochromism exhibited by the fluorinated γ-homologues is unusual. The introduction of strongly electron withdrawing fluorine groups normally results in a decrease in the extent of solvatochromism.[20] The observed behaviour would, at first glance, appear due to the increased ground state dipole moment of the fluorinated quinolinium betaine ($\mu_g \approx 46$D for the long chain C_{10} analogue) relative to unsubstituted counterparts ($\mu_g \approx 31D$ for the corresponding unsubstituted C_{10} analogue). However, for strongly solvatochromic dyes, the observed solvent shifts cannot be explained only in terms of a change in permanent dipole moment on the electronic transition, as the benzylic fluorinated betaine (Figure 3.9), which has a smaller dipole moment ($\mu_g \approx 41D$) relative to its longer chain analogue, exhibits a larger solvatochromic shift. The effect of the surrounding solvent cage ($\mu_g \rightarrow \mu_e$) on the ground state dipole moment of the solute should also be taken into consideration,[4,9,54] as the dipolar solute molecules cause an electronic polarisation of the surrounding molecules, creating a so-called *reaction field*, which affects the dye's ground state dipole moment.[55]

It is considered that the large negative responses observed in the fluorinated adducts is due to a combination of the increased dipole moment which enhances the polarisability of the compound[4,32] and hence creates greater reaction fields, together with the greater specific solute-solvent interactions afforded by the more interactive nature of the fluorine substituents i.e. greater van der Waals interactions. This results in most of the structurally similar betaines being similarly solvated in all solvents and this is seen in Figure 3.14, with similar shaped plots implying similar solvatochromic behaviour. The exception is the relatively insoluble N-methyl homologue, which exhibits limited solvatochromism.

In less polar solvents, fluorinated adducts show a trend towards positive solvatochromism. This reverse solvatochromism, which is not observed in the corresponding unsubstituted compounds, is large and results in an observed bathochromic shift larger than the initial hypsochromic shift at higher polarity.

This is illustrated by $C_{10}H_{21}(4)Q3CNQF_4$ which shows an initial negative shift of –4293 cm^{-1} (170 nm) from dichloromethane to methanol; however from dichloromethane (λ_{max} = 720 nm) to chloroform (λ_{max} = 482 nm) a positive shift of +6858 cm^{-1} (238 nm) is observed (Table 3.4.4).

This reverse solvatochromism is attributed to an aggregation phenomenon, rather than a shift from a charge separated ground state to a neutral one, as in the case of *Brooker's* merocyanine dye.[16,17] Supporting evidence is threefold.

First the ground state dipole moments of the various fluorinated analogues, measured in the relatively low polarity solvent dichloromethane, were determined to be in the order of 40-46 debyes (see Chapter 4). Such large values imply that the adducts are either in a polyene-like or extremely polarised polymethine-like state for low dielectric constant solvents (Figure 3.15).

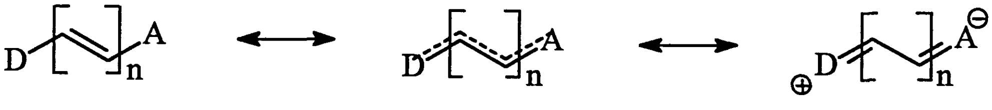

Figure 3.15 Chromophore Solvation States.

It seems unlikely, therefore, that the highly polar adducts would change to a predominately quinoidal ground state structure, as all the evidence suggests that the chromophores prefer a charge-separated polyene or polymethine type configuration even in solvents of low polarity.

Second, in solvents where inverse solvatochromism is observed, a change in the shape of the absorption band structure of the chromophore is noted. For large negative responses, the maxima reveal a broad top transition, as illustrated in Figure 3.16.

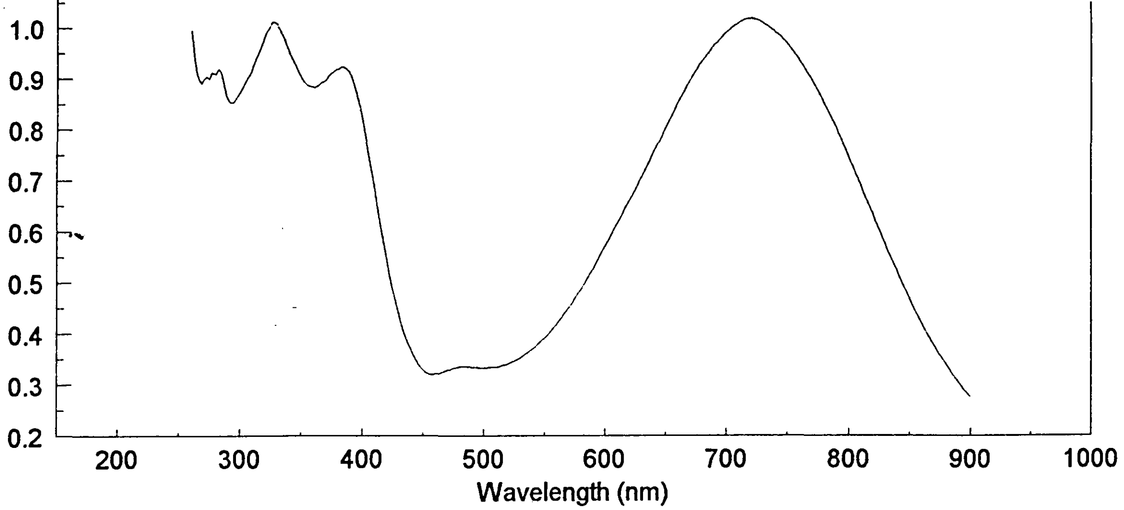

Figure 3.16 $C_{10}H_{21}(4)Q3CNQF_4$ **in Dichloromethane.**

For solvents such as chloroform where the reverse solvatochromic behaviour is noticed, a new absorption maximum emerges which is different to the broad top transition seen in solvents of greater polarity (Figure 3.17).

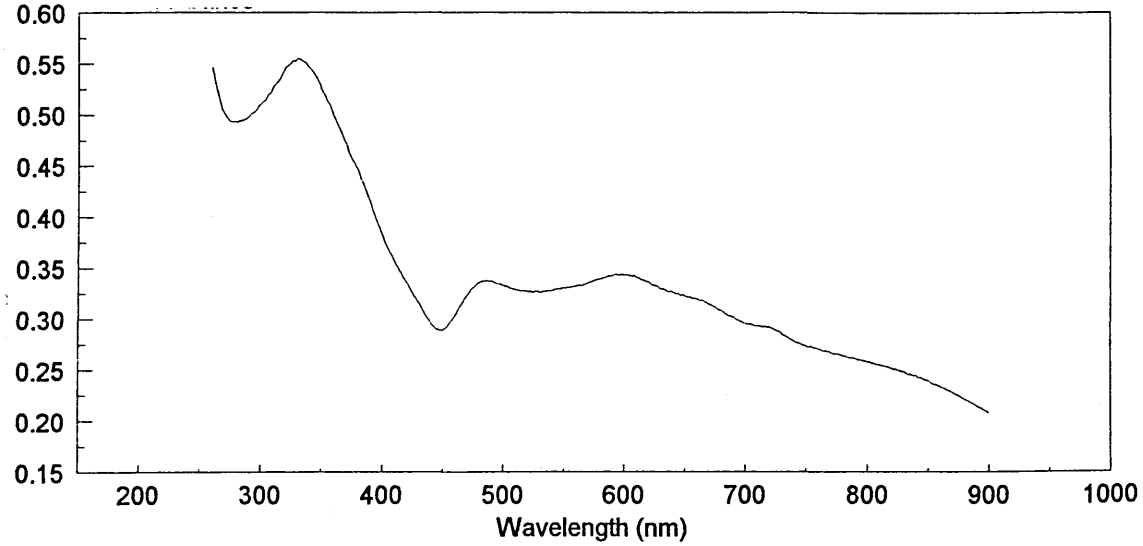

Figure 3.17 $C_{10}H_{21}(4)Q3CNQF_4$ **in Chloroform.**

This phenomenon has been observed in other compounds[20] and is attributed to the formation of aggregated species such as dimer pairs or micelles. Third, the chromophores deviate from Beer-Lambert's law at low concentrations ($<10^{-7}$ mol dm^{-3}) even in polar solvents such as acetone or acetonitrile (Chapter 2).

This phenomenon has been seen before in the closely related DEMI type compounds[7,53,56] which have been found to dimerise at low concentrations in solvents such as acetonitrile or DMF. It is tentatively assumed that the reverse solvatochromism observed here, is due to an aggregation phenomenon rather than a structural change. Further work is required to determine whether the aggregation is micellar in nature or simply dimer pair formation.

The solvatochromism observed in the α-substituted fluorinated betaines shows similar trends to those observed in the γ-substituted compounds in that the α-substituted adducts are similarly solvated in all solvents, although the overall solvatochromic shift observed for the long chain (C_{10} to C_{16}) homologues is much larger. The normalised empirical solvent polarity parameters E_T^N of Reichardt's dye, the intramolecular CT absorption band ν_{max} of a selection of α-substituted betaines, and the corresponding transition energies E_T, are shown in Table 3.4.10.

Solvent		$CH_3(2)Q3CNQF_4$		$C_{10}H_{21}(2)Q3CNQF_4$	
	E_T^N	$\nu_{max}^{\dagger}$	$E_T^{\ddagger}$	$\nu_{max}^{\dagger}$	$E_T^{\ddagger}$
Methanol	0.762	16.89	48.29	18.18	51.98
NMF[a]	0.722	18.18	51.98	18.05	51.61
Nitromethane	0.481	17.54	50.16	17.42	49.81
Acetonitrile	0.460	17.54	50.16	17.42	49.81
DMSO[b]	0.444	18.12	51.79	18.12	51.79
DMF[c]	0.386	17.67	50.51	17.54	50.16
Acetone	0.355	16.78	47.97	16.67	47.65
Benzonitrile	0.333	15.72	46.72	15.63	44.67
2-Butanone	0.327	16.34	46.72	16.08	45.97
Dichloromethane	0.309	15.67	44.81	14.00	40.04
4M2P[d]	0.269	15.92	45.53	15.53	44.39

Chloroform	0.259	NS*	NS*	20.75	59.32
THF[e]	0.207	16.18	46.26	14.33	40.96
Chlorobenzene	0.188	NS*	NS*	12.53	35.83

[a] N-methylformamide (NMF), [b] dimethylsulphoxide (DMSO), [c] N,N-dimethylformamide (DMF), [d] 4-methyl-2-pentanone (4M2P), [e] tetrahydrofuran (THF),), * not soluble (NS), † units are $\times 10^3$ cm^{-1} , ‡ units are kcal mol^{-1}.

Table 3.4.10 Solvatochromic Shifts of the R(2)Q3CNQF$_4$ Adducts.

Figure 3.18 illustrates a plot of wavenumber ν_{max} against the normalised solvent polarity E_T^N parameter, for both of the above compounds. For comparison, the variation of ν_{max} with E_T^N for the unsubstituted α-betaine is also illustrated.

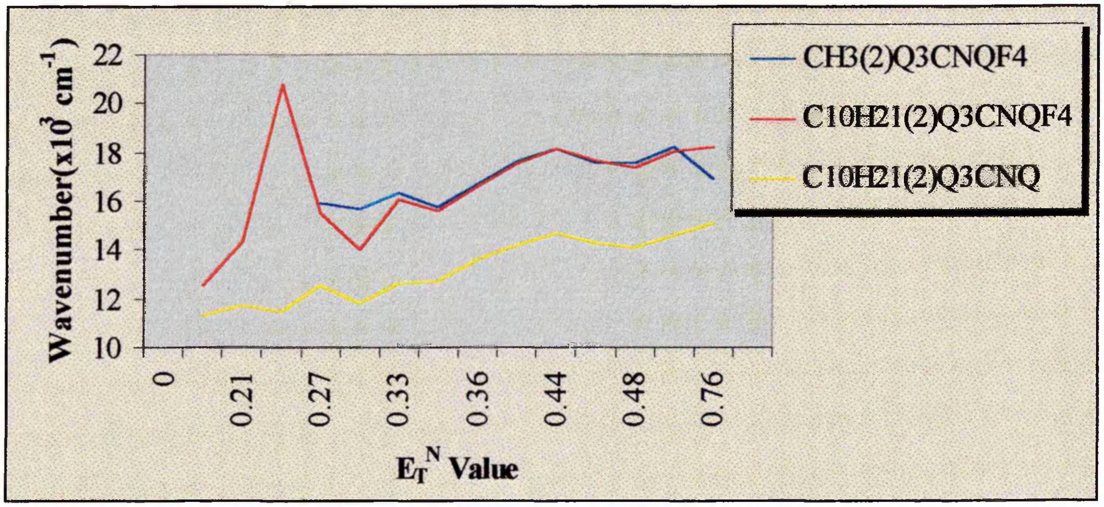

Figure 3.18 Solvatochromic Behaviour of the R(2)Q3CNQF$_4$ Zwitterions.

The graph demonstrates the solvent dependent behaviour of the fluorinated α-substituted analogues with respect to the standard Reichardt betaine by an almost linear correlation of the E_T^N values with the ν_{max} values of the fluorinated adducts. Again, aggregation induced reverse solvatochromism is also observed in low polarity solvents.

The large solvatochromic shifts observed in the fluorinated α-compounds, with exception of the N-methyl homologue, is unusual in many ways. As stated previously, the introduction of electronegative elements into the chromophore was expected to reduce the overall solvatochromism of compounds relative to their unsubstituted derivatives. However, in the case of the long chain α-compounds, which exhibit a larger shift (-5650 cm^{-1}) than that of the isomeric γ-fluorinated compounds (-4293 cm^{-1}), this is not so.

The larger shifts (which are in part due to the fact that in solvents such as chlorobenzene the α-compounds show a normal negative response whereas the γ-compounds exhibit inverse solvatochromic behaviour) result in the trends seen in the unsubstituted isomers being reversed. This consequently results in more pronounced negative solvatochromic behaviour by the α-fluorinated chromophores than their corresponding unsubstituted derivative. This phenomenon has also been observed in the related DEMI type compounds, in which the fluorinated analogue[7] (Figure 3.19) exhibits a solvatochromic shift some –1694cm^{-1} larger than that observed in the parent DEMI compound itself.

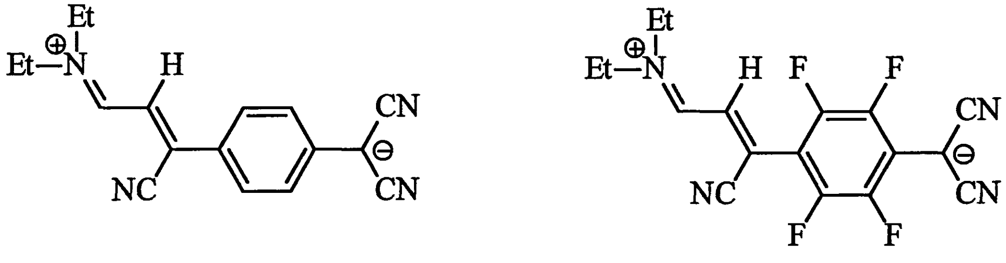

DEMI (-684cm^{-1})

F4-DEMI (-2378cm^{-1})

Figure 3.19 Solvatochromic DEMI Chromophores.

Consequently the α-fluorinated quinolinium betaines, whose much larger solvatochromic shift is approximately half the value of that observed for the Reichardt dye[4] (-9730 cm^{-1}), can be compared to compounds with similar solvatochromic responses such as the

Kosower pyridinium salt,[14] upon which the Z scale solvent polarity parameter is based, or the related stilbazolium dye[57] (Figure 3.20).

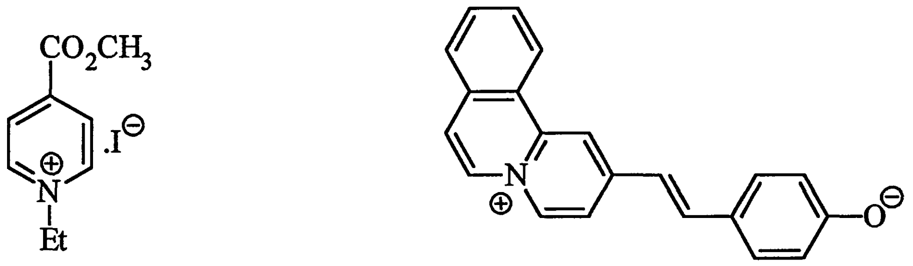

Kosower's Dye ($-5960 cm^{-1}$) Stilbazolium Dye ($-5590 cm^{-1}$)

Figure 3.20 Related Solvatochromic Chromophores.

3.4.4 Solvatochromic Characteristics of $C_3H_7(2)BT3CNQ$ and $C_3H_7(2)BT3CNQF_4$.

The benzothiazolium zwiiterions were studied in numerous solvents of differing polarity. The longest wavelength charge-transfer absorption bands, λ_{max}, of these betaines are listed below.

1) $C_3H_7(2)BT3CNQ$[46]

Solvent	ε_r[49]	λ_{max} (nm)	Solvent	ε_r[49]	λ_{max} (nm)
NMF[a]	182.4	738	Acetone	20.56	786
DMSO[b]	46.45	734	2-Butanone	18.51	794
DMF[c]	36.71	748	4M2P[d]	13.11	804
Acetonitrile	35.94	738	Dichloromethane	8.93	814
Nitromethane	35.87	732	THF[e]	7.58	812
Methanol	32.66	722	Chlorobenzene	5.62	824
Benzonitrile	25.20	808	Chloroform	4.81	818

[a] N-methylformamide (NMF), [b] dimethylsulphoxide (DMSO), [c] N,N-dimethylformamide (DMF), [d] 4-methyl-2-pentanone (4M2P), [e] tetrahydrofuran (THF).

Table 3.4.11 Solvatochromic Shifts of the $C_3H_7(2)BT3CNQ$ Zwitterion.

The observed solvatochromism of this unsubstituted benzothiazolium zwitterion is comparable to that exhibited by the short chain fluorinated quinolinium compounds. A relatively small hypsochromic shift of –1714 cm^{-1} (102 nm) is observed upon going from chlorobenzene (λ_{max} =824 nm) to methanol (λ_{max} = 722 nm) as illustrated in Table 3.4.11.

2) C_3H_7(2)BT3CNQF$_4$

Solvent	ε_r^{49}	λ_{max} (nm)	Solvent	ε_r^{49}	λ_{max} (nm)
NMF[a]	182.4	646	Acetone	20.56	686
DMSO[b]	46.45	636	2-Butanone	18.51	702
DMF[c]	36.71	652	4M2P[d]	13.11	726
Acetonitrile	35.94	664	Dichloromethane	8.93	766
Nitromethane	35.87	672	THF[e]	7.58	762
Methanol	32.66	630	Chlorobenzene	5.62	804
Benzonitrile	25.20	732	Chloroform	4.81	NS[†]

[a] N-methylformamide (NMF), [b] dimethylsulphoxide (DMSO), [c] N,N-dimethylformamide (DMF), [d] 4-methyl-2-pentanone (4M2P), [e] tetrahydrofuran (THF), [†] not soluble (NS).

Table 3.4.12 Solvatochromic Shifts of the C_3H_7(2)BT3CNQF$_4$ Zwitterion.

The fluorinated benzothiazolium derivative exhibits a pronounced negative solvatochromism that is hypsochromically shifted relative to that observed in the above unsubstituted derivative. The absorption maximum exhibits a shift of –3435 cm^{-1} (174 nm) from chlorobenzene (λ_{max} = 804 nm) to methanol (λ_{max} = 630 nm). Significantly, the reverse solvatochromism exhibited by the fluorinated quinolinium compounds, is not observed in the corresponding fluorinated benzothiazolium adduct.

The solvatochromism exhibited by the C_3H_7(2)BT3CNQ zwitterion is unusual. At first glance this push-pull adduct seems to exhibit a normal negative solvatochromism. However, upon closer examination it appears that the charge-transfer absorption band of this zwitterion undergoes significant structural changes with decreasing solvent polarity. In solvents of high polarity (DMSO, DMF, CH_3NO_2 etc) the absorption maximum shows a broad top transition, as seen in the related quinolinium compounds.

In acetone, however, the CT absorption band shows signs of splitting, with a shoulder on the low wavelength side being observed as is illustrated in Figure 3.21. Further splitting occurs as the solvent polarity decreases, with maximum splitting observed in chlorobenzene where two distinct bands appear. This splitting of the absorption band has been observed before in stilbazolium betaines[58] and is attributed to solvent induced broadening of the electronic transitions resulting in a loss of the coarse structure.

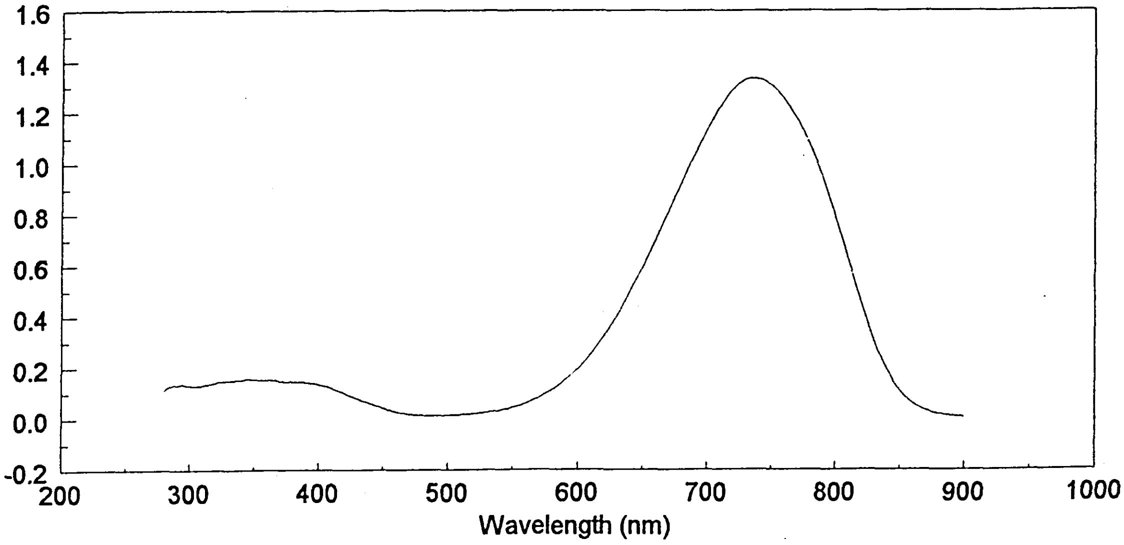

C_3H_7(2)BT3CNQ in Dimethylsulphoxide.

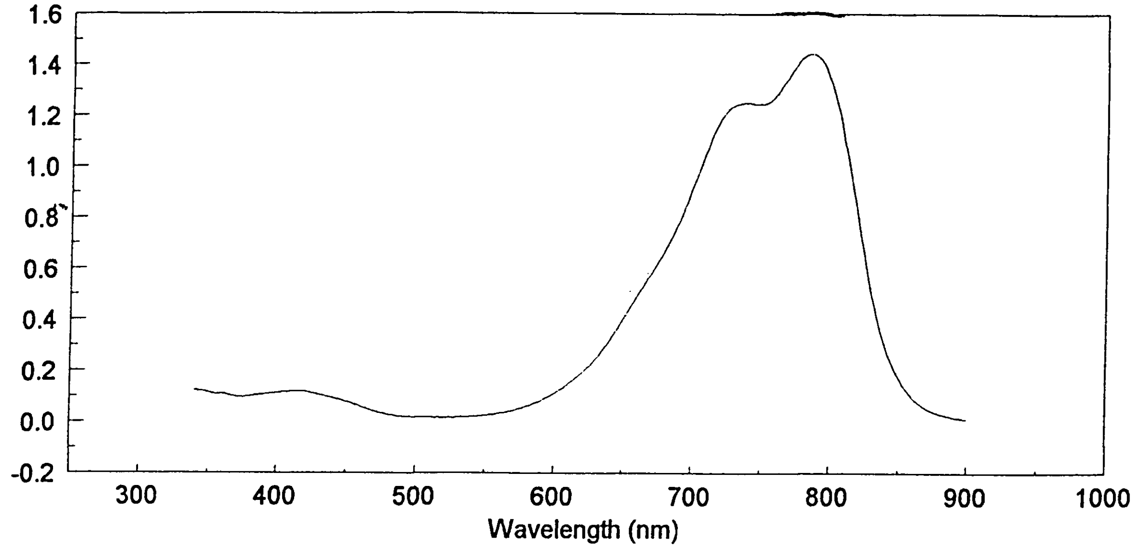

C_3H_7(2)BT3CNQ in Acetone.

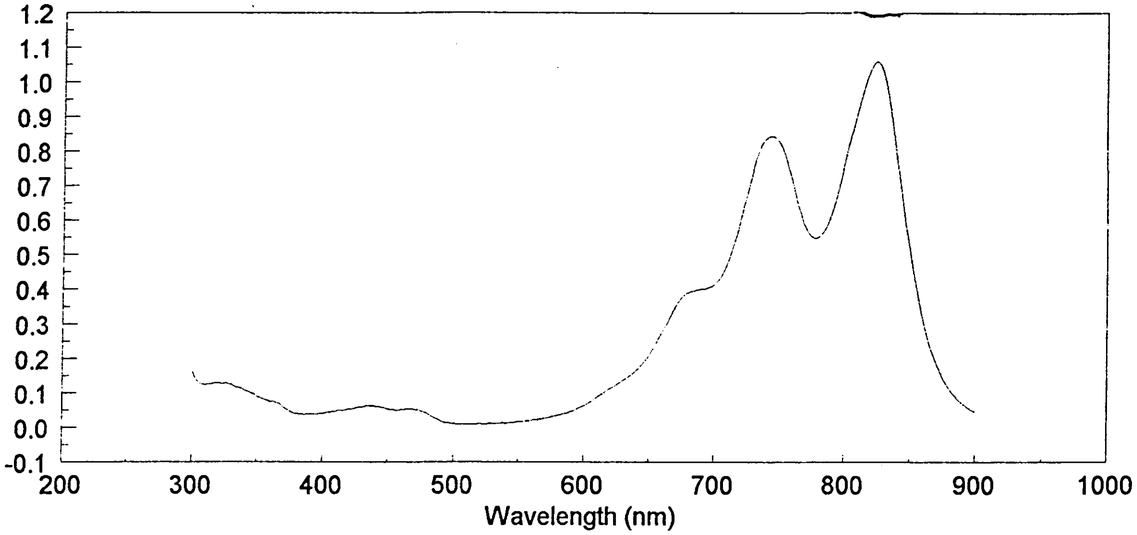

C_3H_7(2)BT3CNQ in Chlorobenzene.

Figure 3.21 C_3H_7(2)BT3CNQ in Various Solvents.

The splitting of the absorption band in this TCNQ-based zwitterion is thought to occur via a similar process. The possibility of the splitting resulting from a structural change is considered unlikely due to the absence of any observed inverse solvatochromism. However splitting due to an aggregation phenomenon cannot be excluded as no Beer-Lambert law studies have been undertaken due to the adduct's limited solubility in most solvents.

On the other hand, the fluorinated benzothiazolium zwitterion (Figure 3.22) shows solvatochromic behaviour typical of other betaines studied in this work.

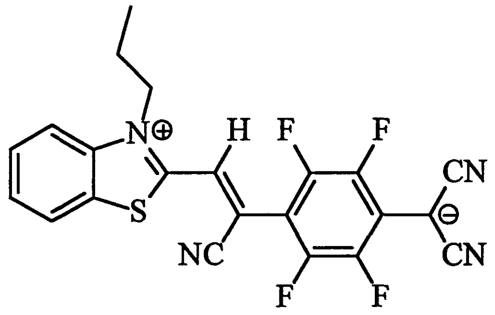

Figure 3.22 $C_3H_7(2)BT3CNQF_4$.

With the exception of chlorobenzene, where a slight shoulder is observed on the low wavelength side, the absorption band shows typical behaviour in that a broad top transition is observed. The normalised E_T^N parameters of Reichardt's dye, the intramolecular CT absorption bands ν_{max} of the two benzothiazolium dyes, and their corresponding transition energies E_T, are listed in Table 3.4.13. When plotted against each other (Figure 3.23), the significantly larger solvatochromic shift of the fluorinated compound relative to its unsubstituted counterpart is clear. The linear relationship between the two plots again demonstrates that the zwitterions are similarly solvated in all solvents and the result correlates well with that of the standard Reichardt betaine.[4]

Solvent		$C_3H_7(2)BT3CNQ$		$C_3H_7(2)BT3CNQF_4$	
	E_T^N	$\nu_{max}^{\dagger}$	$E_T^{\ddagger}$	$\nu_{max}^{\dagger}$	$E_T^{\ddagger}$
Methanol	0.762	13.85	39.6	15.87	45.38
NMF[a]	0.722	13.55	38.74	15.48	44.26
Nitromethane	0.481	13.66	39.06	14.88	42.55
Acetonitrile	0.460	13.55	38.74	15.06	43.06
DMSO[b]	0.444	13.62	38.95	15.72	44.95
DMF[c]	0.386	13.37	38.22	15.34	43.85

Acetone	0.355	12.72	36.00	14.58	41.68
Benzonitrile	0.333	12.38	35.38	13.66	39.06
2-Butanone	0.327	12.59	35.56	14.25	40.73
Dichloromethane	0.309	12.29	35.12	13.06	37.33
4M2P[d]	0.269	12.44	35.56	13.77	39.38
Chloroform	0.259	12.22	34.95	NS*	NS*
THF[e]	0.207	12.32	35.21	13.12	37.52
Chlorobenzene	0.188	12.14	24.70	12.44	35.56

[a] N-methylformamide (NMF), [b] dimethylsulphoxide (DMSO), [c] N,N-dimethylformamide (DMF), [d] 4-methyl-2-pentanone (4M2P), [e] tetrahydrofuran (THF),), * not soluble (NS), † units are $\times 10^3$ cm^{-1} , ‡ units are kcal mol^{-1}.

Table 3.4.13 Solvatochromic Shifts of the Benzothiazolium Zwitterions.

As with all the other compounds studied, anomalies are observed in solvents such as benzonitrile and methacrylonitrile, which give rise to greater shifts than expected. Some authors[44] have attributed this anomaly to weak charge-transfer between solute and solvent.

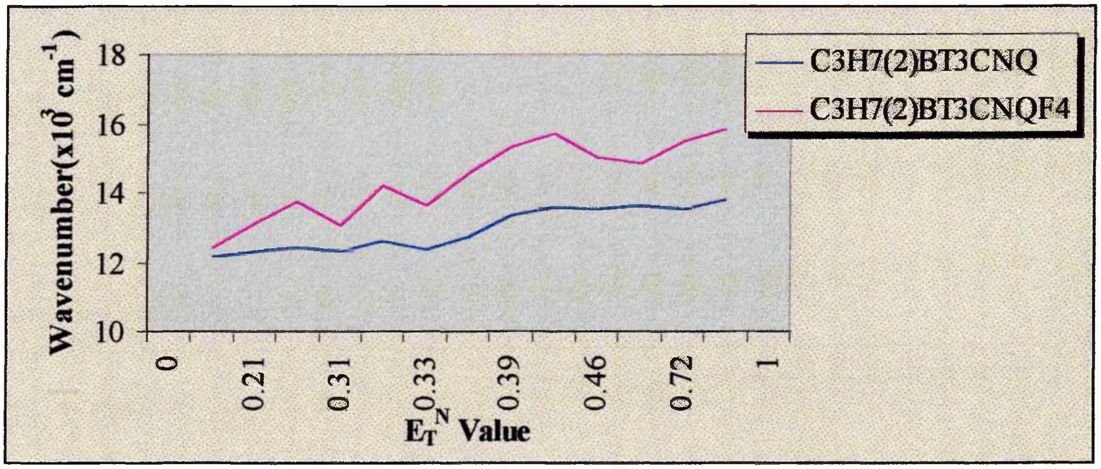

Figure 3.23 Solvatochromic Behaviour of the Benzothiazolium Betaines.

Neither benzothiazolium zwitterion shows signs of reverse solvatochromism. This is unexpected. The fluorinated compound has a similar ground state dipole moment to that of the fluorinated quinolinium zwitterions, which were found to exhibit inverse solvatochromism.

The behaviour of the benzothiazolium adducts follows a similar trend to the α-substituted quinolinium compounds. The fluorinated derivative exhibits a larger shift than the unsubstituted counterpart, although the observed shift relative to the corresponding fluorinated quinolinium compound is smaller. This behaviour is unusual, as the majority of chromophores having benzothiazolium moieties are found to exhibit positive solvatochromism.[54,59]

The solvatochromic shift of the fluorinated benzothiazolium betaine does though compare well with other push-pull type systems such as the previously mentioned long chain pyridinium iminophenolate betaines of *Li et al*[13,34] and the other susbtituted betaines studied here. The unsubstituted benzothiazolium betaine on the other hand exhibits a limited solvatochromic response comparable with the indole based spiropyran system of *Mikeš et al*[60] (Figure 2.24) which exhibits a maximum frequency shift of –2010 cm^{-1} (65 nm) on going from toluene (λ_{max} = 603 nm) to ethanol (λ_{max} = 538 nm).

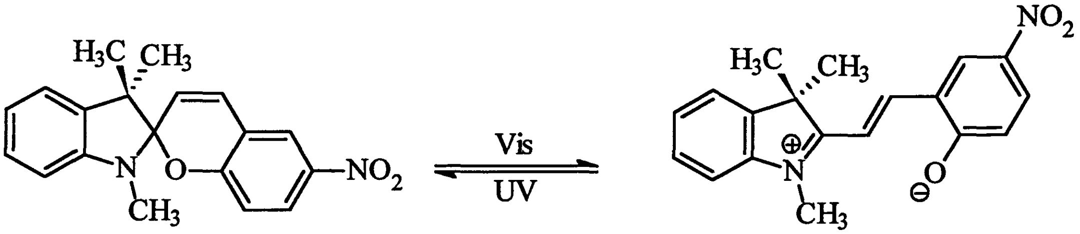

Figure 3.24 Indole Based Spiropyran System.

3.4.5 Solvatochromic Characteristics of $CH_3(2)P3CNQF_4$.

The longest wavelength charge-transfer absorption band in a variety of solvents is listed below in Table 3.4.14. The solvatochromic behaviour shows a slightly larger response to that observed in the fluorinated quinolinium isomer. Its long wavelength charge-transfer absorption band is shifted –3017 cm^{-1} (85 nm) from dichloromethane (λ_{max} = 575 nm) to methanol (λ_{max} = 490 nm) and, inverse solvatochromism is observed in solvents of lower polarity (Table 3.4.14).

Solvent	ε_r^{49}	λ_{max} (nm)	Solvent	ε_r^{49}	λ_{max} (nm)
NMF[a]	182.4	494	Acetone	20.56	532
DMSO[b]	46.45	492	2-Butanone	18.51	542
DMF[c]	36.71	504	4M2P[d]	13.11	550
Acetonitrile	35.94	510	Dichloromethane	8.93	575
Nitromethane	35.87	514	THF[e]	7.58	NS[†]
Methanol	32.66	490	Chlorobenzene	5.62	540
Benzonitrile	25.20	570	Chloroform	4.81	560

[a] N-methylformamide (NMF), [b] dimethylsulphoxide (DMSO), [c] N,N-dimethylformamide (DMF), [d] 4-methyl-2-pentanone (4M2P), [e] tetrahydrofuran (THF), [†] not soluble (NS).

Table 3.4.14 Solvatochromic Shifts of the $CH_3(2)P3CNQF_4$ Zwitterion.

As expected, the position of the absorption band of the pyridinium betaine is hypsochromically shifted relative to that of the corresponding quinolinium compound as a result of its lesser degree of conjugation.[61] Despite this, the pyridinium betaine exhibits a slightly larger solvatochromic shift than its fellow quinolinium compound, as shown in Figure 3.25. For comparison the data for $CH_3(2)Q3CNQF_4$ has also been included in the diagram.

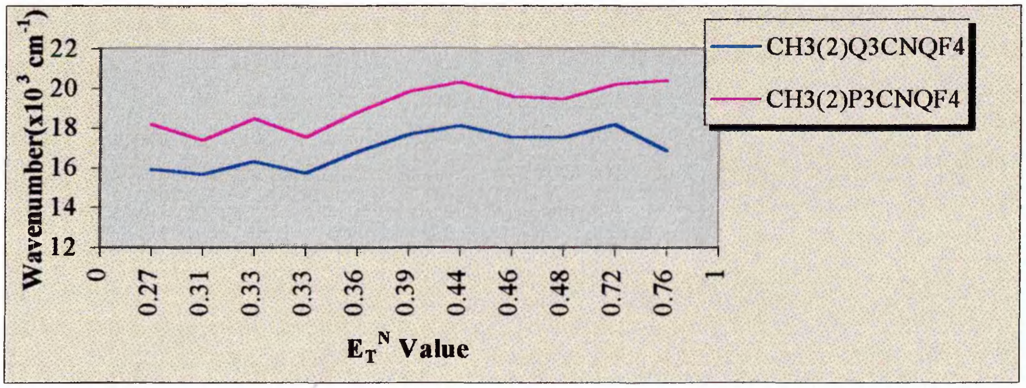

Figure 3.25 Solvatochromic Behaviour of $CH_3(2)P3CNQF_4$.

The solvatochromism exhibited by $CH_3(2)P3CNQF_4$ is comparable with other fluorinated zwitterions. However, the solvatochromic behaviour is limited when compared to structurally similar compounds such as the stilbazolium dye[62] illustrated in Figure 3.26 which exhibits a shift of –5350 cm^{-1} (126 nm) on going from dichloroethane (λ_{max} = 552 nm) to water (λ_{max} = 426 nm). This suggests that the fluorinated pyridinium betaine is best compared to lesser solvatochromic compounds such as the (η^2-TCNE)$W(CO)_5$ complex, whose metal to ligand charge-transfer (MLCT) band shifts –3000 cm^{-1} (158 nm) on changing solvent from chloroform to glyme.[63]

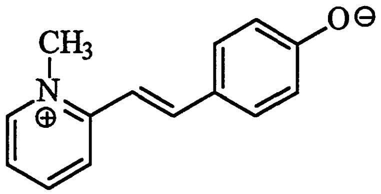

Figure 3.26 Solvatochromic Stilbazolium Dye.[62]

3.5 Halochromic Properties of Quinolinium and Benzothiazolium Zwitterions.

All of the zwitterions studied showed salt-induced halochromism upon treatment with alkali and alkaline earth metal salts in various solvents. This phenomenon has been demonstrated with other solvatochromic dyes[4,13,34,64] and stems from ion-pairing between the metal cation and the dicyanomethanide moiety of the betaine (Figure 3.27). It can be readily demonstrated by simple test tube experiments since the absorption bands of the betaines lie within the visible region of the spectrum.

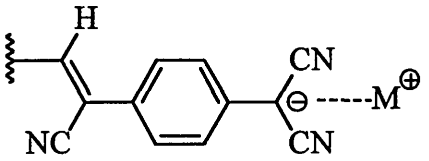

Figure 3.27 Halochromic Ion-Pairing.

In the present study the halochromism of the TCNQ-based betaines was investigated in acetonitrile (polar aprotic) and methanol (polar protic), employing various group I and II metal chlorides and iodides along with a few metal fluoride salts.

So, treatment of a ~ 10^{-3} M solution of $C_{10}H_{21}$(4)Q3CNQ zwitterion in acetonitrile (λ_{max} = 708 nm) with 10^{-1} M magnesium perchlorate solution results in a distinct colour change from turquoise to royal blue (λ_{max} = 614 nm; salt induced shift $\Delta\lambda$ = -94 nm). The longest wavelength absorption maxima of selected betaines [[zwitterion] $\approx 10^{-4}$ M], measured in methanol, with and without added salts, as well as the salt induced band shift, $\Delta\lambda$, after addition of the electrolyte, are shown in Table 3.5.1.

Salt (mol dm^{-3})	R(2)Q3CNQ (where R>10)		R(4)Q3CNQF_4 (where R>10)		R(2)Q3CNQF_4 (where R>10)		C_3H_7(2)BT3CNQF_4	
	λ_{max} (nm)	$\Delta\lambda$ (nm)	λ_{max} (nm)	$\Delta\lambda$ (nm)	λ_{max} (nm)	$\Delta\lambda$ (nm)	λ_{max} (nm)	$\Delta\lambda$ (nm)
WS[‡]	664	-	550	-	550	-	630	-
LiI								
10^{-3} M	660	-4	540	-10	540	-10	n/a[†]	n/a[†]
10^{-1} M	658	-6	536	-14	538	-12	n/a[†]	n/a[†]
NaI								
10^{-3} M	662	-2	540	-10	540	-10	626	-4
10^{-1} M	658	-6	538	-12	540	-10	620	-10
KI								
10^{-3} M	660	-4	540	-10	540	-10	n/a[†]	n/a[†]
10^{-1} M	658	-6	538	-12	538	-12	n/a[†]	n/a[†]
KCl								
10^{-3} M	660	-4	542	-8	540	-10	n/a[†]	n/a[†]
10^{-1} M	658	-6	538	-12	538	-12	n/a[†]	n/a[†]
KF								
10^{-3} M	662	-2	540	-10	540	-10	n/a[†]	n/a[†]
10^{-1} M	660	-4	540	-10	540	-10	n/a[†]	n/a[†]
CsI								
10^{-2} M	664	0	540	-10	540	-10	624	-6
$Mg(ClO_4)_2$								
10^{-3} M	660	-4	540	-10	540	-10	624	-6
10^{-1} M	650	-14	524	-26	526	-24	614	-16
$CaCl_2$								
10^{-3} M	658	-6	542	-8	540	-10	622	-8
10^{-1} M	652	-12	528	-22	530	-20	616	-14

SrCl$_2$								
10^{-3} M	660	-4	540	-10	540	-10	628	-2
10^{-1} M	654	-10	530	-20	532	-18	618	-12
BaCl$_2$								
10^{-3} M	660	-4	540	-10	542	-8	622	-8
10^{-1} M	654	-10	528	-22	532	-18	610	-20

[‡] Without salt (WS), [†] no charge-transfer band observed (n/a).

Table 3.5.1 Halochromic Shifts of Selected Adducts in Methanol.

For comparison, the halochromic shifts observed for the same zwitterions (except C$_3$H$_7$(2)BT3CNQF$_4$) in acetonitrile are listed in Table 3.5.2 along with the shifts observed for the R(4)Q3CNQ series of compounds.

Salt (mol dm^{-3})	R(4)Q3CNQ[†] (where R>10)		R(2)Q3CNQ (where R>10)		R(4)Q3CNQF$_4$ (where R>10)		R(2)Q3CNQF$_4$ (where R>10)	
	λ_{max} (nm)	$\Delta\lambda$ (nm)	λ_{max} (nm)	$\Delta\lambda$ (nm)	λ_{max} (nm)	$\Delta\lambda$ (nm)	λ_{max} (nm)	$\Delta\lambda$ (nm)
WS[‡]	708	-	702	-	566	-	568	-
LiI								
10^{-3} M	706	–2	698	–4	568	+2	574	+6
10^{-1} M	698	–10	696	–6	564	–2	572	+4
NaI								
10^{-3} M	710	+2	702	0	570	+4	570	+2
10^{-1} M	704	–4	696	–6	568	+2	570	+2
KI								
10^{-3} M	708	0	700	–2	568	+2	576	+8
10^{-1} M	706	–2	698	–4	568	+2	574	+6
KF								
10^{-3} M	712	+4	700	–2	568	+2	574	+6
10^{-1} M	710	+2	700	–2	568	+2	576	+8
CsI								
10^{-2} M	710	+2	700	–2	570	+4	568	0
Mg(ClO$_4$)$_2$								
10^{-3} M	694	–14	700	–2	570	+4	576	+8
10^{-1} M	614	–94	678	–24	526	–40	554	–14

[‡] Without salt (WS), [†] halochromic studies were only conducted in acetonitrile for the R(4)Q3CNQ adducts due to the adduct's poor solubility in methanol.

Table 3.5.2 Halochromic Shifts of Selected Adducts in Acetonitrile.

In all cases, hypsochromic salt-induced band shifts were observed upon the addition of electrolytes to solutions of the zwitterion. However, in both methanol and acetonitrile on addition of group I metal salts the expected decrease in halochromism on decreasing cation polarising power (in the order $Li^+ > Na^+ > K^+ > Cs^+$) was not observed.

The vast majority of compounds which exhibit strong halochromic behaviour embody a phenoxide group.[4,40,42,65] It is the resultant strong metal-oxygen interaction that makes such compounds extremely sensitive to immediate changes in the surrounding micro-environment.[4,40,42] In the case of the zwitterions here, the dicyanomethanide moiety interacts with the cation of the electrolyte. This much weaker metal-carbon interaction, results in similar halochromic shifts for different group I salts due to the insensitivity of the chromophore to different monovalent cations of similar effective charge.[66]

The addition of divalent metal electrolytes produce much larger halochromic shifts which correlate well with the dissimilar effective cation charges (i.e. ion charge/ion radius ration)[66] of the group II metal ions. This is illustrated in Figure 3.28 by the near-linear progression of the plot of wavelength of the absorption band against effective cationic charge.

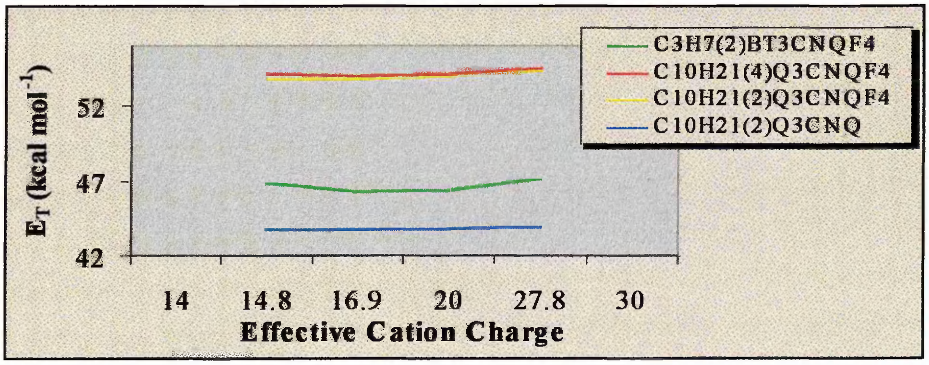

Figure 3.28. Correlation between the salt-induced change in molar transition energy $E_T(30)$ of various adducts and the effective cation charge of the electrolyte.

As concentration of divalent salt is increased, the absorption band shifts to shorter wavelengths due to stabilisation of the dipolar ground state via interaction of the dicyanomethanide centre with the metal ion. For example, the long-wavelength absorption band of the $C_{10}H_{21}(4)Q3CNQF_4$ zwitterion shifts to 524 nm from 550 nm with increasing concentration of $Mg(ClO_4)_2$ in methanol (up to [salt] = 0.1 M).

However, for most adducts increasing concentration of monovalent metal ions - in both solvents - results in no change in the absorption band. This indicates that the adducts interact with added cation to form a complex no longer sensitive to subsequent polarity change on adding further electrolyte. From experimental observation, it seems clear that while the halochromic behaviour of the studied adducts is not great, trends are apparent. In general longer chain fluorinated quinolinium dyes exhibit the largest halochromic shifts - approximately double the values observed in the unsubstituted homologues on the addition of divalent electrolytes in methanol.

The larger observed shifts of the quinolinium zwitterions upon addition of $Mg(ClO_4)_2$ in acetonitrile relative to those in methanol can be attributed to the different solvating properties of the solvents.[4,32,64] Acetonitrile is a good polar aprotic solvent and strongly solvates the cationic part of the electrolyte. In the case of the addition of monovalent electrolyte, the donor solvent acetonitrile solvates the cationic species so much that the dye experiences a relatively weak perturbation from the metal species, as seen in Table 3.5.2. On addition of electrolyte in a polar protic solvent such as methanol, the cation is unable to displace the solvent molecules from the solvating shell of the dicyanomethanide group, resulting in smaller observed shifts. However in methanol the cation is itself solvated by the solvent molecules, with the result that the proton of the solvent R-OH becomes more acidic.

This indirect effect of the cation upon the dye, schematically illustrated in Figure 3.29, can result in the dye experiencing greater perturbation leading to larger shifts - see in Table 3.5.1.

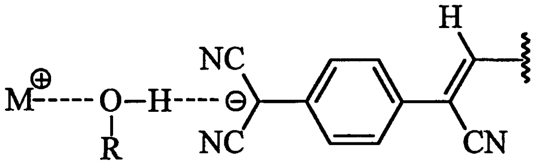

Figure 3.29 Solvent-Aided Halochromic Shifts.

In the case of the $C_3H_7(2)BT3CNQF_4$ zwitterion, the addition of monovalent salts to methanolic solutions of the compound results in a total loss of the charge-transfer absorption band thus mimicking the effect of protonation of the dicyanomethanide swallowtail. Consequently the relatively small shifts observed in methanol result from a complex series of interactions between solute, electrolyte and solvent, making it difficult to assess which interactions are the major contributors to such changes in the absorption spectra of these dipolar compounds.

However it appears that the TCNQ-based zwitterions are poor chromoionophores in terms of differentiating between type of electrolyte and overall halochromic shifts observed, when compared to their phenoxide containing relatives.[4,13,42,64,65]

3.6 References.

1. M. Berthelot and L. Péan de Saint-Gilles, *Ann. Chim. Phys. 3. Sér.*, 1862, **65**, 385.
2. E. S. Amis, *Solvent Effects on Reaction Rates and Mechanisms*, Academic Press, New York, 1966.
3. L. P. Hammett, *J. Am. Chem. Soc.*, 1937, **59**, 96.

4. C. Reichardt, *Solvents and Solvent Effects in Organic Chemistry*, 2nd ed.; VCH Publishers; Weinheim, 1988.

5. L. Claisen, *Liebigs Ann. Chem.*, 1896, **291**, 25.

6. J. F. Coetzee and C. D. Ritchie, *Solute-Solvent Interactions*, Dekker: New York, 1969 and 1976; Vols. 1 and 2.

7. M. Szablewski, P. R. Thomas, A. Thornton, D. Bloor, G. H. Cross, J. M. Cole, J. A. K. Howard, M. Malagoli, F. Meyers, J-L. Brédas, W. Wenseleers and E. Goovaerts, *J. Am. Chem. Soc.*, 1997, **119**, 3144.

8. (a) A. D. Buckingham, P. W. Fowler and J. M. Hutson, *Chem. Rev.*, 1988, **88**, 963. (b) P. L. Huyskens, W. A. P. Luck and T. Zeegers-Huyskens, Eds. *Intermolecular Forces*; Springer: Berlin, 1991.

9. C. Reichardt, *Chem. Rev.*, 1994, **94**, 2319.

10. C. Reichardt, *Angew. Chem.*, 1965, **77**, 30.

11. (a) J. Franck, *Trans. Faraday Soc.*, 1926, **21**, 536. (b) C. U. Condon, *Phys. Rev.*, 1928, **32**, 858.

12. (a) A. Slama-Schwok, M. Blanchard-Desce and J.-M. Lehn, *J. Phys. Chem.*, 1990, **94**, 3894. (b) D. M. Shin and D. G. Whitten, *J. Phys. Chem.*, 1988, **92**, 2945.

13. D. W. Allen and X. Li, *J. Chem. Soc., Perkin Trans. 2.*, 1997, 1099.

14. (a) E. M. Kosower, *J. Am. Chem. Soc.*, 1958, **80**, 3253; 3261; 3267. (b) E. M. Kosower, J. A. Skorcz, W. M. Schwarz and J. W. Patton, *J. Am. Chem. Soc.*, 1960, **82**, 2188. (c) E. M. Kosower, *An Introduction to Physical Organic Chemistry*, Wiley: New York, 1968.

15. B. K. Mishra, M. Kuanar, A. Mishra and G. B. Behera, *Bull. Chem. Soc. Jpn.*, 1996, **69**, 2581.

16. (a) S. F. Alberti and J. Echave, *Chem. Phys.*, 1997, **223**, 183. (b) A. Botrel, A. Le Beuze, P. Jacques and H. Strub, *J. Chem. Soc., Faraday Trans. 2*, 1984, **80**, 1235.

17. L. G. S. Brooker, G. H. Keyes and D. W. Heseltine, *J. Am. Chem. Soc.*, 1951, **73**, 5350.

18. J. O. Morley, R. M. Morley, R. Docherty and M. H. Charlton, *J. Am. Chem. Soc.*, 1997, **119**, 10192.

19. P. Jacques, *J. Phys. Chem.*, 1986, **90**, 5535.

20. M. Niedbalska and I. Gruda, *Can. J. Chem.*, 1990, **68**, 691.

21. E. Grunwald and S. Winstein, *J. Am. Chem. Soc.*, 1948, **70**, 846.

22. L. G. S. Brooker, A. C. Craig, D. W. Heseltine, P. W. Jenkins and L. L. Lincoln, *J. Am. Chem. Soc.*, 1965, **87**, 2443.

23. S. Dähne, F. Shob, K.-D. Nolte and R.Radeglia, *Ukr. Khim. Zh.*, 1975, **41**, 1170.

24. M. J. Kamlet, J.-L. M. Abboud and R. W. Taft, *J. Am. Chem. Soc.*, 1977, **99**, 6027; 8325.

25. E. Buncel and S. Rajagopal, *J. Org. Chem.*, 1989, **54**, 798.

26. B. K. Freed, J. Biesecker, W. J. Middleton, *J. Fluorine Chem.*, 1990, **48**, 63.

27. K. Dimroth, C. Reichardt, T. Siepmann and F. Bohlmann, *Liebigs Ann. Chem.*, 1963, **661**, 1.

28. D. Walther, *J. Prakt. Chem.*, 1974, **316**, 604.

29. J.-E. Dubois, A. Bienvenüe, *Tetrahedron Lett.*, 1966, 1809.

30. I. A. Zhmyreva, V. V. Zelinskii, V. P. Kolobkov and N. D. Krasnitskaya, *Dokl. Akad. Nauk SSSR, Ser. Khim.*, 1959, **129**, 1089; *Chem. Abstr.*, 1961, **55**, 26658e.

31. D. C. Dong and M. A. Winnik, *Can. J. Chem.*, 1984, **62**, 2560.

32. P. Suppan and N. Ghoneim, *Solvatochromism*, The Royal Society of Chemistry, Cambridge, 1997.

33. C. Reichardt, *Liebigs Ann. Chem.*, 1983, 721.

34. X. Li, MPhil Thesis, *Sheffield Hallam University*, 1997.

35. (a) E. Buncel and S. Rajagopal, *Acc. Chem. Res.*, 1990, **23**, 226. (b) M. C. Rezende and L. I. Dal Sasso, *Rev. Roum. Chim.*, 1986, **31**, 323.

36. W. B. Harrod and J. Pienta, *J. Phys. Org. Chem.*, 1990, **3**, 534.

37. I. A. Koppel and J. B. Koppel, *Org. React. (Tartu)*, 1984, **21**, 98; *Chem Abstr.*, 1985, **103**, 12232k.

38. J. G. Dawber, *J. Chem. Soc., Faraday Trans.*, 1990, **86**, 287.

39. V. Gageiro, M. Aillon and M. C. Rezende, *J. Chem. Soc., Faraday Trans.*, 1992, **88**, 210.

40. (a) C. Reichardt, S. Asharin-Fard and G. Schäfer, *Chem. Ber.*, 1993, **126**, 143. (b) C. Reichardt, E. Harbusch-Görnert and G. Schäfer, *Liebigs Ann. Chem.*, 1988, 839. (c) C. Reichardt, S. Asharin-Fard, *Angew. Chem.*, 1991, **103**, 614.

41. (a) C. J. Pedersen, *J. Am. Chem. Soc.*, 1967, **89**, 7017. (b) C. J. Pedersen and H. K. Frensdorf, *Angew. Chem.*, 1972, **11**, 16.

42. C. Reichardt and S. Asharin-Fard, *Angew. Chem., Int. Ed. Engl.*, 1991, **30**, 558.

43. D. D. Perrin, W. L. F. Armarego and D. R. Perrin, *Purification of Laboratory Chemicals*, 2nd ed., Pergamon Press, 1980.

44. R. A. Broughton, PhD Thesis, *Sheffield Hallam University*, 1993.

45. M. Szablewski, PhD Thesis, *Cranfield Institute of Technology*, 1991.

46. C. S. Bradley, PhD Thesis, *Sheffield Hallam University*, 1999.

47. G. J. Ashwell, M. Szablewski and A. P. Kuczynski, In *Lower-Dimensional Systems and Molecular Electronics*; R. M. Metzger, P. Day and G. C. Papavassiliou, Eds.; NATO ASI Series; Plenum: New York, 1991; Vol. B248, p 647.

48. G. J. Ashwell, E. J. C. Dawnay, A. P. Kuczynski, M. Szablewski, I. M. Sandy, M. R. Bryce, A. M. Grainger and M. Hasan, *J. Chem. Soc., Faraday Trans.*, 1990, **86**, 1117.

49. A. J. Riddick, W. B. Bunger and T. K. Sakano, *Organic Solvents., Physical Properties and Methods of Purification.*, 4th ed., John Wiley and Son Inc., New York, 1986.

50. M. Ravi, A. Samanta and T. P. Radhakrishnan, *J. Phys. Chem.*, 1994, **98**, 9133.

51. J. Fabian and R. Zahradnik, *Angew. Chem., Int. Ed. Engl.*, 1989, **28**, 677.

52. S. Inoue, Y. Aso and T. Otsubo, *J. Chem. Soc., Chem. Commun.*, 1997, 1105.

53. P. R. Thomas, PhD Thesis, *University of Durham*, 1998.

54. (a) S. Rajagopal and E. Buncel, *Dyes and Pigments*, 1991, **17**, 303. (b) R. Radeglia and S. Dahne, *J. Mol. Struct.*, 1970, **5**, 339. (c) S. Dahne and K. D. Molte, *J. Chem. Soc., Chem. Commun.*, 1972, 1056.

55. (a) L. Onsager, *J. Am. Chem. Soc.*, 1936, **58**, 1486. (b) C. J. F. Böttcher, *Theory of Electric Polarization*; Elsevier: Amsterdam, 1973, Vol. 1; 1978, Vol. 2.

56. M. Szablewski, *Personal Communication.*

57. S. Arai, H. Arai, M. Hida and T. Yamagishi, *Heterocycles*, 1994, **38**, 2449.

58. (a) J. Catalán, E. Mena, W. Meutermans and J. Elguero, *J. Phys. Chem.*, 1992, **96**, 3615. (b) J. Fabian and H. Hartmann, *Light Absorption of Organic Colorants: Theoretical Treatment and Empirical Rules, Reactivity and Structure Concepts in Organic Chemistry*; Springer Verlag: Berlin, 1980; Vol. 12.

59. (a) I. J. Jano, *Chim. Phys.*, 1992, **89**, 1951. (b) C. A. G. O. Varma and E. J. G. Groenen, *Recl. Trav. Chim. Phys. Paysbas.*, 1972, **91**, 296.

60. (a) F. Mikeš, J. Labský, P. Štrop and J. Králicek, *Polym. Prepr.*, 1982, **23**, 14; *Chem. Abstr.* 1984, **100**, 157349b. (b) A. Samat, D. De Keukeleire and R. Guglielmetti, *Bull. Soc. Chim. Belg.*, 1991, **100**, 679.

61. D. H. Williams and I. Fleming, *Spectroscopic Methods in Organic Chemistry*, 3rd ed., McGraw-Hill, London, 1980.

62. S. T. Abdel-Halim, *J. Chem. Soc., Faraday Trans.*, 1993, **89**, 55.

63. W. Kaim, S. Ernst and S. Kohlmann, *Chem. Unserer. Zeit.*, 1987, **21**, 50.

64. (a) C. Machado, M. G. Nascimento and M. C. Rezende, *J. Chem. Soc., Perkin Trans. 2*, 1994, 2539. (b) S. P. Zanotto, M. Scremin, C. Machado and M. C. Rezende, *J. Phys. Org. Chem.*, 1993, **6**, 637. (c) D. A. Binder and M. M. Kreevoy, *J. Phys. Chem.*, 1994, **98**, 10008.

65. (a) M. L. Moyá, A. Rodriguez and F. Sánchez, *Inorg. Chim. Acta*, 1991, **188**, 185. (b) M. L. Moyá, A. Rodriguez and F. Sánchez, *Inorg. Chim. Acta*, 1992, **197**, 227. (c) C. A. Rodrigues, E. Stadler and M. C. Rezende, *J. Chem. Soc., Faraday Trans.*, 1991, **87**, 701.

66. R. D. Shannon, *Acta Crystallogr. Sect. A: Cryst. Phys., Diffr., Theor. Gen. Crystallogr.*, 1976, **32**, 751.

Chapter 4: Studies on Selected Physical Properties.

4.1 Introduction.

Nonlinear optics (NLO) examines the extension of linear optics to the point where light interacts with, and induces a change in, the medium in which the light propagates. Such studies, which are dependent on the creation of intense pulses of electro-magnetic radiation, have only been achievable with the advent of the laser.[1] This ability to manipulate photonic signals efficiently has revolutionised technologies such as optical communication, optical computing, and dynamic imaging.[2-7] Interest in optical devices is rapidly growing because of the promise of extremely high speed processing and data storage.

Traditionally inorganic materials have dominated the area of NLO and to date most of the nonlinear optical materials used in the fabrication of passive and active photonic devices have been ferroelectric inorganic crystals,[8-11] for example inorganic materials, such as lithium niobate ($LiNbO_3$), gallium arsenide (GaAs) and potassium dihydrogen phosphate (KDP). Crystals are used to double, triple, and combine the frequencies of incident laser light so that different frequencies are achieved in optical experiments or systems.[12,13] However, there are several drawbacks. Crystals are expensive to grow, and are not easily incorporated into electronic devices and in general, the response time of such crystals is slow when compared to other materials. As future requirements for the telecommunications industry include the need for higher speed and higher capacity systems,[14] alternatives to the inorganic NLO materials may be required.

Research during the 1980's exploring the use of organic materials,[15,16] showed some organic chromophores demonstrating extremely large nonlinearities, with much faster responses than those observed in inorganic crystals. The versatility of organic synthesis may allow tailor-made compounds exhibiting the desired application. A variety of carbon-based materials have been investigated for their NLO properties, e.g. polymers,[15] liquid crystals,[17] and organometallic compounds.[18]

4.2 Fundamental Principles of Nonlinear Optics.

If an applied electromagnetic field is allowed to interact with a molecule, a change in polarisation within the molecule occurs (Figure 4.1).

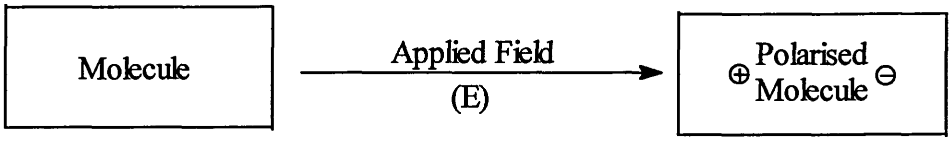

Figure 4.1 Induced Polarisation of a Molecule by Electromagnetic Radiation.

Such molecules may be classified as a *dielectric* and will, therefore, have a *dielectric constant* or *relative permittivity*, ε_r. The degree to which a molecule can be polarised by an applied field is known as the *linear susceptibility*, χ, and is linked to the relative permittivity of the molecule by the following equation:

$$\chi = \varepsilon_r - 1 \qquad \text{Equation 4.1}$$

In the majority of materials, the response of polarisation to an applied electromagnetic field is linear and may be represented by Equation 4.2, where P is the polarisation per unit volume, ε_o is the permittivity of a vacuum and E is the applied field.

$$P = \varepsilon_o \chi E \qquad \text{Equation 4.2}$$

The polarised molecule behaves as an oscillating dipole, producing its own electromagnetic radiation. From Equation 4.2, the polarised species radiates energy of the same frequency and phase as that of the incident radiation.

However, if the electric field strength is sufficiently large, a molecule can deviate from this linear behaviour. For individual molecules, this nonlinear polarising effect, can be expressed as a power series of the local electric field, such that:

$$\Delta\mu = \mu_e - \mu_g = \alpha E + \beta EE + \gamma EEE + \ldots\ldots \qquad \text{Equation 4.3}$$

where $\Delta\mu$ is the induced dipole moment, μ_e and μ_g are the dipole moments in the excited and ground states respectively. The coefficients α, β and γ are the linear, quadratic and cubic hyperpolarisabilities respectively, and β and γ describe a nonlinear response to the incident electric field - for example β is responsible for second order nonlinear optical effects such as second harmonic generation[19] (frequency doubling), frequency mixing,[20] optical rectification[21] and the electro-optic (Pockels) effect.[22]

So far we have described the nonlinear character of a solitary molecule. Equation 4.4 gives the polarisation of an assembly of molecules and introduces the terms $\chi^{(1)}$, $\chi^{(2)}$, $\chi^{(3)}$ which are specific to the bulk material and represent the first, second and third order responses respectively.

$$P = P_o + \chi^{(1)}(E) + \chi^{(2)}(E^2) + \chi^{(3)}(E^3) + \ldots\ldots \qquad \text{Equation 4.4}$$

Equation 4.4 looks very similar to the Equation 4.3. However, the hyperpolarisability coefficients in Equation 4.3 are tensor quantities, and are symmetry dependent. It can be shown that odd order coefficients are non-zero for all molecular environments but even order coefficients are zero for centrosymmetric environments. So, even if a molecule possesses a relatively large molecular hyperpolarisability (β), if it does not retain a non-centrosymmetric environment in the bulk phase, phenomena such as the Pockels effect will not be detected. So in designing new materials for nonlinear optical applications, one should not only consider the polarisability and asymmetric charge distribution of the material but also the bulk phase environment that the material will adopt.

4.3 Second Order Nonlinear Optical Materials and Their Design.

Organic compounds which exhibit second order nonlinear optical activity are usually non-centrosymmetric one dimensional charge-transfer molecules, typically consisting of a conjugated π-electron system, asymmetrically substituted by electron donor and acceptor groups.

Normally, the donor unit is electron rich enabling it to "push" electrons towards the electron deficient acceptor unit via a conjugated π-network. Typical examples of strong electron donating groups include amino (R_2N-), alkylthio (RS-) and alkoxy (RO-) subunits. Common electron accepting groups are nitro (-NO_2), nitrile (-CN) and carbonyl (-CO) functionalities. A generalised model of a typical organic second order NLO molecule is illustrated in Figure 4.2, and 4-(dimethylamino)-4′-nitrostilbene (1, DANS) is a typical example.

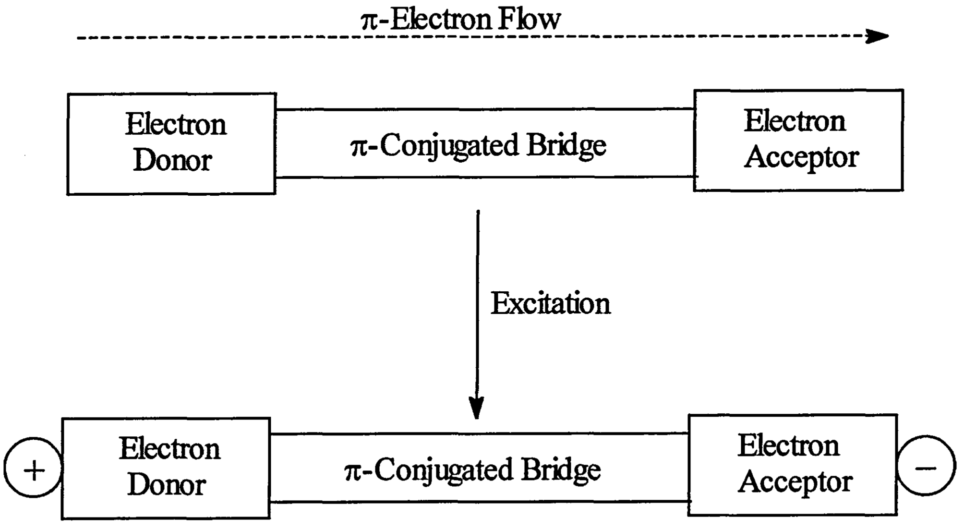
π-Electron Flow
Electron Donor
π-Conjugated Bridge
Electron Acceptor
Excitation
+
Electron Donor
π-Conjugated Bridge
Electron Acceptor
−

Figure 4.2 Generalisation of a Second Order NLO Molecule, Asymmetrically Substituted by Electron Donor and Acceptor Units.

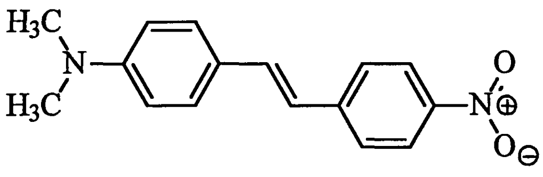
H3C
N
H3C
O
N⊕
O⊖

DANS (1) $\beta_0 = 55 \times 10^{-30}$ esu

The simplest and most widely used theoretical description of the hyperpolarisability of charge-transfer molecules is the Equivalent Field Model (EFM) of *Oudar* and *Chemla.*[23] This model establishes trends in the nonlinearity-molecular structure relationship in terms of relatively simple physical properties, such as charge-transfer between ground and excited states.

However the model of *Oudar* and *Chemla* has limitations. It breaks down for octopolar compounds and certain organometallics,[24] and also if the fundamental frequency and/or the doubled frequency are close to the charge-transfer absorption band of the material.

In a donor-acceptor system, it is the degree of variation in the dipole moment upon excitation, which is important for a large β coefficient, and as chromophores which are charge separated in their ground state will naturally possess a large dipole moment they have been extensively studied. Consider (2) below.

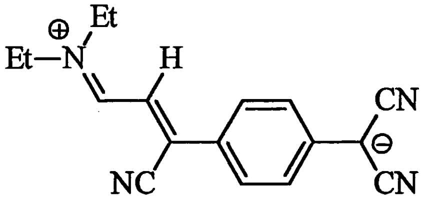

DEMI (2) $\mu\beta(0) = 9500 \times 10^{-48}$ esu

This exceptionally high μβ value is attributed more to the zwitterionic ground state structure of DEMI in solution (μ), rather than the degree of hyperpolarisability (β).[25] The requirement for a molecule to be non-centrosymmetric was mentioned earlier. Due to coulombic attractions in the solid state dipolar compounds such as DEMI (2) usually adopt a head-to-tail arrangement between pairs of molecules, resulting in centrosymmetric dimers. So, although a single molecule may be non-centrosymmetric, a group of molecules may exhibit overall centrosymmetry in the solid state. Such centrosymmetric packing is common in carbon-based materials - only 20% of organic molecules are able to crystallise in a non-centrosymmetric fashion.

As a result, several techniques have been used to fabricate molecules in a non-centrosymmetric alignment in the solid state. These include incorporation of chiral centres,[26] inclusion phenomena,[27] hydrogen bonding,[28] steric hindrance,[29] co-crystallisation,[30] salt formation,[31] dipole-dipole interaction reduction[32] and Langmuir-Blodgett films[33] (discussed in greater detail in Chapter Five) as well as incorporation into a polymer or polymer host.[34]

Early research into organic nonlinear optical materials concentrated on increasing the magnitude of the second-order molecular hyperpolarisability. Substituted benzenes, biphenyls and stilbenes to the more elaborate azobenzenes and Schiff bases,[35-38] were explored to determine the empirical relationship between molecular structure and nonlinear response.

It was shown that the β-value of such organic materials could be increased if the donor and acceptor strengths of the molecule were increased. A similar effect was observed with increasing conjugation length. Table 4.1 illustrates these influences on the molecular hyperpolarisability of thiophene substituted stilbenes. It has been established that there is an optimum donor/acceptor strength for the two components. *Marder et al*[39] have shown that polyenes with dicyanovinyl functionalities exhibit smaller static hyperpolarisabilities (β_0), than the corresponding chromophores bearing an aldehyde functionality.

Compound	μβ 10^{-48} esu (λ = 1.907 μm)[a]
(3) 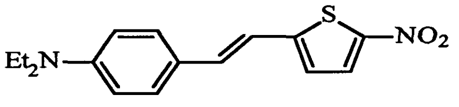	600 (421)
(4) 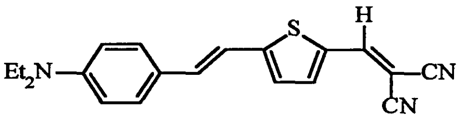	1300 (857)
(5) 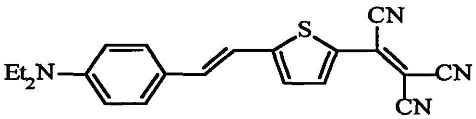	6200 (3023)
(6) 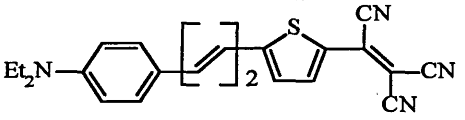	9100 (4146)

[a] Values in parentheses represent $\mu\beta_0$, zero-frequency hyperpolarisability product, obtained from the extrapolation of the measured μ β values from EFISH experiments conducted in 1,4-dioxane using a two-level model.[40]

Table 4.1 Molecular Nonlinearities obtained For Thiophene Substituted Stilbenes Incorporating Different Acceptor Moieties.[40]

Here, it is assumed that the charge-separated state is stabilised by the strong dicyanovinyl groups to such an extent that the optimum level of Bond Length Alternation (BLA) is surpassed. BLA is a means of describing the efficiency of π-electron flow between the donor and acceptor units of the molecule and quantifies the average difference in bond lengths between adjacent single and double bonds (Figure 4.3). Thus the dicyanovinyl chromophore exhibits a relatively smaller static hyperpolarisability (β_0) because the increased zwitterionic ground state character of the molecule means that the BLA within the molecule is increased, despite the fact that molecule has an increased acceptor strength.

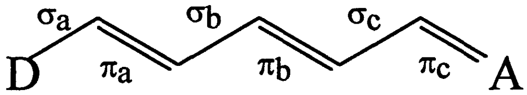

$$\mathrm{BLA} = \frac{[(\sigma_a - \pi_a) + (\sigma_b - \pi_b) + (\sigma_c - \pi_c)]}{3}$$

Figure 4.3 BLA Calculation for a Polyene Backbone.

Structures 7-9 depict three of the most common types of conjugated backbones used in NLO material design and serve as effective models when describing the optimisation of conjugated π-linkages.

In terms of delocalisation, polyene (7) embodies the most effective π-bridge since, ignoring the nature of the donor and acceptor functionalities, the energy barrier for the conversion of one resonance structure to the other should be essentially zero. However, in the vast majority of cases, the donor and acceptor groups will prefer either the neutral or zwitterionic state, thus resulting in an energy gap between the two canonical resonance structures. An exception to this is when the end groups are identical in molecular structure and differ only in charge. For example, the cyanine class of molecule (Figure 4.4) represents a system where both resonance forms contribute equally to the ground state and are therefore degenerate. When the two resonance structures contribute equally, the molecule will exhibit essentially no bond alternation, and will thus have a vanishing β[39] as a result of the molecule reaching the cyanine limit.

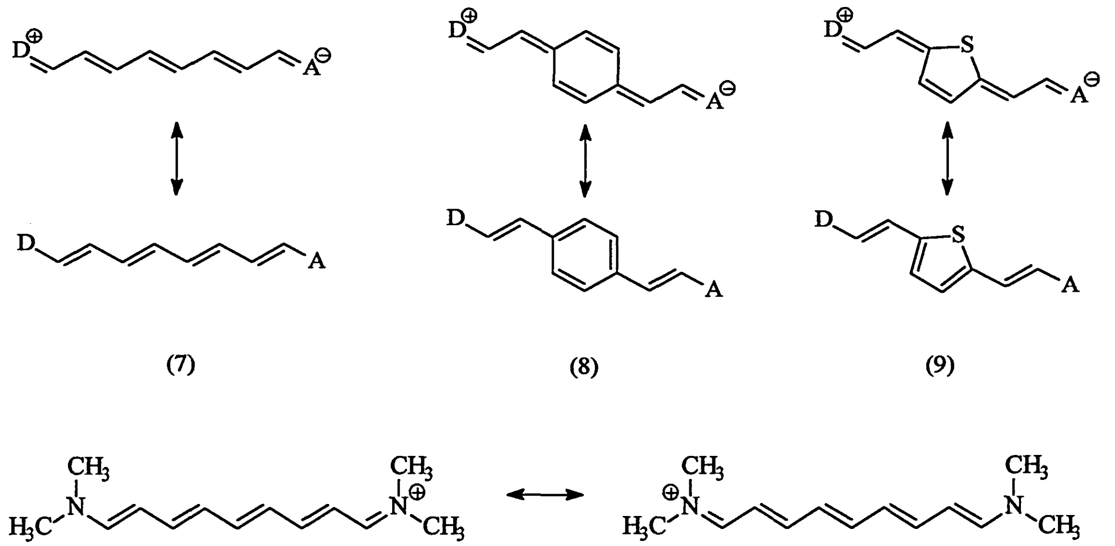

Figure 4.4 Canonical Resonance Structures for the Cyanine Molecule.

Despite the excellent efficiency of the polyene (7) molecules in redistributing electric charges under the influence of electric fields, the synthesis of functionalised polyenes (D-$(CH)_n$-A) is challenging, limiting their use in NLO material design.

Aromatic systems, on the other hand, have been extensively studied. When combined with polyenes in π-conjugated spacers, they offer not only excellent thermal and oxidative stability but also greater synthetic versatility. In terms of BLA, the switch between the two resonance forms in 8 and 9 leads to an appreciable difference in energy. Table 4.2, illustrates the effect of varying the conjugated spacer groups between donor and acceptor functionalities and shows that the value of μβ is enhanced by replacement of the benzene ring system with a thiophene unit, due to the smaller aromatic stabilisation energy of thiophene derivatives compared to benzene.

Compound	$\mu\beta$ 10^{-48} esu ($\lambda = 1.907\mu m$)[a]
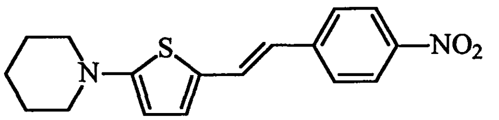	660
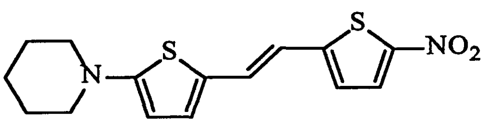	1040
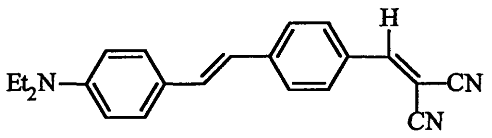	1100
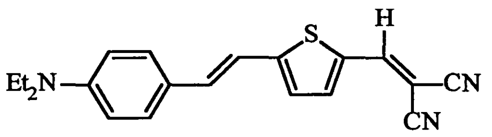	1300

[a] measurements were made in 1,4-Dioxane; $\mu\beta$ was obtained using $1.907\mu m$ incident radiation.

Table 4.2 Molecular Nonlinearities of Selected compounds.[18]

As a result of this work the ground rules for optimising the molecular hyperpolarisability, β, are now well understood: optimising the ground state polarisation via the correct combination of donor/acceptor pairs for a given π-backbone, where the ground-state polarisation is related to the degree of mixing of two limiting charge-transfer forms of the molecule.[39]

For organic materials there are number of different methods which can be used to detect and quantify the level of NLO activity. A brief description of some are listed below:

Kurtz Powder Method.[41]

This technique essentially measures the SHG activity of bulk amorphous or microcrystalline materials. A laser is directed onto a powdered sample and the emitted light at the second harmonic frequency is collected and compared to that of a reference sample, such as quartz or urea. However the method is recognised only as being semi-quantitative, as the degree of nonlinear activity varies with the type and level of crystallinity in the solid; therefore, varying factors, such as the type of solvent used for recrystallisation, will produce different values of SHG efficiency.[42]

Electric Field Induced Second Harmonic Generation (EFISH).[43]

This is one of the most common methods used for determining the β value. Here, a strong electric field is applied to a solution of the NLO material. The interaction of the field with the permanent dipoles of the molecules causes a bias in the orientation of the chromophores. The partial removal of the isotropy allows SHG to occur. The quantity $\mu \beta$ can be determined from the intensity of the second harmonic radiation but a separate measurement for the permanent dipole is required to calculate β. In contrast to the Kurtz technique,[41] the EFISH experiment quantifies second order activity at the molecular level, so that the correlation between structure and property in a compound can be assessed with good accuracy.

Hyper-Rayleigh Scattering (HRS).[44]

This was developed to measure the hyperpolarisabilities of unconventional nonlinear molecules and allows the value of β to be determined without the need for the independent determination of the molecule's dipole moment (μ). Measurements are conducted by focusing an intense laser beam onto an isotropic solution of nonlinear molecules and measuring the intensity of the second harmonic light. This technique has an advantage over EFISH as it can be used to determine β in ionic and apolar compounds as there is no need for an orientating electric field.

Solvatochromic Methods.[45]

Although not as accurate as the EFISH and HRS methods, this technique allows the determination of β from the UV/visible spectra of NLO materials in solution. The technique involves the use of a capacitance bridge to obtain (by calculation) the permanent ground state dipole moment, μ_g, from low polarity solvent solutions of varying concentration. The lowest energy absorption band in the UV/visible spectra of these solutions allows the determination of the excited state dipole moments, μ_e. The value of β can be calculated from the difference term μ_g-μ_e. The advantage of this technique is the relatively inexpensive equipment required and speed.

4.4 TCNQ-Based Nonlinear Optical Materials.

Surprisingly, TCNQ has received scant attention in terms of the number of documented NLO materials that embody the TCNQ framework.[46-50] Nevertheless, of the TCNQ-based compounds that do appear in the literature, the majority exhibit relatively large hyperpolarisabilities.

For example workers at the University of Hyderabad[46] have shown that amino-substituted TCNQ derivatives, such as the one illustrated in Figure 4.5, demonstrate large static hyperpolarisabilities even in the crystalline state. Powder SHG measurements carried out on these compounds,[46] using the Kurtz-Perry powder technique,[51] have shown β(0) values of the order of 60 to 66×10^{-30} esu.

These zwitterionic compounds, which are based upon the diamino-substituted dicyanoquinodimethanes first synthesised by the du Pont group[52] in 1962, retain their non-centrosymmetric lattice in the bulk phase as a result of their stereogenic centres.

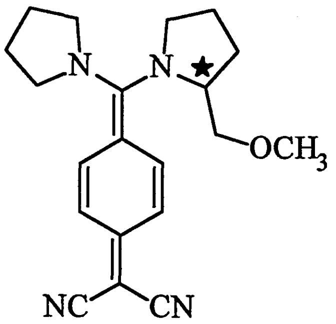

Figure 4.5 Diamino-Substituted Dicyanoquinodimethane NLO Compound.

Materials which contain the tricyanoquinodimethane (TCQ) acceptor moiety rarely exhibit second harmonic activity in the bulk phase. Here, the large acceptor strength of the TCQ moiety[53] means that such molecules are charge-separated in the ground state and as such form an anti-parallel head-to-tail arrangement in the solid phase. For instance the Benzothiazolium (10),[49] and Quinolinium (11)[50] TCQ-based D-π-A systems, have all been shown to exhibit zero SHG activity in the crystalline state.

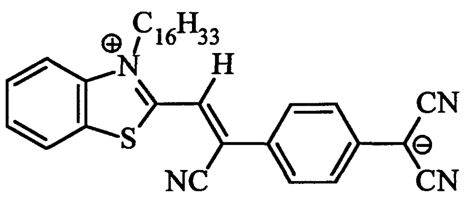

$C_{16}H_{33}$(2)BT3CNQ (10)

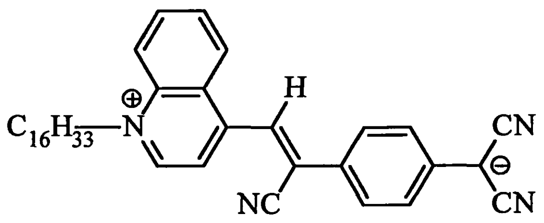

$C_{16}H_{33}$(4)Q3CNQ (11)

However, when suitably aligned in Langmuir-Blodgett films,[49,50] such chromophores exhibit extremely large second harmonic activity, with (11) having the highest second order susceptibility value for any LB multilayer. Because compounds (10) and (11) are structurally related to those studied in this text, it could be assumed that a similarly large nonlinear optical response will be observed here. From theory, quinolinium and benzothiazolium zwitterions should possess a higher second order coefficient because both molecules possess a donor unit with a second aromatic ring. Introducing a second benzene ring into the donor unit means that the aromatic donor system becomes more electron rich, leading to greater polarisation and a larger nonlinear optical response. Also, introducing electron withdrawing and donating substituents into the molecule will affect the observed nonlinear optical response.

And, for R(4)Q3CNQF_4, R(2)Q3CNQF_4 and R(2)BT3CNQF_4, the introduction of the more electronegative fluorine atom into the acceptor moiety has the effect of making the compounds more charge-separated, as the electronegative fluorine helps stabilise the zwitterionic ground state of the molecule. So, this increase in zwitterionic character may imply a larger overall ground state dipole moment (μ). The simple Equivalent Field Model (EFM)[23] shows that this increase in ground state polarisation will theoretically lead to a larger change in dipole moment upon interaction with an applied electro-magnetic field and thus a larger NLO response. However, BLA analysis implies a smaller β value than that of the unsubstituted adduct. So the models give conflicting evidence, and a more rigorous investigation of this structure/property relationship is required.

4.5 Dipole Moments of Highly Dipolar Nonlinear Optical Materials.

4.5.1 Experimental Apparatus and Procedure.

There are numerous methods available, which can be utilised to measure the dielectric constant (ε_r) of a solution.[54-57] Invariably, these involve the measurement of the capacitance (C) of a solution filled cell. Variations on this theme may be adopted[54,56-58] and the design described below was utilised in this work.

The three terminal, solution capacitor is illustrated in Figure 4.6 along with its associated circuit diagram. The apparatus itself consists of a rod of stainless steel placed in the centre of a stainless steel tube, such that a concentric cylindrical capacitor is formed. The centre rod forms the high potential electrode, and the outer tube the low potential electrode. The electrode separation is three millimetres and the total diameter of the cell is approximately fifty millimetres.

The large electrode area and small electrode separation yields a large capacitance for the cell and this allows determination of the dielectric constant. On top of the centre electrode is an earthed ring guard, which removes any fringing of the electric field that may occur at the edges of the centre electrode. Thus, the field remains perpendicular to the surface of the electrodes along the entire electrode surface. The ring guard also ensures that the same volume of solution is measured each time. The entire arrangement is encased in a PTFE case ensuring electrical isolation.

The electrodes are connected to the LCR meter via four BNC coaxial cable sockets. From the circuit diagram, the outer conductors for the sockets are connected to earth, and the centre conductors are connected to the high or low potential and current circuits of the LCR meter, for the centre and outer electrodes respectively.

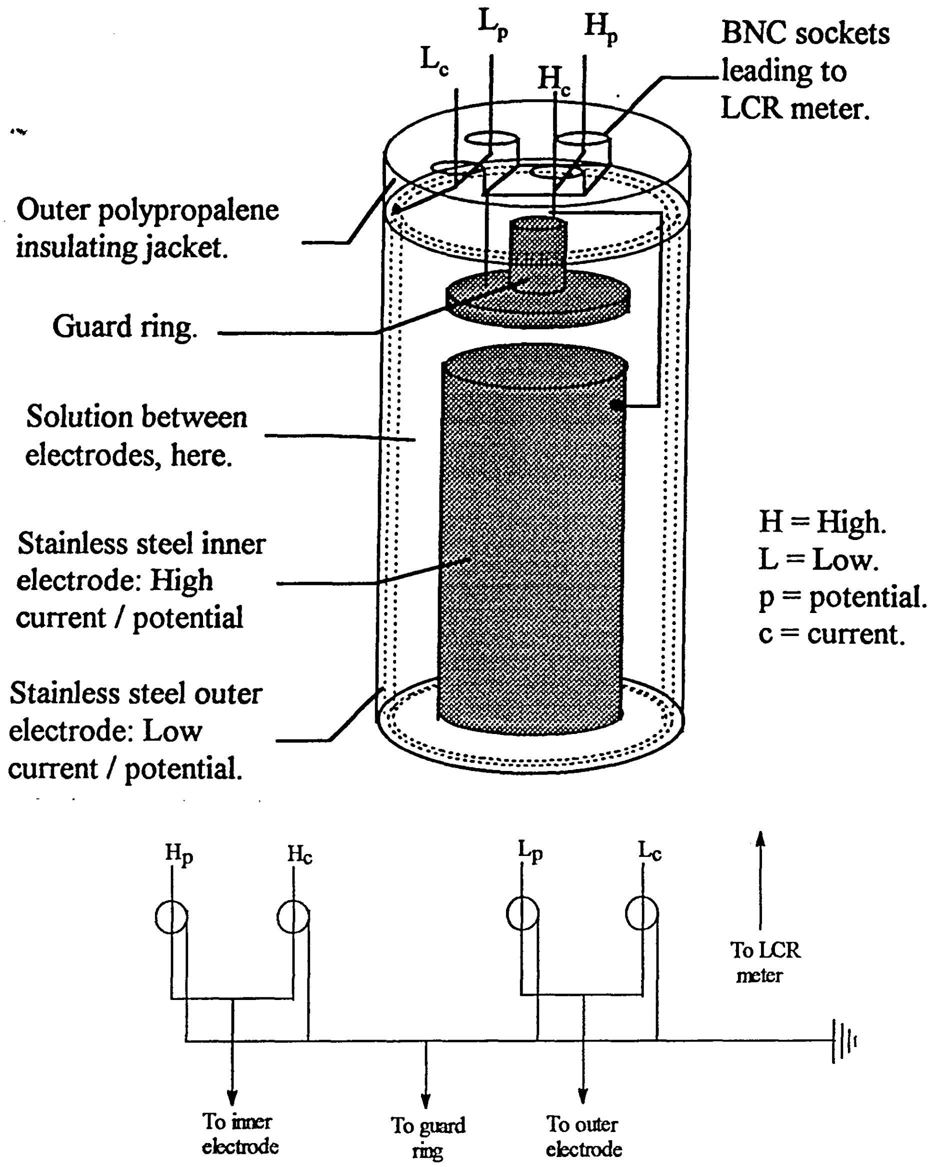
L_p
H_p
L_c
H_c
BNC sockets leading to LCR meter.
Outer polypropalene insulating jacket.
Guard ring.
Solution between electrodes, here.
Stainless steel inner electrode: High current / potential
Stainless steel outer electrode: Low current / potential.
H = High.
L = Low.
p = potential.
c = current.
Hp
Hc
Lp
Lc
To LCR meter
To inner electrode
To guard ring
To outer electrode

Figure 4.6 The Capacitor and Electronic Circuit used in the Measurement of the Dielectric Constant (ε_r) of Solutions.

The LCR meter (Hewlett Packard, HP4278a), used to measure the capacitance of the cell, was operated at 1 MHz, which is well away from any resonance points. To confirm this, in addition to the measurement of the capacitance, the dielectric loss was also measured for each material in solution. The loss was found to be very low for all of the materials, typically ~0.1 - 0.5pF.

A typical experiment was conducted as follows. The capacitance of the dry empty cell was measured. This was found to be approximately 14.57 ± 0.05pF. Measurements of the capacitance of the empty cell were performed immediately prior to the experiment. The dielectric constant, ε_r, for each solution was calculated via the equation:

$$\varepsilon_r = C_S / C_A \qquad \text{Equation 4.5}$$

Where C_S and C_A are the capacitance of the solution filled and empty cell respectively. To ensure that the cell provided accurate and meaningful results, the dielectric constant of various solvents was measured and compared to that reported in the literature.[59] When using solvents with a dielectric constant between 2 and 45, it was found that the measured dielectric constants of the solvents were within 10% of the literature values.[59]

A stock solution of a material of concentration around 10^{-4}-10^{-3} mol dm^{-3} was prepared in dry dichloromethane (HPLC grade), to a volume of 50cm^3 and filtered using a 0.5 μm disposable filter. The solution was then successively diluted, such that two orders of magnitude in concentration were obtained. The capacitance cell was then filled with each solution, the capacitance measured, and the solution returned to its flask. The order in which the experiment was conducted is important as the temperature of each solution may vary and thus affect the value of the dielectric constant measured. Therefore, experiments were conducted from low to high and high to low concentrations in an attempt to eliminate any variation in temperature during the experiment. A graph of the dielectric constant versus the concentration of each solution was then plotted, and an average gradient of the two experimental curves was taken. Experiments for each material were conducted three times to safeguard that the experiment was repeatable and to obtain an average $\partial\varepsilon / \partial C$.

4.5.2 Solution State Dipole Moment Measurements.

The solution state dipole moment was evaluated for a range of materials (see Table 4.3) using the Guggenheim equation[60] as the preferred method of analysis. The Guggenheim method[60] which is a modified version of the Debye formulae,[61] is one of a number of equations[62] that can be used to evaluate solution state dipole moments. The attraction of this method stems from its simplicity, as the dipole moment is determined by measuring the dielectric constant of a solution for a number of solute concentrations C, and relating the experimental gradient $(\partial\varepsilon / \partial C)_0$ at zero concentration to the dipole moment, expressed in Debyes. The data points obtained were fitted to a straight line using a least squares fitting program. Figures 4.7 and 4.8 illustrate characteristic plots for $PhCH_2(4)Q3CNQF_4$ and $C_3H_7(2)BT3CNQF_4$. The dielectric constant at zero concentration was simply obtained by ascertaining the value at which the plot intercepted the Y-axis and the gradient at zero concentration $(\partial\varepsilon / \partial C)_0$ using a least squares fitting program. The average gradients, obtained from the analysis of several experiments for each material, along with obtained dielectric constant values and calculated dipole moments, are presented in Table 4.3.

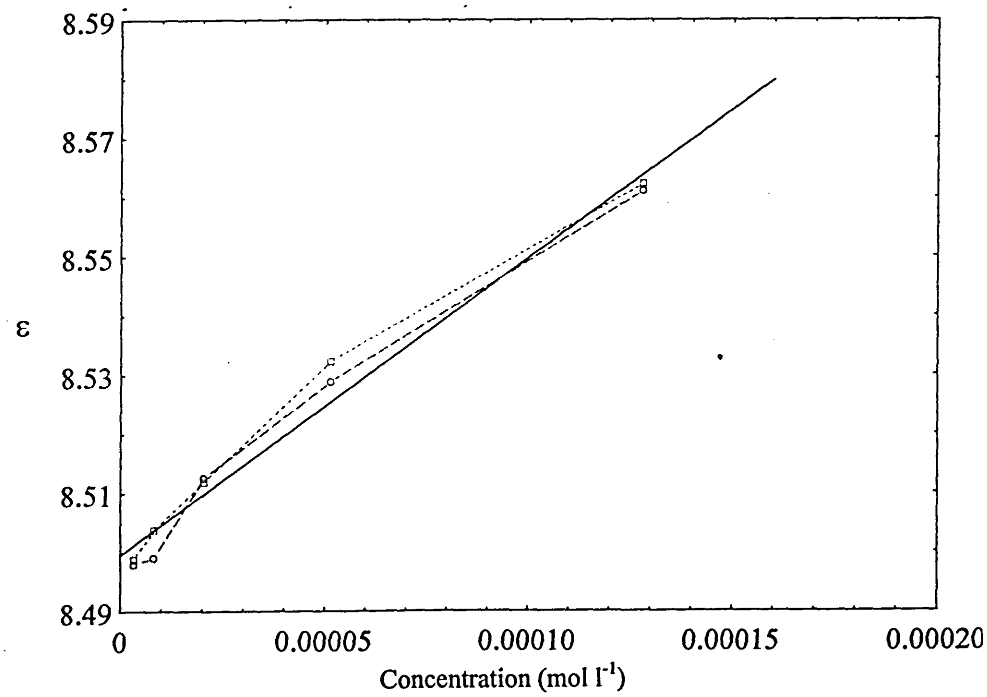

Figure 4.7 Experimental Dipole Moment Plot Obtained for $PhCH_2(4)Q3CNQF_4$.

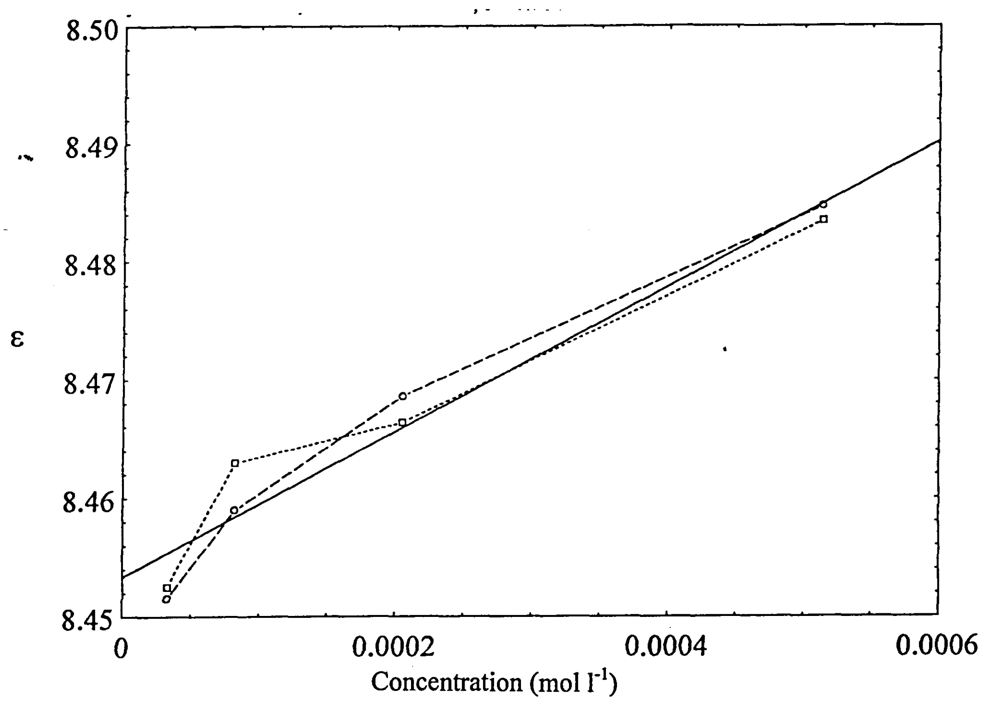

Figure 4.8 Experimental Dipole Moment Plot Obtained for C_3H_7(2)BT3CNQF$_4$.

Material	$(\partial\varepsilon / \partial C)_0$ (mol^{-1} dm^3)	ε_0 (DCM)	μ_s^{gugg} / D
$C_{10}H_{21}$(4)Q3CNQF$_4$	632 ± 98	8.52 ± 1.0	46.3 ± 3.3
$C_{10}H_{21}$(2)Q3CNQF$_4$	565 ± 84	8.30 ± 0.5	44.3 ± 3.0
PhCH$_2$(4)Q3CNQF$_4$	501 ± 76	8.50 ± 1.0	41.3 ± 3.0
$C_{10}H_{21}$(4)Q3CNQ	281 ± 52	8.00 ± 1.0	31.6 ± 2.7
$C_{10}H_{21}$(2)Q3CNQ	177 ± 43	8.50 ± 1.0	24.5 ± 2.7
C_3H_7(2)BT3CNQF$_4$	614 ± 89	8.45 ± 1.0	45.5 ± 1.9
C_3H_7(2)BT3CNTMQ*	178 ± 45	8.54 ± 0.9	24.4 ± 3.1

Table 4.3: Table showing the average gradients obtained from the measurement of the dielectric constant of the materials mentioned in the text, with increasing concentration. In addition the dielectric constant of the solvent at zero concentration is presented along with the dipole moments obtained from experiments using Guggenheim's equation. *denotes the Bis C_3H_7(2)BT3CNTMQ compound discussed in Chapter 2.

The solution state dipole moments are extremely large when compared to other organic materials - in general very few organic materials have dipole moments greater than 7D.[63] Thus the ground state environment of such molecules is strongly zwitterionic, in which the charge centres are located at opposite ends of the molecule as illustrated in Figure 4.9.

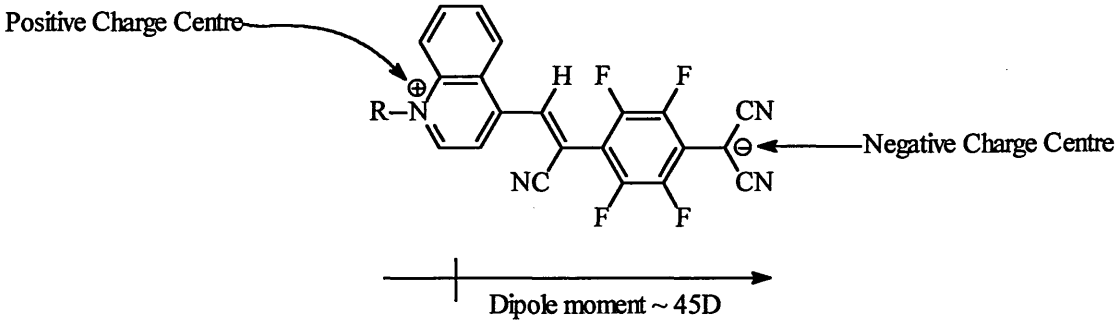

Figure 4.9 Highly Charge-Separated Molecule.

Despite the fact that such compounds all contain the same π-extended backbone, the various adducts do not exhibit similar dipole moments. The fluorinated adducts are much more polar which would explain why they are more insoluble in lower polarity solvents, such as chloroform, chlorobenzene etc. The fluorinated adducts also show very similar dipole moments, with little difference between the quinolinium and benzothiazolium compounds. The TCNQ-based adducts show quite different dipole moments, the γ-substituted compound showing a dipole moment some 7D larger than the α-substituted adduct. The larger values obtained for the γ-substituted TCNQ compound is attributed to the increased distance between the charge centres in the γ-substituted adduct.

However, variation in dipole moments for the quinolinium isomers could be attributed to geometrical shape. Strictly, μ is a vector quantity which implies that the increased dipole moment of the γ-isomer is due to the charge-transfer process of the molecule lying within a near straight-line.[64,65] In the α-substituted adduct, the charge centres do not lie within a near straight-line as the nitrogen heterocycle is meta-substituted. So unlike γ-substituted adducts, the dipole moment of the α-substituted compound is made up of several vectors that act in more than one direction. This results in a much smaller overall vector, and a smaller dipole moment.

The fluorinated compounds show dipole moments, which are far in excess of those observed for the unsubstituted adducts - of the order of 40 to 46 Debyes. The reason for this increase in dipole moment is the electronegative fluorine atoms in the acceptor ring system reducing the overall efficiency of the molecule's charge-transfer process by increasing the ionisation potential of the TCNQ ring system. This has the effect of stabilising a charge-separated ground state (Figure 4.10).

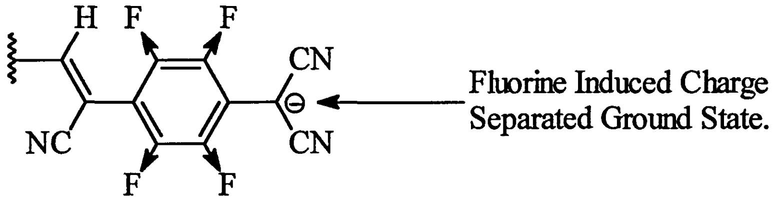

Figure 4.10 Fluorine Induced Stabilisation of the Zwitterionic Ground State.

Apart from indicating that the TCNQF4-based adducts are highly charge-separated, the above experiments also provide significant information on other physical properties.

The investigations involving the fluorinated adducts were conducted in dichloromethane which is a relatively non-polar solvent ($\varepsilon = 8.93$).[59] Because the dipole moments of such adducts are extremely large (40-46D), the probability that the molecules would undergo a change to a neutral ground state in solvents of lower polarity than dichloromethane is considered unlikely. Thus, the observation of reverse solvatochromism in such adducts is attributed to aggregation of the solute molecules in solution rather than a shift from a charge-separated state to a neutral one.[66]

The dipole moment of the fluorinated γ-substituted C_{10} adduct is greater than that observed for the corresponding fluorinated α-substituted compound, although the difference, between the two isomers is much smaller (2D) than that observed for the unsubstituted materials (7D). This disparity is again thought to occur as a consequence of the geometrical differences between the two isomers.

The benzothiazolium compounds exhibit markedly different solution state dipole moments, despite the fact that both compounds demonstrate high-energy intramolecular charge-transfer absorption bands (see Chapter 2). As with the other fluorinated compounds, C_3H_7(2)BT3CNQF_4, displays an exceptionally large dipole moment of 46D. However, despite showing an intramolecular charge-transfer band that is higher in energy than that of C_3H_7(2)BT3CNQF_4, the bis C_3H_7(2)BT3CNTMQ compound was found to have a solution dipole moment some 22D smaller than that of the fluorinated derivative. The reason for this is unclear. However, using the structure proposed in Chapter 2, it is thought, like the α-substituted quinolinium compounds, to arise as a result of the geometrical shape of the molecule. Unlike the other D-π-A materials studied in this text, the bis C_3H_7(2)BT3CNTMQ adduct contains more than one polarisation pathway as the addition of the second benzothiazolium unit to the acceptor ring creates a second possible charge-transfer route (Figure 4.11).

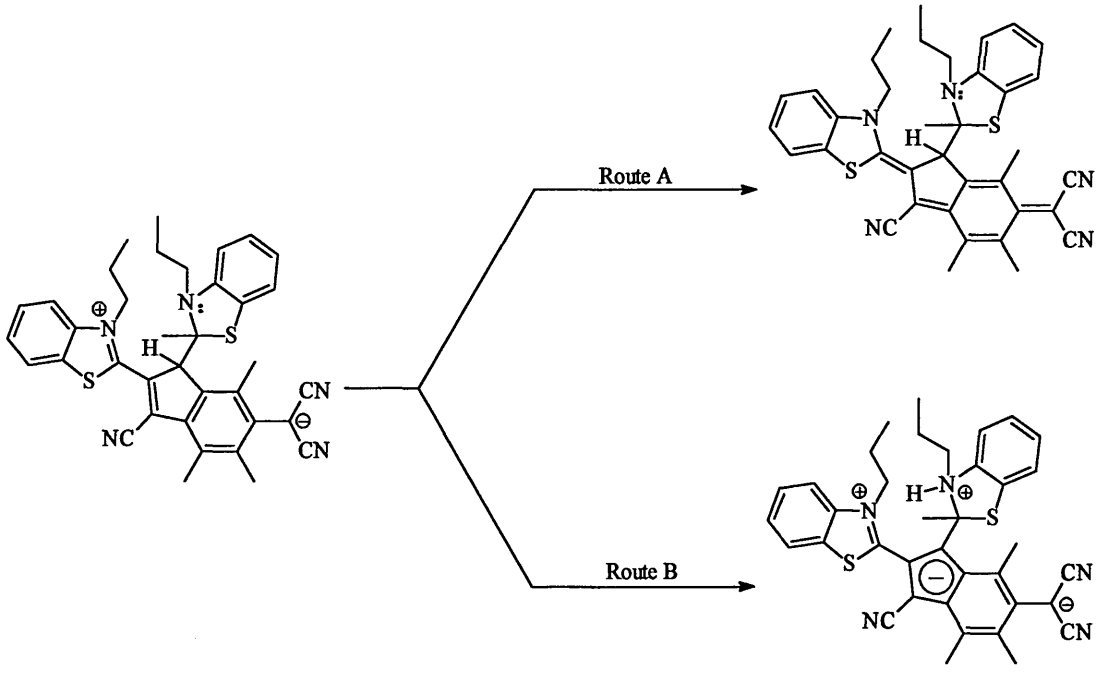

Figure 4.11 Charge-Transfer Pathways in the Substituted C_3H_7(2)BT3CNTMQ Adduct.

Route A, is the transfer of an electron from the negatively charged dicyanomethanide group to the positively charged benzothiazolium heterocycle. Route B, is fairly unusual,[67] in that the ensuing charge-transfer results in the cleavage of a proton from the five membered ring. So the dipole moment may not act in a near straight-line, as is the case in the C_3H_7(2)BT3CNQF_4. Though the chemical structure has not been fully determined, the observation of two closely lying bands in the UV/Vis spectrum obtained for the bis C_3H_7(2)BT3CNTMQ adduct (Figure 2.14, Chapter 2), may indicate two different electronic transitions and provides some supporting evidence.

The dipole moments obtained via the Guggenheim equation compare well with those obtained using different methodologies,[62] e.g. electric field poling of thin polymer films incorporating small fractions of the adduct.[68] For example for (11) and (12) using this method values of 38 ± 5D also support a predominantly zwitterionic ground state.

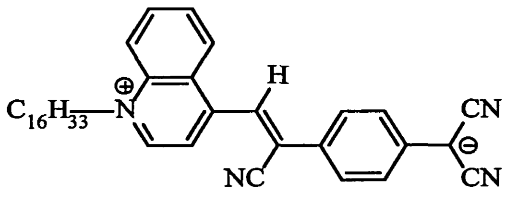

$C_{16}H_{33}(4)Q3CNQ$ (11)

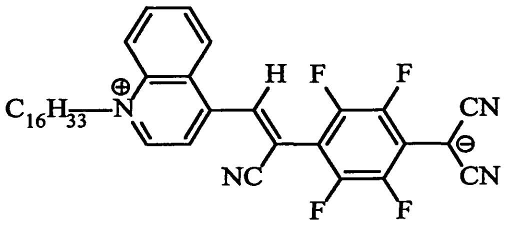

$C_{16}H_{33}(4)Q3CNQF_4$ (12)

Initially the experiments were conducted upon the adducts in chloroform. Chloroform was chosen because its dielectric constant is low ($\varepsilon = 4.806$),[59] However, the solubility of most of the adducts in chloroform is low and measurements were difficult. The fluorinated adducts had also shown reverse solvatochromism in chloroform, implying that the molecules may form aggregates - undesirable as it would affect the accuracy of these results.

The solubility of the adducts was found to be slightly better in dichloromethane which has a higher dielectric constant ($\varepsilon = 8.93$).[59] Despite this, it was found that, due to the low concentration of the solution, the experiments encountered errors, with the extrapolated dielectric constant values (Table 4.3) on average between 5% and 10% different from the standard literature value for dichloromethane.[59]

The dipole moments determined in this study are solution state measurements, not gas phase dipole moments, and are dependent upon the polarity of the media in which the experiments are conducted. As with most other conjugated molecules, the polarisation that occurs within such dipolar compounds is inevitably sensitive to the surrounding environment, which acts to perturb the "vacuum" polarisation of the material and thus alter its dipole moment. Hence when experiments are conducted in reasonably polar solvents, such as dichloromethane, the values obtained do not always equate to the dipole moment of the material in the solid state. Such a solvent induced change of the dipole moment can be clearly seen in the experimental results obtained from the Guggenheim analysis of the structurally related DEMI compound which has substantially different solution state dipole moments when measured in dichloromethane (μ_S = 22D)[62] and dimethylformamide (μ_S = 45D).[69]

This variation in dipole moment is explained by Onsager's reaction field theory.[70] Here, the polarised medium surrounding the molecular dipole is said to exert a "reaction field" back onto the molecule which acts through its linear polarisability, α, to further enhance the dipole. From Figure 4.12, the more polar the medium, the greater the reaction field and the larger the enhancement of the dipole moment.

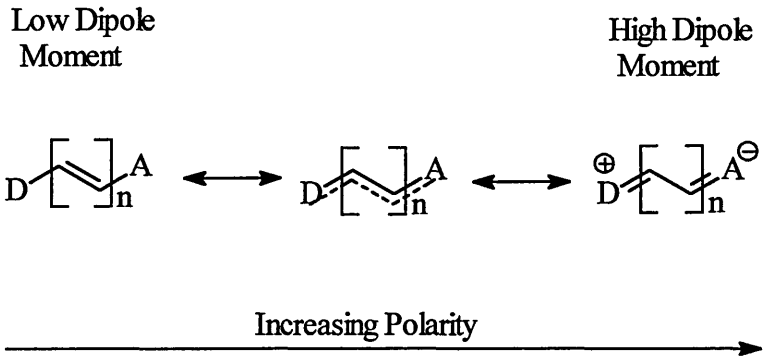

Figure 4.12 Evolution of the Dipole Moment.

Further evidence of increasing zwitterionic character of dipolar compounds, such as DEMI, in increasingly polar media can be obtained from NMR solvatochromism studies. The high sensitivity of the NMR technique means that subtle changes in the electron density of molecular structures can easily be detected, making it a valuable tool for investigations of this type.[71]

4.6 ^{19}F NMR Dipole Moment Evolution Studies.

Nuclear Magnetic Resonance, is one of the most important tools for chemical structural analysis. Magnet nuclei (e.g. ^{1}H, ^{13}C, ^{19}F, etc.) in a molecule experience different local magnetic fields, due, for example, to the varying electron densities around a nucleus. Each nucleus is usually in a unique magnetic environment and as such has a slightly different resonance frequency.

However, apart from structural elucidation of molecules, the NMR technique can also be used for monitoring the changes that occur as a result of changing media polarity. For example if the polarisation within a molecule changes, as a result of different interactions between it and its surroundings, then the electron densities around such nuclei will also change along with the resonant frequencies. Hence, if electron density changes are monitored by the NMR technique as a function of changing solvent polarity, we have a simple technique to monitor the change in dipole moment, as a function of changing solvent polarity.

In terms of the dipole moments obtained here, the NMR technique is an extremely valuable tool for determining how realistic these values are. Any significant changes in the electron density within the compounds with increasing solvent polarity would be manifested by changes in the NMR spectrum. Such a change in ground state polarisation, with increasing media polarity, has been recently observed in the piperidine substituted DEMI derivative (13) [72] in which the protons nearest the charge centres, i.e. H_a, H_b and H_c, all experience significant shifts in their ^{1}H NMR spectra when obtained in increasingly polar solvents.

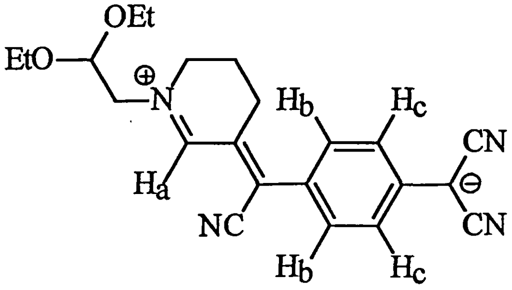

(13)

In this study, only the fluorinated adducts were investigated by NMR. The NMR active ^{19}F nucleus[73] was chosen to monitor any subtle changes in the electron density that might occur with increasing polarity. The weak NMR signal generated by such compounds meant that reasonably good ^{1}H NMR spectra were difficult to obtain. In contrast the ^{19}F spectra obtained for such adducts were of excellent quality (Figure 4.13).

Because the fluorine atoms are situated in a region where the most profound structural changes occur, - the acceptor ring system - they will experience the largest changes in shielding due to shifting π electron density (Figure 4.14).

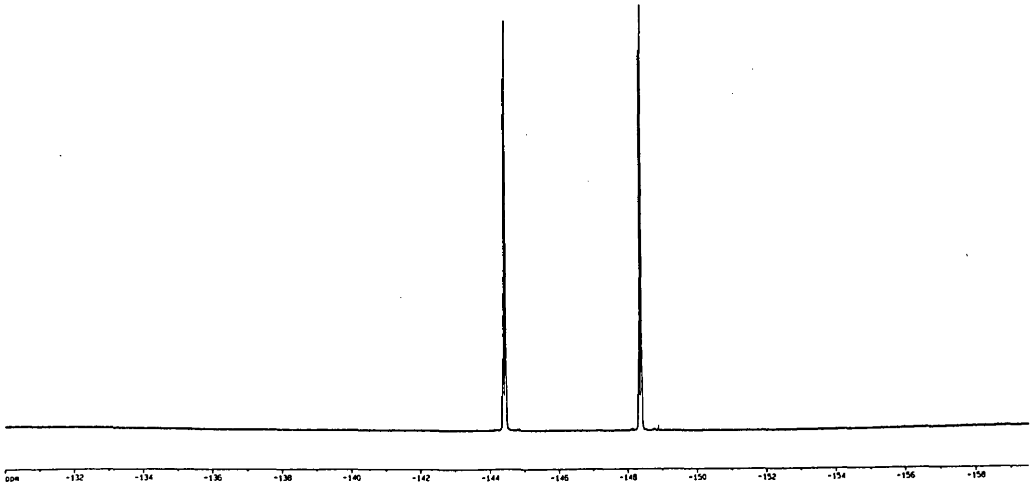

Figure 4.13 ^{19}F NMR Spectra of the $CH_3(2)P3CNQF_4$ Adduct.

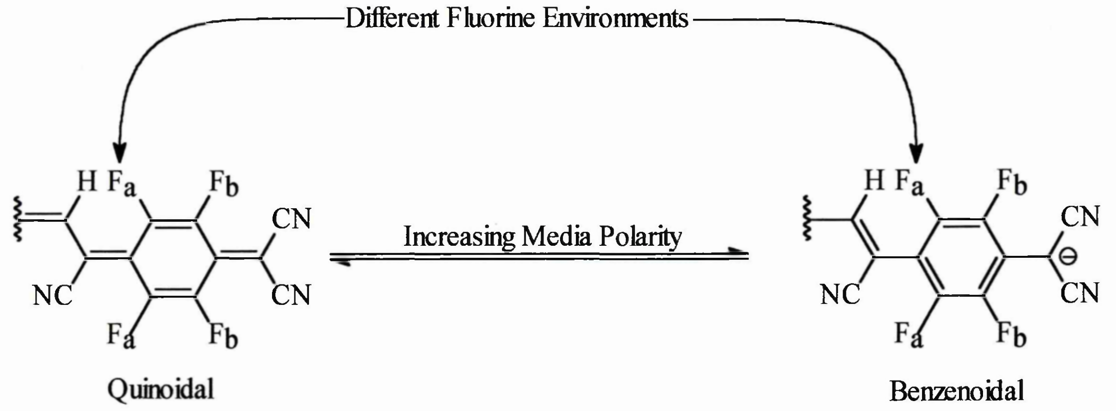
Different Fluorine Environments
H Fa
Fb
CN
NC
CN
Fa
Fb
Increasing Media Polarity
Quinoidal
H Fa
Fb
CN
NC
CN
Fa
Fb
Benzenoidal

Figure 4.14 Polarity Dependent Fluorine Environments.

The ^{19}F NMR spectra for a range of compounds were recorded in deuterated dichloromethane, acetone, nitromethane, acetonitrile and dimethylsulphoxide. However, unlike the DEMI analogues, all of the fluorinated adducts show little change with increasing solvent polarity. This is illustrated in Figure 4.15 by the chemical shifts of the two aromatic/quinoid ring fluorine atoms (F_a and F_b) of the $C_3H_7(2)BT3CNQF_4$ adduct, in progressively more polar solvents.

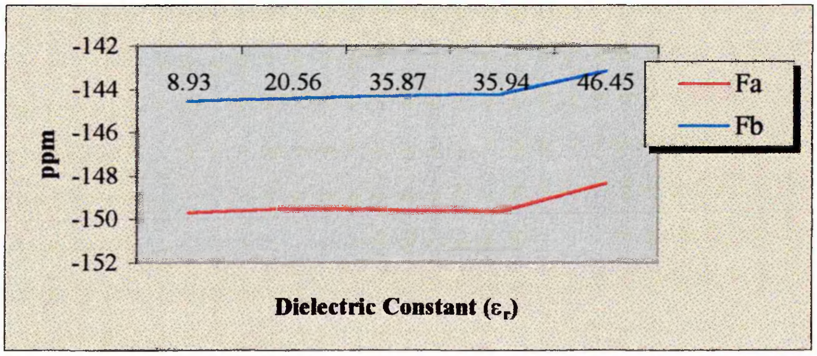

Figure 4.15 ^{19}F NMR Shifts for the $C_3H_7(2)BT3CNQF_4$ Adduct.

In contrast, the adduct's negative solvatochromism (Chapter 3), indicates that, despite the molecules not showing any significant structural alteration, they still undergo a slight increase in polarisation with increasing solvent polarity.

This slight increase in the polarisation with increasing solvent polarity does affect the dipole moment of the material, though not to the same extent as the structurally related DEMI analogues. Therefore it is assumed that dipole moments obtained from the Guggenheim analysis are realistic, and only slightly larger than that of the molecules in the solid state.

4.7 X-Ray Structural Studies.

X-ray crystal structures have been obtained for C_3H_7(2)BT3CNQF_4 (14) and C_4H_9(4)Q3CNQ (15) - these are illustrated in Figures 4.16 and 4.17 respectively, with space groups, unit-cell details, and features of the X-ray analysis in Table 4.4. The three dimensional C_3H_7(2)BT3CNQF_4 structure, which to our knowledge is the only example of a fluorine containing compound of this type, was obtained on a Siemens SMART-CCD diffractometer using the crystallographic facility at Durham University. The atomic co-ordinates, bond lengths, and angles obtained for compound (14) are listed in Tables 4.5, and 4.6, along with the intermolecular hydrogen bond distances and bond angles (Table 4.8).

The C_4H_9(4)Q3CNQ structure, on the other hand, is believed to be the first example obtained for a compound of the much documented R(4)Q3CNQ series,[50,74,75] and was obtained via the Synchrotron instrument at Daresbury. Despite the high final R value the bond lengths and bond angles obtained (Table 4.7) are very similar to those reported by *Bradley et al*[76] and *Ashwell et al*[77] for the structurally related $C_{10}H_{21}$(2)Q3CNQ[76] and CH_3(2)P3CNQ[77] compounds.

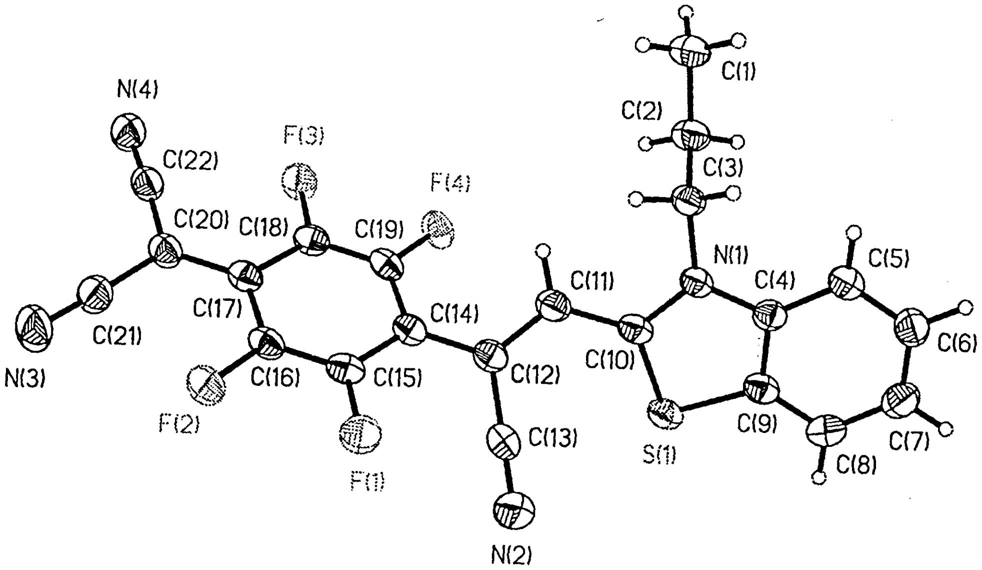
N(4)
C(22)
F(3)
F(4)
C(1)
C(2)
C(3)
C(20)
C(18)
C(19)
N(1)
C(4)
C(5)
C(17)
C(14)
C(11)
C(6)
N(3)
C(21)
C(16)
C(15)
C(12)
C(10)
F(2)
F(1)
C(13)
S(1)
C(9)
C(8)
C(7)
N(2)

Figure 4.16 Molecular Structure of $C_3H_7(2)BT3CNQF_4$ (14) Zwitterion.

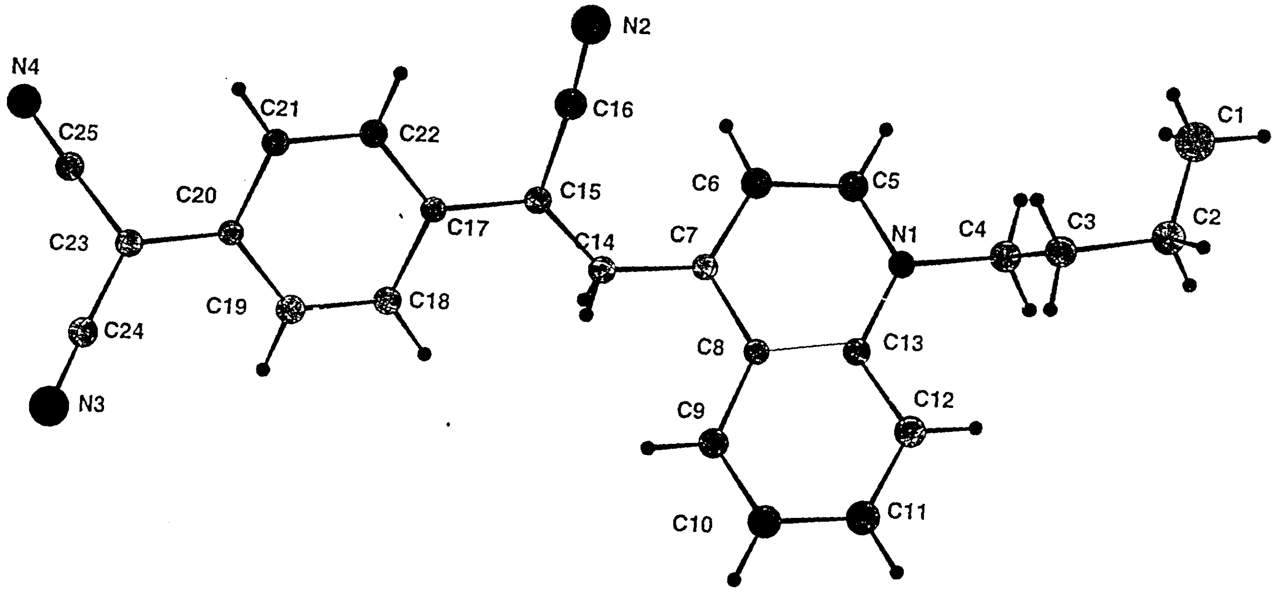
N2
N4
C16
C21
C22
C1
C25
C15
C6
C5
C20
C17
C14
C7
N1
C4
C3
C2
C23
C19
C18
C24
C8
C13
N3
C12
C9
C10
C11

Figure 4.17 Molecular Structure of $C_4H_9(4)Q3CNQ$ (15) Zwitterion.

Table 4.4 Crystal Data Structure Refinement for compounds (14) and (15).

Compound	(14)	(15)
Chemical formula	$C_{22}H_{12}F_4N_4S$	$C_{25}H_{21}N_4$
Chemical formula weight	440.42	377.46
Temperature (K)	150 (2)	160 (2)
Crystal system	Monoclinic	Monoclinic
Space group	$P2_1/c$	$P2_1/c$
Unit cell dimensions	a = 11.2430 (2) Å b = 8.1128 (14) Å c = 20.822 (4) Å β = 101.537 (3) deg	a = 8.7360 (10) Å b = 28.6141 (3) Å c = 7.8456 (10) Å β = 91.402 (10) deg
Volume, Z	1860.80 (6) $Å^3$, 4	1962.98 (4) $Å^3$, 4
Density (calc)	1.572 Mg m^{-3}	1.277 Mg m^{-3}
Radiation type	Mo Kα	-
Wavelength	0.71073 Å	0.68750 Å
No of reflections for cell determination	512	-
θ range for cell determination	13.64 to 22.95 deg	-
Crystal shape	Irregular prism	-
Crystal size	0.45 × 0.25 × 0.13 mm	0.03 × 0.04 × 0.1 mm
Crystal colour	Bright green	Bright green
Diffractometer	Siemens SMART-CCD	-
Absorption coefficient	0.231 mm^{-1}	0.077 mm^{-1}
F (000)	896	796
θ range for data collection	1.85 to 28.28 deg	1.38 to 27.17 deg
Range of h, k, l	-14 < h > 14 -10 < k > 10 -27 < l > 27	-10 < h > 11 -37 < k > 28 -10 < l > 10
Reflections collected	20416	11337
Independent reflections	4609 [R (int) = 0.0245]	4285 [R (int) = 0.0991]
Refinement method	Full matrix least squares on F^2	
Data/ restraints/ parameters	4604 / 0 / 328	2046 / 174 / 264
Goodness of fit on F^2	1.112	2.912
Final R indices [I > 2δ (I)]	R1 = 0.0330 wR2 = 0.0790	R1 = 0.1946 wR2 = 0.4542
R indices (all data)	R1 = 0.0436 wR2 = 0.0883	R1 = 0.2796 wR2 = 0.4974
Extinction coefficient	-	0.007 (4)
Largest diff. Peak and hole	0.317 and –0.294 $Å^{-3}$	1.030 and –1.118 $Å^{-3}$
Data collection	SMART (Siemens, 96)	-
Cell refinement	SMART (Siemens, 96)	-
Data reduction	SAINT (Siemens, 96)	-
Absorption correction	SADABS (Sheldrick, 96)	-
Structure solution	SHELXTL (Siemens, 95)	-

Structure refinement	SHELXTL (Siemens, 95)	-

Table 4.5 Atomic Coordinates (x10^4) and Equivalent Isotropic Parameters for the C_3H_7(2)BT3CNQF_4 Adduct (Å^2 x 10^3).

$$U_{eq} = (1/3)\Sigma_i \Sigma_j U^{ij} a_i^* a_j^* a_i . a_j .$$

	x	y	z	U_{eq}
S1	9671 (1)	4178 (1)	1191 (1)	23 (1)
F1	12919 (1)	6951(1)	3374 (1)	29 (1)
F2	13828 (1)	6800 (1)	4625 (1)	29 (1)
F3	10606 (1)	3264 (1)	4912 (1)	27 (1)
F4	9757 (1)	3307 (1)	3653 (1)	25 (1)
N1	7937 (1)	5748 (1)	1540 (1)	19 (1)
N2	12311 (1)	5737 (2)	1978 (1)	44 (1)
N3	14857 (1)	6081 (2)	6079 (1)	40 (1)
N4	11766 (1)	3527 (2)	6390 (1)	30 (1)
C1	5411 (1)	6418 (2)	2506 (1)	32 (1)
C2	6240 (1)	5443 (2)	2147 (1)	26 (1)
C3	7168 (1)	6593 (2)	1943 (1)	21 (1)
C4	7568 (1)	5564 (2)	861 (1)	20 (1)
C5	6506 (1)	6168 (2)	467 (1)	24 (1)
C6	6340 (1)	5878 (2)	-199 (1)	26 (1)
C7	7191(1)	4985 (2)	-472 (1)	28 (1)
C8	8243 (1)	4392 (2)	-83 (1)	26 (1)
C9	8430 (1)	4707 (2)	590 (1)	22 (1)
C10	9032 (1)	5103 (2)	1782 (1)	20 (1)
C11	9571 (1)	5128 (2)	2474 (1)	23 (1)
C12	10780 (1)	5243 (2)	2737 (1)	21 (1)
C13	11637 (1)	5517 (2)	2312 (1)	26 (1)
C14	11283 (1)	5147 (2)	3438 (1)	20 (1)
C15	12354 (1)	5970 (2)	3738 (1)	21 (1)
C16	12821 (1)	5908 (2)	4395 (1)	21 (1)
C17	12280 (1)	5014 (2)	4846 (1)	20 (1)
C18	11203 (1)	4196 (2)	4540 (1)	21 (1)
C19	10741 (1)	4248 (2)	3882 (1)	20 (1)
C20	12771 (1)	4941 (2)	5529 (1)	22 (1)
C21	13925 (1)	5600 (2)	5816 (1)	27 (1)
C22	12184 (1)	4141 (2)	5988 (1)	23 (1)
H11	4950 (20)	7213 (29)	2215 (11)	52 (6)
H12	5889 (19)	6993 (27)	2869 (10)	44 (6)
H13	4880 (19)	5698 (26)	2677 (10)	43 (5)
H21	5772 (17)	4937 (23)	1761 (9)	31 (5)
H22	6679 (17)	4540 (24)	2432 (9)	35 (5)

H31	6766 (15)	7499 (22)	1682 (8)	23 (4)
H32	7707 (15)	7014 (21)	2329 (8)	23 (4)
H51	5940 (16)	6760 (22)	640 (8)	27 (4)
H61	5633 (17)	6259 (23)	-484 (9)	31 (5)
H71	7067 (16)	4808 (22)	-935 (9)	31 (5)
H81	8825 (16)	3796 (22)	-254 (9)	27 (4)
H111	9043 (17)	5133 (23)	2766 (9)	32 (5)

Table 4.6 Bond Lengths (Å) and Angles (deg) for Compound (14).

S(1)-C(10)	1.7174 (14)	C(5)-C(6)	1.381 (2)
S(1)-C(9)	1.732 (2)	C(5)-H(51)	0.93 (2)
F(1)-C(15)	1.344 (2)	C(6)-C(7)	1.407 (2)
F(2)-C(16)	1.349 (2)	C(6)-H(61)	0.94 (2)
F(3)-C(18)	1.352 (2)	C(7)-C(8)	1.378 (2)
F(4)-C(19)	1.351 (2)	C(7)-H(71)	0.96 (2)
N(1)-C(10)	1.340 (2)	C(8)-C(9)	1.399 (2)
N(1)-C(4)	1.399 (2)	C(8)-H(81)	0.94 (2)
N(1)-C(3)	1.488 (2)	C(10)-C(11)	1.447 (2)
N(2)-C(13)	1.140 (2)	C(11)-C(12)	1.364 (2)
N(3)-C(21)	1.149 (2)	C(11)-H(111)	0.93 (2)
N(4)-C(22)	1.151 (2)	C(12)-C(13)	1.450 (2)
C(1)-C(2)	1.527 (2)	C(12)-C(14)	1.457 (2)
C(1)-H(11)	0.96 (2)	C(14)-C(19)	1.407 (2)
C(1)-H(12)	0.96 (2)	C(14)-C(15)	1.409 (2)
C(1)-H(13)	0.95 (2)	C(15)-C(16)	1.365 (2)
C(2)-C(3)	1.522 (2)	C(16)-C(17)	1.415 (2)
C(2)-H(21)	0.96 (2)	C(17)-C(18)	1.416 (2)
C(2)-H(22)	1.01 (2)	C(17)-C(20)	1.421 (2)
C(3)-H(31)	0.97 (2)	C(18)-C(19)	1.366 (2)
C(3)-H(32)	0.97 (2)	C(20)-C(21)	1.421 (2)
C(4)-C(5)	1.396 (2)	C(20)-C(22)	1.422 (2)
C(4)-C(9)	1.400 (2)		

C(10)-S(1)-C(9)	91.00 (7)	C(9)-C(8)-H(81)	119.8 (11)
C(10)-N(1)-C(4)	113.81 (11)	C(8)-C(9)-C(4)	121.10 (13)
C(10)-N(1)-C(3)	124.15 (11)	C(8)-C(9)-S(1)	128.14 (11)
C(4)-N(1)-C(3)	122.04 (11)	C(4)-C(9)-S(1)	110.76 (10)
C(2)-C(1)-H(11)	110.1 (13)	N(1)-C(10)-C(11)	122.69 (12)
C(2)-C(1)-H(12)	109.8 (12)	N(1)-C(10)-S(1)	112.65 (10)
C(11)-C(1)-H(12)	109 (2)	C(11)-C(10)-S(1)	124.59 (10)
C(2)-C(1)-H(13)	110.8 (12)	C(12)-C(11)-C(10)	125.90 (13)
H(11)-C(1)-H(13)	110 (2)	C(12)-C(11)-H(111)	116.9 (11)
H(12)-C(1)-H(13)	107 (2)	C(10)-C(11)-H(111)	117.1 (11)
C(3)-C(2)-C(1)	109.80 (13)	C(11)-C(12)-C(13)	119.70 (13)

C(3)-C(2)-H(21)	108.6 (11)	C(11)-C(12)-C(14)	123.65 (13)
C(1)-C(2)-H(21)	110.2 (11)	C(13)-C(12)-C(14)	116.63 (12)
C(3)-C(2)-H(22)	109.1 (11)	N(2)-C(13)-C(12)	179.80 (13)
C(1)-C(2)-H(22)	111.4 (11)	C(19)-C(14)-C(15)	113.43 (12)
H(21)-C(2)-H(22)	108 (2)	C(19)-C(14)-C(12)	123.59 (12)
N(1)-C(3)-C(2)	112.53 (12)	C(15)-C(14)-C(12)	122.98 (12)
N(1)-C(3)-H(31)	107.0 (10)	F(1)-C(15)-C(16)	117.21 (12)
C(2)-C(3)-H(31)	110.7 (10)	F(1)-C(15)-C(14)	119.27 (12)
N(1)-C(3)-H(32)	107.1 (10)	C(16)-C(15)-C(14)	123.39 (12)
C(2)-C(3)-H(32)	109.5 (10)	F(2)-C(16)-C(15)	117.53 (12)
H(31)-C(3)-H(32)	110.0 (14)	F(2)-C(6)-C(17)	118.84 (12)
C(5)-C(4)-N(1)	127.10 (12)	C(15)-C(16)-C(17)	123.58 (12)
C(5)-C(4)-C(9)	121.13 (13)	C(6)-C(17)-C(18)	112.64 (12)
N(1)-C(4)-C(9)	111.75 (12)	C(16)-C(17)-C(20)	123.55 (12)
C(6)-C(5)-C(4)	117.31 (13)	C(18)-C(17)-C(20)	123.81 (12)
C(6)-C(5)-H(51)	121.0 (11)	F(3)-C(18)-C(19)	117.40 (12)
C(4)-C(5)-H(51)	121.7 (11)	F(3)-C(18)-C(17)	118.84 (12)
C(5)-C(6)-C(7)	121.77 (14)	C(19)-C(18)-C(17)	123.73 (12)
C(5)-C(6)-H(61)	120.2 (11)	F(4)-C(19)-C(18)	117.13 (12)
C(7)-C(6)-H(61)	118.0 (11)	F(4)-C(19)-C(14)	119.53 (12)
C(8)-C(7)-C(6)	121.02 (14)	C(18)-C(19)-C(14)	123.23 (12)
C(8)-C(7)-H(71)	118.3 (11)	C(17)-C(20)-C(21)	123.02 (12)
C(6)-C(7)-H(71)	120.6 (11)	C(17)-C(20)-C(22)	113.36 (12)
C(7)-C(8)-C(9)	117.65 (13)	N(3)-C(21)-C(20)	176.1 (2)
C(7)-C(8)-H(81)	122.6 (11)	N(4)-C(22)-C(20)	175.8 (2)

Table 4.7 Bond Lengths (Å) and Angles (deg) for Compound (15) .

N(1)-C(5)	1.311 (9)	N(1)-C(13)	1.404 (10)
N(1)-C(4)	1.478 (10)	N(2)-C(16)	1.166 (11)
N(3)-C(24)	1.160 (11)	N(4)-C(25)	1.141 (9)
C(1)-C(2)	1.510 (12)	C(2)-C(3)	1.524 (11)
C(3)-C(4)	1.526 (11)	C(5)-C(6)	1.377 (11)
C(7)-C(14)	1.458 (10)	C(8)-C(13)	1.419 (10)
C(8)-C(9)	1.444 (11)	C(9)-C(10)	1.357 (11)
C(10)-C(11)	1.398 (12)	C(11)-C(12)	1.403 (12)
C(12)-C(13)	1.378 (10)	C(14)-C(15)	1.356 (10)
C(15)-C(16)	1.448 (12)	C(15)-C(17)	1.457 (11)
C(17)-C(22)	1.378 (10)	C(17)-C(18)	1.442 (11)
C(18)-C(19)	1.366 (11)	C(19)-C(20)	1.391 (10)
C(20)-C(21)	1.421 (11)	C(20)-C(23)	1.431 (11)
C(21)-C(22)	1.377 (11)	C(23)-C(25)	1.409 (10)
C(23)-C(24)	1.424 (12)		

C(5)-N(1)-C(13)	120.7 (7)	C(5)-N(1)-C(4)	117.8 (7)
C(13)-N(1)-C(4)	121.5 (6)	C(1)-C(2)-C(3)	113.6 (7)
C(2)-C(3)-C(4)	109.9 (6)	N(1)-C(4)-C(3)	114.4 (6)
N(1)-C(5)-C(6)	123.6 (8)	C(5)-C(6)-C(7)	119.9 (7)
C(6)-C(7)-C(8)	117.0 (7)	C(6)-C(7)-C(14)	123.0 (7)
C(8)-C(7)-C(14)	120.0 (7)	C(13)-C(8)-C(7)	121.2 (7)
C(13)-C(8)-C(9)	115.5 (6)	C(7)-C(8)-C(9)	123.3 (7)
C(10)-C(9)-C(8)	121.5 (8)	C(9)-C(10)-C(11)	120.8 (8)
C(10)-C(11)-C(12)	120.4 (8)	C(13)-C(12)-C(11)	118.4 (8)
C(12)-C(13)-N(1)	119.0 (7)	C(12)-C(13)-C(8)	123.5 (7)
N(1)-C(13)-C(8)	117.5 (6)	C(15)-C(14)-C(7)	130.6 (8)
C(14)-C(15)-C(16)	120.0 (7)	C(14)-C(15)-C(17)	126.9 (7)
C(16)-C(15)-C(17)	113.1 (6)	N(2)-C(16)-C(15)	175.2 (9)
C(22)-C(17)-C(18)	115.8 (7)	C(22)-C(17)-C(15)	122.9 (7)
C(18)-C(17)-C(15)	121.3 (6)	C(19)-C(18)-C(17)	121.1 (7)
C(18)-C(19)-C(20)	122.4 (8)	C(19)-C(20)-C(21)	116.8 (7)
C(19)-C(20)-C(23)	122.4 (7)	C(21)-C(20)-C(23)	120.8 (6)
C(22)-C(21)-C(20)	120.6 (7)	C(21)-C(22)-C(17)	123.3 (8)
C(25)-C(23)-C(24)	114.6 (7)	C(25)-C(23)-C(20)	123.1 (7)
C(24)-C(23)-C(20)	122.3 (7)	N(3)-C(24)-C(23)	174.8 (9)
N(4)-C(25)-C(23)	176.8 (9)		

Table 4.8 Intermolecular Hydrogen Bond Distances (Å) and Angles (deg) for Compound (14).

H(71)...N(2)	2.452 (19)	C(7)...N(2)	3.347 (2)
H(31)...N(3)	2.536 (17)	C(3)...N(3)	3.417 (2)
H(51)...N(3)	2.414 (18)	C(5)...N(3)	3.315 (2)
H(32)...N(4)	2.650 (17)	C(3)...N(4)	3.440 (2)
H(111)...N(4)	2.394 (19)	C(11)...N(4)	3.235 (2)

C(7)-H(71)...N(2)	155.4 (1.5)	C(3)-H(32)...N(4)	139.1 (1.3)
C(3)-H(31)...N(3)	151.0 (1.3)	C(11)-H(111)..N(4)	150.0 (1.6)
C(5)-H(51)...N(3)	164.0 (1.5)		

Both (14) and (15) show a charge-separated ground state. For instance, in C_3H_7(2)BT3CNQF_4 (Figure 4.16), the bond length between C(11) and C(12) illustrates a carbon-carbon double bond, characteristic of the π-electron bridge between the donor and acceptor subunits. The extended C(17)-C(20) and C(12)-C(14) bonds and benzenoidal nature of the acceptor ring in which the C(18)-C(19) and C(15)-C(16) bonds show bond lengths which are somewhere in between that of a carbon-carbon double bond (~1.32 Å)[78] and that of a fully delocalised aromatic system (~1.39 Å)[78] is also indicative of a zwitterionic ground state and this has been further substantiated by the high solution state dipole moment and large negative solvatochromism in the compound (Section 3.4.4 Chapter 3).

In the TCNQ moiety the negative charge, is essentially spread between the two cyano groups C(21)≡N(3) and C(22)≡N(4) (Figure 4.16), as seen by the general lengthening of these bonds (1.149 Å and 1.151 Å respectively) when compared with the corresponding C≡N distance observed in normal cyano groups (~1.140 Å).[78] The consistent shortening of the C(20)-C(21) and C(20)-C(22) bonds, also supports the view that the negative charge is delocalised over the whole of the dicyanomethanide group.

This retention of some quinoidal character is assumed to be due to the presence of the residual cyano group in the molecule, i.e. not part of the dicyanomethanide moiety. As similar characteristics have been found in $C_{10}H_{21}$(2)Q3CNQ,[76] which is also predominantly charge-separated in the ground state. Additionally as can be clearly observed in Table 4.7 (Figure 4.17), the C_4H_9(4)Q3CNQ adduct also shows a degree of quinoidal character in the ground state. Other researchers have shown that species, which do not embody such functionality, have only a relatively small quinoidal contribution to the ground state.[79]

The large solution state dipole moment obtained for $C_3H_7(2)BT3CNQF_4$ indicated that the molecules are much more charge-separated than their unsubstituted TCNQ counterparts. The ^{19}F NMR solvatochromism studies have shown that such fluorinated adducts undergo very little structural alteration in increasingly polar media, implying an extreme resonance form, even in solvents of relatively low polarity. In such a highly charge-separated state the NLO activity of such molecules would be relatively small as the molecule would be extremely bond-alternated. However in the solid state such fluorinated adducts embody some quinoidal character in the ground state and thus bond length alternation (BLA) is not thought to be significant.

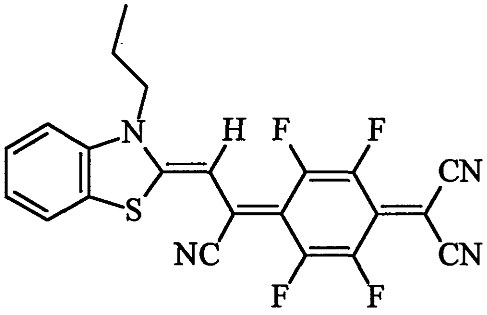

(16) $\mu_{calc} = 25.8$ D

In a purely quinoidal ground state (16) the dipole moment of the $C_3H_7(2)BT3CNQF_4$ adduct, has been estimated to be ~25.8 D, when using commercial molecular modelling software[80] and in excess of 46 Debyes (Table 4.3) in solution. However, in both solution and solid states, such materials are highly charge-separated. Therefore, because of the large difference between the ground and excited state dipole, a large NLO response (Equation 4.3) is expected.

4.7.1 Crystal Packing Effects.

Both adducts were found to exhibit the same centrosymmetric space group, $P2_1/c$ as other TCNQ-based zwitterions, e.g. $CH_3(2)P3CNQ$.[77] This centrosymmetry derives first from the near planarity of the molecules, which encourages plane-to-plane van der Waals contacts, and second from the compounds highly dipolar character, which further favours anti-parallel alignment in which the two molecules pack in a head-to-tail manner. Such an anti parallel alignment can clearly be seen in Figures 4.18a, b and c with the van der Waals contacts obtained for the $C_3H_7(2)BT3CNQF_4$ adduct. The intermolecular contacts between, C(7)-H(71)...N(2), N(2)...H(71)-C(7) [Figure 4.18a] and C(5)-H(51)...N(3), C(3)-H(31)...N(3) [Figure 4.18b] and C(11)-H(111)...N(4), C(3)-H(32)...N(4), N(4)...H(111)-C(11), N(4)...H(32)-C(3) [Figure 4.18c], which are all less than the sum of the van der Waals radii,[81] indicate that the molecules are forming centrosymmetric dimer pairs. This is hardly surprising considering the very large solution state dipole moments obtained for this zwitterion (~46D). The H(32)...N(4) contact is of particular interest, as the intermolecular distance is the longest of all of the inter-molecular contacts, at 2.650 Å, and the angle C(3)-H(32)...N(4) (139.1^0) is a long way from the expected 180^0.

Hence as a consequence, the whole pattern generated by the tabulated hydrogen bonds means that in solid state the $C_3H_7(2)BT3CNQF_4$ adduct forms tridimensional network (Figures 4.19 and 4.20) which is considerable different to the packing observed in other documented zwitterions.[76,77]

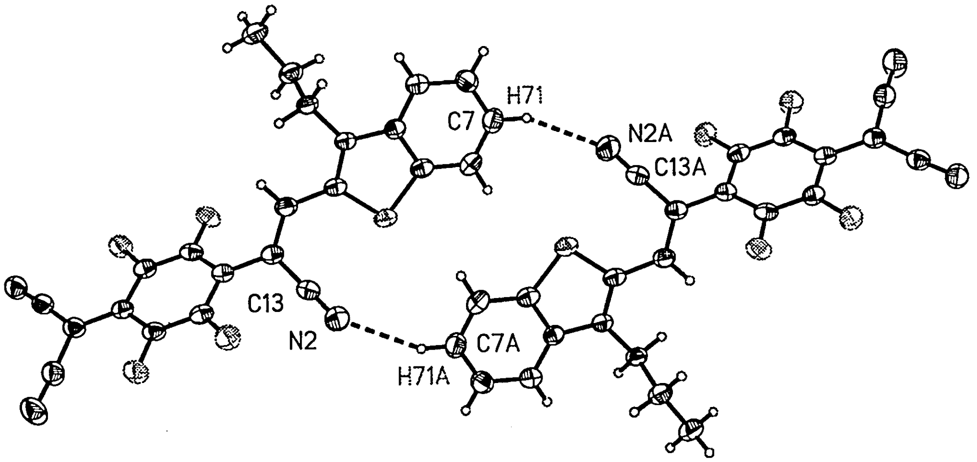
H71
C7
N2A
C13A
C13
N2
C7A
H71A

Figure 4.18a Intermolecular Contacts Shown by the C_3H_7(2)BT3CNQF$_4$ Adduct.

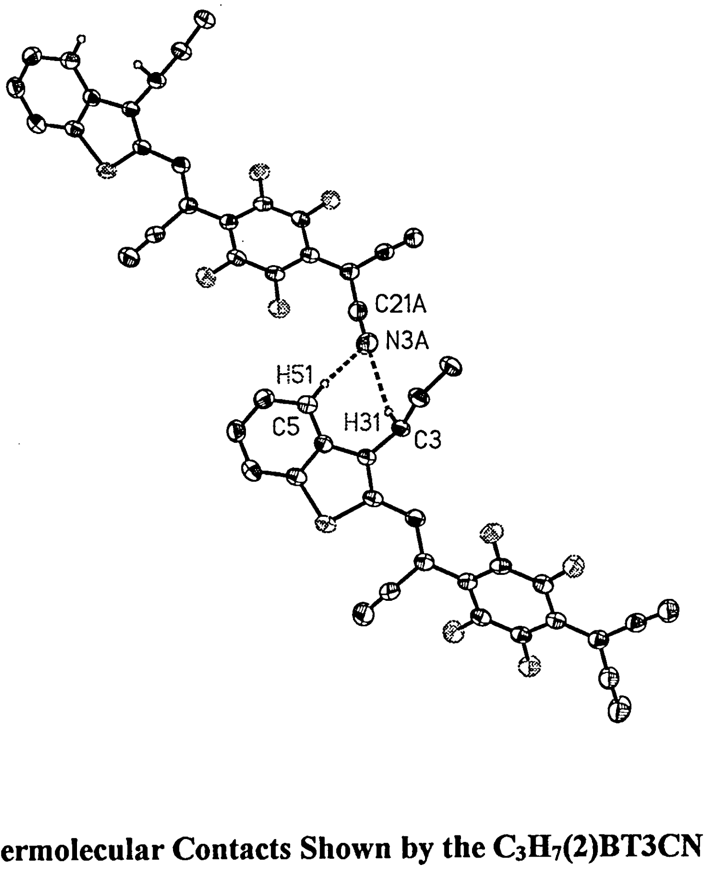
C21A
N3A
H51
C5
H31
C3

Figure 4.18b Intermolecular Contacts Shown by the C_3H_7(2)BT3CNQF$_4$ Adduct.

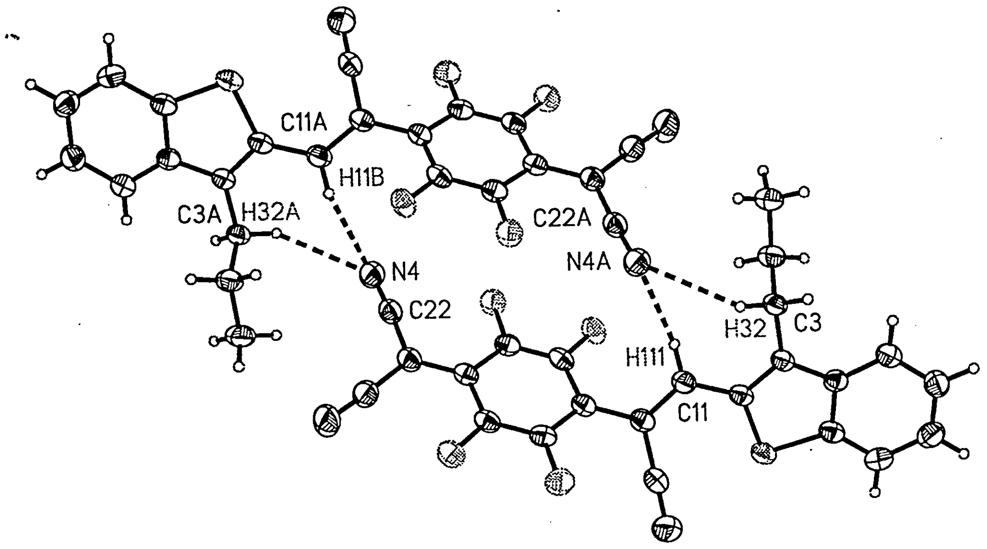
C11A
H11B
C3A
H32A
C22A
N4A
N4
C22
H111
H32
C3
C11

Figure 4.18c Intermolecular Contacts Shown by the C_3H_7(2)BT3CNQF_4 Adduct.

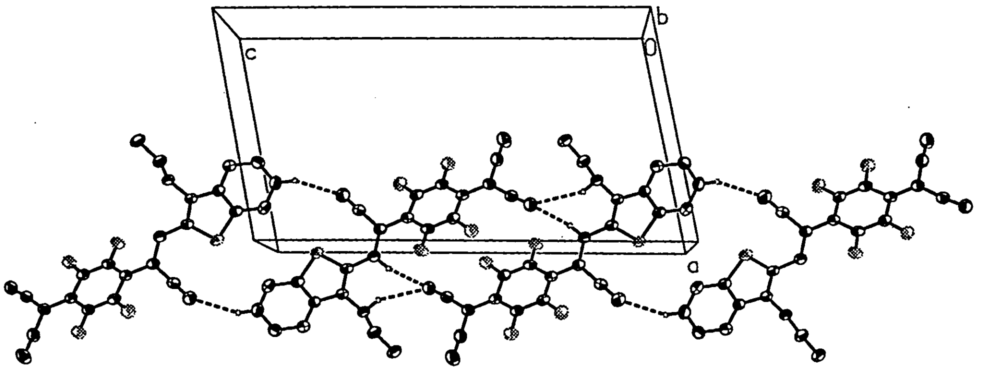

Figure 4.19 C_3H_7(2)BT3CNQF_4 Layers Along the AC Plane.

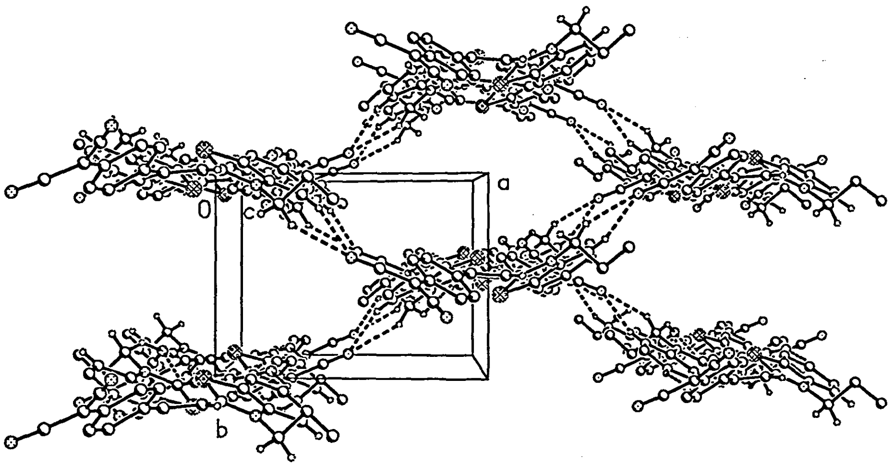

Figure 4.20 The Tridimensional Network Formed by C_3H_7(2)BT3CNQF_4.

For the C_4H_9(4)Q3CNQ zwitterion, only the crystal lattice type (monoclinic) and space group ($P2_1/c$) were confirmed, as the twinned nature of the C_4H_9(4)Q3CNQ crystals meant that very little accurate structural information could be obtained. However, despite this, it appears that, like the C_3H_7(2)BT3CNQF_4 adduct, this zwitterion is also in a centrosymmetric environment, so that second-order nonlinear optical activity for both will be essentially zero. This has been illustrated by Kurtz powder measurements[41] conducted upon the materials at Durham University.[82] The diquinolinium adducts mentioned in Chapter two, e.g. *m*-C_8H_8(4)DQ6CNQ, also exhibited zero SHG activity in the solid state, thus indicating a centrosymmetric crystal. This is again thought to be a consequence of an anti parallel alignment between neighbouring molecules in which the overlap gives zero net dipole moment for the two nearest neighbours.

4.8 Chemical Stability of Adducts.

Materials for electro-optical devices need not only large bulk susceptibilities and optical transparency in the visible region,[16] but chemical and thermal stability as well. For example the strongly solvatochromic merocyanine dyes, due to their charge asymmetry, possess large molecular hyperpolarizabilities (β) e.g. *Brookers* dye 4-[(1-methyl-4(1H)-pyridinylidene)-ethylidene]2,5-cyclohexadien-1-one (Figure 4.21) has been shown to have a high first hyperpolarisability value of 4000×10^{-40} m^4V^{-1} when measured in DMSO at 1.89μm.[16]

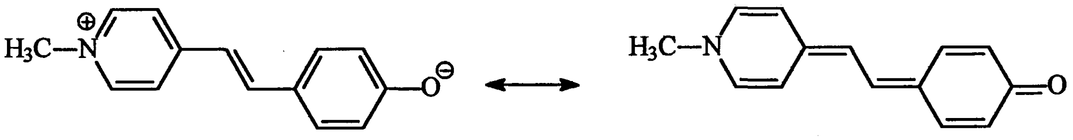

Figure 4.21 High First Hyperpolarisability (β) Merocyanine Dye.

Nevertheless they have found relatively few practical applications due to their chemical instability. In the charge separated form merocyanine dyes are extremely susceptible to protonation which removes their optical nonlinearity[33] by reducing the degree of polarisation that occurs during the irradiation of the material.

The nonlinear and linear optical properties exhibited by the extensively studied DEMI family[47,62,69,72] (Figure 4.22) are very favourable but again there are significant difficulties, which inhibit their use.

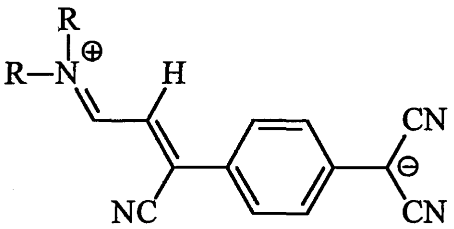

Figure 4.22 DEMI Class of NLO Materials.

Apart from their extreme insolubility[72] in most common solvents, which makes them difficult to work with, their planarity[72,79] and high dipole moments[72,69] means that they readily form aggregates which has consequences in terms of maintaining the non-centric structure. However, it is the compounds' strong optical transition, combined with the presence of ethylenic bonds that poses the most significant problem. This can sensitise the formation of singlet oxygen ($^1O_2$), which due to its reactive nature with olefins and aromatic compounds,[83] can lead to the photo-oxidation of the material in the presence of direct light (Figure 4.23).

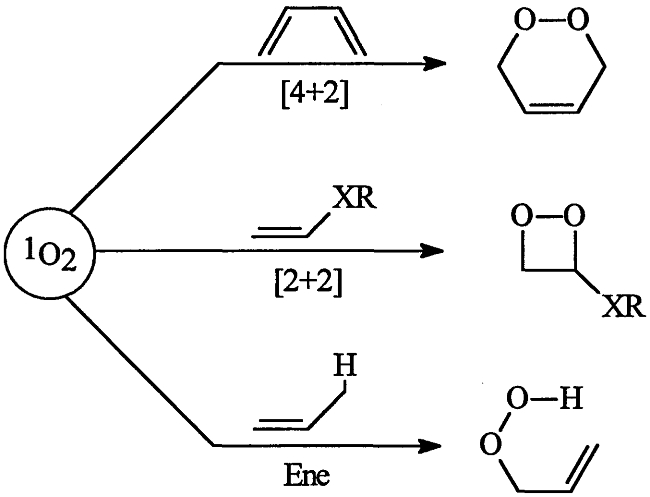

Figure 4.23 Reactions of Singlet Oxygen.

Confirmation of this was achieved using simple Ultra-violet/Visible (UV/Vis) spectroscopy experiments,[82] with oxygenated and deoxygenated samples showing different results after being irradiated over several hours. Deoxygenated samples showed negligible change in position and intensity of their charge-transfer absorption band with time. In contrast the oxygenated samples showed a complete loss of this absorption band as a result of photo-oxidation, confirming that oxygen plays a role in the degradation of such materials. The zwitterionic adducts showed a similar light-dependent behaviour when exposed to sunlight for several days.

4.8.1 Photo-Oxidation Experimental.

The adducts stability to photo-oxidation has been investigated using UV/Visible spectroscopy. For each adduct a series of three solutions were prepared, typically containing a concentration of adduct of 10^{-5}-10^{-6} mol dm^{-3} in anhydrous acetonitrile (Aldrich-Sigma Co.). Solution 1 comprised the adduct dissolved in anhydrous acetonitrile (oxygenated sample), whereas solution 2 comprised the adduct dissolved in anhydrous acetonitrile along with a small amount - typically 1-2mg - of nickel(II) dibutyldithiocarbamate (oxygenated sample + radical scavenger). Solution 3 was the adduct dissolved in anhydrous acetonitrile which had been deoxygenated by repeated cooling with liquid nitrogen under a nitrogen atmosphere (deoxygenated sample).

Once prepared, the solutions were transferred to three, 1cm path length, quartz cuvettes and sealed. The absorption spectrum of each solution was recorded from 210-900nm using a double beam UV/Visible ATI Unican V2 spectrophotometer, and reference. The sealed cuvettes were placed into the darkened interior of a UV lamp viewing cabinet (UVP inc., model CC-10), encased in aluminium foil and placed out of direct sunlight and irradiated using a short wavelength (254nm) UV lamp (UVP inc., model UVGL-58). The UV/Vis spectra were then measured at various time intervals, typically every hour, and the change (if any) in maximum absorption intensity of the longest wavelength charge-transfer absorption band measured.

4.8.2 Experimental Results.

All of the adducts studied suffer from photo-oxidation as a result singlet oxygen formation (Figure 4.24). The irradiation of an acetonitrile solution of C_3H_7(2)BT-3CNQF$_4$ resulted in the loss of the charge-transfer process. As with the DEMI compounds,[72,82] the evidence supports the assumption that chemical alteration of the molecule resulting in loss of the charge-transfer process, is in fact singlet oxygen based photo-oxidation.

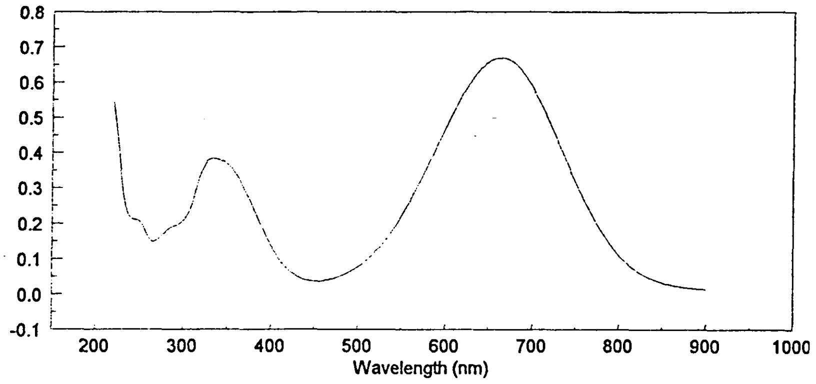

Figure 4.24a C_3H_7(2)BT3CNQF$_4$ in Acetonitrile Before Irradiation.

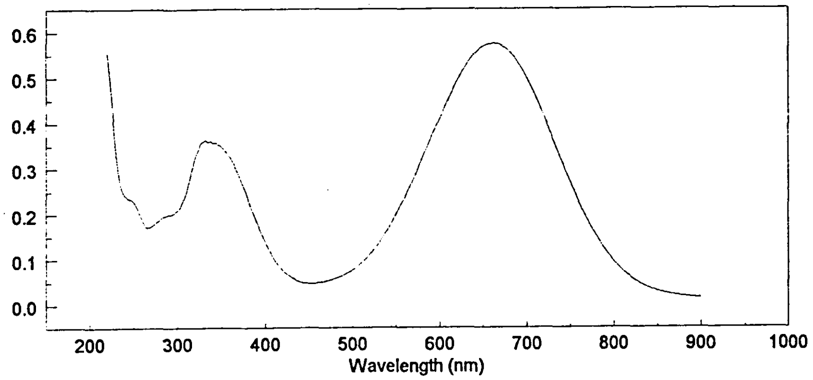

Figure 4.24b C_3H_7(2)BT3CNQF$_4$ in Acetonitrile After Four Hours Irradiation.

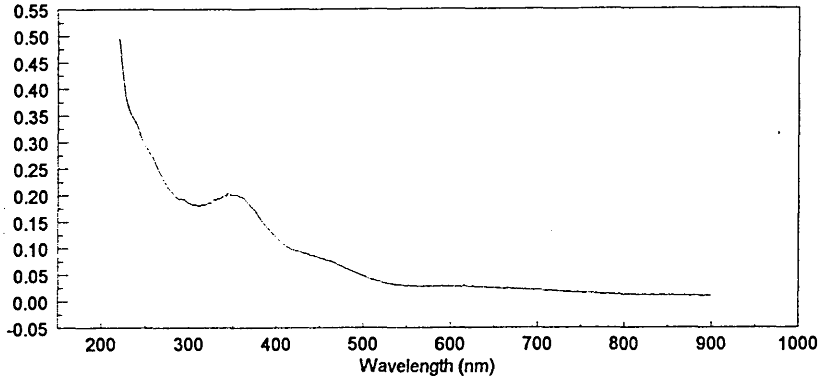

Figure 4.24c C_3H_7(2)BT3CNQF$_4$ in Acetonitrile After Eight Hours Irradiation.

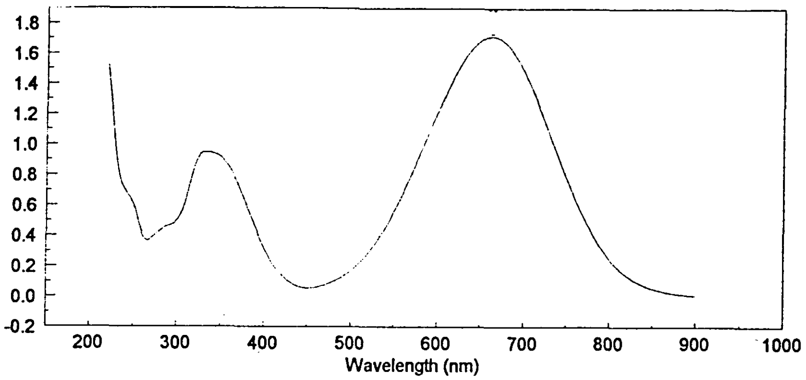

Figure 4.25a $C_3H_7(2)BT3CNQF_4$ in Deoxygenated Acetonitrile Before Irradiation.

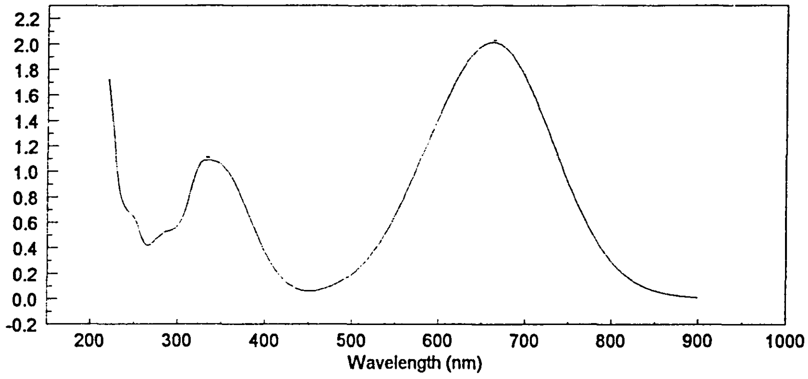

Figure 4.25b $C_3H_7(2)BT3CNQF_4$ in Deoxygenated Acetonitrile After Eight Hours Irradiation.

When the solvent is deoxygenated, irradiation results in no change in the charge-transfer absorption band (Figure 4.25). The stability to photo-oxidation was compared for $TCNQF_4$-based and TCNQ-based adducts. The results for all were essentially the same as described above, though the rate at which the photo-oxidation occurred did vary, with degradation in the fluorinated adducts being much more rapid than in the TCNQ-based adducts. Table 4.9 lists the irradiation times required to completely degrade the charge-transfer absorption bands, along with the position, λ_{CT}, of the charge-transfer absorption band of each adduct in acetonitrile.

Zwitterion	Irradiation Time (Hours)	λ_{CT} (CH_3CN)
C_3H_7(2)BT3CNQF$_4$	8.0	664 nm
$C_{10}H_{21}$(4)Q3CNQF$_4$	8.5	566 nm
$C_{10}H_{21}$(2)Q3CNQF$_4$	8.5	568 nm
$C_{10}H_{21}$(4)Q3CNQ	11.0	708 nm
$C_{10}H_{21}$(2)Q3CNQ	11.0	702 nm

Table 4.9 Irradiation Times.

The increased rate at which the fluorinated adducts are photo-oxidised is thought to be a consequence of the fluorinated compounds having much greater solution dipole moments (Table 4.3). This increased polarisation, along with the stronger optical transition possessed by the fluorinated compounds relative to their non-fluorinated counterparts, means that the former are able to sensitise singlet oxygen formation more easily.[83] However no clear indication as to the type of pathway the photo-oxidation takes has been established. The number of products which can be formed as a result of reaction between the adduct and singlet oxygen is extensive and more than one product may be formed, as is illustrated in Figure 4.26

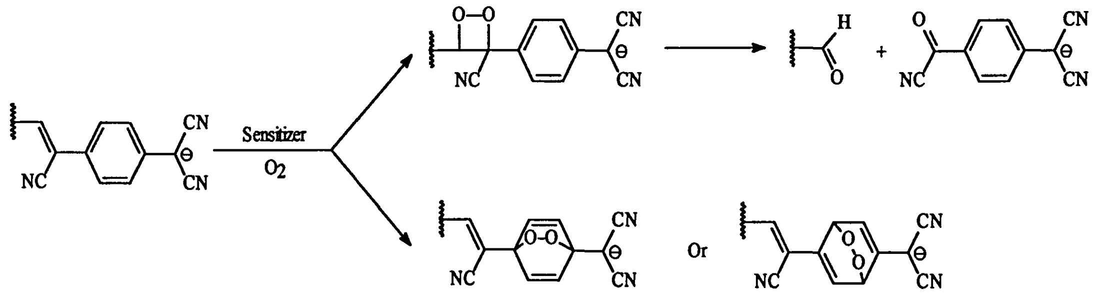

Figure 4.26 Possible Oxyfunctionalised Products from the Photo-Oxidation Process.

The photo-oxidation reaction did however give some indication as to type of mechanism that the reaction follows. When a radical scavenger, such as nickel (II) dibutyldithiocarbamate, was added, a similar response to that for the deoxygenated samples occurred. This is illustrated in Figure 4.27 and indicates that the photo-oxidation process is most likely occurring via a free radical mechanism. In the absence of the radical scavenger the irradiation of the oxygenated sample results in photo-oxidation.

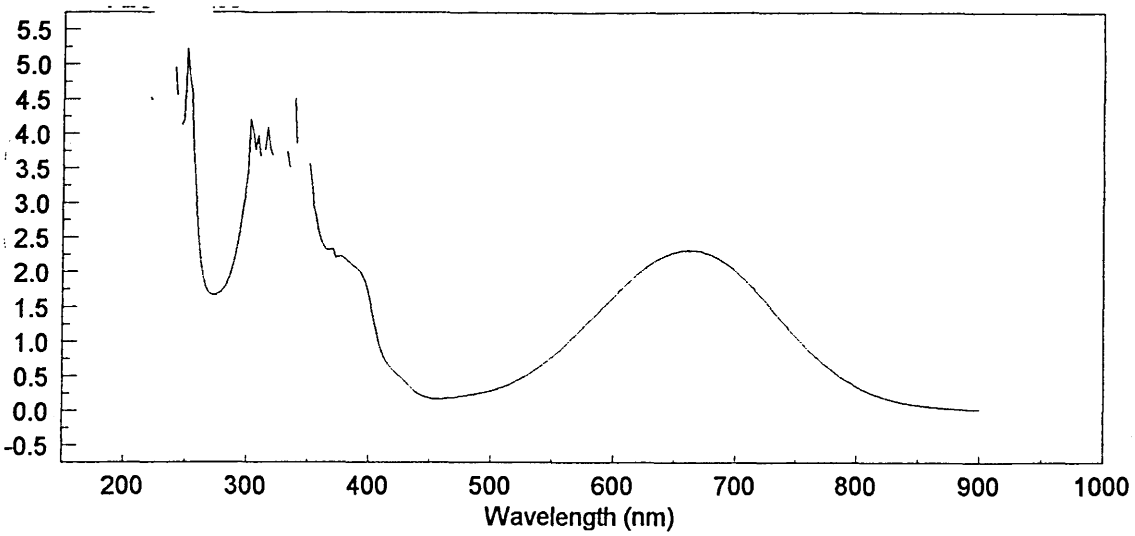

Figure 4.27a $C_3H_7(2)BT3CNQF_4$ and Nickel(II)Dibutyldithiocarbamate in Acetonitrile Before Irradiation.

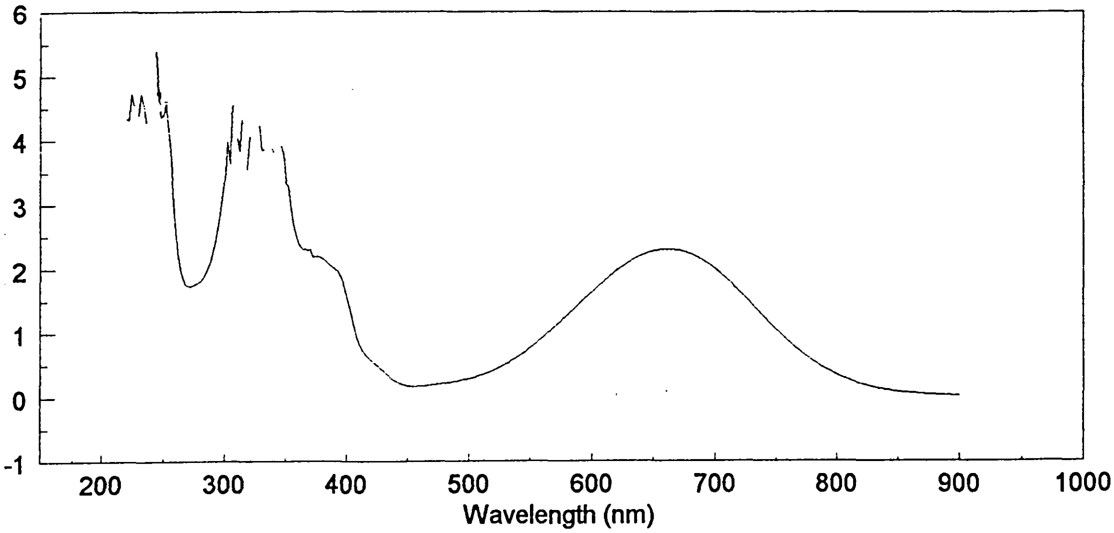

Figure 4.27b $C_3H_7(2)BT3CNQF_4$ and Nickel(II)Dibutyldithiocarbamate in Acetonitrile After Eight Hours Irradiation.

In conclusion, the zwitterionic adducts, like the structurally related DEMI compounds,[72,82] suffer from photolytic instabilities. Along with their limited solubilities this may inhibit their use in nonlinear optical devices.

4.9 References.

1. T. H. Maiman, *Nature*, 1960, **187**, 493.
2. K. Clays and A. Persoons, *Phys. Rev. Lett.*, 1982, **66**, 2980.
3. R. W. Boyd, *Nonlinear Optics*; Academic Press: New York, 1992.
4. Y. R. Shen, *The Principles of Nonlinear Optics*; W. A. Benjamin: New York, 1965.
5. J. G. Bergman and S. K. Kurtz, *Mater. Sci. Eng.*, 1969, **5**, 235.
6. G. R. Meredith, *J. Mater. Educ.*, 1987, **9**, 719.
7. J. Zyss, *J. Mol. Electron.*, 1985, **1**, 25.
8. F. Zernike and J. Midwinter, *Applied Nonlinear Optics*; Wiley: New York, 1973.
9. R. S. Weis and T. K. Gaylord, *Appl. Phys. A.*, 1985, **37**, 191.
10. M. E. Lines and A. M. Glass, *Principles and Applications of Ferroelectrics and Related Materials*; Clarendon: Oxford, 1977.
11. M. B. Klein, G. J. Dunning, G. C. Valley, R. C. Lind and T. R. O'Meara, *Opt. Lett.*, 1986, **11**, 575.
12. A. Yariv, *Optical Electronics*; 3rd Ed., Holt Rinehart and Winston: London, 1985.
13. R. W. Boyd, *Nonlinear Optics*; Academic Press Inc: London, 1992.
14. (a) J. M. Senior, *Optical Fibre Communications, Principles and Practices;* 2nd Ed., Prentice Hall: London, 1992. (b) M. N. Islam, *Ultrafast Fibre Switching Devices and Systems*; Cambridge Studies in Modern Optics, **12**, Cambridge University Press: Cambridge, 1992.
15. P. N. Prasad and D. J. Williams, *Introduction to Nonlinear Optical Effects in Molecules & Polymers*, Wiley, New York, 1995.

16. D. S. Chemla and J. Zyss, *Nonlinear Optical Properties of Organic Molecules and Crystals*, Academic Press, New York, 1987, Vols 1 and 2.
17. I.-C. Khoo, *Liquid Crystals. Physical Properties and Nonlinear Optical Phenomena*, Wiley, New York, 1995.
18. N. J. Long, *Angew. Chem., Int. Ed. Engl.*, 1995, **34**, 21.
19. A. Yariv, *Quantum Electronics*, Wiley, New York, 1975, 407.
20. A. Yariv, *Quantum Electronics*, Wiley, New York, 1975, 437.
21. P. W. Smith, *Opt. Eng.*, 1980, **4**, 456.
22. A. Yariv, *Quantum Electronics*, Wiley, New York, 1975, 327.
23. J. L. Oudar and D. S. Chemla, *J. Chem. Phys.*, 1977, **66**, 2664.
24. T. Verbiest, S. Houbrechts, M. Kauranen, K. Clays and A. Persoons, *J. Mater. Chem.*, 1997, **7**, 2175.
25. P. R. Thomas, *Personal Communication.*
26. (a) J. Zyss, J. F. Nicoud and M. Coquillay, *J. Chem. Phys.*, 1984, **81**, 4160. (b) R. J. Tweig and K. Jain, *ACS Symposium Series*, 1983, **233**, 57.
27. (a) Y. Wang and D. F. Eaton, *Chem. Phys. Lett.*, 1985, **120**, 441. (b) S. Tomaru, S. Zembutsu, M. Kawachi and M. Kobayashi, *J. Chem. Soc., Chem. Commun.*, 1984, 1207.
28. (a) J. Zyss and G. Berthier, *J. Chem. Phys.*, 1982, **77**, 3635. (b) M.C.Etter and G. M. Frankenbach, *Chem. Mater.*, 1989, **1**, 10.
29. B. F. Levine, C. G. Bethea, C. D. Thurmond, R. T. Lynch and J. L. Bernstein, *J. Appl. Phys.*, 1979, **50**, 2523.
30. N. Okamoto, T. Abe, D. Chen, H. Fujimara and R. Matsushima, *Opt. Commun.*, 1990, **74**, 421.
31. S. R. Marder, J. W. Perry and W. P. Schaefer, *Science*, 1989, **245**, 626.
32. J. Zyss, D. S. Chemla and J. F. Nicoud, *J. Chem. Phys.*, 1981, **74**, 4800.

33. (a) I. R. Girling, P. V. Kolinsky, N. A. Cade, J. D. Earls, and I. R. Peterson, *Opt. Commun.*, 1985, **55**, 289. (b) G. H. Cross, I. R. Peterson, I. R. Girling, N. A. Cade, M. J. Goodwin, N. Carr, R. S. Sethi, R. Marsen, G. W. Gray, D. Lacey, M. Mc Roberts, R. M. Scrowston and K. J. Toyne, *Thin Solid Films*, 1988, **156**, 39.
34. (a) T. J. Marks and M. A. Ratner, *Angew. Chem., Int. Ed. Engl.*, 1995, **34**, 155. (b) O. F. J. Noordman and N. F. van Hulst, *Chem. Phys. Lett.*, 1996, **253**, 145. (c) Y. Karakus, D. Bloor and G. H. Cross, *J. Phys. D: Appl. Phys.*, 1992, **25**, 1014. (d) D. H. Choi, W. M. K. P. Wijekoon, H. M. Kim and P. N. Prasad, *Chem. Mater.*, 1994, **6**, 234.
35. K. D. Singer, J. E. Soln, L. A. King, H. M. Gordon and C. W. Dirk, *J. Opt. Soc. Am. B.*, 1989, **6**, 1339.
36. L. T. Cheng, W. Tam, S. R. Marder, A. E. Stiegman and C. W. Spangler, *J. Phys. Chem.*, 1991, **95**, 10643.
37. L. T. Cheng, W. Tam, S. H. Stevenson, G. R. Meredith and S. R. Marder, *J. Phys. Chem.*, 1991, **95**, 10631.
38. A. E. Stiegman, E. Graham, K. J. Perry, L. R. Khundkard and J. W. Perry, *J. Am. Chem. Soc.*, 1991, **113**, 7565.
39. (a) F. Meyers, S. R. Marder, B. M. Pierce and J. L. Brédas, *J. Am. Chem. Soc.*, 1994, **116**, 10703. (b) S. R. Marder, C. B. Gorman, B. G. Tieman and L.-T. Cheng, *J. Am. Chem. Soc.*, 1993, **115**, 3006. (c) B. G. Tieman, L.-T. Cheng and S. R. Marder, *J. Chem. Soc., Chem. Commun.*, 1993, 735.
40. (a) A. K.-Y. Jen, V. P. Rao, K. Y. Wong and K. J. Drost, *J. Chem. Soc., Chem. Commun.*, 1993, 91. (b) V. P. Rao, A. K-Y. Jen, K. Y. Wong and K. J. Drost, *J. Chem. Soc., Chem. Commun.*, 1993, 1119.
41. J. P. Dougherty and S. K. Kurtz, *J. Appl. Crystallogr.*, 1976, **9**, 145.

42. S. R. Marder in *Inorganic Materials* (Eds.: D. W. Bruce and D. O' Hare), Wiley, Chichester, 1992, 136.

43. J. L. Oudar and H. Le Person, *Opt. Commun.*, 1975, **15**, 258.

44. (a) K. Clays and A. Persoons, *Rev. Sci. Instrum.*, 1992, **63**, 3285. (b) K. Clays and A. Persoons, *Phys. Rev. Lett.*, 1991, **66**, 2980.

45. (a) S. A. Rani, J. Sobhanadri and T. A. P. Rao, *Spectrochim. Acta. Part A.*, 1995, **51**, 2473. (b) C. Runser, A. Fort, M. Barzoukas, C. Combellas, C. Suba, A. Thiébault R. Graff and J. P. Kintzinger, *Chem. Phys.*, 1995, **193**, 309.

46. (a) M. Ravi, D. N. Rao, S. Cohen, I. Agranat and T. P. Radhakrishnan, *J. Mater. Chem.*, 1996, **6**,1119. (b) M. Ravi, D. N. Rao, S. Cohen, I. Agranat and T. P. Radhakrishnan, *Chem. Mater.*, 1997, **9**, 830. (c) M. Ravi, D. N. Rao, S. Cohen, I. Agranat and T. P. Radhakrishnan, *Current Science.*, 1995, **68**, 1119. (d) M. Ravi, S. Cohen, I. Agranat and T. P. Radhakrishnan, *Structural Chemistry.*, 1996, **7**, 225.

47. G. H. Cross, D. Bloor and M. Szablewski, *Nonlinear Opt.*, 1995, **14**, 219.

48. P. Boldt, G. Bourhill, C. Bräuche, Y. Jim, R. Kammler, C. Müller, J. Rase and J. Wichern, *J. Chem. Soc., Chem. Commun.*, 1996, 793.

49. G. J. Ashwell, M. Malhotra, M. R. Bryce and A. M. Grainger, *Synth. Met.*, 1991, **86**, 1117.

50. (a) G. J. Ashwell, E. J. C. Dawnay, A. P. Kuczyñski, M. Szablewski, I. M. Sandy, M. R. Bryce, A. M. Grainger and M. Hasan, *J. Chem. Soc., Faraday. Trans.*, 1990, **86**, 1117. (b) G. J. Ashwell, G. Jefferies, E. J. C. Dawnay, A. P. Kuczyñski, D. E. Lynch, Y. Gongda and D. G. Bucknall, *J. Mater. Chem.*, 1995, **5**, 975.

51. S. K. Kurtz and T. T. Perry, *J. Appl. Phys.*, 1968, **39**, 3798.

52. L. R. Hertler, H. D. Hartzler, D. S. Acker and R. E. Benson, *J. Am. Chem. Soc.*, 1962, **84**, 3387.

53. V. P. Rao, A. K.-Y. Jen, K. Y. Wong and K. J. Drost, *J. Chem. Soc., Chem Commun.*, 1993, 1118.

54. N. Hill, W. E. Vaughan, A. H. Price and M. Davies, *Dielectric Properties and Molecular Behaviour.*, Van Nostrand Reinhold Co. Ltd., London, 1969.

55. B. K. P. Scaife, *Principles of Dielectrics.*, Oxford University Press., 1989.

56. O. C. Van Belle, P. Bordewick and A. Rip., Volume 1; *Dielectrics in Static Fields.*, Elsevier, London, 1993.

57. D. Gray, PhD Thesis, *University of Durham*, 1994.

58. M. Farsari, PhD Thesis, *University of Durham*, 1996.

59. J. A. Riddick, W. B. Bunger and T. K. Sakano, *Organic Solvents., Physical Properties and methods of Purification.*, 4th ed., John Wiley and Son Inc., New York, 1986.

60. E. A. Guggenhiem, *Trans. Farad. Soc.*, 1949, **45**, 714.

61. (a) P. Debye, *Phys. Z.*, 1912, **12**, 97. (b) P. Debye, Collected Papers, *Interscience*, New York, 1954; *Polar Molecules*, Dover, New York, 173.

62. P. R. Thomas, PhD Thesis, *University of Durham*, 1998.

63. J. March, *Advanced Organic Chemistry*, 4th ed., John Wiley and Son Inc , New York, 1992, 16.

64. M. C. Petty, *Langmuir-Blodgett Films, An Introduction*, Cambridge University Press, 1996.

65. C. J. F. Böttcher, *Theory of Electric Polarisation*; Elsevier: Amsterdam, 1973, Vol. 1; 1978; Vol. 2.

66. P. Jacques, *J. Phys. Chem.*, 1986, **90**, 5535.

67. (a) G. J. Ashwell, *Thin Solid Films*, 1990, **186**, 155. (b) G. J. Ashwell, *Nature*, 1990, **347**, 617.

68. D. Healy, P. R. Thomas, M. Szablewski and G. H. Cross, *Proc. SPIE.*, 1995, 2527, 32.

69. M. Szablewski, P. Thomas, G. Cross and J. Cole, *Organic Thin Films for Photonic Applications*, Sept 1995, Portland, Oregon, *Opt. Soc. Am., A.C.S.*

70. L. Onsager, *J. Am. Chem. Soc.*, 1936, **58**, 1486.

71. A. Fort, C. Runser, C. Barzoukas, C. Combellas, C. Suba and A. Thiebault, *Proc. SPIE.* 1984, 2285, 5.

72. M. Szablewski, P. R. Thomas, A. Thornton, D. Bloor, G. H. Cross, J. M. Cole, J. A. K. Howard, M. Malagoli, F. Meyers, J. L. Brédras, W. Wenseleers and E. Goovaerts, *J. Am. Chem. Soc.*, 1997, **119**, 3144.

73. R. J. Abraham, J. Fisher and P. Lotus, *Introduction to NMR Spectroscopy*, John Wiley and Sons Inc, New York, 1988.

74. R. M. Metzger, B. Chen, U. Höpfner, M. V. Lakshmikantham, D. Vuillaume, T. Kawai, X. Wu, H. Tachibana, T. V. Hughes, H. Sakurai, J. W. Baldwin, C. Hosch M. P. Cava, L. Brehmer and G. J. Ashwell, *J. Am. Chem. Soc.*, 1997, **119**, 10455.

75. (a) N. A. Bell, R. A. Broughton, J. S. Brooks, T. A. Jones and S. C. Thorpe, *Int. J. Electronics.*, 1994, **76**, 751.(b) R. A. Broughton, PhD Thesis, *Sheffield Hallam University*, 1993.(c) N. A. Bell, R. A. Broughton, J. S. Brooks, T. A. Jones and S. C. Thorpe, *J. Chem. Soc., Chem. Commun.*, 1990, 325.

76. C. S. Bradley, PhD Thesis, *Sheffield Hallam University*, 1999.

77. R. M. Metzger, N. E. Heimer and G. J. Ashwell, *Mol. Cryst. Liq. Cryst.*, 1984, **107**, 733.

78. J. March, *Advanced Organic Chemistry*, 4th ed., John Wiley and Son Inc , New York, 1992, 21 and references within.

79. J. C. Cole, J. M. Cole, G. H. Cross, M. Farsari, J. A. K. Howard and M. Szablewski, *Acta. Cryst.*, 1997, **B53**, 812.

80. Nemesis, Version **2.0**, Oxford Molecular Ltd., (1990-1994).

81. A. Bondi, *J. Phys. Chem.*, 1964, **68**, 441.

82. M. Szablewski, *Personal Communication.*

83. M. Prein and W. Adam, *Angew. Chem., Int. Ed. Engl.* 1996, **35**, 477.

Chapter 5: Langmuir-Blodgett Films, Experimental, Results and Discussion.

5.1 Historical Introduction.

Man's experience with insoluble films on water stretches back to antiquity. The Babylonian people considered the spreading of oil on water to be a form of divinity.[1] The Japanese used the phenomenon in a more practical nature - their *sumo-nagashi* art form involves the passing of paper through a suspension of dyes spread on a water subphase, to produce a patchwork design of dark and light areas.[2] The calming effect of "oil on troubled water" has also been known to fishermen throughout the ages.

However, formal study of monomolecular films really started in the eighteenth century. *Benjamin Franklin*, an American statesman and scientist, on a visit to England in 1774, read a paper to the Royal Society.[3] In this he described his experiment on the pond at Clapham Common, in which a teaspoon of oil dropped onto the pond was observed to extend to an area of approximately half an acre. In common with the observations of mariners he also reported on its calming influence. Yet it was *Lord Rayleigh*,[4] some years later, who deduced that such a volume of oil, spread over such an area, would produce a layer one molecule thick.

Alongside the work of Lord Rayleigh, a German schoolgirl, *Agnes Pockels*,[5] carried out experiments to determine molecular sizes in which she developed a method for manipulating oil films on water. However the true significance of Raleigh's and Pockel's work was not fully appreciated for some three decades until an American scientist, *Irving Langmuir,* employed by the General Electric Corporation, developed the experimental and theoretical concepts which underlie our modern understanding of the behaviour of molecules in insoluble monolayers.[6]

This early work, studying the behaviour of long chain fatty acids enabled Langmuir to evaluate the shapes and sizes of molecules, work for which he was awarded the Nobel prize in 1932.[7] In an early communication[6] Langmuir described the design of his now famous film balance, or trough, and outlined how it could be used to deduce the molecular size and orientation of monolayers at the air-subphase interface.

The first detailed description of the sequential build up of monolayers onto a solid substrate was made by one of Langmuir's co-workers, *Katherine Blodgett.*[8] Such assemblies are now termed Langmuir-Blodgett (LB) films. With the advent of World War Two much research interest into LB films ceased, and the subject was rarely studied until *Hans Kuhn* in the 1960's studied the organisation of monolayers and their spectroscopic properties.[9] Since this time, the number of research groups has grown dramatically. The expertise of today's chemists and physicists has facilitated the design of molecules which possess specific functional properties and which can be studied using the Langmuir-Blodgett technique. The technique enables in principle the preparation of thin films possessing well-defined thickness and molecular infrastructure, which display numerous exciting physical phenomena.

For instance, current interest in thin organic films has been stimulated by the fact that organic chromophores[10] have faster optical switching responses than the current generation of inorganic materials, such as $BaTiO_3$, $LiNbO_3$. Hence by utilising the LB technique the use of such organic materials in electrooptic applications may be realised.

5.2 Isotherm Measurement.

Molecules which embody both a hydrophilic (water-soluble) and hydrophobic (water-insoluble) part are termed *amphiphilic*. When dissolved in an appropriate solvent, such molecules may spread upon a suitable subphase to form a monomolecular layer at the air-subphase interface. After time has been allowed for the solvent to evaporate, the remaining molecules may be compressed by means of an appropriate mechanical barrier. Any resulting physical changes the molecules experience during the compression are demonstrated on a plot of surface pressure against area per molecule (or film area) at constant temperature - the resultant *isotherm*. A measurement of surface pressure (Π), as a function of the area occupied by the film, is an important experiment; it allows the size and molecular orientation of the molecules at the air-subphase interface to be determined. A typical Π-A isotherm plot for stearic acid is illustrated in Figure 5.1.

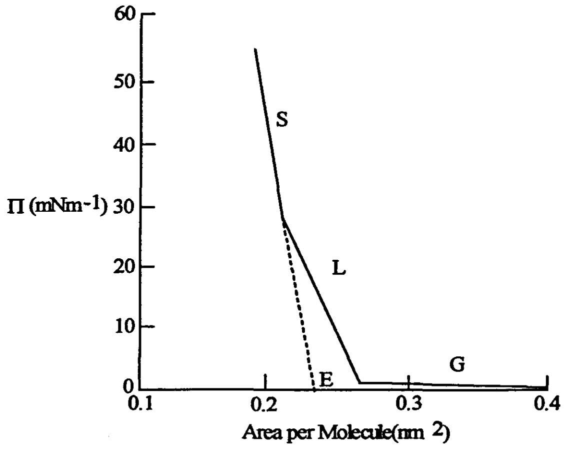

Figure 5.1 The Surface Pressure-Area Isotherm of Stearic Acid on a Water Subphase.

The floating monolayer can be considered a two dimensional system which, upon compression, undergoes phase changes that are the two dimensional equivalence of the normal pressure versus volume isotherm for a gas/liquid/solid. Consequently the monolayer is described as a two dimensional gas obeying the equation:

$$PA = kT \qquad \text{Equation 5.1}$$

Where P is the surface pressure, A is the effective area per molecule, k is the Boltzmann constant and T is the thermodynamic temperature.

Upon compression, the surface pressure increases, and the monolayer, initially in a gaseous state (G), becomes compressed via a liquid phase (L) to a condensed solid (S) phase as illustrated in Figure 5.1. However, many of the materials,[11-15] which have been shown to produce stable, good quality LB films do not produce the classical, three phase isotherms exhibited in fatty acids. In some materials where phase changes are observed, the transitions arise as a result of more complicated processes than just simple compression of the material. For instance, the extensive work carried out on pyridinium-TCNQ salts by *Barraud et al*,[16] showed that the plateaus observed can be explained by the formation of dimer pairs on the subphase. Non-classical behaviour of other compounds is attributed to gross re-orientation of the amphiphile on the subphase during compression,[17] or simply resulting from some form of chemical interaction, such as oxidation, polymerisation etc., taking place between the monolayer film and one (or both) of the adjacent bulk phases.[18]

The extrapolated point E in Figure 5.1 represents the area at zero pressure and is taken as the cross sectional area of the amphiphile on the subphase which in the case of the classical material, stearic acid,[19,20] is found to be ≈ 0.19 nm^2. Information gained from an isotherm is important as it gives a clear indication of the behaviour and limits to which the monolayer of the studied material can be exposed. So an essential pre-requisite to the deposition of multilayer films is the full characterisation of the material's behaviour on the subphase.

However the quality of the isotherm is critically dependent upon the purity of the subphase.[21] Normally the purest grade available of subphase and solvents are used, to aid reproducibility. The choice of subphase is dependent upon the solubility and properties of the material under investigation. Although the vast majority of monolayer research is carried out using ultra pure water, other subphases have been used - hydrocarbons and mercury for example which allow the use of water-soluble solvents. The use of glycerol to study TCNQ-based amphiphiles,[22] reduces potential monolayer solubility in a water subphase due to the necessary use of more polar solvents.

The presence of divalent metal ions such as calcium and cadmium in the subphase can, in many cases, improve the cohesion of conventional fatty acids and other ionised monolayers. The incorporation of metal ions into the monolayer is relatively straightforward and the effects are shown in Figure 5.2.

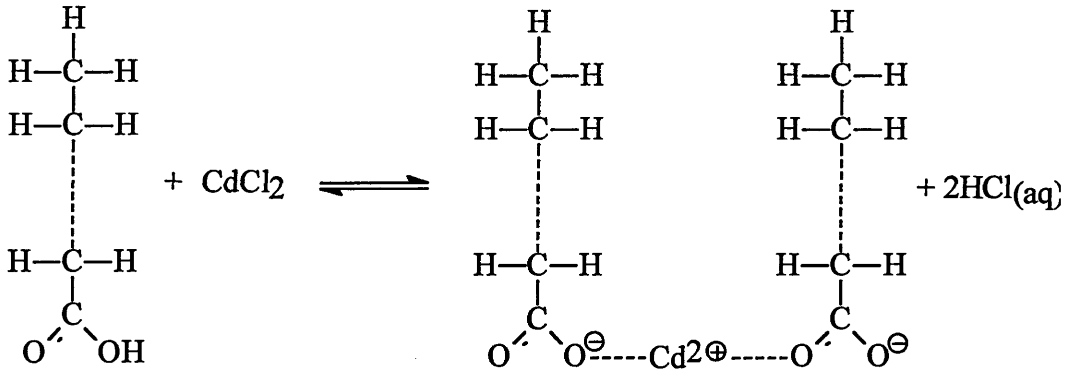

Figure 5.2 Molecular Arrangement of Fatty Acid Salts at the Subphase Interface.

Amphiphiles having ionisable head groups are also dependent upon the pH of the subphase, as the presence of any proton source will prevent the hydrolysis of the material. This may result in a loss of cohesion within the monolayer, which potentially can lead to the formation of defects within any LB films fabricated. The combined effects of pH and divalent metal ion addition are illustrated in Figure 5.3.

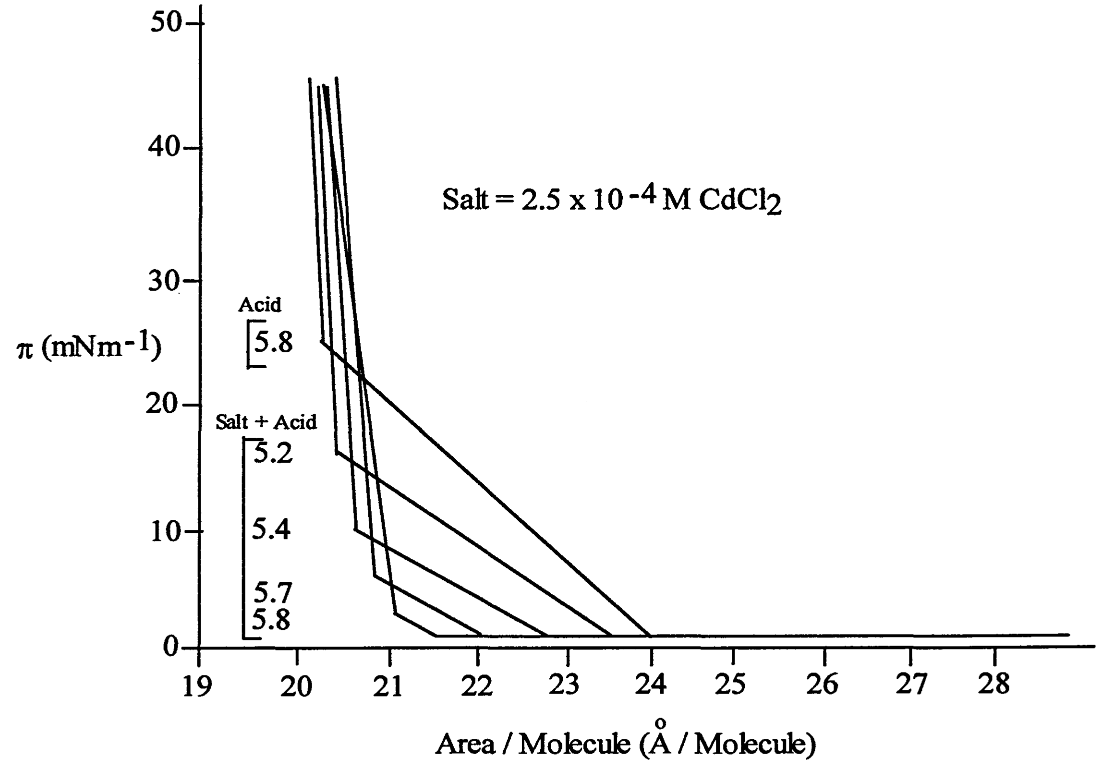

Figure 5.3 Effect of pH Variation and Divalent Metal Ion on Stearic Acid Films.

The quality of the monolayer is crucial as it dictates the properties of LB films subsequently prepared. If the monolayer contains defects, then the LB film may contain defects. If these defects are incorporated into electrical devices this may limit the amount of current to which they could be exposed, reducing the potential use. The presence of defects can be substantially limited, but not removed, if slow evaporating solvents are used in the initial spreading of the monolayer, i.e. mesitylene and long chain hydrocarbons such as hexadecane. The experimental considerations and precautions taken in producing reproducible isotherms will be discussed in greater detail in Section 5.5.

5.3 Deposition Principles and Mono/Multilayer Fabrication.

The Langmuir-Blodgett (LB) technique, first introduced by Irving Langmuir[6] and applied extensively by Katherine Blodgett,[8] involves the vertical lifting of a suitable substrate through a floating monolayer, maintained at a predetermined surface pressure. The movement of this substrate through the air-monolayer interface results in monolayer material being transferred to the substrate surface. If this transference is repeated sequentially a multilayer structure is produced. In principle, it is possible to prepare highly ordered multilayer LB films consisting of several hundred monolayers or more.[12,13] Such sequential removal of monolayer material on each traversal of the monolayer-air interface may result in a head-to-head and tail-to-tail stacking of the amphiphilic molecules within the film. This centrosymmetric mode of deposition illustrated in Figure 5.4 is called Y-type deposition.

Although this is the most frequently encountered mode of deposition,[19,20] instances in which the floating monolayer is only transferred to the substrate as it is being inserted into the subphase, or only as it is being removed are also observed. These deposition modes are called X-type (monolayer transfer on the down stroke only) and Z-type (monolayer transfer on the upstroke only) and are illustrated in Figure 5.5. In terms of preparing LB films, which possess good nonlinear optical behaviour, then the X- and Z-type structures are very important, as both give rise to the required non-centrosymmetric arrangement of dipoles necessary for second harmonic generation.[10]

As the schematics show, on each deposition cycle, material may or may not be transferred to the solid support. The transference of monolayer material to the substrate manifests itself as a decrease in the area occupied by the monolayer, held at constant pressure. This is called the *transfer* (η) or *deposition* (τ) ratio and is simply defined as the decrease in the area occupied by the film on the subphases surface divided by the coated area of the solid substrate.

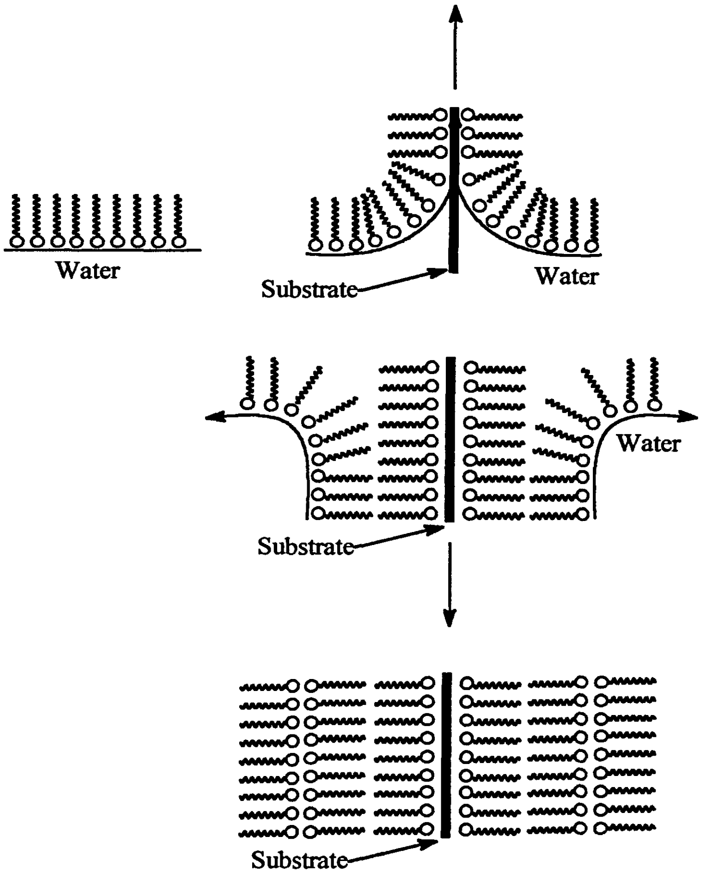
Water
Substrate
Water
Water
Substrate
Substrate

Figure 5.4 Y-Type Langmuir-Blodgett Film Deposition.

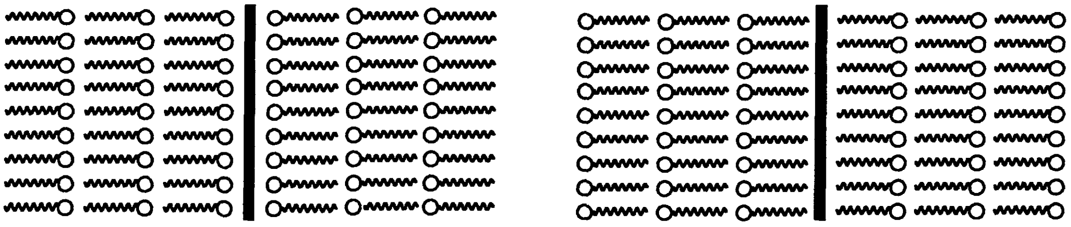
(a) (b)

Figure 5.5 (a) Z-Type Deposition; (b) X-Type Deposition.

i.e.

$$\text{Transfer or Deposition Ratio} = \frac{A_L}{A_S} \qquad \text{Equation 5.2}$$

Where A_L is the decrease in the area occupied by the monolayer on the water surface and A_S is the area of substrate covered by the monolayer.

The value of η or τ gives an indication of the integrity of monolayer transference, and which mode of deposition is occuring.[11,19] Ideally the value should be either unity or zero - values differing substantially from these imply that the molecules are rearranging or that transference of the monolayer is incomplete. It should be noted, however, that the deposition type can change as the LB film is being formed, e.g. *Bradley et al*[15] on the fabrication of large multilayer films incorporating the R(2)Q3CNQ class of compound.

The vertical dipping LB process is not the only way to transfer a floating monolayer to a solid support or, indeed, to build up multilayer films. Other techniques have been employed. Possibly one of the more popular techniques is the horizontal lifting LB technique (HLLB) original developed by *Langmuir* and *Schaefer* in the thirties.[23] As the name implies, the substrate is held horizontally and lowered onto the monolayer from above, as illustrated in Figure 5.6. This approach has been used by various authors,[20,24,25] as it is useful for the transfer of highly rigid monolayers to solid supports, the floating monolayer being subjected to fewer disruptive forces than in the vertical LB method.

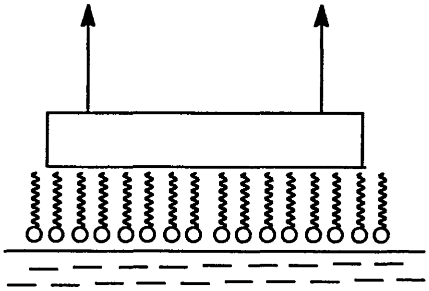

Figure 5.6 Langmuir-Schaefer or HLLB Technique for Depositing Floating Monolayers.

The Langmuir-Blodgett technique for preparing organised assemblies is an extremely important tool - it does not require the use of expensive vacuum and heating processes of other techniques.[26] It provides for the production of very thin organic films of a defined structure and thickness. Together with the synthetic ability of the chemist to design appropriate materials interest has been aroused in the industrial applications to which organic assemblies can be applied.

5.4 Langmuir-Blodgett Film Forming Materials and their Applications.

Classically, most of the research on LB films studied the long chain fatty acids of which n-octadecanoic acid (stearic acid), illustrated in Figure 5.7, is perhaps the most widely studied.

Stearic acid contains two functional groups, a long chain hydrocarbon "tail" and a carboxylate "head". The non-polar hydrocarbon tail is hydrophobic. The carboxylate head group is hydrophilic. Hence the balance between these two opposing forces results in the formation of an insoluble monolayer at the air-water interface. Any change in this amphipathic balance can significantly affect the monolayer properties of the material. For example acetic acid has a very short alkyl chain and this confers total water solubility.

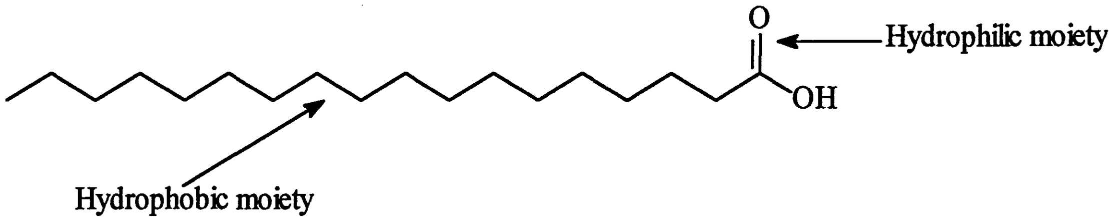

Figure 5.7 Stearic Acid ($C_{17}H_{35}COOH$).

Other fatty type acids which have been extensively studied include arachidic acid ($C_{19}H_{39}COOH$) and behenic acid ($C_{21}H_{43}COOH$).[19] This early work established the fundamental molecular requirements for LB film forming materials- the key prerequisite being that individual molecules should embody a hydrophilic and hydrophobic moiety.

The introduction of carbon-carbon double bonds into the fatty acid structure has been shown to markedly affect film forming properties.[20] For instance the presence of a terminal double bond in ω-tricosenoic acid (Figure 5.8) greatly reduces the disruption of the close-packed hydrocarbon chains that is commonly observed when the double bond is situated in a mid-chain position.[11] The subsequent LB films formed from this terminal alkene acid have been extensively studied as a result of their polymerisation when exposed to an electron beam.[27]

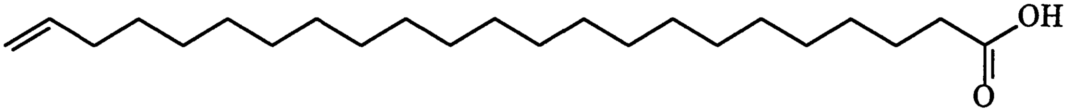

Figure 5.8 ω-Tricosenoic Acid [$CH_2=CH-(CH_2)_{20}-COOH$].

Films of ω-tricosenoic acid have also been found to exhibit excellent thermal and mechanical stability. The major limitation with LB films formed from fatty acid derivatives is that they are generally insulators and have very low temperature tolerances. This limits their use for many practical applications, though ω-tricosenoic acid has been the subject of research geared towards their potential use in field effect semiconductor devices,[28] where they have been incorporated as active insulators in compound semiconductors.[29]

The ability to form insoluble monolayers at the air-water interface is not limited to long chain fatty acids alone. The number of film forming materials now known is large and increasing. The variation of hydrophilic head groups is diverse, with various functional groups, ranging from nitrile[30] and amide[31] groups to sulphur[32] containing systems, being incorporated.

At the forefront of this area of research is the development of sensors and potential molecular electronic devices from organic conductors, nonlinear optical materials and organic magnets. However the majority of crystalline materials of this type do not always have a well-organised molecular architecture, making it difficult for the material to display its intended physical property.

For example the TTF-TCNQ charge-transfer complex, which has been found to be highly conducting at room temperature,[33] is relatively insoluble and thus difficult to handle. However the synthesis of amphiphilic TTF (1) and TCNQ (2) derivatives (Figure 5.9) and subsequent fabrication using the LB technique[7] has enabled investigation into their potential for device fabrication.[34] The LB technique enables the individual molecules to stack face-to-face, thereby ensuring efficient electron flow along the direction of the stack.

Bryce and his colleagues at Durham university[34] have exploited this by producing conducting multilayer structures of a TTF based thioester (1, Figure 5.9) which to date has the highest conductivity observed for a TTF based LB film.

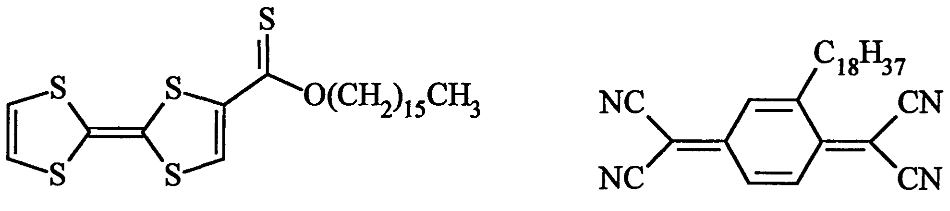

(1) (2)

Figure 5.9 Amphiphilic TTF and TCNQ Derivatives.

There is an increasing need for data storage and the quest for ever faster signal processing and data manipulation. The last decade has seen an increased study of nonlinear optical materials, which find use as frequency doublers[12] and photochromic memory devices.[35] However, for such materials to display nonlinear optical properties, certain molecular design criteria are required - the conjugation of a donor unit to an acceptor unit and a non-centrosymmetric arrangement of the molecular dipole's within the crystals structure - the latter in practice is difficult to achieve, as 70% of most crystalline materials pack centrosymmetrically. The great advantage of the LB technique here is that both X- and Z- deposition modes can give rise to the required non-centrosymmetric arrangement of dipoles.

Production of films with a non-centrosymmetric type film structure can also be obtained by interleaving the active chromophore with inactive spacers[36] so that the alignment of the active material is essentially non-centrosymmetric (though this can dilute the effect of the active chromophore and result in large multilayer structures being required for device manufacture).

If the NLO efficiency of such materials is to be improved, in principle every layer should be active but to date, of the homomolecular films, only 2-docosylamino-5-nitropyridine, DCANP,[13] and the quinolinium zwitterion, $C_{16}H_{33}$(4)Q3CNQ,[12] have shown a quadratic increase in SHG in thicknesses of a few hundred layers, and this quadratic enhancement is only retained if long range order is maintained.[38] Of the two examples, the quinolinium zwitterion has been shown to exhibit a second order susceptibility value, $\chi_{zzz}^{(2)}$ of 180 pm V^{-1} for a 200 layer film, the highest reported second order susceptibility for any LB multilayer film.[12]

The years of research into the alignment of nonlinear optical materials via the LB technique has produced important insights for future workers. The experience gained has recently been utilised by synthetic chemists at Cranfield University. They have shown that unconventional two legged cationic dyes, such as the ones illustrated in Figure 5.10, which embody hydrophobic chains at opposite ends of a hydrophilic chromophore, invariably form non-centrosymmetric Z-type structures,[14,37-39] providing that the hydrophobic alkyl groups are of the appropriate length.[38] Multilayer films have shown quadratic enhancement of the second harmonic intensity with number of layers, to a thickness of ~ 0.6 μm for the case of compound (4). This is the thickest homomolecular Z-type structure reported to date,[37] although thicker non-centrosymmetric films have been reported when incorporating inactive spacers.[36,40]

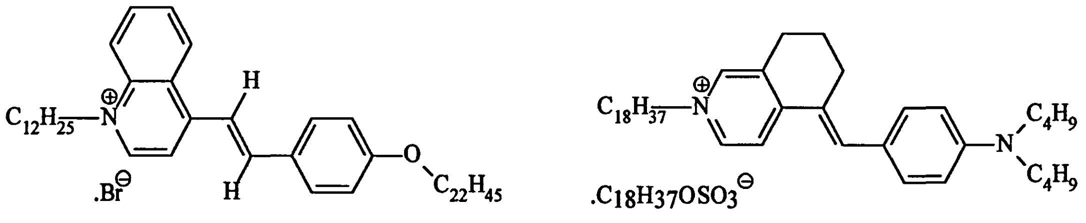

(3) (4)

Figure 5.10 Two Legged Dyes Forming Z-type LB Structures.

The formation of non-centrosymmetric structures from such materials is a result of the interdigitation of the alkyl chains at the air-water interface.[41] The temptation for the monolayer to invert during deposition, placing like ends together, as observed in the majority of other amphiphilic materials, is resisted as a result of each end of the molecule being hydrophobic.

The quadratic SHG enhancement observed in such materials and the applicability of the technique to different classes of dyes suggests that alternate-layer deposition is no longer a prerequisite for the formation of non-centrosymmetric films.

The second order susceptibilities, $\chi_{zzz}^{(2)}$, observed in such two legged dyes[14,37-39] are in general much smaller- 30 pm V^{-1} (160 layers), in the case of compound (4)[37] than that observed for the more widely studied, potentially multifunctional $C_{16}H_{33}$(4)Q3CNQ compound.[12] As well as SHG, $C_{16}H_{33}$(4)Q3CNQ also shows photochromic[12] and molecular rectification behaviour,[42,43] though the hypothesis that the asymmetric current-voltage characteristics observed implies molecular rectification is a highly controversial one.[44]

Other two legged dyes which have shown extensive nonlinear optical behaviour have included the unusually symmetrical squaraine dyes (Figure 5.11), which were developed by Ashwell and co-workers at the University of Cranfield.[45]

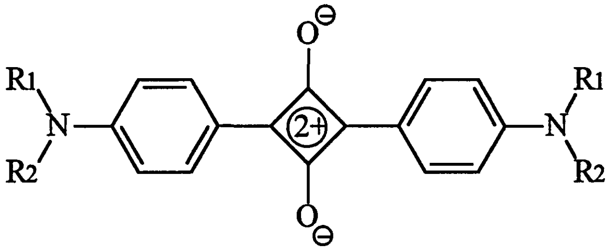

Figure 5.11 A Typical Squaraine Dye.

The unusual feature of the squaraine dyes is that they are centrosymmetric in nature and hence would be expected to be inert to SHG. However, SHG has been observed from LB films of a variety of analogues with anilino[46] and heterocyclic[47] donors. The SHG is not inherent to the molecule and furthermore, the intensity is too strong to be associated with the glass|LB interface. Instead, it is attributed to aggregate dimer pair formation within the film structure. The molecules are assumed to adopt a T-shaped arrangement and the SHG arises from intermolecular charge-transfer between the acceptor and donor moieties. This has been substantiated by mass spectroscopic data on the materials, where peaks are observed for the fragmentation of the dimeric aggregates.

However, in all of the above examples, the materials, which form stable monolayers at the air-subphase interface, contain long hydrophobic alkyl chains. Hydrophobic groups may severely restrict any practical applications of the materials. Two factors may explain this: first, the presence of such groups can introduce a large degree of instability,[11] and second, the more interesting properties of the organic molecule can be diluted by the long aliphatic chain. Recently, more robust organic materials containing less aliphatic character have been deposited as LB films. These have included phthalocyanines[48] (5, Figure 5.12) and porphyrins[49] (6, Figure 5.12), which have been shown to have potential commercial applications as sensors when deposited on platinum interdigitated electrodes. Devices incorporating such heterocycles have been found to exhibit a useful room temperature response on exposure to environmental pollutants such as nitrogen dioxide gas at the occupational hygiene level.[50]

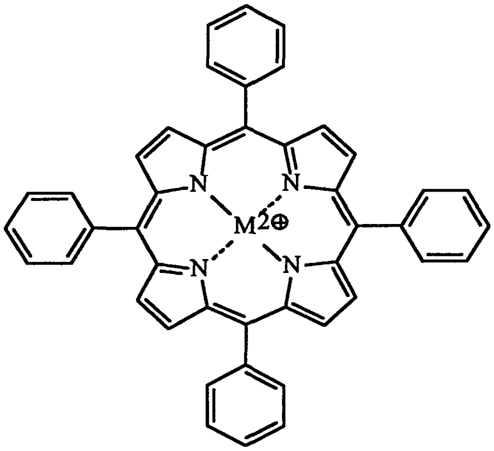

(5)

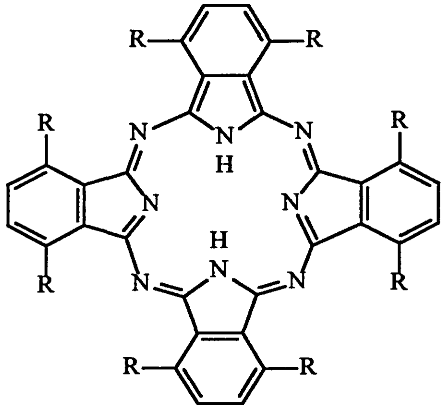

(6)

Figure 5.12 Non-aliphatic LB Film Forming Materials.

Although study of LB films of these materials has shown that they have imperfect structures when compared to long chain fatty acids, this is perhaps a price to be paid for the greater mechanical and thermal stability they exhibit. This stability has led to their greater use - they are incorporated into a greater number of devices than other compounds.

Interesting work by *Vincett et al*[51] has shown that anthracene molecules, substituted with alkyl chains as short as four carbon units, could be fabricated as LB films. It is generally agreed that this observation arises as a result of the fused ring system of anthracene contributing towards the hydrophobic part of the molecule. Thus shorter alkyl chains could be incorporated into ring systems, and still maintain the necessary amphiphilic balance. Thus the dilution problem associated with long chain compounds can be kept to a minimum, potentially improving the overall efficiency of nonlinear optical materials.

What this chapter has shown is that the ability to design and build organic molecules of an appropriate structure, coupled with the LB technique's ability to orientate these systems into defined structures of precise order and thickness, leaves open the door on future developments in this area.

5.5 Langmuir-Blodgett Films - Experimental.

This section discusses the design and operation of the mini-trough used in this work. Other experimental considerations regarding isotherm recording, film stability, etc are discussed in Section 5.7.

5.5.1 The Joyce-Loebl Mini Trough Monolayer Coating Unit.

This commercially available trough is a further development of a well-proven design, which has been used successfully in many universities and industrial establishments. The mini-trough is a miniaturised version of the larger type 4 Joyce-Loebl constant perimeter trough which was originally developed by scientists at ICI and Durham University using the ideas of *Blight et al.*[52]

The two principal types of operation of a Langmuir Trough - isotherm plotting and monolayer removal to a substrate - are fully automated. The mechanical sections of the trough are corrosion resistant. The unit itself is housed in a clean cabinet with a glass hinged lid. The main feature of this, and indeed any other Langmuir trough, are shown schematically in Figure 5.13.

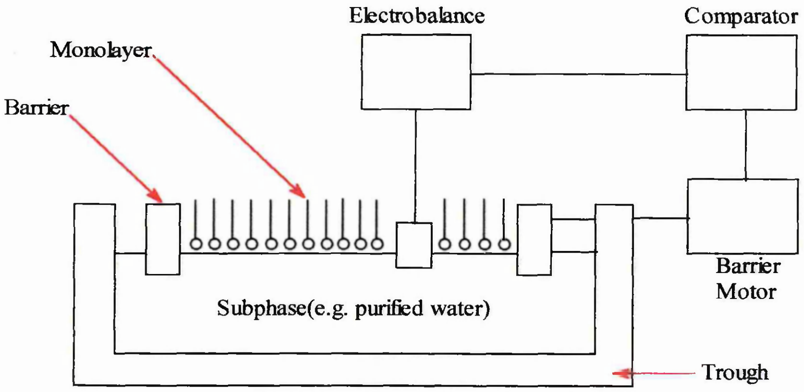

Figure 5.13 Schematic Diagram of the Essential Features of a Langmuir Trough.

5.5.2 The Compression System.

Traditionally, the container, which holds the liquid subphase, forms an integral part of the boundary of the compression system. To enable adequate surface pressure control and prevent any potential film leakage, a seal is incorporated between the edge of the trough and the moveable barrier. An important feature of the Joyce-Loebl trough is the incorporation of a constant perimeter PTFE coated glass fibre barrier that defines the working area of the liquid surface. Enclosing the monolayer within a continuous band keeps the problems of film leakage and contamination to a minimum. The liquid container in the Joyce-Loebl mini-trough is made of a FEP Teflon sheet mounted on a stainless steel assembly.

The compression barrier, illustrated in Figure 5.14, is a PTFE fibre belt of width 2cm, and is held in place by a system of five PTFE rollers, two of which are secured to a mobile gantry. The size of the area covered by the film is carefully controlled by means of a highly geared motor maintaining the barrier taut at all times. A gantry is located and suspended by PTFE bearings sliding smoothly along square cross-section rails. A range of speeds are available - range of area change 0-40 cm^2/s - when using the instrument in either a compression or expansion mode.

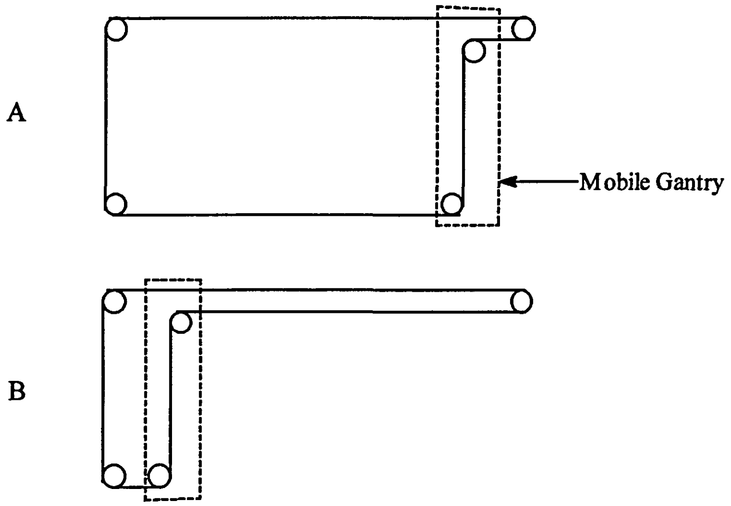

Figure 5.14 Molecules Deposited Within an Area Defined by PTFE Barrier as Shown A) Maximum Area: B) Minimum Area.

5.5.3 Surface Pressure Measurement.

The Wilhelmy plate technique used to monitor the surface pressure is well established, reliable and enables the surface pressure to be measured accurately over a wide range. The Wilhelmy balance is based on a thin plate, which is semi-immersed in the subphase and attached to a microbalance directly above it (Figure 5.15). Providing that the contact angle between the plate and the subphase is zero, then the counterbalancing forces on the microbalance can be directly linked to the surface pressure, provided that the microbalance is sensitive enough to cope with the small forces involved.

The Wilhelmy plate itself can be made from various materials, although one of the more effective ones is typically a piece of Whatman Grade 1 chromatography paper which is attached to the balance head with a length of fine wire.

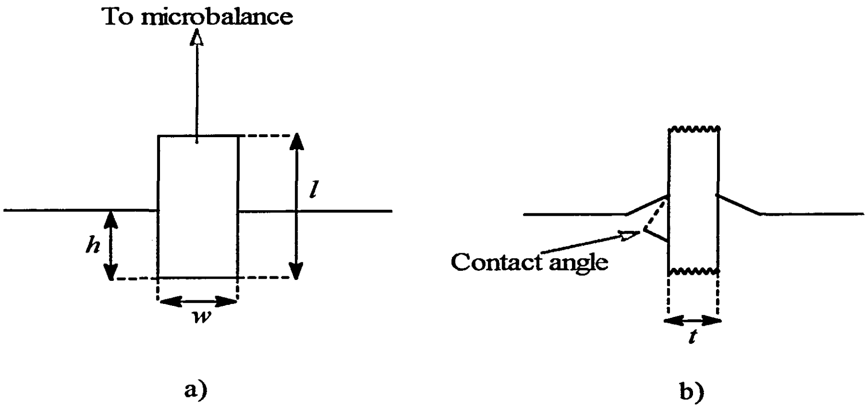

Figure 5.15 A Wilhelmy Plate a) Front view; b) Side View.

The forces acting on the plate are due to gravity and surface tension downwards and buoyancy, due to the displaced water upwards. Hence for a rectangular plate of dimensions l, w and t and of material of density ρ_w immersed to a depth h in a liquid of density ρ_L, the net downward force is given by:

$$F = \rho_w g l w t + 2\gamma(t + w)\,\mathrm{Cos}\theta - \rho_L g t w h \qquad \text{Equation 5.3}$$

where γ is the surface tension; g is the gravitational constant and θ is the contact angle on the plate. The surface pressure π is regarded as being the reduction in surface tension occurring when the subphase is covered by a monolayer i.e. it is the expanding pressure of the monolayer opposing the naturally contracting tension of the subphase surface. Thus:

$$\pi = \gamma_0 - \gamma_1 = \Delta\gamma \qquad \text{Equation. 5.4}$$

where γ_0 = surface tension of the pure liquid, γ_1 = surface tension of the subphase covered with a monolayer. Hence:

$$F = (2\gamma_0 - \gamma_1)(t + w) \quad \text{Equation 5.5}$$

assuming that the contact angle is zero (hence Cos $\theta = 1$). Thus if the plate is of negligible thickness and width 1cm and ignoring the upward force due to the displaced monolayer, then:

$$F = 2\Delta\gamma \quad \text{Equation 5.6}$$

That is, the weight measure in milligrams is equal to twice the surface pressure measured in mNm^{-1}.

5.6 Trough Operation

This section outlines the necessary steps to set up the Langmuir Mini trough. The detail is quite general, and is not specific to any one material or indeed any subphase.

5.6.1 Cleanliness.

The need for scrupulous cleanliness has already been illustrated and its importance cannot be stressed too highly. Many of the problems encountered in monolayer technology emanate from the presence of impurities and other "*surface active*" contaminants in the equipment or materials used. Rigorous cleaning procedures and the use of ultrapure solvents are essential, as well as carrying out experiments in the cleanest environment possible.

The trough was cleaned at least three times a week using successive washings of dichloromethane or chloroform, propan-2-ol and high purity water. The PTFE barrier and rollers were also cleaned at the same time, using the same procedure. The housing of the trough i.e. metal cage and anti-vibration table were also found to be a source of contamination and, as a result, cleaned periodically using the same method as stated above.

5.6.2 Trough Calibration.

Before use, all of the individual instruments i.e. pH meter, microbalance and chart recorder were calibrated in accordance with their respective manufacturer's instructions, and recalibrated periodically.

5.6.3 Calibration of Surface Area.

For accurate, reproducible isotherms the abscissa of the X-Y chart recorder must be calibrated. This requires knowledge of the maximum and minimum areas contained within the confines of the constant perimeter barrier. The approximate values of these are 500 and 100 cm^2 respectively, although all researchers should determine the exact values of these for themselves. The speed at which the barrier is moving prior to the measurement of minimum area is particularly important, as this will affect exactly where the barrier stops after the trip micro switch has been activated. It is recommended that the barrier speed, which is used for monolayer compression, also be used for the area calibration.

5.6.4 Calibration of Surface Pressure.

When the microbalance has been correctly calibrated by the use of standard weights, then the surface pressure is directly related to the dimensions of the Wilhelmy plate as discussed in Section 5.5.3. Hence, the ordinate of the X-Y chart recorder can be most conveniently calibrated by the addition of known weights to the microbalance arm.

5.6.5 The Subphase.

Most Langmuir trough work requires an aqueous subphase. The water used should be of the highest quality available. In this work a Millipore "Milli-Q" water purification unit was employed, feeding water of 18 MΩ resistance directly into the trough as and when required. This system makes use of an initial reverse osmosis stage, followed by a system of "polishing" filters, which ultimately removes contaminants at the biological level. In certain cases the addition of divalent metal ions to the subphase is required (to aid certain film stability as discussed earlier). In such cases the metal salt added must also be of the purest grade available. Similarly with the addition of acid or alkali to raise or lower the pH of the subphase. It is advisable to change the subphase, cleaning the trough at the same time, at least every other day, and certainly after a weekend or whenever the system has not been used for any lengthy period of time.

5.6.6 Surface Cleaning.

Adequate cleaning of the subphase surface before monolayer spreading is essential if reproducible results are to be obtained. Such cleaning can be conveniently done by attaching a clean glass pasteur pipette (preferably new) to a suitable suction pump and then removing the surface layers by suction. Depending on the mains pressure then a simple water pump will suffice or, if not, then a pump capable of taking a mixture of air and water is necessary.

The usual approach is first to reduce the area to a minimum and then clean the surface of the subphase with the pasteur pipette/pump arrangement. The effectiveness of this cleaning procedure can be monitored by opening the barrier to its maximum area, then compressing it at a slow speed and measuring any change in surface pressure. Any appreciable increase in the surface pressure is indicative of surface contamination and the process should be repeated.

Ideally, if the subphase is totally clean then there should be no change in surface pressure upon opening and closing the barrier to its maximum and minimum limits. For the Joyce-Loebl instrument a value of surface pressure of less than 0.5 mNm^{-1} (corresponding to 1.0 mg) is usually acceptable.

This cleaning technique has been criticised by some monolayer researchers.[48] Such trough systems, where the barrier cannot close to give an absolute zero area, may still have an appreciable surface area left which, on compression, could show surface contamination. The spreading and compression of a well-characterised amphiphile (i.e. stearic acid) and observing any deviations from the standard isotherm can overcome this problem.

5.6.7 Monolayer Material Preparation and Spreading.

Monolayer-forming materials are applied to the subphase by first dissolving them in a suitable solvent. Some common solvents used in monolayer spreading are listed in Table 5.1, along with some of their properties.

Solvent	Mpt (°C)	Bpt (°C)	Solubility Kgm^{-3} H_2O
n-Hexane	-94	69	0.01
Cyclohexane	6.5	81	0.07
Chloroform	-64	61	8.0
Diethyl Ether	-116	35	75

Table 5.1 Common Solvents used in Langmuir-Blodgett Monolayer Preparation.

However these solvents are all relatively non-polar and will not dissolve some of the more polar amphiphiles that have been documented.[13,15,19] This has led to the development of special techniques such as the use of mixed solvents,[11,53] which provides the necessary solubility for the monolayer material but does not introduce serious water solubility problems. Examples include mixtures of the compounds listed in Table 5.1 with simple alcohols.[11]

When producing monolayer solutions, exceptionally high levels of accuracy are required. The mass of the adduct dissolved in the solvent was in this work measured to one hundredth of a milligram. The amount of solvent used was typically one millilitre, delivered by a Gilson pipette.

The usual way of spreading a monolayer solution is via a microsyringe onto the subphase surface. The amount of solution deposited, which is known to the nearest ten microlitres, should be calculated to give a compressed monolayer with the barrier positioned approximately half way between its maximum and minimum limits. The material is added from just above the surface, one-drop at a time, allowing each drop to spread onto the subphase. When the appropriate amount has been added to the surface, time (generally 5-10 minutes) is allowed for any excess solvent to evaporate. The hinged glass lid may be opened during this period to aid ventilation.

5.6.8 Temperature of the Subphase.

Changes in the properties of a monolayer forming material can be due to increasing or decreasing the temperature of the subphase. The temperature can be altered by incorporating a small electrical heat exchanger into the trough, and measuring the temperature with an appropriate probe.

5.6.9 Compression of the Monolayer.

Before monolayer compression, the microbalance must be zeroed. This is done by first adding or removing weights from the pan to give a coarse zero, and then adjusting the zero control of the microbalance. Cleaning the subphase will also change any zero reading that is obtained as it removes water from the trough, so changing the Wilhelmy plate arrangement. Therefore all cleaning should be carried out before the system is zeroed. Compression is usually done slowly, with a typical time scale for an isotherm measurement being about 5-10 minutes. Once the essential features of the isotherm have been recorded, the barrier is returned to its original open position. This avoids the collapse of the monolayer if it is compressed too far, although, when studying a new material for the first time, the collapse pressure is usually recorded.

5.6.10 Control of Surface Pressure.

To facilitate monolayer removal to the substrate or for stability experiments, it is useful to be able to control the surface pressure of the monolayer. A negative feedback loop provides the facility to maintain the system at a constant pressure, whereby the removal or collapse of the monolayer is compensated by the closing of the barrier by an appropriate amount. A feedback time constant puts additional damping into the feedback loop and can thus change the response time of the system.

5.6.11 Transfer of Monolayer.

Much of the details of monolayer transfer to a substrate and, in particular the ways in which materials may be deposited as a floating monolayer, have been mentioned in the previous sections. The size of the film required, i.e. number of layers, the drying time, if any, between successive layers, the speed of deposition and the depth can all be selected and controlled by the system. The deposition process is most conveniently monitored using a two-channel recorder to measure both the surface pressure and surface area against time. Thus if the system is behaving correctly, then a decrease in area should be observed as material is removed from the subphase, due to the negative feedback loop maintaining the surface pressure at the predetermined value. Hence if the area remains steady then this would indicate that there is no material being transferred.

5.7 Langmuir-Blodgett Films - Results and Discussion.

The systematic study of the film forming potential of the various donor-π-acceptor adducts prepared in this work was carried out in collaboration with scientists at the Health and Safety Laboratories in Sheffield and the Department of Engineering at Durham University. Very briefly, the investigation concentrated upon three main areas:

1. The film forming behaviour of the materials on the subphase.
2. The attempted deposition of the materials as LB films.
3. Comparison of these results with those of the previously studied R(4)Q3CNQ[11] and R(2)Q3CNQ series[15]

5.7.1 Langmuir Film Studies on R(4)Q3CNQF$_4$ and R(2)Q3CNQF$_4$ Adducts.

The systematic investigation into the potential film forming abilities of the R(4)Q3CNQF$_4$ and R(2)Q3CNQF$_4$ compounds was as a direct consequence of the film forming abilities shown by the unsubstituted R(4)Q3CNQ and R(2)Q3CNQ type compounds.[11,12,15,54-58] The R(4)Q3CNQ compounds, which were first studied nearly a decade ago, exhibit film behaviour which is dependent upon the hydrophobic chain length, R. For analogues, with chain lengths greater than 14 carbon atoms, the subsequent films formed are non-centrosymmetric in nature and give rise to a very strong nonlinear optical effect in which the charge-transfer band observed arises from an intramolecular process. In contrast, when the alkyl chain length of the adduct is less than fifteen carbon units, the ensuing films formed are centrosymmetric and give rise to a charge-transfer process which is intermolecular and results in such films exhibiting very weak nonlinear optical effects such as SHG.

As a result of the molecular structure of the substituted compounds prepared in this work being very similar to that of the corresponding unsubstituted compounds, it led one to suspect that such substituted adducts would also form similar insoluble monomolecular films at the air-water interface. The practical interest in these materials stems from the unique multifunctional properties exhibited by the $C_{16}H_{33}$(4)Q3CNQ adduct, in that (i) it is photochromic;[35] (ii) it has been found to exhibit Y- and Z- type LB film structures,[11,12] with the Z-type structures showing second harmonic intensity that increases quadratically with the number of layers[12] and (iii) Mg| ($C_{16}H_{33}$(4)Q3CNQ monolayer)|Pt devices show asymmetric current-voltage curves,[42,43] – a possible consequence of molecular rectification.

It was hoped that substituted derivatives would exhibit properties of a similar nature. Consequently the major interest in the substituted compounds was to see if they exhibit a similar chain length dependency as that of the R(4)Q3CNQ compounds as, despite the extensive research into these materials over nearly a decade, a definitive explanation of this phenomenon has not been forthcoming. If such a dependency occurs in the substituted derivatives then it should provide further information upon which to help to clarify why certain compounds gives significantly different areas per molecule when deposited at the air-water interface.

Another interesting observation is that R(4)Q3CNQ compounds can be deposited in more than one way. *Ashwell et al*[12] have observed that such adducts undergo Z-type deposition, with the non-centrosymmetric film structure being maintained to >200 layers. In contrast *Broughton et al*,[11] amongst other researchers,[15] have shown that such compounds may be deposited in a Y-type fashion in which the Y-type films are possibly orientated in a herringbone type arrangement (Figure 5.16). This ordering has been reported before in 2-docosylamino-5-nitropyridine (DCANP)[13] which has a Y-type structure in which the molecular layers pack head-to-head and tail-to-tail. Such arrangements are usually centrosymmetric but, in this case, the layers adopt a non-centrosymmetric herringbone arrangement, which is significant in terms of NLO applications.

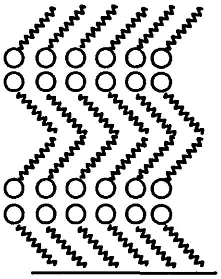

Figure 5.16 Non-Centrosymmetric Y-Type Herringbone Arrangement.

Therefore the investigation into the substituted tetrafluoro adducts was to include the fabrication of multilayer films with both Y- and Z-type structures so that phenomena such as second harmonic generation could be potentially observed in different structure types.

The major problem associated with using the R(4)Q3CNQF_4 adducts was their sparing solubility in most organic solvents, and that many of these solvents were not suitable for spreading upon a water subphase. For the α-substituted adducts the problem was not serious, as the materials were soluble in dichloromethane. Thus, solutions of the α-compounds could be prepared of amenable concentration in the range 0.3-1.1 mg ml^{-1}.

The γ-substituted adducts on the other hand were very difficult to handle, as even their solubility in dichloromethane was very limited (<0.1 mg ml^{-1}) and meant that very large volumes of solution had to be spread onto the subphase, typically 1-2 ml. The subsequent isotherms that were obtained for the γ-adducts were very similar to those of the corresponding TCNQ-based adducts, in that featureless plots were obtained. The molecular areas occupied by the materials were very small with typical area per molecule's being around 0.14 nm^2, as in the case of $C_{10}H_{21}$(4)Q3CNQF$_4$. A typical isotherm, of $C_{10}H_{21}$(4)Q3CNQF$_4$, is illustrated in Figure 5.17. The area per molecule values obtained for the γ-derivatives are puzzling for several reasons.

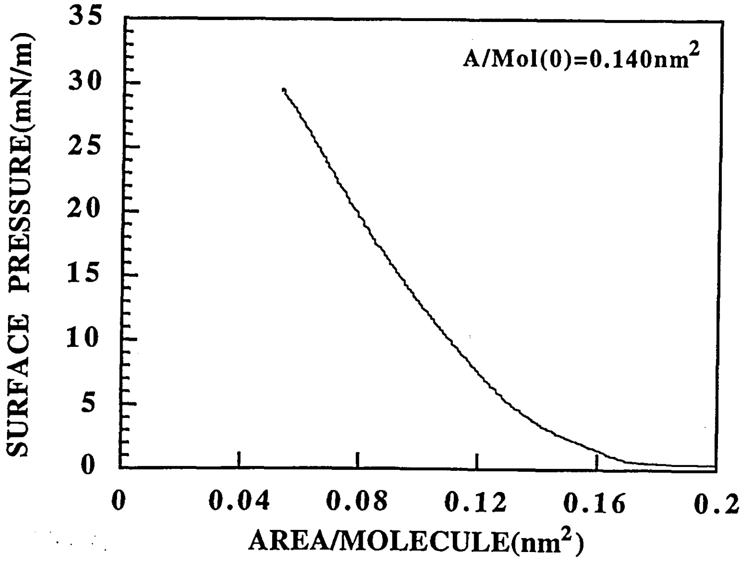

Figure 5.17 Isotherm of $C_{10}H_{21}$(4)Q3CNQF$_4$.

First previous studies have shown that the cross sectional area of the widest part of the chromophore, the quinolinium cation,[54] is 30 Å^2 wide. The value of 0.14 nm^2 (14 Å^2) is below the minimum value that would be observed if the chromophore of the molecule was aligned perpendicular to the substrate.[54] (Figure 5.18)

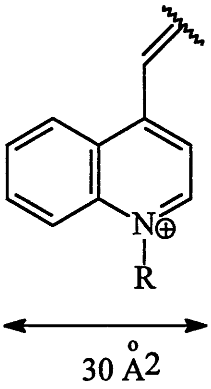

Figure 5.18 Widest Part of the Chromophore.

Second, the single fluorinated zwitterion with the same chromophore, studied by *Szablewski et al*[58] (Figure 5.19) gave an area per molecule value of 85 Å when spread from a dichloromethane solution.

There are a number of possible reasons for this. One possibility is that the very low values arise as a result of the material not forming a full monolayer on the surface of the trough. It has been previously shown in Chapter Two that, when dissolved in low concentrations, the spectral absorption bands of the fluorinated adducts deviate from the Beer-Lambert law, thus indicating aggregate formation.

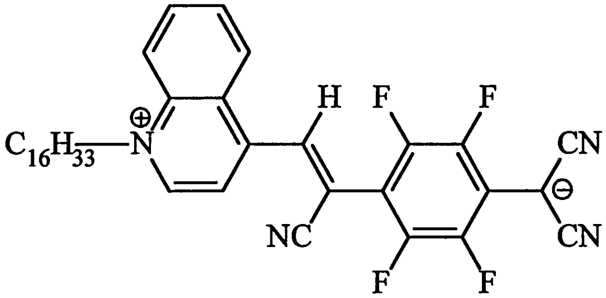

Figure 5.19 Szablewski's Fluorinated LB Material.

Poor solubility of the adducts led to dilute spreading solutions, typically of the order ~0.05 mg ml^{-1}, being prepared. Such low concentrations could result in the formation of aggregates, possibly in the form of dimer pairs, whereby the individual molecules adopt an anti-parallel arrangement. (Figure 5.20)

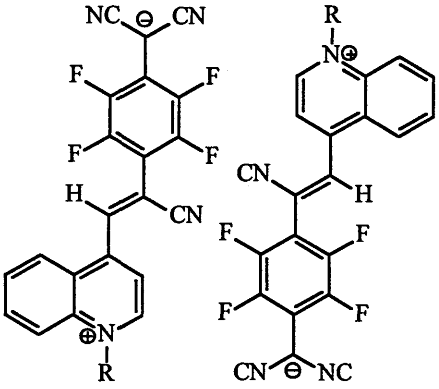

Figure 5.20 Dimer Pair Formation.

Another problem arises from the poor solubility of the materials in dichloromethane. The lower concentration of material dissolved in dichloromethane means that larger quantities of solution need to be deposited onto the subphase. Delivering different quantities of sample to the subphase can result in potentially different isotherms.[12,20] This, and the possible formation of aggregates at low concentration, may explain the puzzling results. Alternative solvents in which the materials are more soluble may overcome this problem.

The choice of alternative solvents from which the adducts could be spread, is fairly limited as, in general, the fluorinated γ-adducts are only soluble in relatively polar solvents such as acetone, DMF, DMSO etc. (see Chapter 3). Most of these solvents are water-soluble and hence cannot be used when a water subphase is used in LB experiments. Therefore alternative methods were sought.

Initially a binary solvent mixture was tried which involved dissolving the adduct in a dichloromethane/acetone mixture. This methodology has been used before,[59] whereby the solubility of the material under investigation is increased by the incorporation of a more polar solvent into the spreading solution. This enables more concentrated solutions to be prepared which are much easier to handle.

However, in the case of the γ-derivatives, the amount of acetone needed to make a concentrated DCM/acetone sample of the order of 1mg ml^{-1} was too great and water solubility problems arose. Subsequent isotherms gave molecular areas that were similar to those obtained when dichloromethane was used alone. As a result of this the binary solvent method was abandoned in favour of a single spreading solvent.

Three solvents were identified - methacrylonitrile, 2-butanone and 4-methyl-2-pentanone. All three solvents were found to have the necessary properties required of a spreading solvent.[20] However the use of these solvents posed new problems.

2-Butanone and 4-methyl-2-pentanone, despite them having relatively high partial vapour pressures,[60] were found to be involatile when deposited onto the surface of the subphase. This was thought to be as a result of hydrogen bonding between the water molecules of the subphase and the carbonyl groups in the solvent molecules.

The use of methacrylonitrile, despite its highly toxic nature, was initially promising as the fluorinated adducts were readily soluble in it and its high partial vapour pressure and insolubility in water meant that it would easily evaporate from the surface of the trough. However, as with the other solvents the use of methacrylonitrile did have limitations. Methacrylonitrile is a light-sensitive compound and readily undergoes polymerisation[61] and is stabilised with 0.005% p-hydroxyanisole, which is itself surface active. So, though methacrylonitrile is itself a very good solvent for spreading solutions of fluorinated γ-compounds, its stabilisation with *p*-hydroxyanisole precludes its use as a LB spreading solvent. This is illustrated in Figure 5.21 by the steeply sloped isotherm obtained when a 100μl sample of methacrylonitrile was deposited onto the trough and left for twenty minutes before being compressed. The methacrylonitrile evaporates leaving *p*-hydroxyanisole which on compression exhibits the isotherm shown in Figure 5.21.

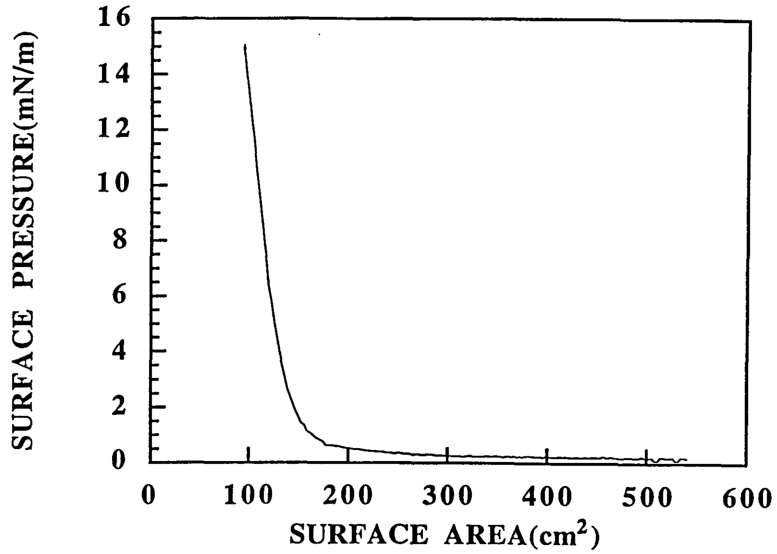

Figure 5.21 Isotherm Obtained from the use of Methacrylonitrile.

As a result of solubility problems associated with R(4)Q3CNQF$_4$ compounds, investigation into the film forming behaviour of this class of adduct was not possible. The insolubility of such compounds does highlight one of the major disadvantages of the LB technique in that, even if a material is amphiphilic, it does not necessarily mean that it can be studied.

R(2)Q3CNQF$_4$ adducts are almost all soluble in dichloromethane. Hence the preparation of concentrated solutions, typically ~1 mg ml^{-1}, of the various adducts is relatively easy.

Unlike the previously documented R(2)Q3CNQ compounds, which show featureless surface pressure *vs.* surface area isotherms (Figure 5.22), the fluorinated R(2)Q3CNQF$_4$ adducts show very different monolayer behaviour. The isotherms observed for such compounds are not featureless and show the onset of a plateau region at ~21 mNm^{-1}. This is illustrated in Figures 5.23 and 5.24 with the surface pressure *vs.* surface area isotherm obtained for a selection of fluorinated α-adducts.

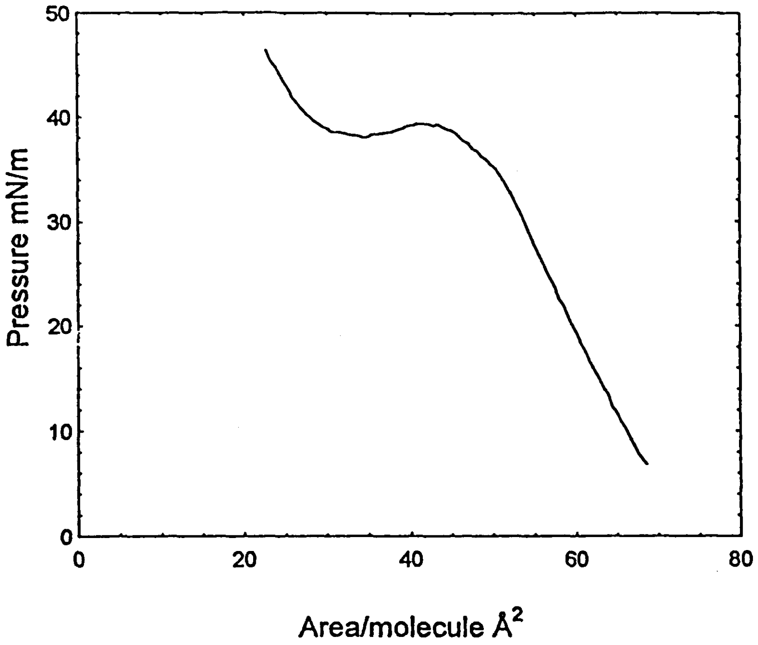

Figure 5.22 Isotherm Showing Change in Surface Pressure (mNm^{-1}) Against Area Per Molecule (Å^2) for R(2)Q3CNQ.

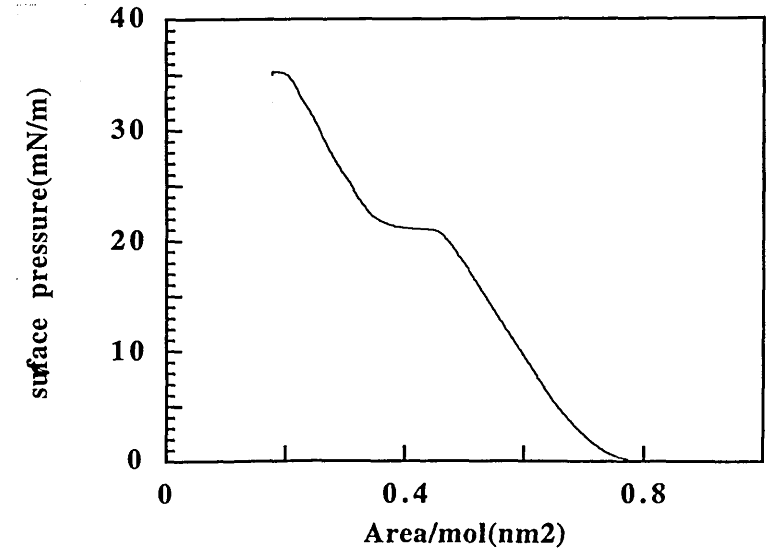

Figure 5.23 Isotherm Showing Change in Surface Pressure (mNm^{-1}) Against Area Per Molecule (Å^2) for $C_{10}H_{21}$(2)Q3CNQF$_4$.

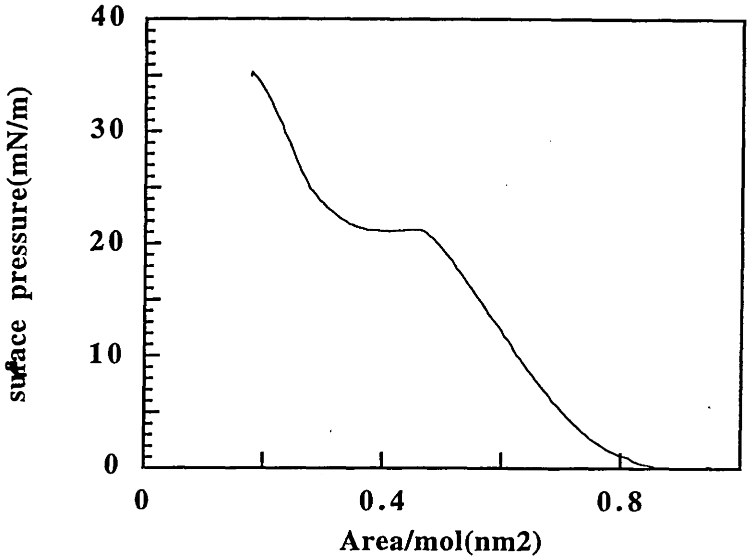

Figure 5.24 Isotherm Showing Change in Surface Pressure (mNm^{-1}) Against Area Per Molecule (Å^2) for $C_{16}H_{33}$(2)Q3CNQF$_4$.

The areas per molecule at $\pi = 0$ mNm^{-1} are listed in Table 5.2 and are generally in the range 70-85 Å^2.

Zwitterion	π_0 (mNm^{-1})	π_{25} (mNm^{-1})
$C_{10}H_{21}$(2)Q3CNQF$_4$	0.75 nm^2	0.30 nm^2
$C_{13}H_{27}$(2)Q3CNQF$_4$	0.81 nm^2	0.27 nm^2
$C_{16}H_{33}$(2)Q3CNQF$_4$	0.85 nm^2	0.31 nm^2

Table 5.2 Areas Per Molecule for Selected Adducts at π_0 and π_{25}.

When compared with the end-on van der Waals area of 24 Å^2 for the —C(CN)$_2$ [calculated from the mean dimensions of CH_3(2)P3CNQ][62] and the calculated face area of 114 Å^2 for the Q3CNQ chromophore [calculated from the molecular dimensions of CH_3(2)P3CNQ][62] and [1,4-di(4-quinoliniummethyl)benzene](TCNQ)$_3$[63]] it is clear that the chromophores do not lie face down on the water surface at $\pi = 0$ mNm^{-1}, unlike their unsubstituted counterparts.[15,55] Instead they are assumed to adopt a tilted arrangement on the water subphase as illustrated in Figure 5.25 below.

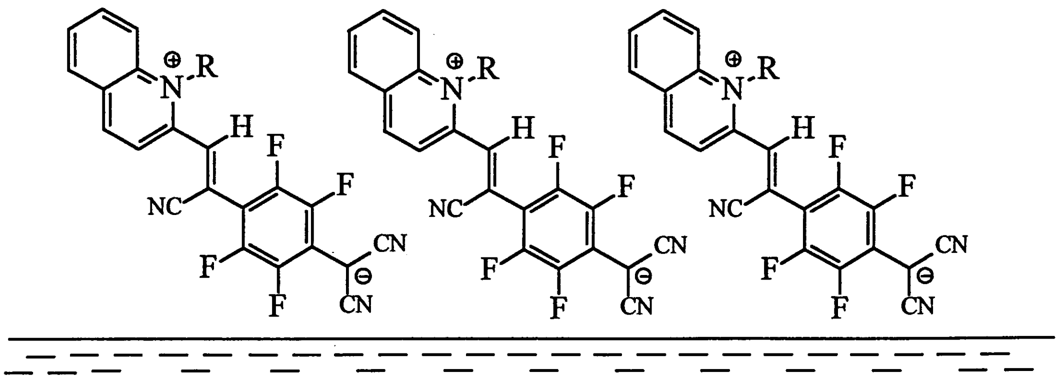

Figure 5.25 Probable Chromophore Orientation.

These calculations are based on data obtained from the crystallographic studies of an unsubstituted TCNQ-based zwitterionic adduct[62] and hence could be viewed with some caution. However the X-ray crystal structure obtained for the $C_3H_7(2)BT3CNQF_4$ (see Chapter 4) gives similar molecular dimensions to those observed in the compounds upon which this calculation is based. It is not unreasonable therefore to assume that the fluorinated α-substituted adducts will have similar molecular dimensions to those of their unsubstituted TCNQ-based compounds.

The initial gradient of the isotherms is not steep which also suggests that the molecules are tilted upon compression. As the monolayer is compressed further the surface pressure then increases, the isotherm showing a gradient similar to the one observed before the onset of the constant pressure region. This increase in surface pressure continues until at ~35-40 mNm^{-1} collapse occurs. This collapse pressure appears dependent upon the adduct, the concentration of the solution used and the speed at which the monolayer was compressed, although the collapse pressure is reproducible, with an accuracy of ± 0.5 mNm^{-1} being observed for successive isotherms.

The observation of constant pressure regions in isotherms is not new and has been observed in several amphiphilic materials.[16,64] Their observation here is unexpected - other documented zwitterionic D-π-A TCNQ-based materials,[11,12,15,55,58] studied by the Langmuir-Blodgett technique have, in general, exhibited featureless isotherms.

Such constant pressure regions have been shown to occur for a number of reasons. In fatty acids[11] these regions are associated with enthalpy changes within the monolayer, such as the energy change observed when the monolayer changes from an expanded to a condensed monolayer. This first order thermodynamic transition mimics the enthalpy change observed when a gas condenses to a liquid state, or a liquid solidifying, in a three dimensional system.

Amongst other compounds,[37,38] the structurally related quinolinium materials studied by *Ashwell et al*[37] (Figure 5.26) have also shown plateau like regions in their isotherms.

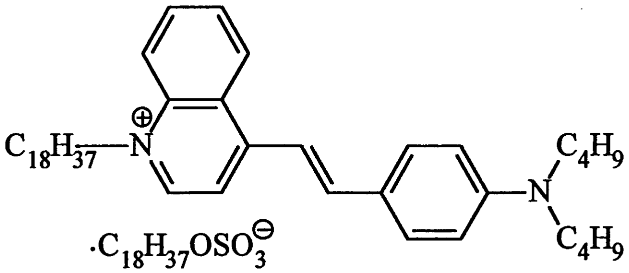

Figure 5.26 Octadecylsulphate Salt of E-N-Octadecyl-4-[2-(4-dibutyl-aminophenyl)ethenyl] quinolinium.

Here, they are thought to occur as a result of structural rearrangements within the monolayer,[37] which involves a change from a horizontal to a vertical alignment of the chromophore within the film's structure.

They may also be the result of aggregate formation,[16] with individual molecules of the deposited material forming dimers as well as micelles or vesicles within the film structure. For example, the extensive studies of *Barraud et al*,[16] mentioned earlier, indicated that the constant pressure regions observed in the isotherms of TCNQ-based charge-transfer materials (Figure 5.27) were due to dimer pair formation within the monolayer.

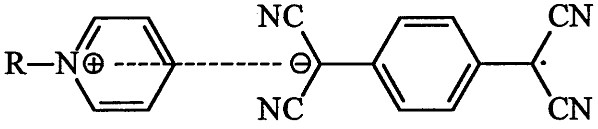

Figure 5.27 Barraud's Charge-Transfer Salt.

The possibility an enthalpy change is thought unlikely as it is not observed in any of the structurally related unsubstituted TCNQ-based compounds. The gradient of the isotherm after the plateau is not very steep, with the isotherm still showing considerable changes in area per molecule - approximately 0.1 nm^2, even after the transition. If the transition was due to an expanded-to-condensed phase enthalpy change, molecules in the condensed phase would be closely packed and would not be expected to show such a large change in area per molecule with increasing surface pressure. The film would become strained and collapse.

The likelihood that the plateau arises as a result of a change in the alignment of the fluorinated chromophores, (cf. Ashwell[37,38]) may be more plausible. The observed area per molecule before the plateau indicates that the chromophores are aligned nearly parallel to the surface of the subphase, whereas the molecular areas occupied by the material after the plateau are typically of the order of 35-40 Å^2.This is only just larger than the cross sectional van der Waals area of the quinolinium cation,[54] and is the alignment exhibited by the R(4)Q3CNQ compounds. By considering the molecular dimensions of the α-substituted compounds, the chromophores could reorientate themselves on the surface of the trough as the surface pressure increases, so that the chromophores become perpendicular to the surface of the subphase (Figure 5.28).

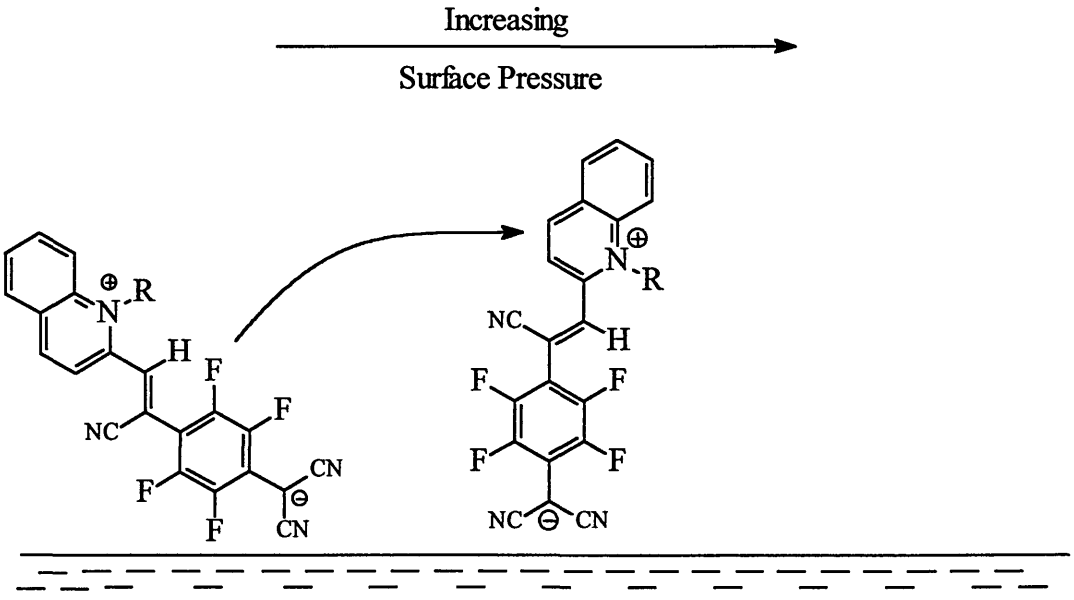

Figure 5.28 Reorientation of $R(2)Q3CNQF_4$ Monolayer.

If the monolayer were compressed and then expanded, in a fully dynamic system it would be expected that there would be no change in the pressure-area profile. This is because, on compression, each molecule would be anticipated to organise itself into its preferred orientation and upon expansion would return to its original state. While molecules can attain a preferred orientation upon compression, they can also be preferentially influenced by neighbouring molecules upon successive expansions and compressions, thus retaining an aggregated type state. This phenomenon is known as hysteresis, and has been acknowledged as a problem for some time.[20] It can be identified by conducting routine compression-expansion experiments upon the material under investigation to see whether such an aggregation phenomenon is present.

In the case of the R(2)Q3CNQF$_4$ compounds, hysteresis experiments appear to show that the plateau is not just a simple case of molecular reorientation of the molecules. Hysteresis plots show that aggregation is a clear problem as the repeated compression and expansion of the monolayer, resulted in a change in the pressure-area profile of the material. The hysteresis plot obtained for the C$_{10}$H$_{21}$(2)Q3CNQF$_4$ adduct is illustrated in Figure 5.29 and shows that, as the monolayer is repeatedly expanded and compressed, the profile of the isotherm changes.

As the molecular dimensions occupied by the molecules at certain points - such as initial pressure rise and plateau transition along with the size of the plateau - are all significantly smaller than those observed in the previous compression, then some form of aggregation of the molecules in the monolayer may be occurring. This is also borne out by the observation of a decrease in the maximum surface pressure obtained, as the final compression (thin dotted line in Figure 5.29), shows a smaller maximum surface pressure value than observed in the first compression (solid line in Figure 5.29). This may be due to disruption in the monolayer due to aggregation which cause residual defects in the monolayer structure.

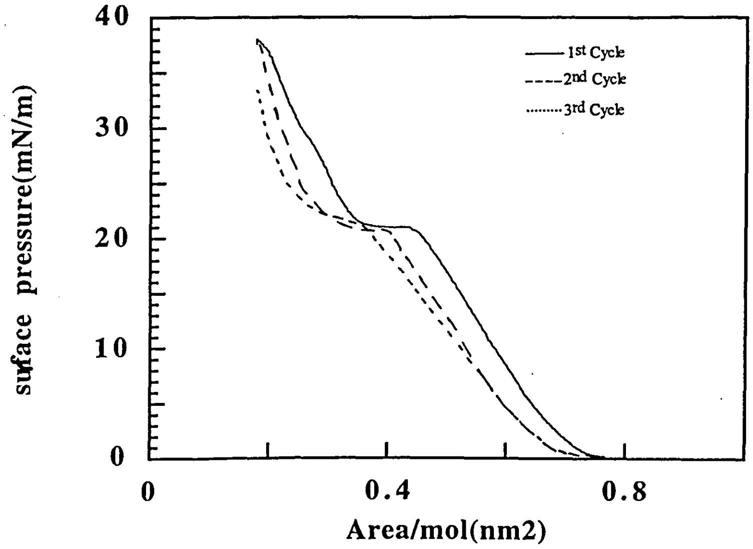

Figure 5.29 Three Successive Compression/Expansion Cycles Showing the Film Hysteresis of C$_{10}$H$_{21}$(2)Q3CNQF$_4$.

So it is suggested that the constant pressure region arises as a result of aggregate formation of the molecules. Other evidence supporting this proposal comes from area *vs.* time stability experiments.

If the materials are to be successfully transferred to a solid substrate and fabricated as LB films, then the compressed monolayer should be stable at the chosen deposition pressure. Thus, the barrier can be held at a particular surface pressure and the film area monitored with time. If the material is undergoing structural reorientation, due to aggregation problems, for example, then a decrease in the film area will be observed as a consequence of the feedback system maintaining the surface pressure at the predetermined value. Figure 5.30 clearly shows that the films are unstable with respect to time. Such behaviour is unsuitable for transferring films to a solid support and is supportive of aggregate formation within the monolayer.[16,19,20]

The stability plot shows that the films do not collapse, despite the fact that during the experiments the barrier is very nearly at its minimum area. In the normal isotherm studies, on collapse, a fine black solid was observed on the subphase surface. In the stability plots this was not observed.

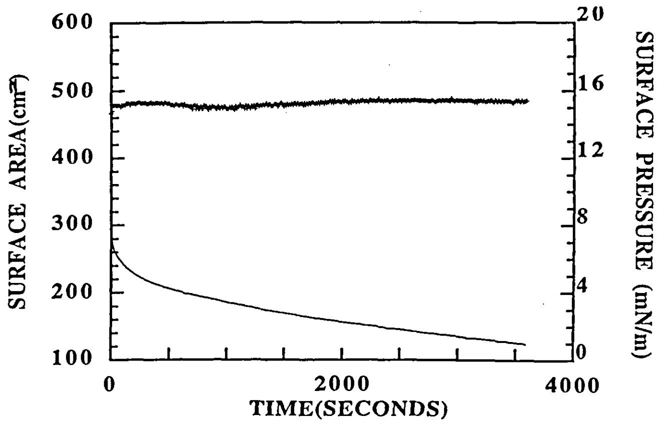

Figure 5.30 Stability of $C_{10}H_{21}(2)Q3CNQF_4$ at 25 mNm^{-1}.

The loss of film area could also occur as a result of the material forming micelles,[19,20] that dissolve into the subphase, thus resulting in a loss of film area. The reasons supporting this are as follows. First the surface pressure used in the area *vs.* time stability experiments was 25 mNm^{-1} which, as previously shown, is beyond the point at which the molecules are thought to form aggregates, i.e. the constant pressure region. Hence, if the constant pressure region is due to the molecules changing their alignment to a more vertical like arrangement, then the subsequently realigned monolayer would in theory still be expected to be stable and thus show no loss of film area in an area *vs.* time stability experiment. As this is not the case it thus indicates that a different process is occurring.

Second, if the film were collapsing, the development of a black solid in a *wave like* formation would be observed. It is not. Thus, loss of film area could occur via the formation of micelles, which are readily soluble in the subphase due to the molecules possessing a strong polar head group relative to the non-polar part of the molecule. The formation of these micelles is illustrated in Figure 5.31.

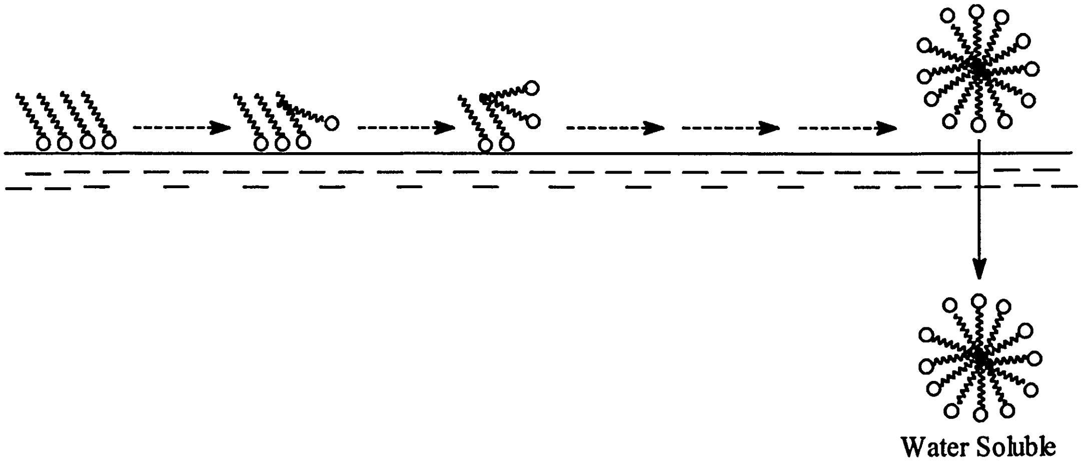

Figure 5.31 Cross Sectional View of the Proposed Micelle Formation.

Although the loss of film area can clearly be assigned to an aggregational problem, the very nature of the aggregation remains unclear. It may arise from a combination of both micelle and dimer pair formation but a more detailed study would be necessary to establish this. (see Chapter 6).

Poor film stability means poor LB films. To improve film stability, a series of experiments was carried out whereby the pH of the subphase was altered, and the effect of divalent metal ions such as cadmium assessed.

When the pH of the subphase was decreased, by the addition of Aristar grade hydrochloric acid, isotherms were similar to those prior to addition of acid. Again a plateau was observed, and the films were unstable under area *vs.* time analysis. The only marked difference between the isotherms was that at lower pH, larger molecular areas for the various transitions were observed. For example the area at which the pressure initially starts to increase was found to be 90-100 Å^2 for the isotherms obtained at pH 3-4, compared to 70-85 Å^2 for the isotherms obtained under normal conditions at pH 5.8.

The difference is attributed to the fact that at lower pH values the negatively charged dicyanomethanide swallowtail of the adduct is prone to protonation. As a result of this protonation of the swallowtail, the adduct loses its potential for electrostatic interaction with neighbouring adducts and water molecules in the subphase. Here, cohesion between neighbouring molecules will be less and as such occupy larger molecular areas as shown in Figure 5.32.

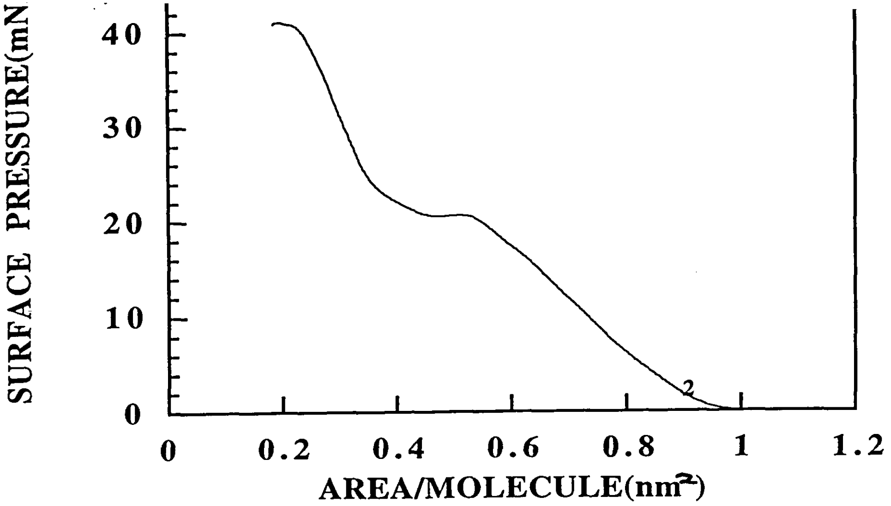

Figure 5.32 Isotherm Showing Change in Surface Pressure (mNm^{-1}) Against Area Per Molecule (Å^2) for $C_{10}H_{21}$(2)Q3CNQF$_4$ at pH 3-4.

The addition of Aristar grade sodium hydroxide pellets to the subphase, which subsequently increased the pH of the subphase to ~11, had a dramatic effect upon the shape of the isotherms obtained, in that the plateau was absent. The isotherms (Figure 5.33), were essentially featureless and similar to those obtained for the R(2)Q3CNQ class of compound.[15,55]

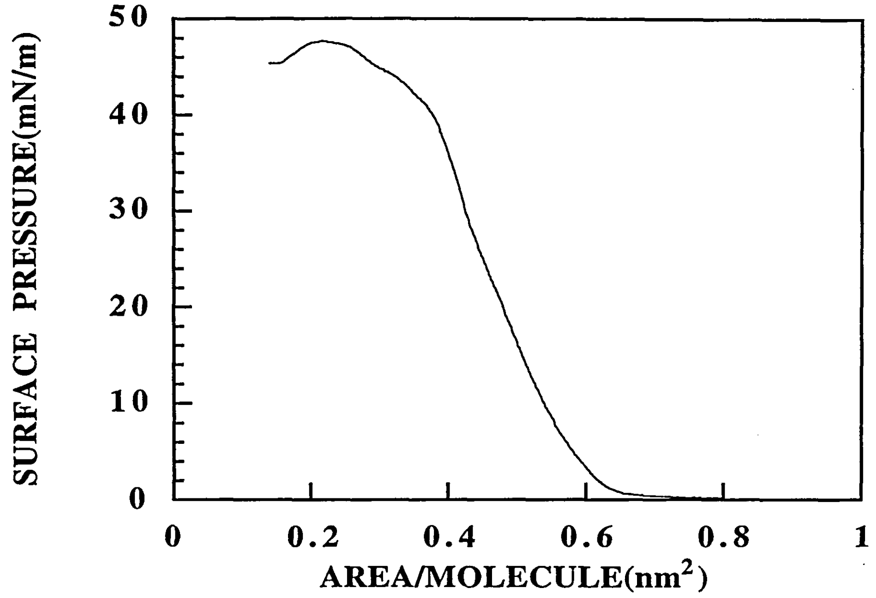

Figure 5.33 Isotherm Showing Change in Surface Pressure (mNm^{-1}) Against Area Per Molecule (Å^2) for $C_{10}H_{21}$(2)Q3CNQF$_4$ at pH 11.

The molecular areas at which the pressure initially started to increase were slightly smaller, and were typically of the order 60-65 Å^2. The isotherms also showed higher surface pressures for the same amount of material deposited relative to those at pH 3-4 and normal conditions. This enabled the collapse of the monolayer to be determined much more easily, around 42-44 mNm^{-1}. It was thought that the sodium hydroxide addition was stabilising the monolayer by making the subphase more polar and thus encouraging the monolayer to remain as a single entity rather than from forming dimer pairs or micelles. However area *vs.* time analysis showed the film was very unstable and progressively lost area under compression (Figure 5.34).

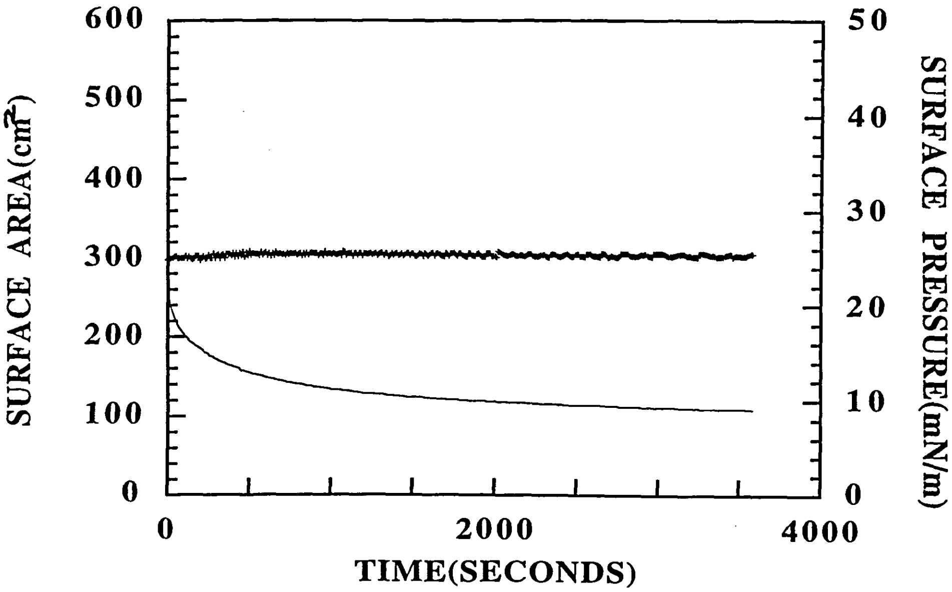

Figure 5.34 Stability of $C_{10}H_{21}(2)Q3CNQF_4$ at pH 11(25 mNm^{-1}).

It was also thought that the addition of divalent metal ions to the subphase would aid stability as this has been used before to stabilise the monolayer of ionic materials.[11,12] Addition of cadmium chloride to the subphase, which resulted in a 10^{-4} M solution, had little effect upon the monolayer - isotherms were very similar to those under normal conditions. Again constant pressure regions are observed around ~21 mNm^{-1} which are ascribed to an aggregation phenomenon. However, such materials have been found to be photochromic,[35] which has led some authors[11] to attribute reorientation of the monolayer to a photochromic reaction at the air-water interface. Here this is thought unlikely as materials which have potentially been shown to reorientate themselves via a photochromic reaction, have all shown stable film behaviour,[11] unlike the films studied in this work.

The only major differences observed on the addition of cadmium chloride, were that the initial molecular areas occupied by the material were slightly larger. This is illustrated in Figure 5.35. At zero surface pressure the adducts, when spread onto a $CdCl_2$ containing subphase, occupy an area of the order 95-105 Å^2, thus inferring that the individual molecules of the monolayer lie face down on the water surface. This is observed in the R(2)Q3CNQ adducts.[15,55]

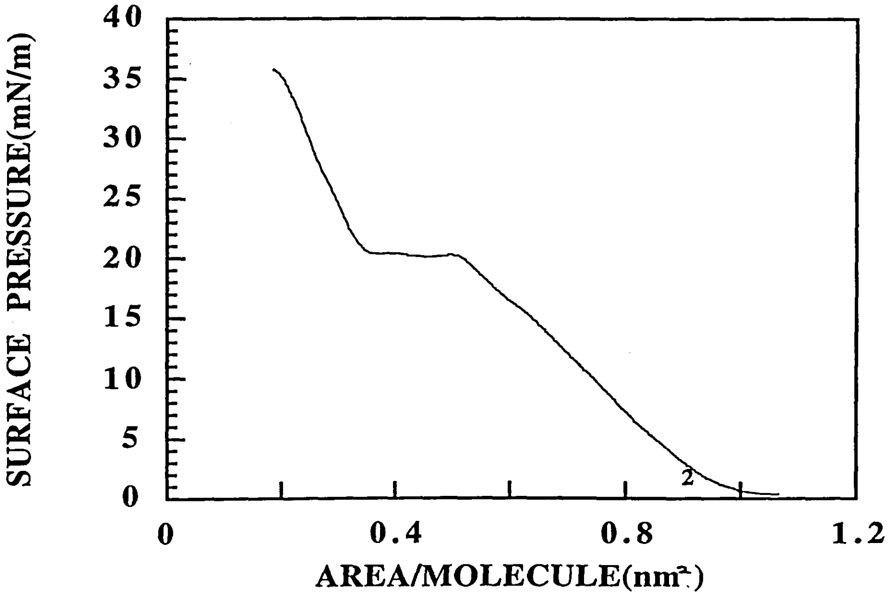

Figure 5.35 Isotherm Showing Change in Surface Pressure (mNm^{-1}) Against Area Per Molecule (Å^2) for $C_{10}H_{21}(2)Q3CNQF_4$ Obtained from a $CdCl_2$ Subphase.

Also the plateau region is much larger for a $CdCl_2$ subphase. This infers that the proposed aggregation process is much longer on a subphase containing divalent metal ions, suggesting better film stability. However, again (Figure 5.36) the films are very fragile and collapse rapidly upon compression.

All experimental evidence had shown that films derived from such compounds are not stable with respect to time and as such subsequent LB films are unlikely to be of a precise order. The larger ground state dipole moments observed in such compounds (see Chapter 4), relative to those observed in the unsubstituted TCNQ-based compounds, would in theory give such compounds potentially greater nonlinear optical responses such as increased second harmonic generation,[10] as a result of the increased polarisation within the chromophore of such materials, but the poor stability shown by the fluorinated adducts has shown that suitable LB films of such potentially exciting materials is limited.

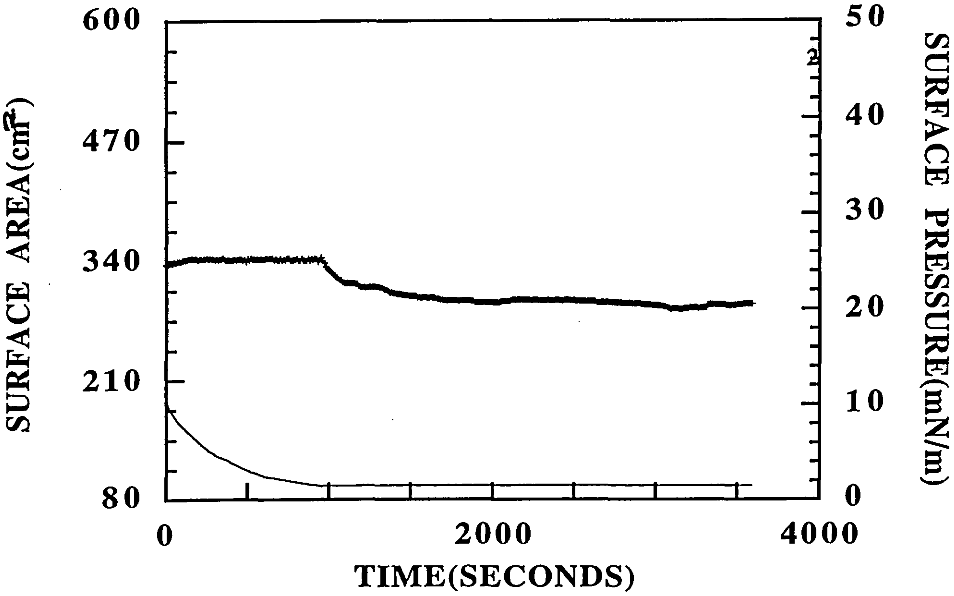

Figure 5.36 Stability of $C_{10}H_{21}(2)Q3CNQF_4$ under $CdCl_2$ Conditions (25 mNm^{-1}).

5.8 References.

1. D. Tafor, *J. Colloid Interface Sci.*, 1980, **75**, 240.
2. T. Terada, R. Yamamoto and T. Watanabe, *Sci. Pap. Inst. Phys. Chem. Res. Jpn.*, 1934, **23**, 173.
3. Cited, e.g., in *The complete works of Benjamin Franklin*, Vol. V, J. Bigelow, ed., G. P. Putnam's Sons, New York, 1887, p.253.
4. Lord Rayleigh, *Phil. Mag.*, 1899, **48**, 337.
5. A. Pockels, *Nature*, 1891, **43**, 437.
6. I. Langmuir, *J. Am. Chem. Soc.*, 1917, **39**, 1848.
7. G. Cooke, *Chem. Br.*, 1997, **33**, 54.
8. K. B. Blodgett, *J. Am. Chem. Soc.*, 1934, **56**, 495.
9. H. Kuhn, D. Möbius and H. Bucher, *Physical Methods in Chemistry*, 1972, **1**, 577.
10. D. R. Kanis, M. A. Ratner and T. J. Marks, *Chem. Rev.*, 1994, **94**, 195.
11. R. A. Broughton, PhD Thesis, *Sheffield Hallam University*, 1993.
12. G. J. Ashwell, G. Jefferies, E. J. C. Dawnay, A. P. Kuczyñski, D. E. Lynch, Y. Gongda and D. G. Bucknall, *J. Mater. Chem.*, 1995, **5**, 975.
13. G. Decher, B. Tieke, C. Bossard and P. Günther, *J. Chem. Soc., Chem. Commun.*, 1988, 933.
14. G. J. Ashwell, T. Handa, G. Jefferies and D. Hamilton, *Colloids and Surfaces A: Physicochem. Eng. Aspects*, 1995, **102**, 133.
15. C. S. Bradley, PhD Thesis, *Sheffield Hallam University*, 1999.
16. A Barraud, M. Flörsheimer, H. Möhwald, J. Richard, A. Ruaudel-Teixier, and M. Vandevyver, *J. Colloid. Interface. Sci.*, 1988, **121**, 491.
17. M. J. Grundy, R. J. Musgrove, R. M. Richardson, and S. J. Roser, *Langmuir*, 1990, **6**, 519.
18. C. Bubeck, *Thin Solid Films*, 1988, **160**, 1.

19. M. C. Petty, *Langmuir-Blodgett Films, An Introduction*, Cambridge University Press, 1996.

20. G. L. Gaines Jr, *Insoluble Monolayers at Liquid-Gas Interfaces*, Wiley-Interscience, New York, 1966.

21. O. Albrecht, *Thin Solid Films*, 1989, **178**, 563.

22. T. Nakamura, M. Matsumoto, F. Tahei, M. Tanaka, T. Sehiguchi, E. Manda and Y. Kawabata, *Chem. Lett.*, 1986, 709.

23. I. Langmuir and V. J. Schaefer, *J. Am. Chem. Soc.*, 1938, **60**, 1351.

24. M. C. Petty and W. A. Barlow, Film Deposition, in *Langmuir-Blodgett Films*, ed. G. G. Roberts, 131-221, Plenum Press, New York, 1990.

25. J. H. Schulman, R. B. Waterhouse, and J. A. Spink, *Kolloid-Z.*, 1956, **146**, 77.

26. J. K. O'Rourke, PhD Thesis, *Sheffield Hallam University*, 1994.

27. A. Barraud, C. Rosilio and A. Ruaudel-Teixier, *J. Colloid. Interface. Sci.*, 1977, **62**, 1509.

28. K. K. Kan, G. G. Roberts, and M. C. Petty, *Thin Solid Films.*, 1983, **99**, 291.

29. R. W. Munn, *Chem. Br.*, 1984, 518.

30. E. Stenhagen, Surface Films, in *Determination of Organic Structures by Physical Methods*, eds. E. A. Braunde and F. C. Nachod, 1955, 325-371, Academic Press, New York.

31. C. A. Jones, PhD Thesis, *University of Durham*, 1987.

32. T. J. Lewis, D. M. Taylor, J. P. Llewellyn, S. Salvagno and C. J. M. Stirling, *Thin Solid Films.*, 1985, **133**, 243.

33. J. Ferraris, D. O. Cowan, V. V. Walatka and J. M. Perlstein, *J. Am. Chem. Soc.*, 1973, **95**, 948.

34. M. R. Bryce and M. C. Petty, *Nature*, 1995, **374**, 771.

35. G. J. Ashwell, *Nature*, 1990, **347**, 617.

36. I. R. Girling, P. V. Kolinsky, N. A. Cade, J. D. Earls, and I. R. Peterson, *Opt. Commun.*, 1985, **55**, 289.

37. G. J. Ashwell, G. Jefferies, C. D. George, R. Ranjan, R. B. Charters and R. P. Tatam, *J. Mater. Chem.*, 1996, **6**, 131.

38. G. J. Ashwell, P. D. Jackson, G. Jefferies, I. R. Gentle and C. H. L. Kennard, *J. Mater. Chem.*, 1996, **6**, 137.

39. G. J. Ashwell, P. D. Jackson and W. A. Crossland, *Nature*, 1994, **368**, 438.

40. P. Hodge, Z. Ali-Adib, D. West and T. A. King, *Macromolecules*, 1993, **26**, 1789.

41. G. J. Ashwell, T. W. Walker, I. R. Gentle, G. J. Foran, G. S. Bahra and C. R. Brown, *J. Mater. Chem.*, 1996, **6**, 969.

42. G. J. Ashwell, J. R. Sambles, A. S. Martin, W. G. Parker and M. Szablewski, *J. Chem. Soc., Chem. Commun.*, 1990, 1374.

43. R. M. Metzger, B. Chen, U. Höpfner, M. V. Lakshmikantham, D. Vuillaume, T. Kawai, X. Wu, H. Tachibana, T. V. Hughes, H. Sakurai, J. W. Baldwin, C. Hosch, M. P. Cava, L. Brehmer, and G. J. Ashwell, *J. Am. Chem. Soc.*, 1997, **119**, 10455.

44. A. Broo, and M. C. Zerner, *Chem. Phys.*, 1995, **196**, 423.

45. G. J. Ashwell, T. Handa, P. Leeson, K. Skjonnemand, G. Jefferies and A. Green, *J. Mater. Chem.*, 1998, **8**, 377.

46. G. J. Ashwell, G. Jefferies, D. G. Hamilton, D. E. Lynch, M. P. S. Roberts, G. S. Bahra and C. R. Brown, *Nature*, 1995, **375**, 385.

47. G. J. Ashwell and P. Leeson, *Electrical and Related Properties of Organic Solids* (ed. R. W. Munn, A. Miniewicz and B. Kuchta), NATO ASI series, 1997, **24**, 297.

48. S. Baker, M. C. Petty, G. G. Roberts and M. V. Twigg, *Thin Solid Films*, 1982, **99**, 53.

49. R. H. Tredgold, S. D. Evans, P. Hodge, R. Jones, M. G. Stocks and M. C. J. Young, *Brit. Polym. J.*, 1987, **19**, 397.

50. D. Crouch, S. C. Thorpe, M. J. Cook, I. Chambrier and A. K. Ray, *Sensors and Actuators B*, 1994, **18-19**, 411.

51. P. S. Vincett, W. A. Barlow, F. T. Boyle, J. A. Finney and G. G. Roberts, *Thin Solid Films*, 1979, **60**, 265.

52. L. Blight, C. W. N. Campbell, and V. J. Kyte, *J. Colloid. Sci.*, 1965, **20**, 393.

53. C. Pearson, A. S. Dhindsa, L. M. Goldenberg, R. A. Singh, R. Dieing, A. J. Moore, M. R. Bryce and M. C. Petty, *J. Mater. Chem.*, 1995, **5**, 1601.

54. G. J. Ashwell, E. J. C. Dawnay, A. P. Kuczyñski, M. Szablewski, I. M. Sandy, M. R. Bryce, A. M. Grainger and M. Hasan, *J. Chem. Soc., Faraday Trans.*, 1990, **86**, 1117.

55. G. J. Ashwell, *Thin Solid Films*, 1990, **186**, 155.

56. N. A. Bell, R. A. Broughton, J. S. Brooks, T. A. Jones and S. C. Thorpe, *J. Chem. Soc., Chem. Commun.*, 1990, 325.

57. N. A. Bell, R. A. Broughton, J. S. Brooks, T. A. Jones and S. C. Thorpe, *Int. J. Electronics*, 1994, **76**, 751.

58. M. Szablewski, PhD Thesis, *Cranfield Institute of Technology*, 1991.

59. C. Pearson, *Personal Communication.*

60. A. J. Riddick, W. B. Bunger, and T. K. Sakano, *Organic Solvents., Physical Properties and Methods of Purification.*, 4th ed., John Wiley and Son Inc., New York, 1986.

61. A. Streitwiesser, C. H. Heathcock and E. M. Kosower, *Introduction to Organic Chemistry*, 4th ed., MacMillan Publishers, 1992.

62. R. M. Metzger, N. E. Heimer and G. J. Ashwell, *Mol. Cryst. Liq. Cryst.*, 1984, **107**, 733.

63. G. J. Ashwell, D. D. Eley, S. C. Wallwork, M. R. Willis, G. F. Peachey and D. B. Wilkos, *Acta. Crystallogr. B.*, 1977, **33**, 843.

Chapter 6: Conclusions

6.1 Summary.

The aim of this work has been to synthesise and study the molecular properties exhibited by zwitterionic donor-π-acceptor systems that incorporate substituted TCNQ-based electron acceptors such as 2,3,5,6-tetramethyl-7,7,8,8-tetracyano-p-quinodimethane (TMTCNQ), 11,11,12,12-tetracyano-9,10-anthraquinodimethane (TCAQ) and 2,3,5,6-tetrafluoro-7,7,8,8-tetracyano-p-quinodimethane ($TCNQF_4$). Previous work has shown that such donor-π-acceptor materials, which incorporate TCNQ, display numerous electro-optical properties.[1-3] However, the vast majority of structural alterations that have occurred have been associated with the donor part of the molecule, with simple TCNQ being used as the acceptor. Here we have extended the range of D-π-A adducts known by incorporating either electron withdrawing, i.e. fluorine, or electron-donating, i.e. methyl and aromatic, functionalities into the TCNQ acceptor moiety.

The substituted tetramethyl-(TMTCNQ) and anthracene-(TCAQ) acceptors were prepared via slightly modified $TiCl_4$-mediated condensation procedures,[4,5] in which the TCNQ-derivative was prepared directly from the corresponding quinone in a single step. The more powerful $TCNQF_4$ acceptor, on the other hand, was prepared via the five step synthetic strategy used by *Wheland et al*[6] as the attempted single step dicyanomethylation of p-fluoranil failed. The quinolinium-, diquinolinium-, pyridinium- and dipyridinium-electron donor units were also prepared via standard literature methods,[7] essentially involving the N-alkylation of the appropriate nitrogen heterocycle with an alkyl halide to form quaternised salts. These were then allowed to react with the appropriate TCNQ-derivative to yield the desired zwitterionic adduct.

The adducts were all prepared using the N-methylpiperidine (or piperidine) / acetonitrile (or methanol) method developed by *Broughton et al*[7] and included an extensive series of TMTCNQ- and $TCNQF_4$-based quinolinium zwitterions, as well as benzothiazolium-, pyridinium- and diquinolinium-based compounds.

Attempts to prepare adducts of the sterically strained TCAQ acceptor, were unsuccessful. Yields of the TMTCNQ-based adducts were generally poor (8-15%) and all of the adducts showed varying degrees of solvent inclusion in the solid state.

The most interesting member of the TMTCNQ-based family of materials was found to be C_3H_7(2)BT3CNTMQ. Unlike the other TMTCNQ-based materials, the reaction used to prepare this adduct not only produces the yellow zwitterion but also consumes it as well to produce a red isolable solid for which the following structure has been proposed (on the basis of the spectroscopic and analytical data obtained).

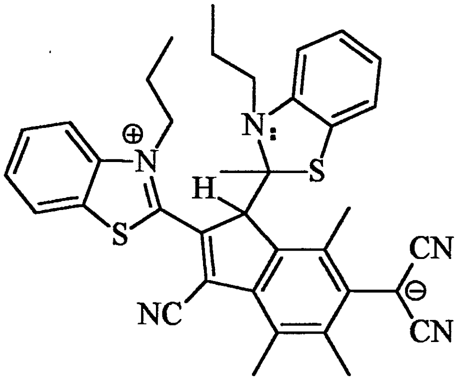

The effects of introducing electro-positive and electro-negative functionalities into the framework of such dipolar compounds has been demonstrated in the ultra violet / visible spectroscopy studies with the position of the longest wavelength charge-transfer absorption band of the chromophore being sensitive to the environment in which molecule is situated.

For example the introduction of the more electronegative fluorine atom resulted in a shift to higher energies relative to that of the TCNQ-based counterpart.

Solvatochromic effects of the TCNQ- and $TCNQF_4$-based adducts were studied in eighteen solvents and these were explained using both the dielectric constant and normalised empirical solvent polarity parameter E_T^N scales. The absorption spectrum of each adduct typically showed an intense broad structureless transition, which for the long-chain quinolinium adducts was independent of chain length and is attributed to an intramolecular back charge-transfer process from the negatively charged dicyanomethanide group to the positively charged nitrogen moiety. All of the materials showed a hypsochromic (blue) shift with increasing solvent polarity, with shifts for the $TCNQF_4$ adducts being greater than for the TCNQ adducts. In contrast the C_3H_7(2)BT3CNQ adduct has been shown to undergo significant structural changes with decreasing solvent polarity. When measured in low polarity solvents the absorption band resembles a double camel hump rather than a structureless broad transition, due to solvent induced broadening of the electronic transitions, resulting in the concomitant loss of the coarse structure.

In general the negative solvatochromic responses exhibited by the $TCNQF_4$-based materials were found to be much larger than those in the TCNQ-based materials. For example $C_{10}H_{21}$(2)Q3CNQF$_4$ showed a negative solvatochromic shift some -1902 cm^{-1} larger than that observed in the corresponding $C_{10}H_{21}$(2)Q3CNQ adduct. The fluorinated zwitterions also showed other differences. In solvents of low polarity a bathochromic shift in the charge-transfer band is observed. Such reverse-solvatochromism - observed in all but the C_3H_7(2)BT3CNQF$_4$ adduct - is attributed to an aggregation of molecules in solution rather than a structural change to a neutral ground state (the solution state dipole moments of various fluorinated analogues were determined to be in the order of 40-46 Debyes). Other evidence supporting this has come from ^{19}F NMR solvatochromism studies, which have shown that the electron density around the acceptor system changes very little with increasing solvent polarity.

The zwitterions are also halochromic, with the charge-transfer absorption band being shifted hypsochromically, on addition of electrolytes.

The X-ray crystal structures of C_3H_7(2)BT3CNQF_4 and C_4H_9(4)Q3CNQ compounds indicate their zwitterioinc nature. The former is the first example of a fluorinated TCNQ containing adduct of this type while the later is the only crystal structure of the γ-substituted quinolinium series.

Unlike, the R(4)Q3CNQ and R(2)Q3CNQ family of compounds, R(4)Q3CNQF_4 and R(2)Q3CNQF_4 compounds are very poor LB film forming materials due to their sparing solubility in appropriate organic solvents. Isotherms obtained for the fluorinated γ-adducts were very similar to those of the corresponding TCNQ-based adducts, but are unstable. In contrast to R(2)Q3CNQ,[3,8] isotherms of R(2)Q3CNQF_4 contain a plateau, which may be attributed to a realignment of the molecules within the floating monolayer, possibly due to the aggregation. Hysteresis plots appear to confirm this.

6.2 Future Work.

1. Further synthetic work to isolate the TMTCNQ-based compounds and those listed in Appendix I.

2. Further investigations into the Langmuir-Blodgett film forming properties of R(4)Q3CNQF$_4$ and R(2)Q3CNQF$_4$, to develop a method for producing non-centrosymmetrical films.

3. Experimental determination of the nonlinear optical behaviour of the materials with techniques such as Hyper Rayleigh Scattering (HRS), enabling structure/property relationships to be better understood and thus provide a means to optimise nonlinear optical activity in a specific delocalised π-framework.

5. Further investigations into the nature of the products formed from the photo-oxidation reactions that such adducts undergo with oxygen.

6.3 References.

1. G. J. Ashwell, E. J. C. Dawnay, A. P. Kuczyñski, M. Szablewski, I. M. Sandy, M. R. Bryce, A. M. Grainger and M. Hasan, *J. Chem. Soc., Faraday Trans.*, 1990, **86**, 1117.
2. (a) R. M. Metzger, B. Chen, U. Höpfner, M. V. Lakshmikantham, D. Vuillaume, T. Kawai, X. Wu, H. Tachibana, T. V. Hughes, H. Sakurai, J. W. Baldwin, C. Hosch, M. P. Cava, L. Brehmer and G. J. Ashwell, *J. Am. Chem. Soc.*, 1997, **119**, 10455. (b) G. J. Ashwell, J. R. Shambles, A. S. Martin, W. G. Parker and M. Szablewski, *J. Chem. Soc., Chem. Commun.*, 1990, 1374. (c) G. J. Ashwell, E. J. C. Dawnay and A. P. Kuczynski, *J. Chem. Soc., Chem. Commun.*, 1990, 1355.
3. (a) G. J. Ashwell, *Thin Solid Films*, 1990, **186**, 155. (b) G. J. Ashwell, *Nature*, 1990, **347**, 617.
4. A. Aumüller and S. Hünig, *Liebigs. Ann. Chem.*, 1984, 618.
5. A. Kini, M. Mays and D. Cowan, *J. Chem. Soc., Chem. Commun.*, 1985, 286.

6. R. C. Wheland and E. L. Martin, *J. Org. Chem.*, 1975, **40**, 3101.
7. (a) R. A. Broughton, PhD Thesis, *Sheffield Hallam University*, 1993. (b) N. A. Bell, R. A. Broughton, J. S. Brooks, T. A. Jones and S. C. Thorpe, *J. Chem. Soc., Chem. Commun.*, 1990, 325.
8. C. S. Bradley, PhD Thesis, *Sheffield Hallam University*, 1999.

Appendix I.

Appendix I lists the other diquinolinium and dipyridinium adducts that were prepared and characterised in this study, although their purity was not considered to be of a sufficient enough level to include in the main text of this thesis.

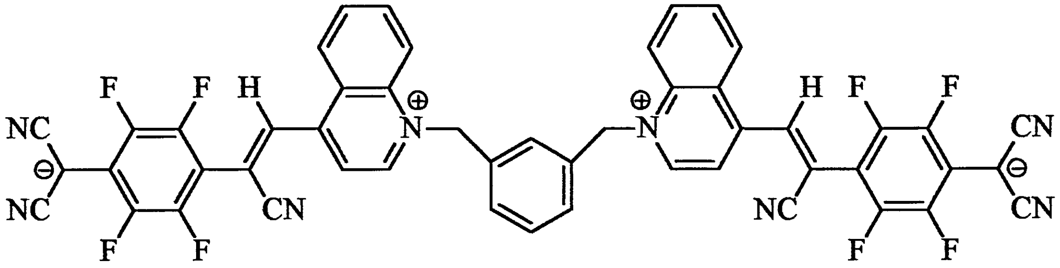

m-C_8H_8(4)DQ6CNQF_4

Characterisation:

IR (KBr): 3444 (O-H str), 2183, 2152 (C≡N str), 1497 (C=C str) cm^{-1}.

^{1}H NMR: Insufficient sample.

MS (FAB): not obtained.

C, H, N analysis: insufficient sample.

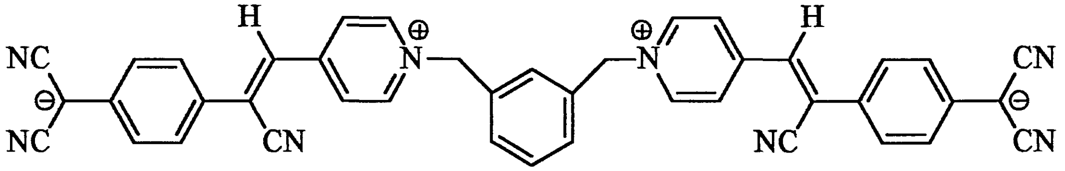

m-C_8H_8(4)DP6CNQ

Characterisation:

IR (KBr): 3437 (O-H str), 2180, 2125 (C≡N str), 1510 (C=C str) cm^{-1}.

^{1}H NMR (d_1-TFA): signal too weak

MS (FAB): *m/z* =642 (3%, M^+), 465 (2%, M^+-TCQ).

$C_{42}H_{26}N_8$ (642.68)	Calc:	C 78.49	H 4.08	N 17.43 %
	Found:	C 73.22	H 4.57	N 13.48 %
$C_{42}H_{26}N_8.2CH_3OH$ (706.76)		C 74.77	H 4.84	N 15.85 %

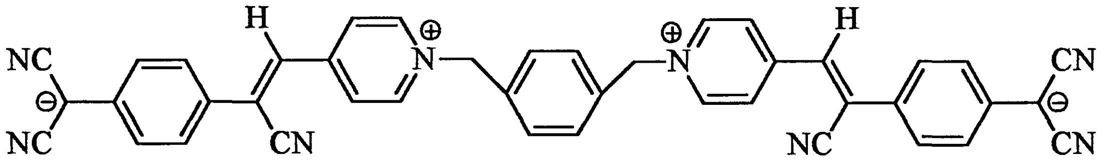

p-C_8H_8(4)DP6CNQ

Characterisation:

IR (KBr): 3431 (O-H str), 2188, 2127 (C≡N str), 1570 (C=C str) cm^{-1}.

^1H NMR (d_1-TFA): insufficient sample

MS (FAB): *m/z* =642 (4%, M^+), 465 (1%, M^+-TCQ).

$C_{42}H_{26}N_8$ (642.68)	Calc:	C 78.49	H 4.08	N 17.43 %
	Found:	C 73.62	H 4.77	N 14.48 %
$C_{42}H_{26}N_8.2CH_3OH$ (706.76)		C 74.77	H 4.84	N 15.85 %

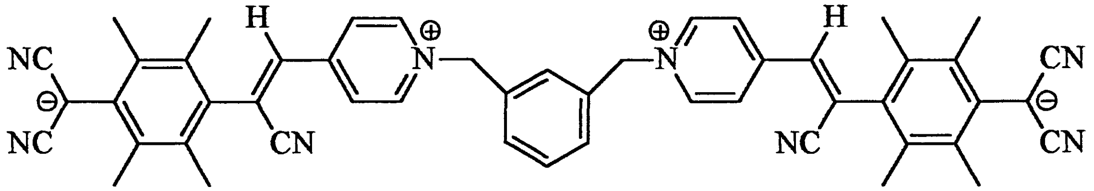

m-C_8H_8(4)DP6CNTMQ

Characterisation:

IR (KBr): 3421 (O-H str), 2159, 2082 (C≡N str), 1546 (C=C str) cm^{-1}.

^1H NMR: Insufficient sample.

MS (FAB): not obtained.

C, H, N analysis: insufficient sample.

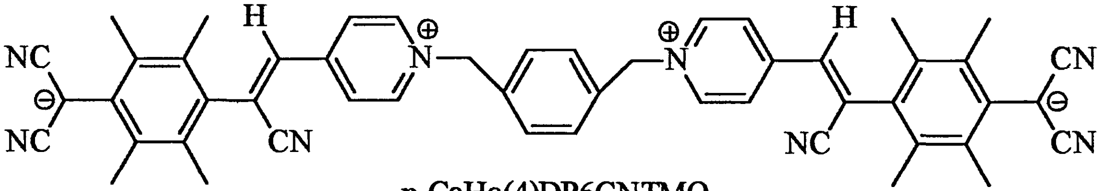

p-C_8H_8(4)DP6CNTMQ

Characterisation:

IR (KBr): 3421 (O-H str), 2155, 22083 (C≡N str), 1539 (C=C str) cm^{-1}.

^1H NMR: Insufficient sample.

MS (FAB): not obtained.

C, H, N analysis: insufficient sample.

Appendix II.

Appendix II contains a selection of DSC and TGA plots obtained for the diquinolinium zwitterions, demonstrating the embodiment of solvent molecules in the structure of such novel compounds.

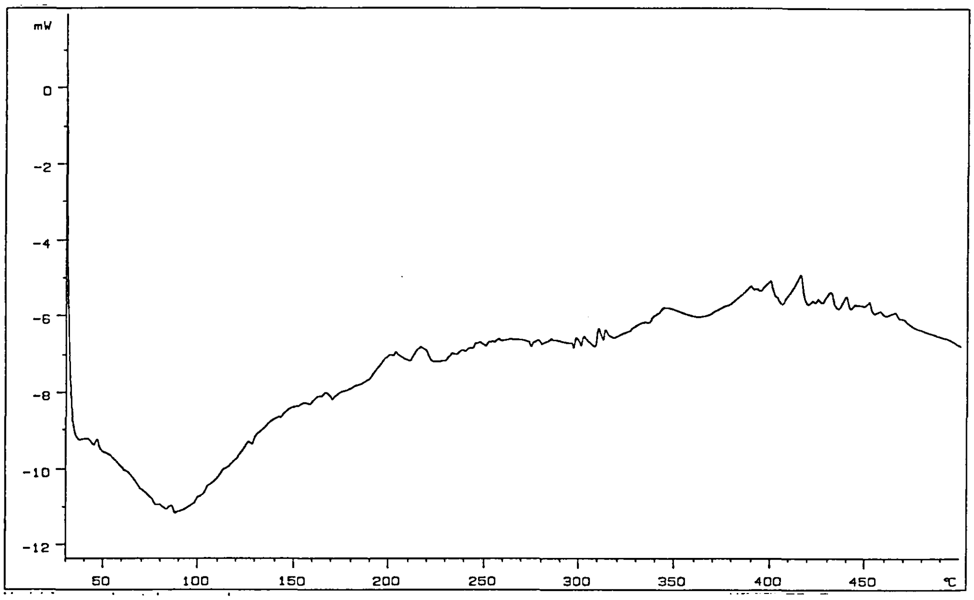

DSC Plot Obtained for *m*-C_8H_8(4)DQ6CNQ.

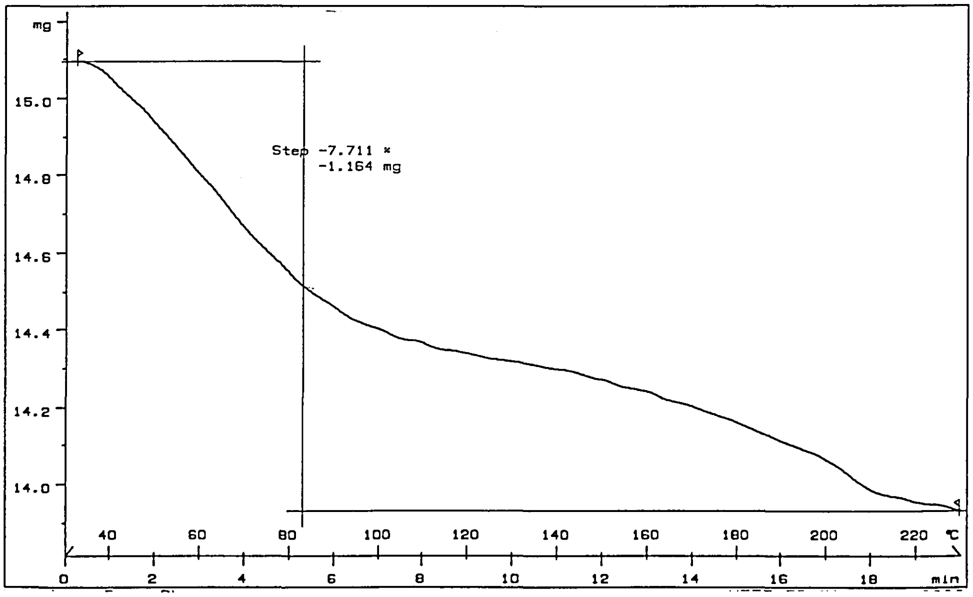

TGA Plot Obtained for *m*-C_8H_8(4)DQ6CNQ.

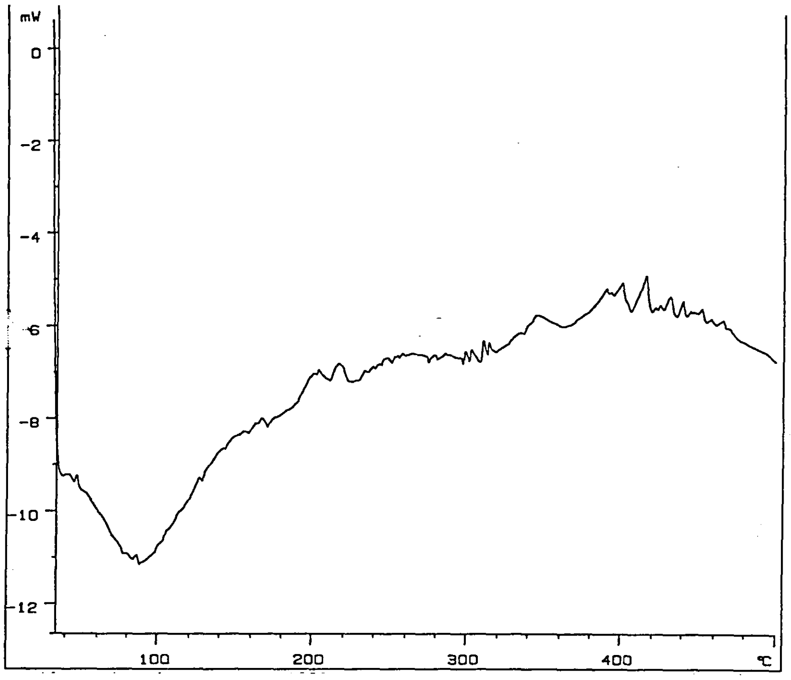

DSC Plot Obtained for p-C_8H_8(4)DQ6CNQ.

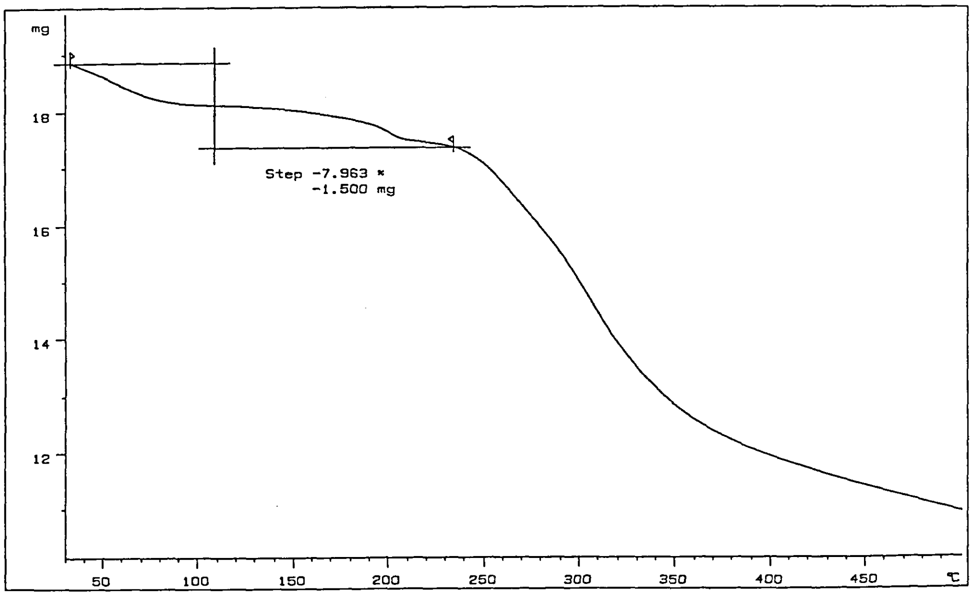

TGA Plot Obtained for p-C_8H_8(4)DQ6CNQ.